Small-Molecule-Based Crosslinking and Bioconjugation of Biomolecules

Lee-Ann Keane, B.Sc. (Hons)

Thesis presented as fulfilment for the degree of

Doctor of Philosophy (Ph.D.)

of the

National University of Ireland, Galway

School of Chemistry

National University of Ireland, Galway

October 2019

Supervisors: Dr. Eddie Myers and Prof. Fawaz Aldabbagh

Head of School: Dr. Patrick O'Leary

Declaration

I declare that the work included in this thesis is my own work and has not previously been submitted for a degree to this or any other academic institution.

Lee-Ann Keane.

Abstract

For the first two years of my 4-year Ph.D. programme, I conducted research under the supervision of Prof. Fawaz Aldabbagh. This research is outlined in Chapters 2 and 3. Following Prof. Aldabbagh's appointment at Kingston University, London in 2017, I remained at NUI Galway where I joined the research group of Dr. Eddie Myers, who joined as a new member of staff of the School of Chemistry, NUI Galway. This research is outlined in Chapters 1 and 4.

Chapter 1

The chemical modification and bioconjugation of proteins is an expanding yet challenging area of chemical biology. The superior nucleophilicity of cysteine presents it as a uniquely reactive bioconjugation handle. Inefficient photoinitiated methods and enzymatic methods (formylglycine-generating enzyme) are known for the oxidation of the thiol moiety of cysteine into the corresponding aldehyde (formylglycine). In this chapter, a photoinitiated transformation of the thiol group of a cysteine residue by using a phenacyl bromide reagent is described. Depending on the substitution pattern of the aryl ring of the phenacyl bromide, different products are obtained. Substitution with electron-donating groups allowed the generation of a disulfide in high conversion whereas an unsubstituted phenacyl bromide produced a novel isothiazolone in high conversion upon photolysis. Substitution with electron-withdrawing groups allowed high conversion to an enethiolate to be obtained upon photolysis. The efficient generation of an enethiolate from a cysteine residue by using a small molecule provides a means to incorporate a bioconjugation handle, which could be used for rapid and selective modification of cysteine residues within protein.

Chapter 2

Benzo[1,2,4]triazin-7-ones have previously been shown to exhibit submicromolar cytotoxicity against breast and prostate cancer cell lines and strong correlations to the naturally occurring anti-cancer agent, pleurotin. Given that the incorporation of a pyridine moiety into cytotoxic compounds has also been shown to significantly alter cytotoxicity against cancer cell lines, two newly synthesized pyrid-2-yl benzo[1,2,4]triazin-7-ones have been evaluated for cytotoxicity by using the MTT assay and National Cancer Institute (NCI) COMPARE analysis. The stable free radical precursors of the pyrid-2-yl benzo[1,2,4]triazin-7-ones were also subject to cytotoxicity evaluation with comparisons made to TEMPO, a stable free radical known to

exhibit cytotoxicity. Both stable free radical precursors showed specificity towards the prostate cancer cell line but were several orders of magnitude less cytotoxic than the corresponding pyrid-2-yl benzo[1,2,4]triazin-7-ones. Both pyrid-2-yl benzo[1,2,4]triazin-7-ones exhibited increased cytotoxicity against most cancer cell lines compared with the parent phenyl benzo[1,2,4]triazin-7-one analogue as shown by the NCI. NCI COMPARE analysis of the pyrid-2-yl benzo[1,2,4]triazin-7-ones showed strong correlations to the naturally occurring anti-cancer compound pleurotin. The discovery of anti-cancer activity and correlations to pleurotin for pyrid-2-yl benzo[1,2,4]triazin-7-ones presents these novel iminoquinones as potential anti-cancer agents.

Chapter 3

The synthesis of alicyclic ring-fused [1,2-*a*]benzimidazoles has attracted attention as precursors to benzimidazolequinones, a known class of bioreductive anti-tumour agents. Current synthetic protocols often require the use of transition metal catalysts, high molar mass hypervalent iodine reagents and strong bases. The most convenient method involves the oxidative cyclization of *o*-cyclic amine substituted anilines using hydrogen peroxide and trifluoroacetic acid. In this chapter hydrogen peroxide and methanesulfonic acid were used to synthesize an azocane-fused[1,2-*a*]benzimidazole, which was further oxidized into the benzimidazolequinone. The incorporation of halogen atoms onto the quinone moiety has previously been shown to enhance cytotoxicity and provides the potential for these moieties as synthetically useful intermediates. In this work, the combination of hydrogen peroxide with hydrohalic acids (H_2O_2/HX) has been used to synthesize a new series of halogenated azocane-fused[1,2-*a*]benzimidazoles and benzimidazolequinones through a one-pot oxidative cyclization, halogenation and demethylation of *o*-cyclic amine substituted anilines. The cytotoxicity of a series of ring-fused[1,2-*a*]benzimidazolequinones has been evaluated using the MTT assay. Although halogenation offered little effect on cytotoxicity, most quinone analogues exhibited submicromolar cytotoxicities against prostate and breast cancer cell lines. The novel H_2O_2/HX protocol allows efficient generation of potent, anti-cancer ring-fused benzimidazolequinones.

Chapter 4

Covalently crosslinked proteins, in long-lived connective tissues, are among the major modifications caused by the Maillard process. Advanced glycation end products (AGEs) accumulate over time and are generated to a greater extent in diabetes. Glucosepane is a major protein (lysine–arginine) crosslink, yet its mechanism of formation is poorly understood. Previous studies have suggested a key α-dicarbonyl intermediate, which is formed through a series of tautomerizations from the well-known Amadori product (derived from glucose and lysine). Cyclization of this intermediate with a proximal arginine residue yields glucosepane. In this work, isotopic labelling studies have been used to explore the possibility of an alternative mechanism for the formation of glucosepane, an intramolecular 1,5-hydride shift. The detection of a mass consistent with that of unlabelled glucosepane suggested that a 1,5-hydride shift does not occur from either the C6 position of the Amadori product to the C2 position or from the C5 position of the protonated imine intermediate to the C1 position. However, a mass consistent with that of labelled DOGDIC, a protein crosslink (AGE) was detected when 6-$[^2H]_2$-glucose was used as starting material. The inconsistency of this observation with the currently accepted mechanism of formation of DOGDIC prompted the suggestion of an alternative mechanism of formation and structure of DOGDIC. Elucidation of the formation pathways of these major protein crosslinks is a significant step for the development of effective therapeutics against the accumulation of AGEs in tissues.

Acknowledgements

First and foremost, I would like to sincerely thank my supervisors Dr. Eddie Myers and Prof. Fawaz Aldabbagh for the allowing me to pursue a Ph.D. and for their invaluable guidance, advice and patience afforded to me over the course of my research.

I gratefully acknowledge the generous financial support of College of Science, NUI Galway, which enabled the research carried out in this doctoral thesis.

I would like to acknowledge Prof. Olivier Thomas and the Thomas research group (School of Chemistry, NUI Galway) for advice and collaboration on chapter four of this thesis.

Many thanks to Prof. Patrick McArdle (School of Chemistry, NUI Galway) for obtaining all X-ray crystallography data in this thesis.

Thanks to the technical and administrative staff of the School of Chemistry, NUI Galway.

I would like to thank our collaborators Prof. Panayiotis Koutentis and the Koutentis research group (University of Cyprus) for the synthesis of all compounds evaluated in chapter two of this thesis.

I would also like to acknowledge Dr. Michael Carty (Department of Biochemistry, NUI Galway) for advice and the use of the tissue culture laboratory.

I wish to acknowledge the Development Therapeutics Program at the US National Cancer Institute, for carrying out the growth inhibition studies in chapter two and three of this thesis.

Thank you to all my fellow postgraduates, both past and present, for all of their invaluable help, advice, humour and friendship and for making my time in Galway so enjoyable.

Finally, I would like to thank my family for their continuous support through the years.

Abbreviations

Ac	acetyl
AGE	advanced glycation end product
ADC	antibody drug conjugate
ARC	accelerating rate calorimetry
Bn	benzyl
Boc	*tert*-butoxycarbonyl
BSA	bovine serum albumin
Bu	butyl
°C	degrees Celsius
Calcd	calculated
CNS	central nervous system
CSA	camphorsulfonic acid
Cys	cysteine
d	days
DBAA	α,α′-dibromoadipyl(bis)amide
DBU	diazabicyclo[5.4.0]undec-7-ene
DCM	dichloromethane
DEPT	distortionless enhancement by polarization transfer
DIC	*N*,*N*′-diisopropylcarbodiimide
DMEM	Dulbecco's modified eagle's medium
DMF	*N*,*N*-dimethyl formamide
DMSO	dimethyl sulfoxide
DNA	deoxyribonucleic acid
DSC	differential scanning calorimetry
DTNB	5,5′-dithiobis-(2-nitrobenzoic acid)/Ellman's reagent
EEDQ	2-ethoxy-1-ethoxycarbonyl-1,2-dihydroquinoline
EDG	electron donating group
ESI	electrospray ionization
Et	ethyl
equiv	equivalent
EWG	electron-withdrawing group

FAD	flavin adenine dinucleotide
FBS	fetal bovine serum
FDA	Food and Drug Administration
FGE	formylglycine-generating enzyme
fGly	formylglycine
Grb2	growth factor receptor-bound protein
GFP	green fluorescent protein
Gly	glycine
h	hours
HiF-1α	hypoxia-induced factor
Hib	*Haemophilus influenza* type b
HMQC	heteronuclear multiple quantum coherence
HOBt	hydroxybenzotriazole
HPLC	high-performance liquid chromatography
HRMS	high-resolution mass spectra
Hz	Hertz
IC_{50}	concentration required to reduce cell viability by 50%
LC_{50}	lethal concentration: resulting in a 50% reduction of cells measured at the end compared to that at the start
LC-MS	liquid chromatography – mass spectrometry
m-	*meta*-
M	molar
Me	methyl
MEM	minimum essential media
MHz	megahertz
Min	minute
MMC	mitomycin C
μM	micromolar
mM	millimolar
mp	melting point
MSH	*o*-mesitylenesulfonylhydroxylamine
MTT	3-(4,5-dimethylthiazol-2-yl)-2,5-diphenyltetrazolium bromide

m/z	mass-to-charge
NADH	nicotinamide adenine dinucleotide
NADPH	nicotinamide adenine dinucleotide phosphate
NCI	National Cancer Institute
NMR	nuclear magnetic resonance
NQO1	NAD(P)H:quinone oxidoreductase
o-	*ortho*-
obsd	observed
p-	*para*-
PDI	protein disulfide isomerase
PEG	polyethylene glycol
pet. ether	petroleum ether
Ph	phenyl
PIFA	phenyliodine(III) bis(trifluoroacetate)
PLP	pyridoxal-5-phosphate
ppm	parts per million
Pro	proline
PTM	post translational modification
R	carbon side chain
R_f	retention factor
rt	room temperature
SET	single electron transfer
SH2	src homology 2
SRB	sulforhodamine B
tert-	t*ertiary*-
TCEP	tris(2-carboxyethyl)-phosphine
TEMPO	(2,2,6,6-tetramethylpiperidin-1-yl)oxyl
TES	triethylsilane
TFA	trifluoroacetic acid
TLC	thin-layer chromatography
TOFMS	time-of-flight mass spectrometer
Tr	trityl (triphenylmethyl)

Trx	thioredoxin
TrxR	thioredoxin reductase
UV	ultra-violet

Chapter 1

Light-Mediated Bioinspired Transformations of Cysteine Derivatives

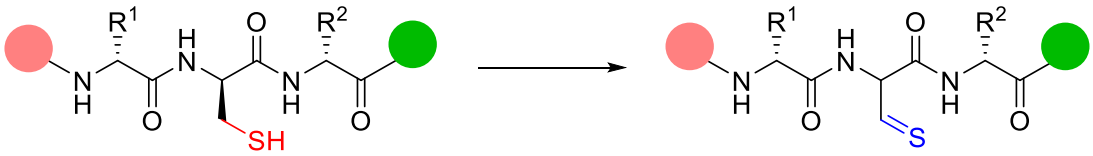

1.1 Introduction

1.1.1 Bioconjugation

Chemical modification of proteins is an expanding area of chemical biology.[1] Bioconjugation is a particular type of modification that involves the formation of a covalent bond between two or more molecules, at least one being a biomolecule. Semisynthetic or synthetic molecules, such as small-molecule drugs, peptides, carbohydrates, bio- and synthetic polymers can be attached to a biomolecule, such as a protein (Scheme 1.1).[2]

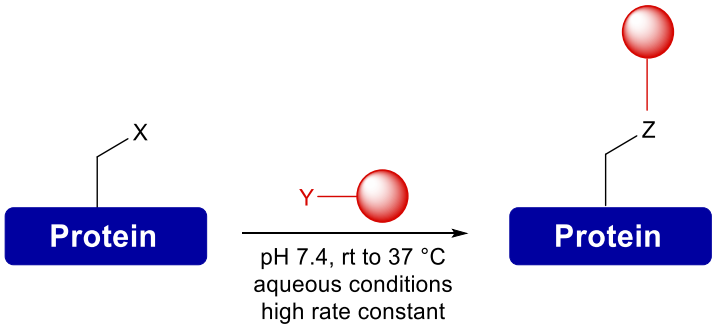

Scheme 1.1: Bioconjugation of proteins.[3]

Bioconjugation can confer changes to biomolecular structure and function and introduce desirable physiochemical properties.[4] For example, the incorporation of polymers, such as polyethylene glycol (PEG), can extend the circulating half-life of protein therapeutics, thus decreasing the dosing frequency to obtain the desired clinical effect. For example, PEGylated Adynovate is used for the treatment of haemophilia A and has a half-life that is 1.4–1.5 fold longer than that of the non-PEGylated Prophylaxis, thus allowing for two doses per week instead of three.[5,6] Selective delivery of cytotoxic drugs to cancer cells can be achieved through coupling of the drug to an antibody. For example, the antibody–drug conjugate (ADC), ado-trastuzumab emtansine, is used for the treatment of breast cancer. In this ADC, the drug, maytansine, is conjugated to the trastuzumab antibody, which selectively targets HER2-overexpressing breast cancer cells.[7,8] Fluorescent labelling, using green fluorescent proteins (GFP), allows the otherwise difficult analysis and tracking of proteins by using fluorescence microscopy.[1,9,10] Indeed, from as early as the 1920s bioconjugates have had medical applications. Avery and Goebel reported the stimulation of an immune response in a non-immunogenic bacterial capsular polysaccharide upon conjugation to a protein carrier.[11] Later in 1987, this observation led to ProHIBIT®, the first conjugate vaccine for the treatment of *Haemophilus influenza* type b (Hib) coming to market.[5]

The complexity of biomolecules presents some challenges for the development of a bioconjugation process. Bioconjugation processes should be chemoselective so as to modify one amino acid residue of interest over others (e.g. only cysteine residues in the presence of lysine residues). Chemoselectivity is often challenging as the amino acids of interest are often surrounded by other functional groups such as amines, amides, carboxylic acids, alcohols and thiols, which can also be transformed under the reaction conditions. Bioconjugation processes should be regioselective. For example, one may want to transform a particular lysine residue in the presence of other lysine residues. Such site-selectivity leads to optimized function and greatly simplifies purification and characterization of the products.[4] Bioconjugation processes should be operational under biologically ambient conditions, i.e. aqueous media, near neutral pH (pH 6–8) and at low to ambient temperatures (≤ 37 °C), so as to prevent the denaturation of protein, thus preserving structure and function. Surfactants and salts, which are often needed for protein stability, should also be tolerated by the process.[1,12] Bioconjugation processes should be rapid. Ideally, full conversion of substrate should be achievable with reaction rates on the order of 1–1000 $M^{-1}s^{-1}$ and above.[4] This rapid reactivity would allow protein modification under dilute conditions if second-order kinetics apply where the rate depends on reactant concentration.[13,14] However, the use of organic solvents, heating beyond ambient temperature and prolonged reaction times can be acceptable in some cases, particularly for robust and structurally simple biomolecules such as certain oligosaccharides and peptides.[4]

1.1.2 Proteins

The primary building blocks of proteins are amino acids. There are over 300 naturally occurring amino acids, 20 of which are used in protein biosynthesis by the ribosome, the exact sequence of amino acids being encoded by RNA. These amino acids, specifically those with reactive functional groups, can be chemically or enzymatically modified, which are often referred to as posttranslational modifications (PTM). PTMs include the oxidation of peptidyl proline into 4-hydroxyproline (a major component of collagen) by the enzyme prolyl hydroxylase[15,16] and the formation of disulfide bonds between cysteine residues within proteins.[17] Amino acids are chemically linked by peptide bonds (amide bonds). The general amino acid structure consists of a tetrahedral α carbon atom with four substituents; a carboxyl group, an amino group, a hydrogen atom and a variable side chain. Isolated amino acids often occur as zwitterions at physiological pH (pH = 7.4) as they contain at least one carboxylic acid group (pK_a = 2–3) and at least one amino group (pK_a = 9–10), leading to the carboxylate and ammonium forms,

respectively. The overall charge is neutral. If the pH is lower than the pK_a value of the amino and carboxylic acid groups, they will exist in their protonated forms. If the pH is higher than the pK_a value of the amino and carboxylic acid groups, they will exist in their deprotonated forms. The pK_a value of the dissociable group is affected by its environment. A nonpolar environment raises the pK_a of a carboxyl group, which makes it a weaker acid, and lowers the pK_a of an amino group, which makes it a stronger acid. Therefore the pK_a of a functional group will vary depending on its location within a protein.[16] For example, the pK_a value of the active-site cysteine in glutaredoxin is 3.5.[18,19] Thioredoxin, from *Escherichia coli*, contains a cysteine residue with a pK_a value of 6.7.[20] The C-terminal active-site cysteine in protein disulfide isomerase (PDI), an endoplasmic reticulum enzyme, has a pK_a value greater than 10.[21] The properties associated with amino acids, such as acidity or basicity, and hydrophilicity or hydrophobicity depend on their side chain. Hydrophilic amino acids have polar/ionized side chains. Lysine and arginine are positively charged at neutral pH and glutamic acid and aspartic acid are negatively charged. Hydrophobic amino acids such as alanine and valine, have aliphatic side chains. Arginine is a basic amino acid. At neutral pH its guanidinium side chain (pK_a 12.48) is protonated. Aspartic acid is an acidic amino acid. At neutral pH its carboxylic acid side chain (pK_a 3.65) is negatively charged (Figure 1.1).[15]

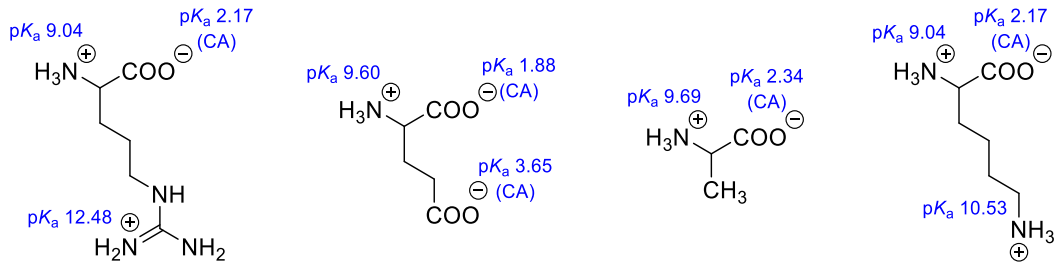

Figure 1.1: Basic and acidic amino acids, arginine and aspartic acid. Hydrophobic and hydrophilic amino acids alanine and lysine. CA = conjugate acid.

1.1.3 Cysteine

Of the 20 canonical amino acids, there are two that contain sulfur atoms—cysteine and methionine, which are the rarest of the amino acids. Cysteine accounts for 2.2%[22] and methionine accounts for 2.3% of all amino acid residues in human proteins.[23] This low abundance in proteins allows the opportunity for single-site protein modification.[12] Methionine contains a relatively unreactive thioether, whereas cysteine contains an ionisable thiol group, which is highly nucleophilic in the anionic thiolate form (Scheme 1.2).[24,25]

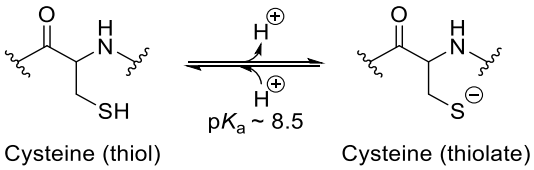

Scheme 1.2: Structure of cysteine residue within a protein with average pK_a value, which can vary depending on particular protein environment.

The determining factor for cysteine's nucleophilicity and reactivity is the pK_a value of its side chain. The pK_a value denotes the pH at which the thiolate and thiol populations are equal.[24] In an aqueous environment, the pK_a value of a free cysteine side chain is approximately 8.6, which is relatively acidic. In proteins, and as mentioned above, this value can range from 3.5 to 10 owing to the influence of environmental factors such as the nearby polar groups.[24–26] The thiol pK_a value can be lowered by certain neighbouring amino acid residues. It can be stabilized by protonated or positively charged amino acids but destabilized by negative charges. Wilson *et al*.[26] found that glutamic acid lowered the pK_a value of Cys106 in the Parkinsonism-associated protein DJ-1 (a protein that protects cells against oxidative stress) from 8.3 to 5.4 through a stabilizing interaction with the thiolate. In its thiolate form, cysteine is more reactive, acting as a nucleophile; the lower the pK_a value of cysteine thiol, the more likely it will be in the more reactive thiolate form.[27] The primary ammonium group of lysine residues typically have pK_a values that are higher than those of typical cysteine residues. Therefore, at physiological pH (pH 7.4) the side chain of lysine residues is largely protonated, thus being non nucleophilic. However, even at pH values where both the thiolate form of cysteine and the free amine form of lysine coexist, the thiolate is more nucleophilic, reacting faster than lysine with electrophiles, thus engendering selective modification of cysteine over lysine.[15] Brotzel and Mayr[26] investigated the nucleophilicity of amino acids such as cysteine. A nucleophilicity parameter (*N*) was calculated using the second-order rate constant for the reaction between cysteine and

benzhydrylium tetrafluoroborates in water at 20 °C. The dianion of cysteine has an *N* value of 23.43, which is the most nucleophilic of the canonical amino acids investigated. The *N* value for lysine was not given; however, the *N* value for 3-amino propanoic acid, which is similar in structure to lysine, is 13.26. From second-order rate constants, the thiolate of cysteine was found to be approximately 6000 times more reactive than the α-amino group of alanine and 4000 times more reactive than 3-amino propanoic acid. The nucleophilicity parameter is defined by the correlation: $\log k_{20\ °C} = s(N+E)$, where k is the second-order rate constant in $M^{-1}s^{-1}$, s is the nucleophile-specific slope parameter and E is the electrophilicity parameter.[26] Its high nucleophilicity allows for more facile, selective reactions with electrophiles, thereby making cysteine one of the more favoured amino acids for selective modification.[24,25]

1.1.4 Direct Chemical Modification of Cysteine

Because of its desirable physiochemical properties, as described above, cysteine is the most commonly targeted amino acid residue for transformation. A selection of the most common transformations of cysteine are described below.

1.1.4.1 α-Halocarbonyl Compounds

α-Halocarbonyl electrophiles are widely used for cysteine modification. Goddard and Michaelis first reported iodoacetamides for the modification of keratins. Keratins have a high percentage of disulfides (10–15%). These disulfides were reduced with alkaline thioglycolate to the corresponding thiol, substituted with iodoacetamides and the new properties of the substituted protein studied.[28,29] Iodo analogues are typically used for this transformation as iodide is a better leaving group compared with the other halogens, thus leading to high conjugation reaction rates. These transformations are typically conducted at physiological pH (pH 7.2–9.0) and away from light, thus limiting the generation of I_2 through the oxidation of the iodide ion,[28,30] which can react with other amino acid residues such as tryptophan and histidine. This reaction is selective for thiols at pH 8.3. Less reactive chloroacetamides are also used as the iodoacetyl group can slowly react with free amino groups, the thioether group of methionine, and the nitrogen atoms of the histidine imidazole when the pH is above 7.[28]

Davis and Flitsch[31] developed a method for selectively glycosylating proteins at one or more sites. Acetyl-protected amino-*N*-acetylglucosamine **1** was coupled with iodoacetic acid in a condensation reaction using 2-ethoxy-1-ethoxycarbonyl-1,2-dihydroquinoline (EEDQ) and then deprotected using sodium methoxide to give iodoacetamide **2**. The free cysteine of bovine

serum albumin (BSA) protein **3** was selectively alkylated with glycosylated iodoacetamide **2** at pH 8, leading to a glycosylated lysine derivative **4**, containing the unnatural, yet non-imposing thioether linkage (Scheme 1.3).[31]

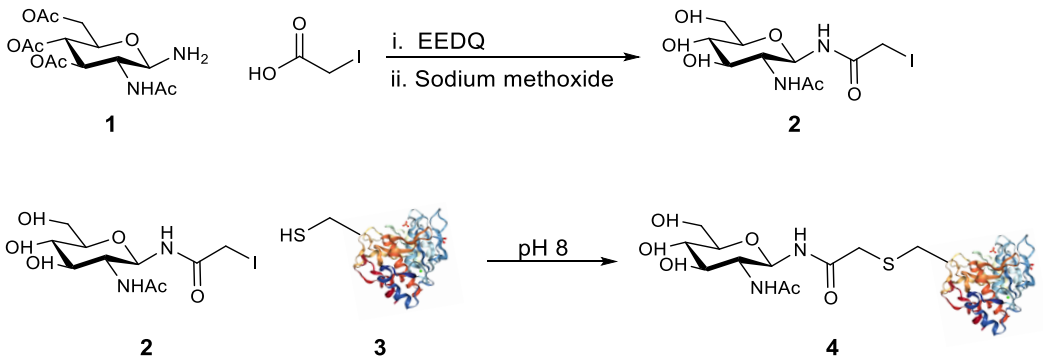

Scheme 1.3: Selective glycosylation of cysteine in BSA protein using an iodoacetamide.

Raftery and Cole reported the aminoethylation of cysteine of insulin B chain (isolated as thiosulfonate) with β-bromo-ethylenimine at pH 8.6 to give a lysine mimic, aminoethyl insulin B. The aminoethyl cysteine was cleaved by hydrolysis using trypsin, which is a lysine-directed protease (Scheme 1.4).[32] Aminoethyl-cysteine is chemically and structurally similar to lysine. The acidity of the ammonium protons is slightly increased due to the electron-withdrawing effect of the thioether (− 1.1 pK_a unit). When the lysine γ-methylene is substituted with a sulfur atom, the length of the side chain increases slightly (~ 0.28 Å).[33]

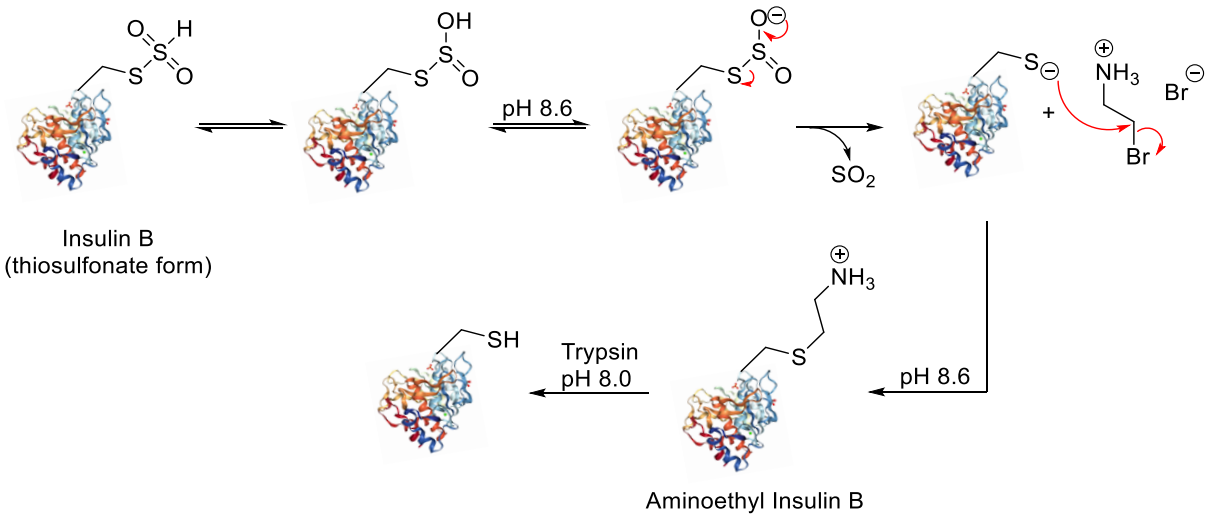

Scheme 1.4: Aminoethylation of Insulin B.

1.1.4.2 Maleimides

Maleimides (maleic acid imides) exhibit high selectivity for reaction with cysteines/thiolates in proteins. The high electrophilicity of the alkene within the maleimide structure comes from the conjugation with the electron-withdrawing carbonyl groups and its strained structure. These structural characteristics decrease the energy of the alkene lowest unoccupied molecular orbital (LUMO), the π* orbital, thus leading to a faster reaction between the electrophile and nucleophile.[34–36] Unlike iodoacetamides, maleimides do not react with histidine or methionine. Conjugation with maleimides is typically carried out at pH 6.5–7.5 so as to prevent the side reaction with amines, which can react at higher pH values.[28,37] Mantovani *et al.* reported the conjugation of BSA protein **5** to α-maleimide polyethylene glycol (PEG)-terminated polymer **6** at pH 7.4 (Scheme 1.5).[28,38]

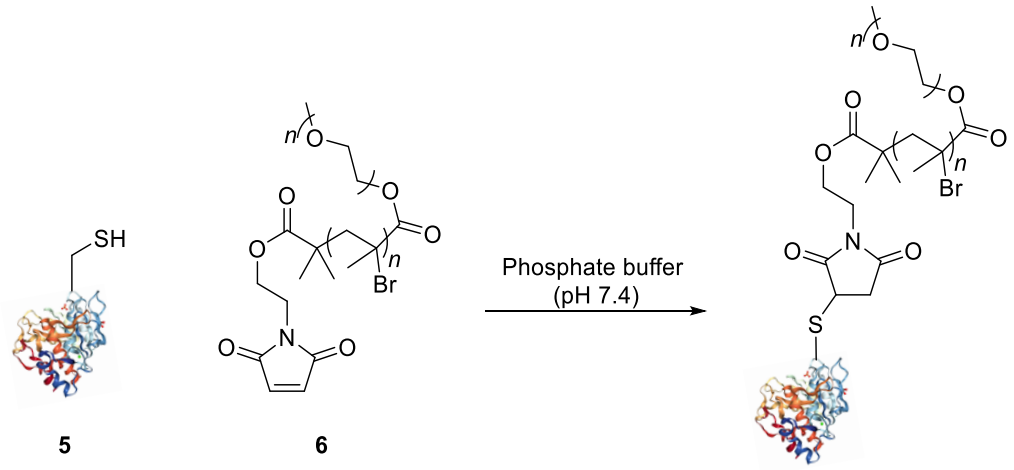

5 6

Scheme 1.5: Conjugation of BSA protein to polyethylene glycol (PEG)-terminated polymers by an α-maleimide.[31]

The stability of the maleimide adduct makes the regeneration of the unmodified protein difficult, a process that requires strongly basic conditions and high amounts of imidazole. Smith *et al.* introduced monobromomaleimide derivatives, which underwent conjugative addition with the cysteine thiol of the growth factor receptor-bound protein (Grb2) SH2 domain (L111C) **7** at pH 8. Addition of tris(2-carboxyethyl)-phosphine (TCEP) allowed 85% conversion back to the original protein **7** (Scheme 1.6), thus demonstrating the reversible modification of cysteine residues by bromomaleimides. Protein–maleimide conjugate **8** also underwent a thiol conjugate addition with glutathione, thus giving access to protein–peptide conjugate **9** with 95% conversion.[39]

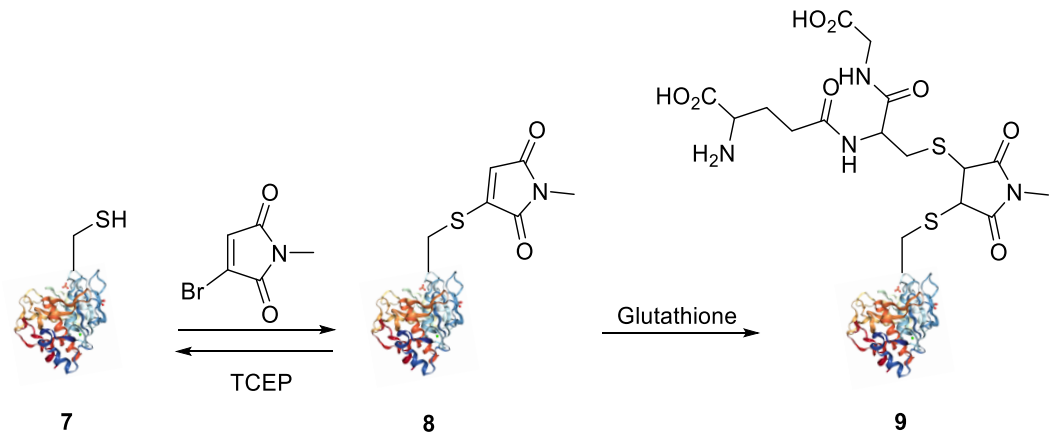

Scheme 1.6: Modification of the Grb2 SH2 domain (L111C) protein with N-methylbromomaleimide followed by TCEP cleavage or further conjugation with glutathione.[31]

1.1.4.3 Disulfide Exchange

Diverse disulfides have been used for cysteine modification by disulfide exchange. Attack of the cysteine thiolate at one of the sulfur atoms of the disulfide bond breaks the S–S bond, leading to the formation of a new mixed disulfide. Steiner *et al.*[31] prepared a disulfide-linked antibody–drug conjugate. Antibodies linked by C-terminal disulfide bridges **10** were reduced using TCEP forming one free cysteine per monomer **11**. The free cysteine can act as a nucleophile when exposed to either Ellman's reagent (5,5′-dithiobis-(2-nitrobenzoic acid), DTNB) or phenylselenyl bromide. Addition of the cytotoxic thiol analogue of the drug cemadotin forms the homogeneous mixed disulfide-linked antibody–drug conjugate **12**. The free cysteine can also act as a nucleophile upon addition of a disulfide pyridyl cemadotin analogue yielding mixed disulfide **12** (Scheme 1.7).

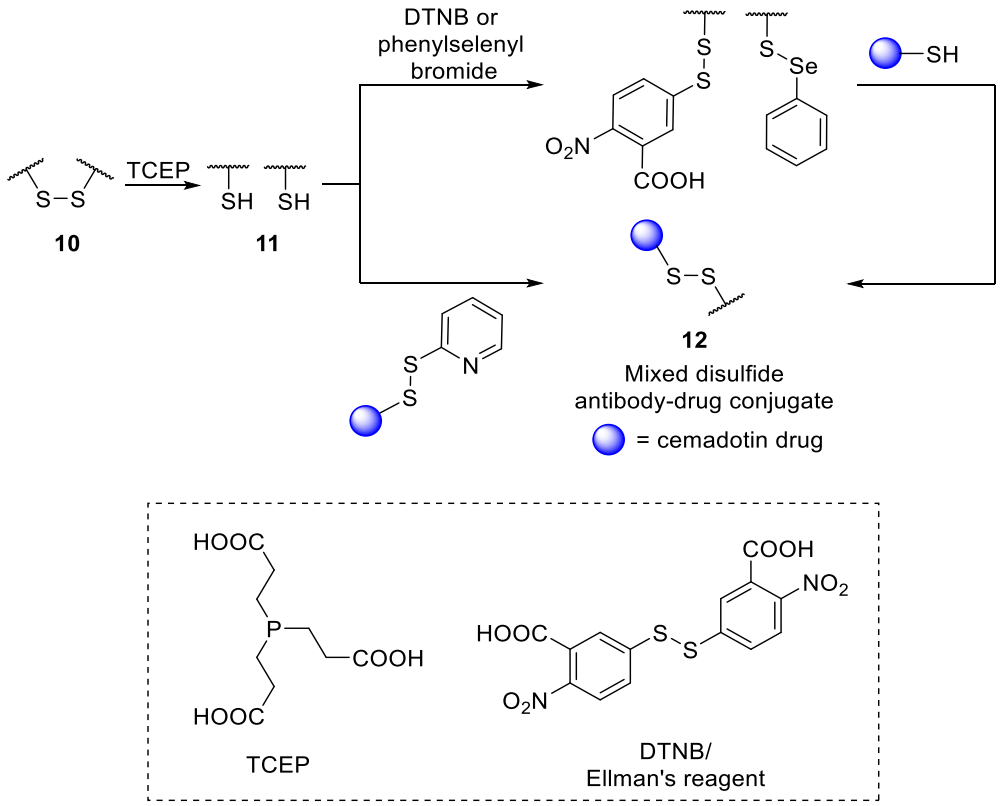

Scheme 1.7: Generation of mixed disulfide antibody–drug conjugates through electrophilic and nucleophilic approaches.[31]

Both conjugation reactions were rapid (minutes) and proceeded with high conversion (> 95%). The driving force of this reaction is the low pK_a value of the aromatic thiol, thus preventing the competing formation of the symmetrical disulfide.[40]

1.1.5 Transformation of Cysteine into Other Functional Groups for Subsequent Bioconjugation

More selective methods for cysteine modification have recently been described. The incorporation of bioorthogonal functional groups not naturally present in proteins allows new reactions that cannot proceed with natural amino acids. In addition, these functional groups should not interfere with the biological environment. The "tag-and-modify" strategy is one such method. This approach allows the installation of a reactive group, which can be either a natural or an unnatural amino acid residue (the "tag"), followed by selective modification.[9] There are many methods available for the introduction of "tags" onto proteins, some of which are described below.[41]

1.1.5.1 Dehydroalanine

Through the formal elimination of dihydrogen sulfide (H_2S), nucleophilic cysteine is transformed into electrophilic dehydroalanine, which can then undergo reaction with nucleophiles (Scheme 1.8). The dehydroalanine moiety can be installed through methods such as oxidative elimination or dialkylation–elimination.[28]

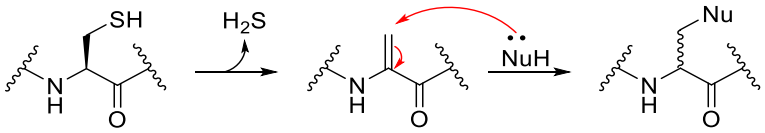

Scheme 1.8: Transformation of cysteine into dehydroalanine, followed by reaction with a nucleophile.[31]

Oxidative elimination of a thiolate using *o*-mesitylenesulfonylhydroxylamine (MSH) as an oxidizing agent has been used to rapidly convert the cysteine residue of protein mutant S156C SBL **13** into dehydroalanine **14** by oxidative elimination under basic conditions (Scheme 1.9).[28,42,43]

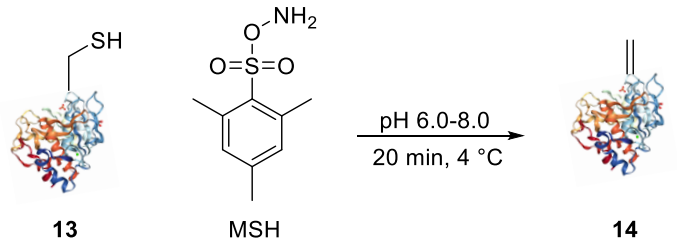

Scheme 1.9: Conjugation of cysteine residue of the protein mutant S156C SBL with MSH.[43]

Recently, Chalker *et al.*[42] reported a general method for the conversion of cysteine into dehydroalanine in a dialkylation–elimination reaction. α,α′-Dibromoadipyl(bis)amide (DBAA) was used under mild reaction conditions (pH 7–8, 37 °C) and high yields were reported. A single cysteine mutant of the protein subtilisin from *Bacillus lentus* (SBL-S156C) **15** was used as a protein substrate. The thiol moiety was alkylated with DBAA at room temperature. Ring-forming dialkylation followed by elimination was carried out at 37 °C and Ellman's assay confirmed the conversion of cysteine to dehydroalanine **16**. The dehydroalanine moiety **16** was then reacted with 2-mercaptoethanol at pH 8 (Scheme 1.10).[28,42]

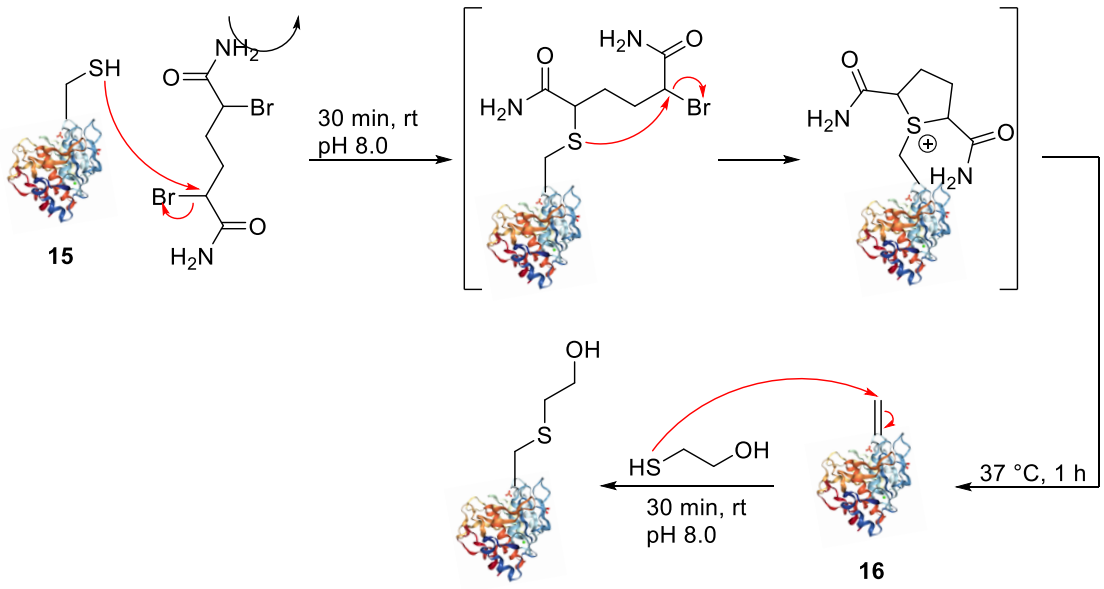

Scheme 1.10: Dehydroalanine-mediated conjugation of 2-mercaptoethanol with SBL-S156C containing a single cysteine residue.[42]

1.1.6 Incorporating Aldehydes into Proteins

One common drawback with the types of methodology described above is the difficulty in obtaining site-selectivity when more than one amino acid (cysteine) side chain is present in the protein. Recent strategies have focused on the incorporation of functional groups that are not naturally found in proteins. The protein is then subjected to a substrate that specifically reacts with the non-natural moiety on the protein without interacting with any other functional group on the protein, thus allowing the generation of homogenously modified proteins. The aldehyde functional group is rarely found within proteins (see below). Upon installation of this reactive carbonyl moiety, it is possible to carry out reactions that are specific to aldehydes, thus facilitating site-selective labelling of proteins. There are both chemical and enzymatic methods available for introducing an aldehyde functional group into a protein and there are also a growing number of aldehyde-based ligation protocols to choose from.[44]

1.1.6.1 Chemical Strategies for the Incorporation of Aldehydes

Aldehydes can be inserted into a protein through chemical methods. The oxidative cleavage of β-amino alcohol residues, namely, serine **17** and threonine **18**, that are located at the N-terminus of a peptide/protein can be achieved by using sodium periodate, as reported by Stroh *et al.*[45] (Scheme 1.11). The transformation leads to a highly reactive N-terminal α-oxo aldehyde **19**. This reaction has the advantage of being partially selective as the oxidation of β-amino alcohols

is 100–1000 times faster than that of vicinal diols (1,2-diol), which can be found in carbohydrates. However, under these oxidative conditions, other amino acids such as methionine and cysteine can also undergo oxidation.[45,46] An excess of ethylene glycol is commonly used to quench excess reagent and the oxidized protein is then purified.[46,47]

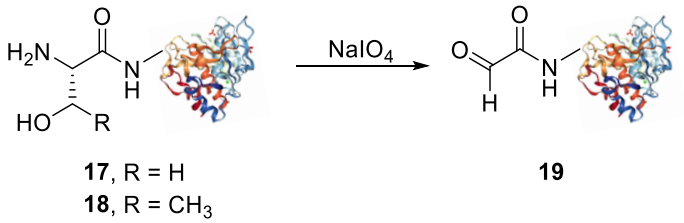

Scheme 1.11: Sodium periodate mediated oxidation of serine and threonine.[46]

Gilmore *et al.*[48] developed a pyridoxal-5-phosphate (PLP) mediated oxidation, which selectively oxidized N-terminal amino groups of proteins into aldehydes or ketones (Scheme 1.12). A variety of proteins and peptides bearing different amino acids at the N-terminus were used. For example, N-terminal glycine residue of horse heart myoglobin protein **20** was oxidized to glyoxylamide **22** under mild conditions (37 °C, pH 6.5) with 90% conversion. Condensation between the amino group of the glycine residue and the aldehyde of PLP forms imine **21**. This imine contains an α proton with a lower pK_a value (versus a non-terminal imine), which allows tautomerization to occur. Hydrolysis of the imine forms N-terminal aldehyde **22**.[46,48]

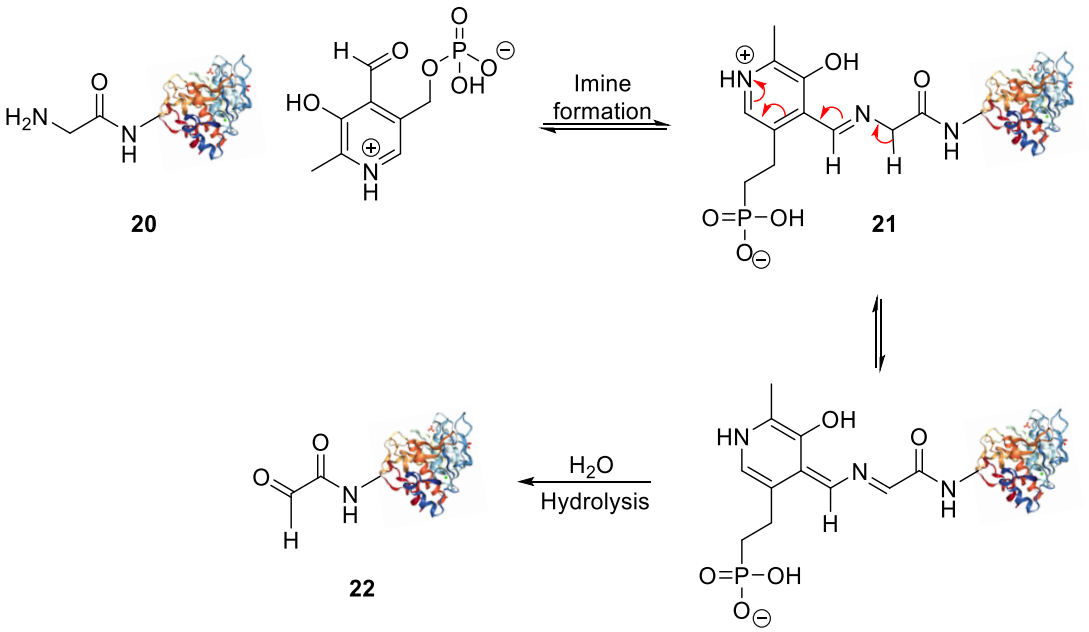

Scheme 1.12: Oxidation using pyridoxal-5-phosphate (PLP).[46]

1.1.6.2 Enzymatic Strategies for the Incorporation of Aldehydes

Enzymatic strategies have been used to install the aldehyde moiety. The aldehyde-containing amino acid residue formylglycine (fGly) is formed through the enzymatic oxidation/hydrolysis of cysteine residues, which are located within the consensus sequence of CxPxR (x being any amino acid). This conversion of a thiol into an aldehyde is achieved by using the formylglycine-generating enzyme (FGE, Scheme 1.13).

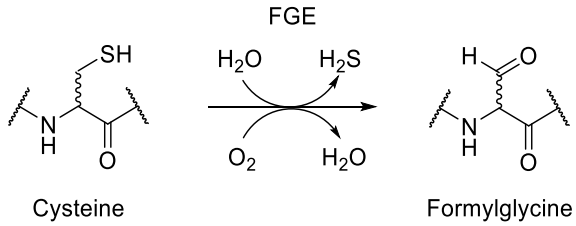

Scheme 1.13: Formylglycine-generating enzyme (FGE) mediated conversion of cysteine into formylglycine.

In nature, the enzyme, FGE, is essential for the activity of sulfatase enzymes. FGE installs the catalytic fGly residue in the active site of sulfatase enzymes and this residue is responsible for sulfate ester hydrolysis. Boltes *et al.*[49] proposed a mechanism for sulfate ester hydrolysis (Scheme 1.14). The fGly is in the hydrated geminal diol form **23**, which is its predominate resting state. A divalent cation, Ca^{2+} or Mg^{2+} is present in the active site of type I sulfatases and helps to bind and polarize the substrate. An aspartate residue hydrogen bonds with one of the hydroxy groups of fGly geminal diol **23** and the other hydroxy group hydrogen bonds with a histidine nitrogen atom. The fGly geminal diol **23** nucleophilically attacks the sulfur of sulfatase ester substrate **24**, which is stabilized by hydrogen bonding with lysine and histidine residues, forming sulfoenzyme intermediate **25** and alcohol. There are two pathways by which desulfation can occur: histidine-catalysed elimination (E2) from fGly geminal diol complex **25a** or hydrolysis of complex **25b** through an S_N2 substitution at the sulfur atom. Both of these pathways lead to the breakdown of sulfoenzyme intermediate **25** by cleavage of the S-O ester bond and release of sulfate **26** or hydrogen sulfate **27**. Aldehyde **28** is regenerated and is hydrated back to its geminal diol resting state **23** (Scheme 1.14).[50]

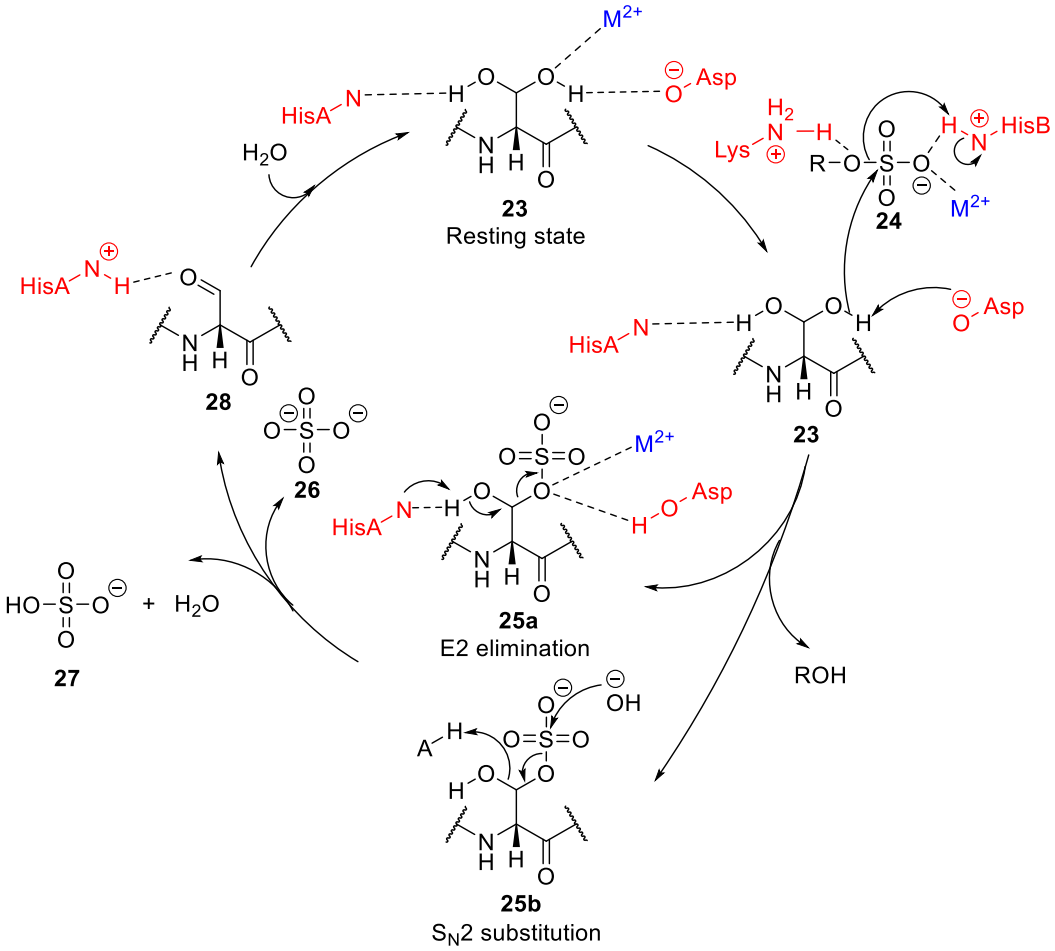

Scheme 1.14: Sulfate ester hydrolysis by sulfatases.[50]

In 2019 Appel *et al.*[51] proposed a mechanism for the conversion of cysteine into fGly by FGE (Scheme 1.15). The FGE active site cysteine 277 and cysteine 272 are coordinated to Cu(I) **29**. The cysteine substrate binds to the Cu(I) forming a three-coordinate complex **30**. Oxidation of Cu(I) to Cu(II) with O_2 forms peroxy radical **31**, which abstracts a hydrogen atom from the attached substrate, thus forming a carbon-centred radical of substrate **32**, which fragments to give thioaldehyde **33** with reduction of Cu(II) to Cu(I). Hydrolysis of thioaldehyde **33** gives fGly product **34**. The resulting hydroperoxy metal species **35** undergoes a two-electron reduction to return to its resting Cu(I) state **29** (Scheme 1.15).

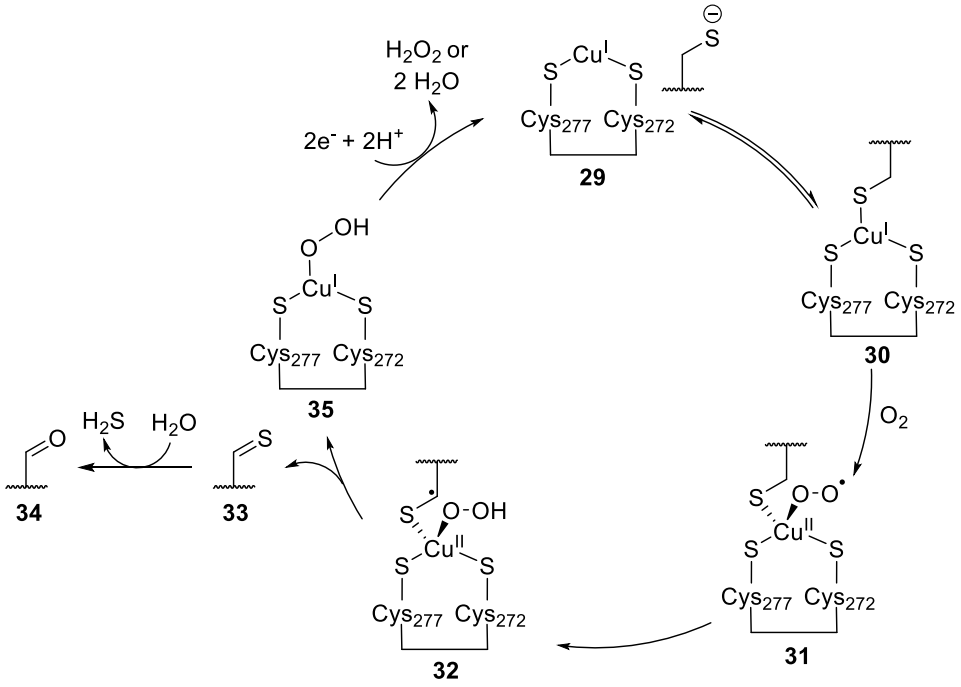

Scheme 1.15: Mechanism for the conversion of cysteine into fGly by FGE.[51]

Beyond its role in the sulfatase active site, the electrophilic aldehyde moiety of the fGly residue is a useful handle for bioconjugation. However, fGly must first be installed in the protein of interest.[52] The insertion of nucleotides into the gene of interest allows the genetic encoding of the five-amino acid sequence, CXPXR (where X is often serine, threonine, alanine, leucine or glycine). This short amino acid sequence is recognized by FGE.[53,54] Co-expression of this protein with the CXPXR sequence and FGE allows selective oxidation of the cysteine residue within the sequence into fGly.[53] Once the aldehyde moiety has been installed on a target protein it can then be used as a bioconjugation handle in a variety of site-selective chemical modifications and some examples are given below.

1.1.7 Chemical Strategies for Protein Modification with Aldehyde Handles

1.1.7.1 Hydrazone/Oxime Ligations

One of the most established ligation reactions involving aldehydes is the formation of hydrazones and oximes through condensation reactions with hydrazines and hydroxylamine/aminooxy reagents, respectively (Scheme 1.16).[45,46,48]

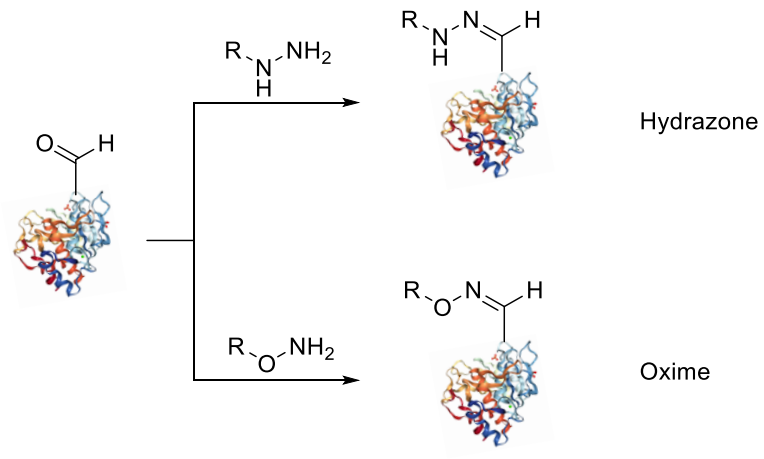

Scheme 1.16: Hydrazone and oxime ligations.

Carbohydrates have been incorporated into proteins through oxime ligation.[46,55,56] Antibody–drug conjugates with either hydrazine or oxime linkages have been reported.[46,57,58] However, there are some drawbacks associated with use of this type bioconjugate linkage. The resulting C=N bond is susceptible to hydrolysis. As hydrazones are more susceptible to hydrolysis,[28,46] they can be converted into a more stable hydrazine through a reduction protocol.[46,59] Furthermore, the optimum pH value for carrying out these ligation reactions is 4.5. At neutral pH, poor reactivity and long reaction times are observed (rate constants of 10^{-3} M^{-1} s^{-1}).[13,60] However, the use of nucleophilic catalysts, such as aniline, can allow efficient condensation at neutral pH values. Inspired by the work of Cordes and Jencks,[61] Dirksen *et al.*[62] ligated two unprotected peptides, glyoxylyl-LYRAG **36** and aminooxy-acetyl-GRGDSGG **37** (Scheme 1.17) in the absence and presence of a *p*-methoxyaniline catalyst. The uncatalyzed ligation was carried out at pH 7. The concentration of the reactive electrophile, the protonated carbonyl group, is very low at pH 7.0 (pK_a −4 to −10). Glyoxylyl-LYRAG peptide **36** undergoes a condensation reaction with the primary amine (pK_a 4.6) of aminooxy-acetyl-GRGDSGG peptide **37** to form oxime **39**. The observed half-time of this reaction (i.e. the time that is required for 50% conversion) was 7.6 days and the rate constant was 0.0015 M^{-1} s^{-1} with an overall yield of 30%.

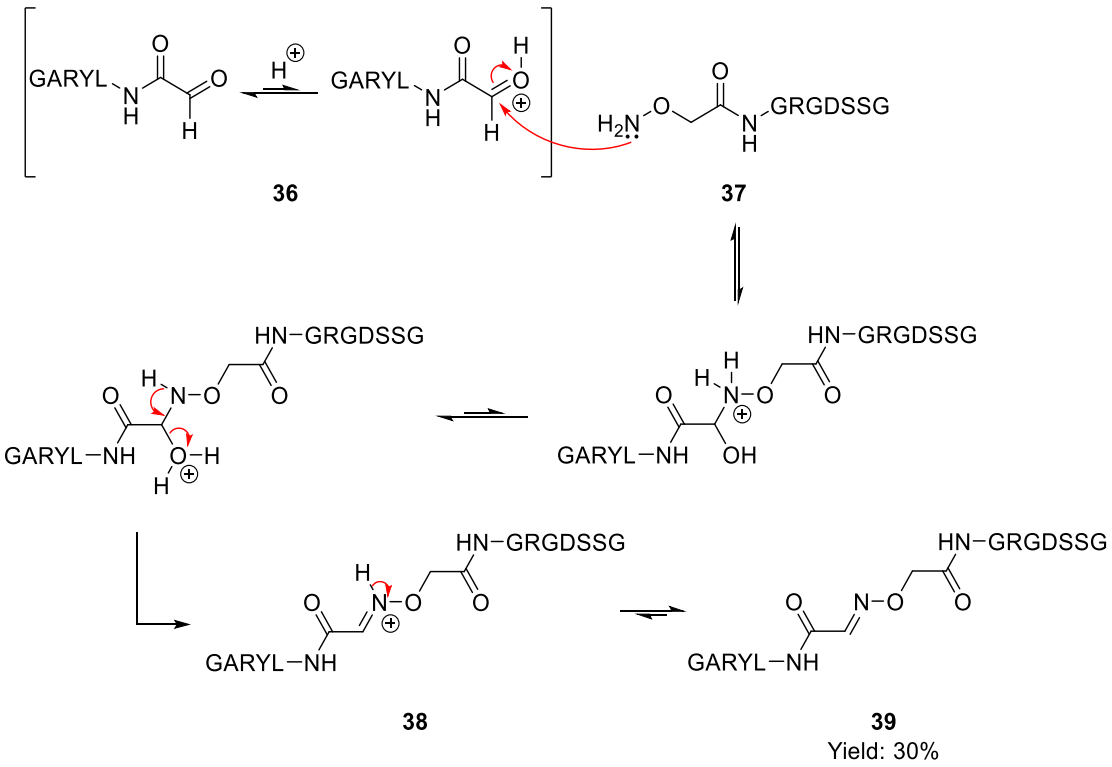

Scheme 1.17: Ligation of peptides glyoxylyl-LYRAG and aminooxy-acetyl-GRGDSGG without aniline catalyst.

In the presence of 100 mM *p*-methoxyaniline as catalyst at pH 7, the half-time was observed to be 280 min and the rate constant was 0.061 $M^{-1} s^{-1}$. The yield was 94% (Scheme 1.18). The rate enhancement was attributed to the generation of a high concentration of the reactive electrophile, protonated aniline imine **40** compared with the low concentration of the reactive electrophile **36** (protonated carbonyl (pK_a −4 to −10), Scheme 1.17) in the uncatalyzed ligation. Rapid transamination of protonated aniline imine **40** with the hydroxyamine **37** leads to oxime **39**, regenerating the *p*-methoxyaniline catalyst (Scheme 1.18).[62]

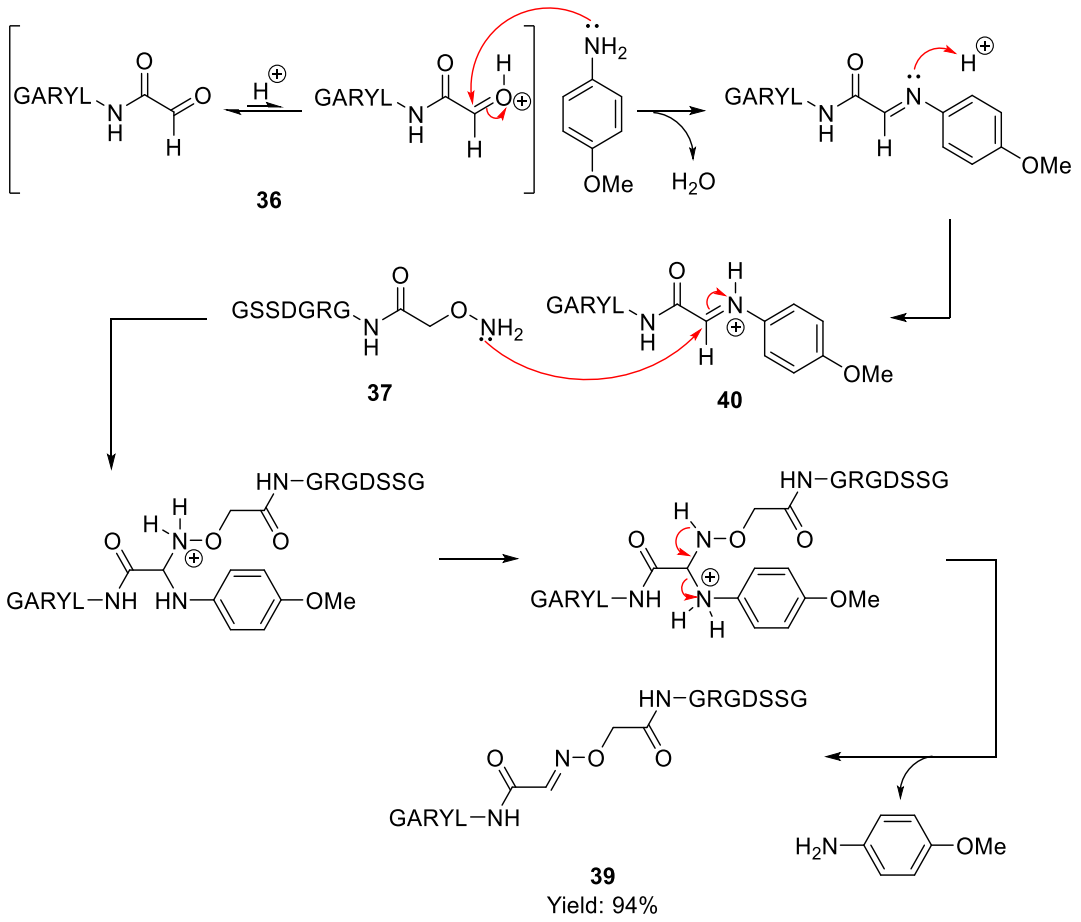

Scheme 1.18: *p*-Methoxyaniline catalysed oxime ligation.

1.1.7.2 Pictet–Spengler Reactions of Proteinaceous Aldehydes

The Pictet–Spengler transformation is a cyclization reaction involving tryptamines and aldehydes where an initially-formed iminium intermediate undergoes an intramolecular cyclization. Sasaki *et al.*[54] applied this approach for the labelling of N-terminal of horse heart myoglobin protein **41**. This protein is a 153 amino acid residue heme-binding protein with an N-terminal glycine. The N-terminal glycine residue was first converted into α-keto aldehyde **42** by transamination using pyridoxal-5-phosphate. This transformation was followed by the Pictet–Spengler reaction with tryptamine (3-(2-aminoethyl)indole) **43**, which is the preferred electron-rich substrate for Pictet–Spengler reactions under mild conditions (pH 6.5, 37 °C, 18 h) (Scheme 1.19). This approach can be applied generally to recombinant proteins and is not restricted to myoglobin containing a N-terminal glycine residue.[63]

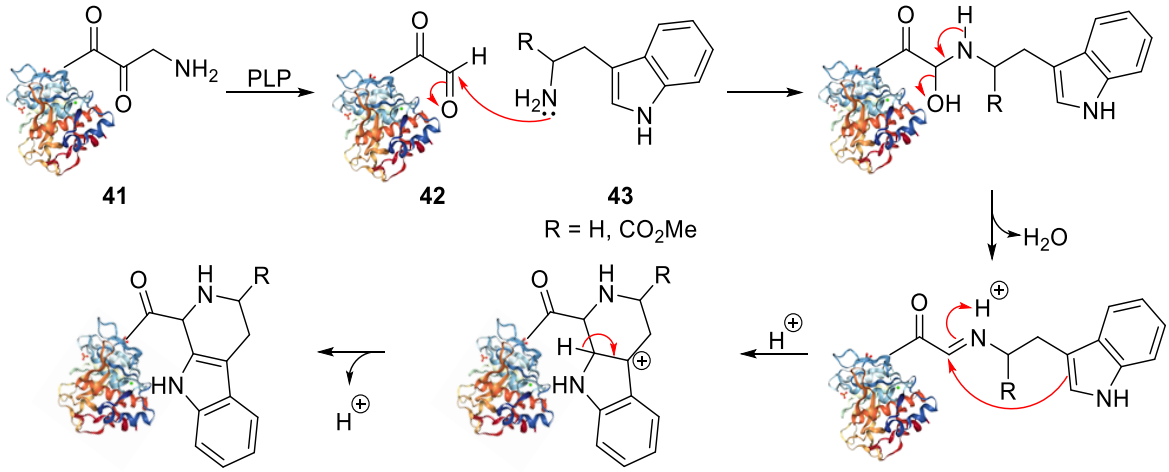

Scheme 1.19: Pictet–Spengler mediated coupling of tryptamine with horse heart myoglobin.

The Pictet–Spengler ligation strategy has been applied to the development of antibody–drug conjugates. The antibiotic natural product, maytansine **44**, was linked to the anti-Her2 antibody, trastuzumab **45**, through a Pictet–Spengler reaction (Scheme 1.20). The fGly handle was installed on trastuzumab through FGE (see Section 1.1.6.2), thus enabling site selectivity and drug conjugation.[50]

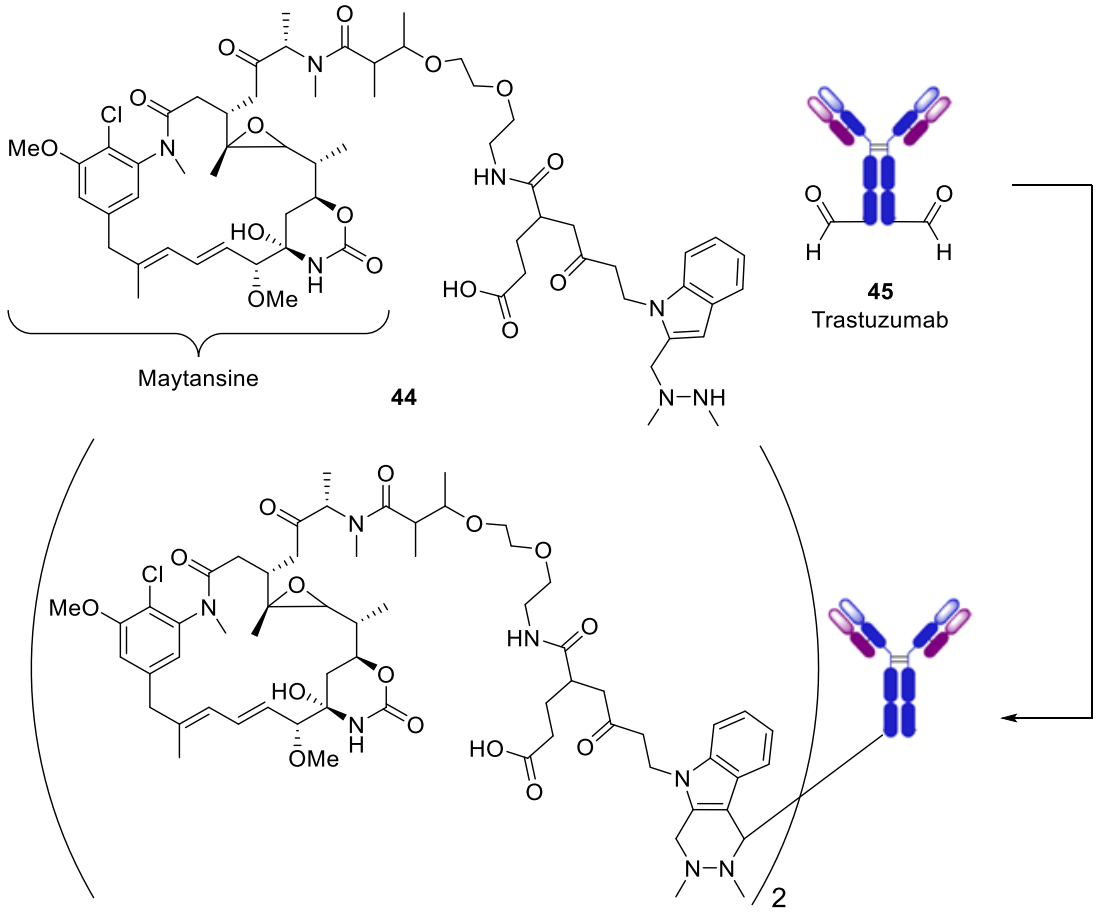

Scheme 1.20: Pictet–Spengler mediated coupling of maytansine and trastuzumab.[50]

1.1.8 Project Background

In the 1970s, Clark and Lowe[64,65] carried out the photochemical conversion of the thiol group of cysteine into a hydroxy group, thus converting cysteine into serine. The active site cysteine residue of the enzyme, papain **46**, was selectively alkylated with the phenacyl bromide, 2-bromo-2′,4′-dimethoxyacetophenone **47**. It was proposed that photolysis (λ > 320 nm) of alkylated enzyme **48** in aqueous solution at pH 7.4 allowed a Norrish Type II cleavage to thioaldehyde intermediate **49**. Hydrolysis of intermediate **49** with loss of hydrogen sulfide generated the corresponding aldehyde (formyl glycine) **50**. Reduction of aldehyde **50** to a hydroxy group with sodium borohydride gave the serine residue **51**, which was confirmed by amino acid analysis (Scheme 1.21).

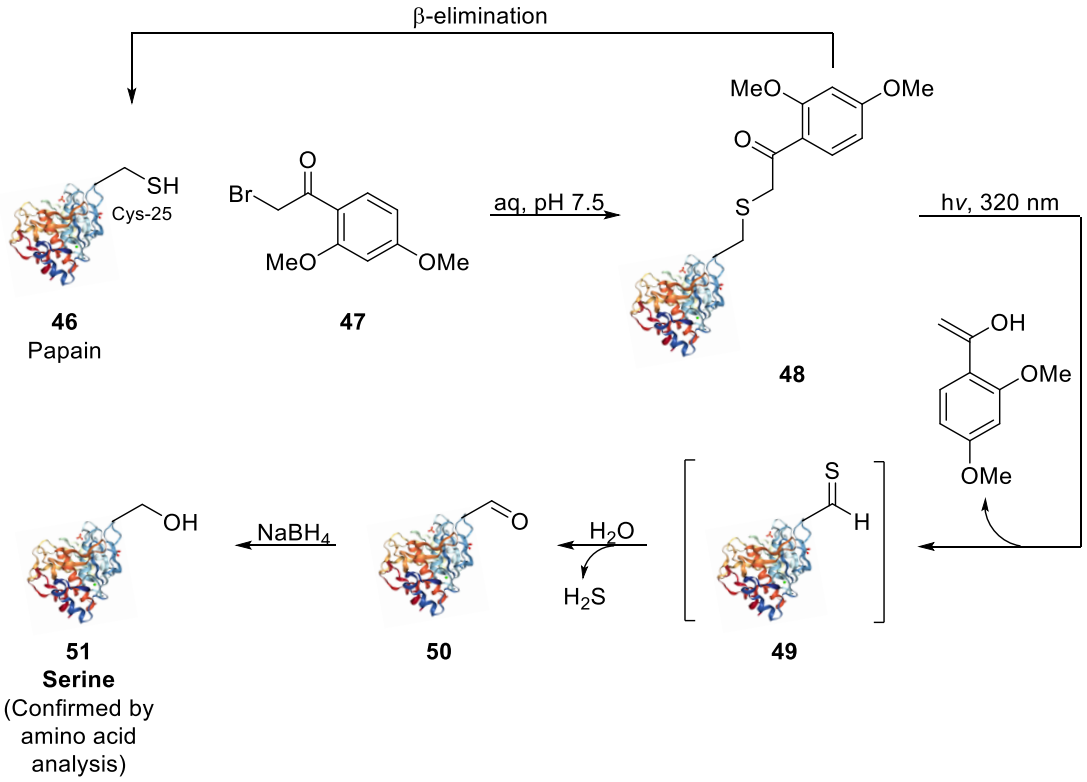

Scheme 1.21: Alkylation of Cys-25 residue, located in the active site of papain, with 2-bromo-2′,4′-dimethoxyacetophenone followed by photolysis to the thioaldehyde. Hydrolysis of the thioaldehyde generated the corresponding aldehyde, followed by reduction to serine.[64]

The photolysis of alkylated enzyme **48** resulted in the regeneration of 76% of native protein **46**. Therefore, the alkylation/photolysis cycle needed to be repeated three times to obtain high conversion into modified protein **50**. Regeneration of native enzyme **46** was likely favoured due to the steric restriction associated with the alkylated cysteine residue of enzyme **48**, which

could make the desired conformation for the Norrish type II cleavage unfavourable. The more favourable β-elimination to directly cleave the C–S bond between the phenacyl group and the sulfur atom would produce a thiyl and ketyl radical. Hydrogen abstraction by the thiyl radical would lead to regeneration of native enzyme **46**. After the final photolysis, suspected product **50** was purified by chromatography using an affinity column of sepharose-aminocaproyl-glycyl-L-phenylalanyl-L-arginine with a 20 mM ethylenediaminetetra-acetic acid (EDTA) and water gradient. Reduction of purified protein **50** was carried out using sodium borohydride. Reduction product protein **51** was purified using the same affinity column and method and was confirmed by amino acid analysis to contain a serine residue.

The reduction was also performed using sodium boro[^{3}H]hydride after purification by chromatography. The reduction was followed by hydrolysis of the [^{3}H]-labelled protein. Radioactivity was only evident in the amino acid analyser fractions containing serine. When the reduction using sodium boro[^{3}H]hydride was carried out immediately after the three cycles of alkylation/photolysis, the hydrolysed and purified protein products contained [^{3}H]-cysteic acid (derived from [^{3}H]-cysteine, Scheme 1.22) and [^{3}H]-serine, thus providing supporting evidence that the initial photolysis product was thioaldehyde **49**, which then slowly undergoes hydrolysis to aldehyde **50**.

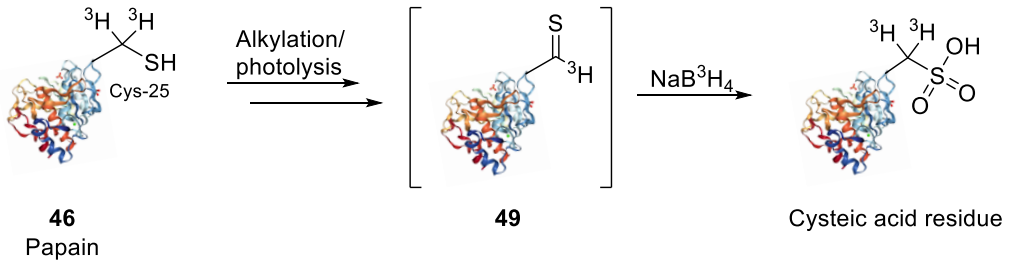

Scheme 1.22: Detection of [^{3}H]-cysteic acid residue after sodium boro[^{3}H]hydride reduction.

Since Clark and Lowe's work on the conversion of cysteine into serine[64,65] *via* a thioaldehyde, there has been no other reports, to our knowledge, of the use of this approach for the chemical modification of proteins or the development of a more efficient process.

1.2 Aims and Objectives

This chapter is focused on the design of a reagent that will allow rapid and selective photoinitiated oxidative transformation of the thiol group of a cysteine residue into alternative functional groups, such as an aldehyde or a thioaldehyde, which can be used for bioconjugation. This investigation would attempt to build upon Clark and Lowe's inefficient photochemical conversion of cysteine into serine. Furthermore, given the current use of the enzyme, FGE, as a protein engineering tool for the oxidative transformation of the thiol group of cysteine (within a specific amino acid sequence) into an electrophilic aldehyde, this photochemical transformation would allow a bioconjugation handle (aldehyde or thioaldehyde) to be generated without the requirement for a specific amino sequence or extensive protein engineering. A cysteine-based model peptide, which mimics a cysteine residue embedded within a protein or peptide and presents a free thiol moiety, will first be prepared. Alkylation of this cysteine residue with a range of phenacyl halides will generate a library of phenacyl sulfides. Exposure of these phenacyl sulfides to UV light should induce a Norrish Type II fragmentation, thereby generating a thioaldehyde (Scheme 1.23), which could then undergo hydrolysis to the aldehyde.[66]

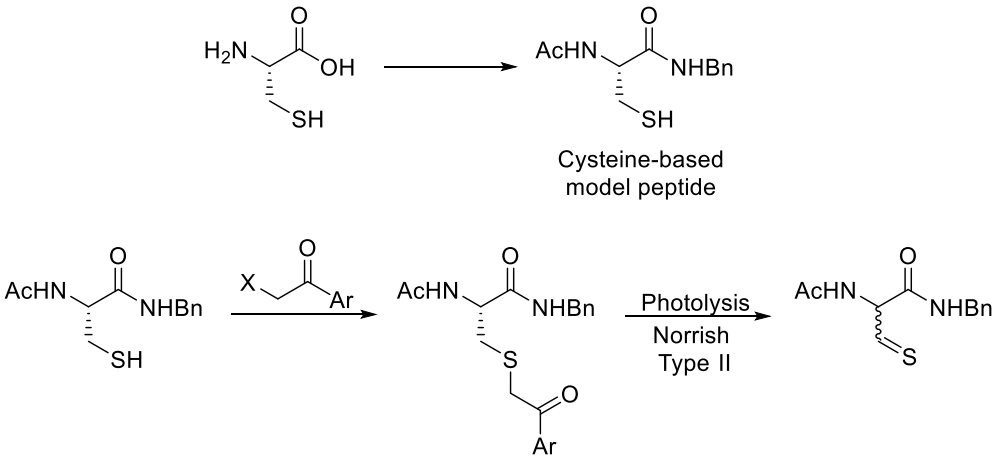

Scheme 1.23: Light-mediated transformation of the thiol group of cysteine into a thioaldehyde group by using a phenacyl halide reagent.

1.3 Results and Discussion

1.3.1 Preparation of Cysteine-Based Peptide Model

The cysteine derivative was prepared by following a literature procedure reported by Zheng *et al*.[67] Chloride-to-tosylate anion exchange of cysteine hydrochloride monohydrate **52** was first carried out to prepare a more soluble derivative for tritylation of the thiol moiety, a process that requires organic solvents. A solution of L-cysteine hydrochloride monohydrate **52** in dilute aqueous HCl was treated with *p*-toluenesulfonic acid, leading to precipitation of the cysteine *p*-toluenesulfonate salt **53**, which was isolated in 77% yield (Scheme 1.24).

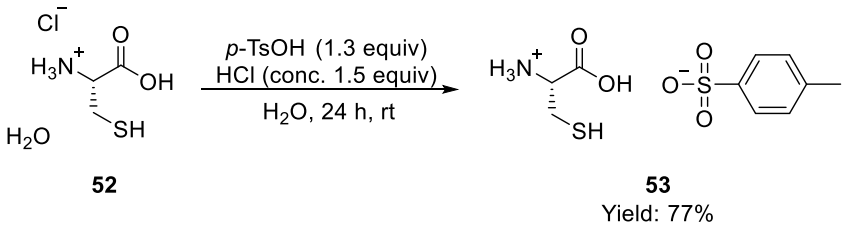

52 **53**
Yield: 77%

Scheme 1.24: Anion exchange of L-cysteine hydrochloride monohydrate.

Tritylation of the thiol group of L-cysteine toluenesulfonate salt **53** was carried out by treating an anhydrous DMF solution of salt **53** with trityl chloride. After 48 h, aqueous sodium acetate (10%) was added and the precipitated trityl-protected cysteine **54** was collected by filtration. The filtrate was washed with diethyl ether to remove the triphenylmethanol by-product, which may have derived from residual water present in the DMF, giving *S*-(triphenylmethyl)cysteine **54** in 87% yield (Scheme 1.25).

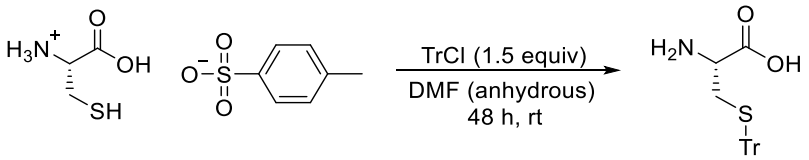

53 **54**
Yield: 87%

Scheme 1.25: Tritylation of L-cysteine toluenesulfonate salt.

The free amine was converted into the acetamide under Schotten–Baumann conditions. Aqueous NaOH (4 M) was added dropwise to a solution of **54** in 1,4-dioxane and water until the pH reached 9–10. Acetic anhydride was added slowly at 0 °C along with concomitant addition of aqueous NaOH (4 M) to maintain the pH range of 9–10. The reaction mixture was stirred for 12 h at room temperature and then acidified with aqueous HCl (2 M) to pH 6.

Evaporation of the solvent followed by purification by column chromatography gave the *N*-acetyl-*S*-(triphenylmethyl)cysteine product **55** in 97% yield (Scheme 1.26).

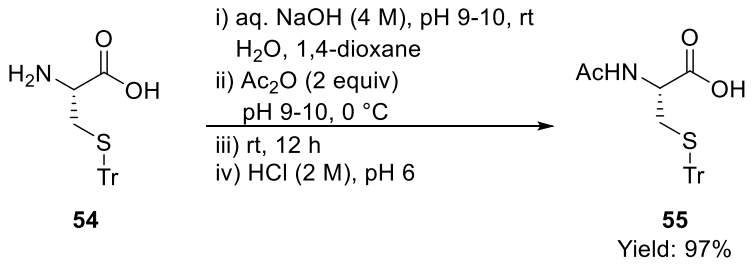

Scheme 1.26: Acetylation of *S*-(triphenylmethyl)cysteine.

Conversion of carboxylic acid **55** into benzyl amide **56** was achieved through carbodiimide-based peptide coupling with freshly distilled benzylamine. 6-Chloro-1-hydroxybenzotriazole (6-Cl-HOBt) and *N*,*N*′-diisopropylcarbodiimide (DIC) were added to a solution of **55** in DMF at 0 °C. Benzylamine was added and the reaction mixture was stirred at 0 °C for 1 h and at room temperature for 12 h. Purification was carried out by using flash column chromatography; however, the *N*,*N*′-diisopropylurea by-product **57** could not be completely removed. Attempts to recrystallize the product from a range of solvent systems failed to provide pure material. Therefore, *N*-2-acetyl-*N*-benzyl-*S*-(triphenylmethyl)cysteinamide **56** and *N*,*N*′-diisopropylurea **57** were isolated as a ~3.5:1 mixture (determined through NMR analysis) with the hope of removing the *N*,*N*′-diisopropylurea **57** at a later stage (Scheme 1.27).

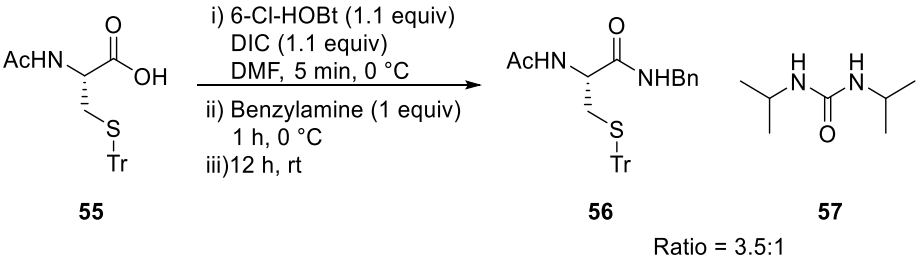

Scheme 1.27: Peptide coupling of *N*-acetyl-*S*-(triphenylmethyl)cysteine with benzylamine.

The mechanism of this coupling is as follows. Deprotonation of carboxylic acid **55** by DIC forms carboxylate **58**. Nucleophilic attack of carboxylate **58** on the protonated carbodiimide forms *O*-acylisourea mixed anhydride **59**. Nucleophilic attack of 6-Cl-HOBt on anhydride **59** releases the diisopropyl urea by-product **57**. The ester intermediate **60** is then nucleophilicly

attacked by benzylamine to generate the amide product **56**, thus regenerating 6-Cl-HOBt. The formation of urea **57** is the driving force for this reaction (Scheme 1.28). To prevent racemization and acetyl transfer, which would form an unreactive *N*-acylurea, the reaction is carried out at 0 °C and the amine is added last.[68]

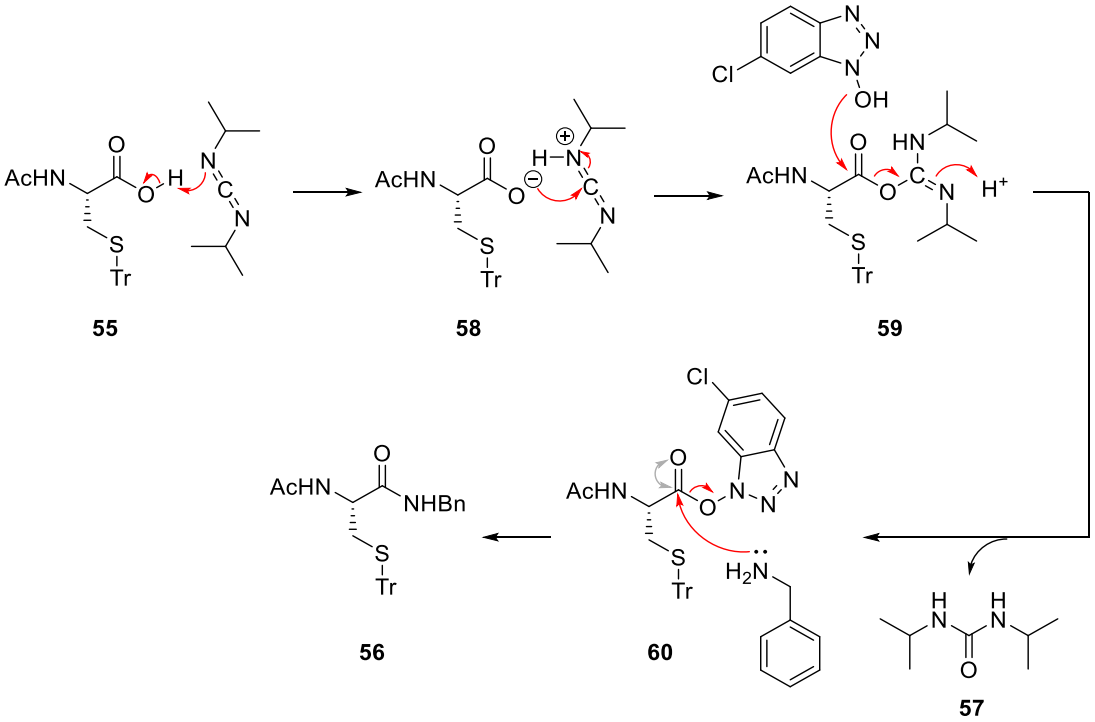

Scheme 1.28: Peptide coupling mechanism.

As 6-Cl-HOBt and HOBt are known to be explosive and can no longer be shipped to Ireland, an alternative approach using ethyl cyano(hydroxyimino)acetate (Oxyma, Figure 1.2) and DIC, as proposed by Funosas *et al.*,[69] was applied to generate *N*-2-acetyl-*N*-benzyl-*S*-(triphenylmethyl)cysteinamide **56** in 73% yield (isolated as a mixture of product **56** and diisopropyl urea **57**, ratio 3.5:1). Funosas *et al*[69] found that Oxyma inhibits racemization and its coupling efficiency was superior to that of HOBt and comparable to that of HOAt. Differential scanning calorimetry (DSC) and accelerating rate calorimetry (ARC) studies carried out by Albericio *et al.* showed that Oxyma decomposed at a slower rate and released a third of the pressure compared with benzotriazole-based additives, such as HOBt and HOAt (1-hydroxy-7-azabenzotriazole). Therefore a lower risk of explosion is associated with Oxyma.[69]

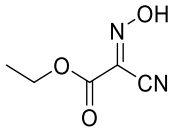

Figure 1.2: Oxyma (ethyl cyano(hydroxyamino)acetate).

Deprotection of the trityl protecting group was achieved by using the combination of a large excess of the proton donor, trifluoroacetic acid (TFA), and a slight excess of the hydride donor, triethylsilane (TES) to give *N*-2-acetyl-*N*-benzylcysteinamide **61** in 50% yield (Scheme 1.29).[70]

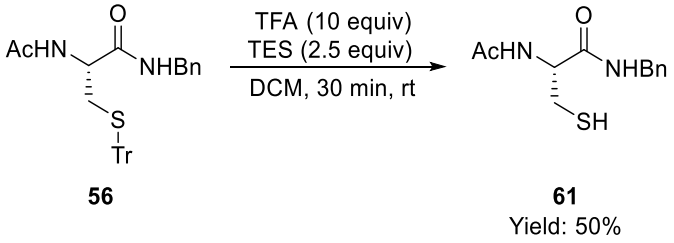

Scheme 1.29: Deprotection of the trityl group.

Deprotonation of TFA by **56** gives a sulfonium ion intermediate **62**. Loss of the trityl cation **63** gives product **61**. Due to the $Si^{\delta+}$–$H^{\delta-}$ polarization of TES a hydride transfer occurs to the electron-deficient trityl cation **63**, forming triphenylmethane **64** (Scheme 1.30). Excess triethylsilane is volatile (boiling point 108 °C) and can be easily removed.[70]

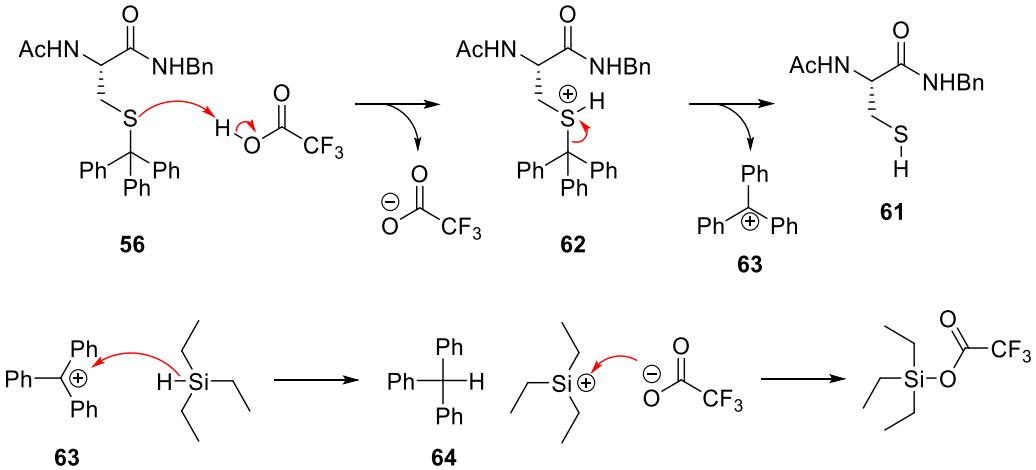

Scheme 1.30: Deprotection of the trityl group in the presence of TFA and TES.

1.3.2 Alkylation of Cysteine-Based Peptide Model

With the cysteine substrate, *N*-2-acetyl-*N*-benzylcysteinamide **61**, in hand, alkylation of the thiol moiety was performed by using a range of phenacyl bromide derivatives. Alkylation with reactive halogen compounds requires cysteine to be in its thiolate form (pH 8/9 in aqueous solution).[71] Alkylations of *N*-2-acetyl-*N*-benzylcysteinamide **61** were carried out by using an excess of the phenacyl bromide derivative under biologically ambient conditions, that is, aqueous phosphate buffer (pH 9, 0.1 M) and a minimum amount of DMF for solubility. All reaction mixtures were stirred at room temperature for 12 h. With the eventual aim of carrying out this transformation in a protein environment, it was important to use biologically ambient conditions (i.e. 37 °C, pH 6–8 and aqueous solution) so as to preserve protein structure and function.[1] Moderate yields were obtained for all of the below transformations. This was due to the formation of minor side products, which were not isolated.

Alkylation of *N*-2-acetyl-*N*-benzylcysteinamide **61** with 2-bromoacetophenone gave the *N*-2-acetyl-*N*-benzyl-*S*-(2-oxo-2-phenylethyl)cysteinamide product **65** in 62% yield (Scheme 1.31).

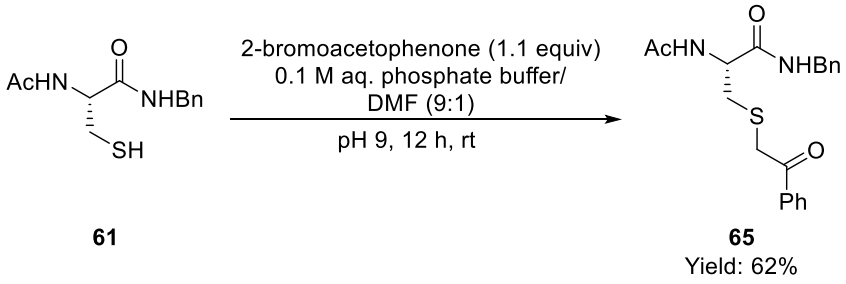

Scheme 1.31: Alkylation of *N*-2-acetyl-*N*-benzylcysteinamide with 2-bromoacetophenone.

This reaction is expected to occur by an S_N2 process. In the presence of basic phosphate buffer, thiol **61** is in equilibrium with its conjugate base, the thiolate, which is the active nucleophile. The thiolate anion then undergoes an S_N2 reaction with the phenacyl bromide (Scheme 1.32).

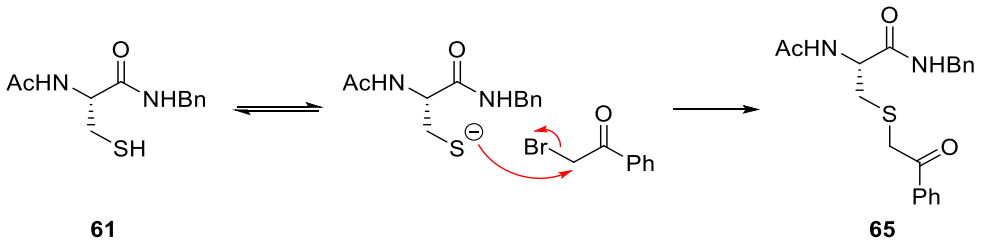

Scheme 1.32: S_N2 reaction between *N*-2-acetyl-*N*-benzylcysteinamide and 2-bromoacetophenone.

The cysteine-based peptide model was also alkylated with 2-bromo-2′,4′-dimethoxyacetophenone giving α-thioketone **66** in 60% yield (Scheme 1.33). As this phenacyl bromide was used by Clark and Lowe[64,65] in the photochemical conversion of cysteine in the protein, papain, into serine, this derivative would be used for comparison with current state of the art.

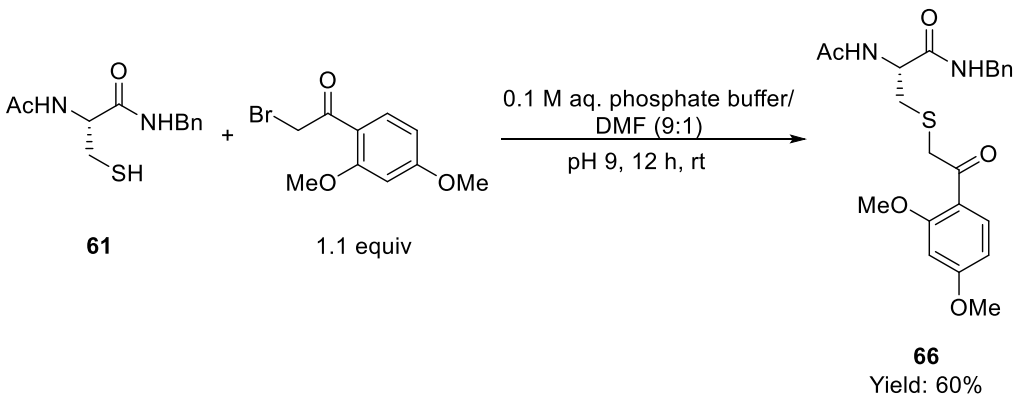

Scheme 1.33: Alkylation of *N*-2-acetyl-*N*-benzylcysteinamide with 2-bromo-2′,4′-dimethoxyacetophenone.

Based on Wagner and Siebert's[72] study on the effect of inductively electron-withdrawing substituents on Norrish Type II reactivity (Section 1.3.3.3), phenacyl bromides with both cyano and trifluoromethyl substituents were used to functionalize cysteine-based peptide model **61**. Alkylation of cysteine-based peptide model **61** with 3-(2-bromoacetyl)benzonitrile gave the corresponding α-thioketone **67** in 60% yield (Scheme 1.34).

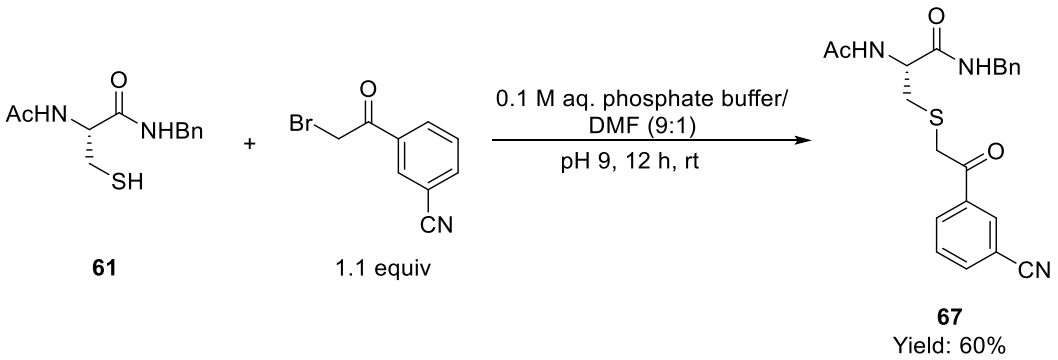

Scheme 1.34: Alkylation of *N*-2-acetyl-*N*-benzylcysteinamide with 3-(2-bromoacetyl)benzonitrile.

For comparison, the cysteine-based peptide model **61** was also alkylated with 4-(2-bromoacetyl)benzonitrile giving α-thioketone **68** in 50% yield (Scheme 1.35).

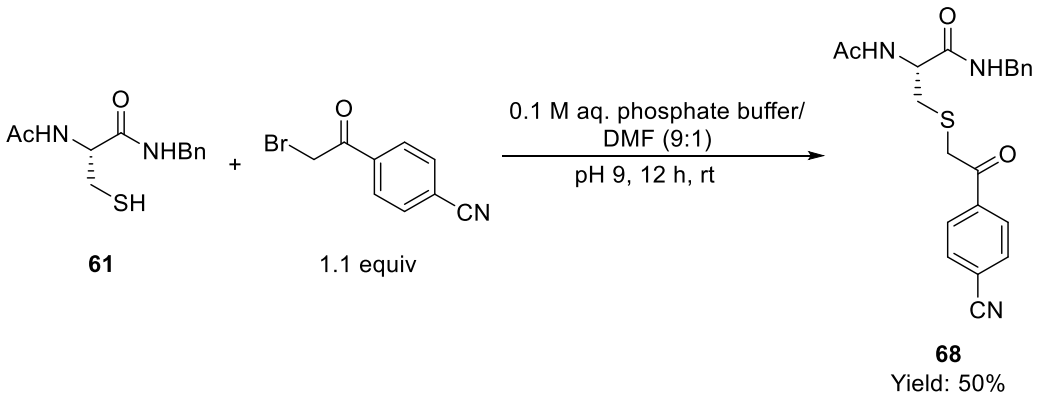

Scheme 1.35: Alkylation of *N*-2-acetyl-*N*-benzylcysteinamide with 4-(2-bromoacetyl)benzonitrile.

The cysteine-based peptide model **61** was also alkylated with 3-(trifluoromethyl)phenacyl bromide giving α-thioketone **69** in 73% yield (Scheme 1.36).

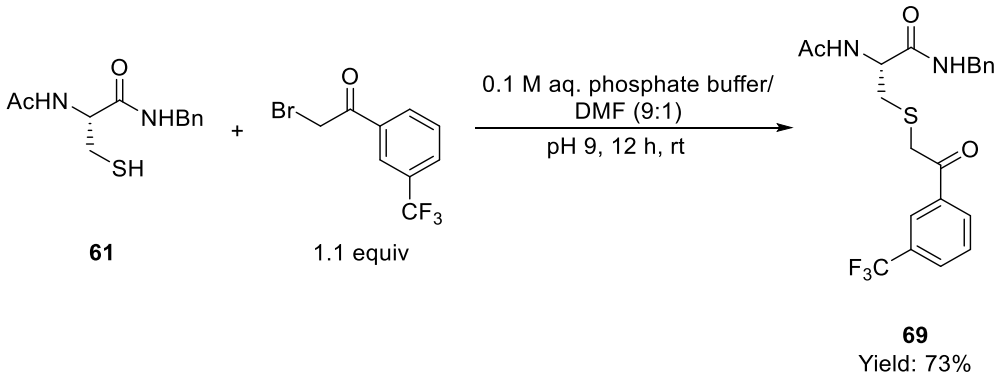

Scheme 1.36: Alkylation of *N*-2-acetyl-*N*-benzylcysteinamide with 3-(trifluoromethyl)phenacyl bromide.

To increase the inductive electron-withdrawing effect through substitution of both *meta* positions, alkylation of the cysteine-based peptide model **61** with 3′,5′-bis(trifluoromethyl)-2-bromoacetophenone was carried out giving α-thioketone **70** in 62% yield (Scheme 1.37).

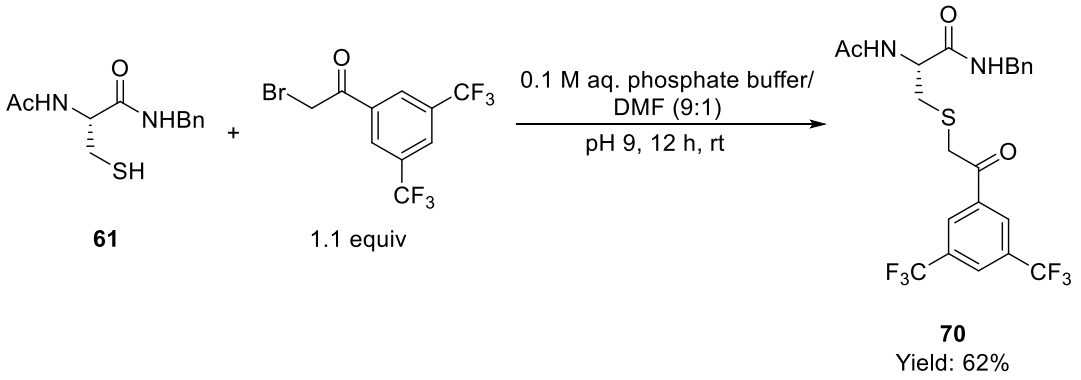

Scheme 1.37: Alkylation of *N*-2-acetyl-*N*-benzylcysteinamide with 3′,5′-bis(trifluoromethyl)-2-bromoacetophenone.

1.3.3 Norrish Type II Photoelimination

With cysteine-based peptide model **61** successfully alkylated to give a range of α-thioketone derivatives (compounds **65**–**70**), we were now in a position to study the photofragmentation of these molecules. Below is an introduction to the Norrish Type II reaction.

Photolysis of *N*-2-acetyl-*N*-benzyl-*S*-(2-oxo-2-phenylethyl)cysteinamide **65** to the thioaldehyde is proposed to cause Norrish Type II cleavage giving thioaldehyde (or enethiol) **71** and acetophenone **72** as products (Scheme 1.38).[73]

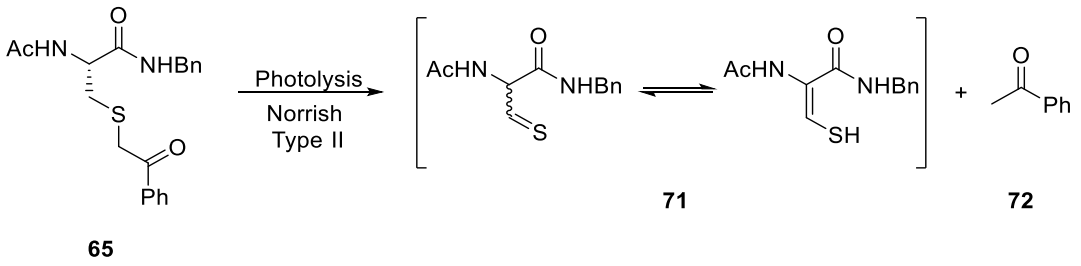

Scheme 1.38: Norrish Type II cleavage of *N*-2-acetyl-*N*-benzyl-*S*-(2-oxo-2-phenylethyl)cysteinamide.

In general, this photochemical reaction begins with the photochemical excitation of the carbonyl group of an aromatic aldehyde or ketone **73** generating a species with 1,2-biradical character **74**. Biradical **74** undergoes an intramolecular γ-hydrogen transfer, generating 1,4-biradical intermediate **75**, which can undergo fragmentation to form enol **76** and alkene **77**. The Norrish Type II reaction may also be in competition with the Yang cyclization. This intramolecular radical combination of the 1,4-biradical leads to cyclobutanol product **78** (Scheme 1.39).[74–76]

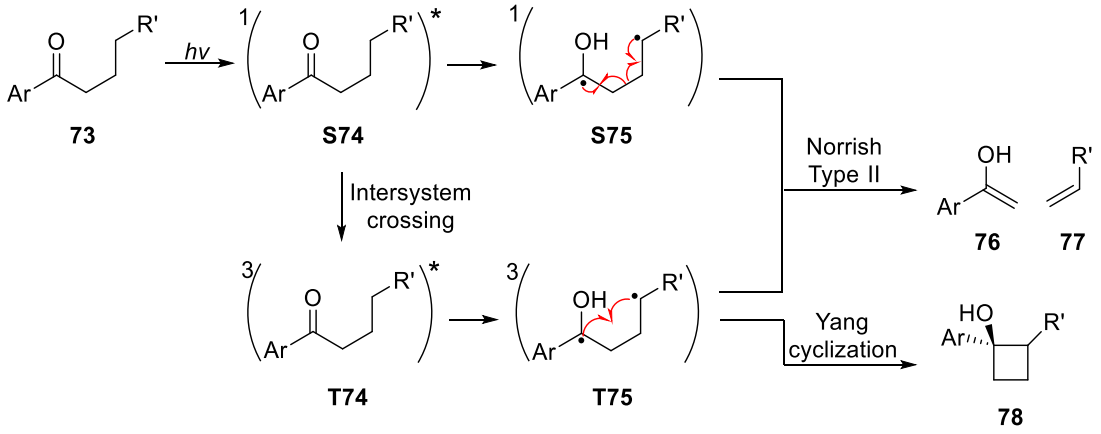

Scheme 1.39: Norrish Type II cleavage and Yang cyclization.[74]

1.3.3.1 Nature of Excited State: Comparison of n,π* and π,π* Triplets

The nature of the excited state is important for the Norrish Type II process. Photoexcitation of a carbonyl, for example an aromatic ketone, promotes an electron from a lower-energy molecular orbital to a higher-energy molecular orbital. The two lone pairs of electrons in the non-bonding orbitals (n) on the oxygen atom are lower in energy than the antibonding π* molecular orbital. The n,π* transition occurs when an electron is promoted from the n orbital to the π* molecular orbital.[75] The n,π* state produces an unpaired electron in a nonbonding, n orbital of the more electronegative oxygen atom (as opposed to placing all unpaired electrons on carbon). This excited state shows reactivity that is similar to that of an alkoxy radical, which is highly unstable owing to electron deficiency at the oxygen atom, thus leading to new bonds to be formed. The other electron is promoted to a nucleophilic π* orbital.

In aromatic ketones, a π,π* transition can also occur; here an electron is promoted from a bonding π molecular orbital to an antibonding π* molecular orbital. There is little spin density on the oxygen atom as the electron in the half-vacant bonding molecular orbital is mainly delocalized in the aromatic ring (Scheme 1.40).[77,78]

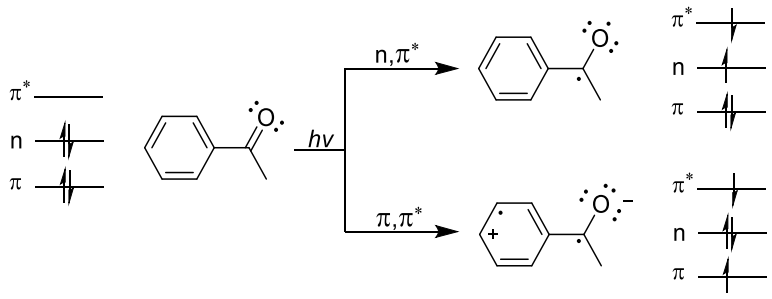

Scheme 1.40: n,π* and π,π* triplet states.[66]

In the ground state, the electrons are spin-paired. When excitation of an electron occurs, the electron can either adopt an antiparallel spin, which is known as a singlet state, or a parallel spin, which is known as a triplet state.[75,79] Upon excitation, an electron is promoted to the first singlet excited state.[66] The triplet state populations arise from intersystem crossing (ISC) from singlet states, which are first populated upon excitation. Both singlet and triplet excited states display Norrish Type II reactivity. Singlet state reactions typically exhibit low quantum yields and the singlet state often returns to the ground state. However, the triplet excited state is more productive for hydrogen abstraction.[77] For example, for 2-pentanone, the singlet state quantum yield for Norrish Type II reactivity is 0.025, whereas the corresponding triplet state quantum yield is > 0.36.[75] Aromatic ketones can have the n,π* or the π,π* as the lowest triplet state.[72] ISC to either the n,π* or π,π* lowest triplet state occurs rapidly in phenyl ketones (< 10^{11} s^{-1} versus 10^{8} s^{-1} for saturated ketones) thus allowing transformations, such as hydrogen abstraction leading to Norrish Type II, to occur from the triplet state.[80] The relative energy of the π,π* and n,π* state is influenced by the substituents on the aromatic ring.[77,78]

1.3.3.2 Substituent Effects: Electron-Donating Groups

Aromatic ketones can have the n,π* or the π,π* state as the lowest triplet state. Ring-unsubstituted phenyl ketones have n,π* lowest triplet states and a π,π* triplet state that is a few kcal/mol higher in energy. Electron-donating ring substituents cause an inversion of the triplet states such that the π,π* triplet state is lower in energy than the n,π* triplet state. These types of ketones do undergo hydrogen abstraction reactions such as Norrish Type II; however, most of the measured reactivity comes from low concentrations of the n,π* triplet state, which is in thermal equilibrium with the π,π* triplet state.[75,81]

Wagner *et al.*[82] studied the effect of various electron-donating ring substituents on rate constants for Norrish Type II hydrogen abstraction in ring-substituted valerophenones (Scheme 1.41). Electron-donating (+R) substituents at any ring position decrease both quantum efficiencies[72,83,84] and rate constants[72,85] for triplet state hydrogen abstraction. For example, the quantum yields for *para*-, *meta*- and *ortho*-methoxy substituted valerophenones were 0.10, 0.014 and 0.15 compared with 0.33 for unsubstituted valerophenone.

The overall hydrogen abstraction rate constant ($k_{\mathrm{H}}^{\mathrm{obs}}$) depends on the Boltzmann distribution of the reactive states (Equation 1; the population of each state is denoted as χ and ΔE is the energy difference between n,π* and π,π* triplet states). Most reactivity arises from the n,π* state when $\Delta E(E_{\mathrm{n},\pi^*-\pi,\pi^*}) < 5$ kcal mol^{-1}.[75,77]

$$k_{\mathrm{H}}^{\mathrm{obs}} = \chi_{\mathrm{n},\pi} k_{\mathrm{H}}^{\mathrm{n},\pi} + \chi_{\pi,\pi} k_{\mathrm{H}}^{\pi,\pi}$$

$$\chi_{\mathrm{n},\pi} = (1 - \chi_{\pi,\pi}) = \mathrm{e}^{-\Delta E/RT}/[1 + \mathrm{e}^{-\Delta E/RT}]$$

Equation 1.1: Hydrogen abstraction rate constant equation.

The hydrogen abstraction rate constants (k_{obs}) can depend on the position of a substituent (Table 1.1).[75] The introduction of electron-donating groups in the *para* position, such as *p*-OMe, decreases the population of the reactive n,π* state as they inductively stabilize the π,π* triplet more than they stabilize the n,π* triplet. Most of the reactivity arises from low populations of the n,π* triplet. The π,π* triplets are known to undergo hydrogen abstraction with low spin density on oxygen; however, the rate constants are much lower compared with the hydrogen abstraction rate for n,π* triplets.[77]

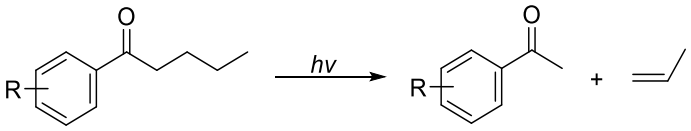

Scheme 1.41: Norrish type II reaction of ring-substituted valerophenone.[72]

Table 1.1: Electron-donating substituent effect on hydrogen abstraction rate constants (k_{obs}), the n,π* triplet percentage populations and the rate constant for hydrogen abstraction for the n,π* triplet state (k_{n,π^*}).

Substituent	k_{obs} (10^7 s^{-1})	n,π* (%)	k_{n,π^*} (10^7 s^{-1})
H	13	99	13
o-OMe	0.30	3	10
m-OMe	0.02	0.15	15
p-OMe	0.06	1	6

The methoxy substituents on Clark and Lowe's phenacyl halide substrate, 2-bromo-2′,4′-dimethoxyacetophenone (Scheme 1.21, Section 1.1.8) may have contributed to the low conversion to the Norrish Type II fragmentation product, as observed during photochemical conversion of cysteine into serine.[64,65,77,78]

1.3.3.3 Substituent Effects: Electron-Withdrawing Groups

Wagner *et al.*[72] also studied the effect of electron-withdrawing substituents on rate constants for Norrish Type II hydrogen abstraction by ring-substituted valerophenones (Scheme 1.42). Inductively electron-withdrawing ring substituents, such as cyano and CF_3 groups, increase the rates of triplet state hydrogen abstraction as the n,π* triplet reactivity for γ-hydrogen abstraction increases and the electron density of the carbonyl oxygen becomes more deficient (Table 1.2).[72] The cyano group stabilizes n,π* triplets by induction and π,π* triplets by conjugation. Cyano substituents at the *ortho* and *meta* position exhibit this inductive effect. Therefore, the n,π* triplet state remains lower in energy than the π,π* triplet state.[75] Cyano substituents at the *para* position are in conjugation with the carbonyl group, thus in comparison with the *meta*-cyano group, the *para*-cyano group stabilizes the π,π* triplet state by conjugation more than the n,π* triplet state.[72,75] The small increase in rate for the CF_3 substituted valerophenones is probably due to the inductive effect on the reactivity of the electrophilic n,π* triplet state.[72,82]

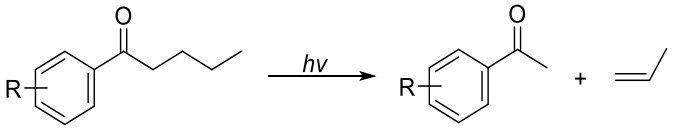

Scheme 1.42: Norrish type II reaction of ring-substituted valerophenone.[72]

Table 1.2: The effect of electron-withdrawing substituents on the rate constants of hydrogen abstraction (k_{obs}), the n,π* triplet percentage populations and k_{n,π^*}.

Substituent	k_{obs} (10^7 s^{-1})	n,π* (%)	k_{n,π^*} (10^7 s^{-1})
H	13	99	13
o-CN	23	99	23
m-CN	30	99	30
p-CN	6.8	21	32
o-CF_3	13	>99	13
m-CF_3	32	>99	32
p-CF_3	28	>99	28

1.3.4 Photolysis of Parent Model Compound

A solution of each model compound (compounds **65**–**70**) in a 1:1 mixture of deuterated methanol and deuterated phosphate buffer (pD 7.0, 0.1 M) was prepared. As the model compounds were not soluble in deuterated phosphate buffer it was necessary to add deuterated methanol. Each solution was degassed with argon for approximately 15 mins in a quartz NMR tube to avoid any photooxidation processes that may occur due to the presence of dissolved oxygen. Photolysis was performed using a Rayonet photochemical reactor and 350 nm ultraviolet lamp (Figure 1.3). ^{1}H NMR spectroscopy was used to monitor all reactions. Average NMR conversions are given (see Section 1.3.8).

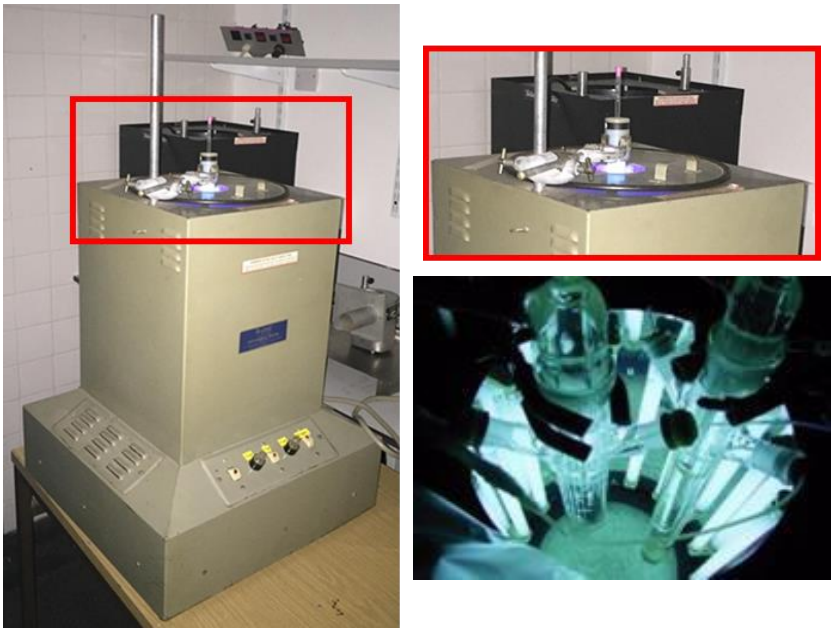

Figure 1.3: Rayonet photochemical reactor.

Photolysis of the parent model compound *N*-2-acetyl-*N*-benzyl-*S*-(2-oxo-2-phenylethyl)cysteinamide, **65** was investigated first (Scheme 1.43).

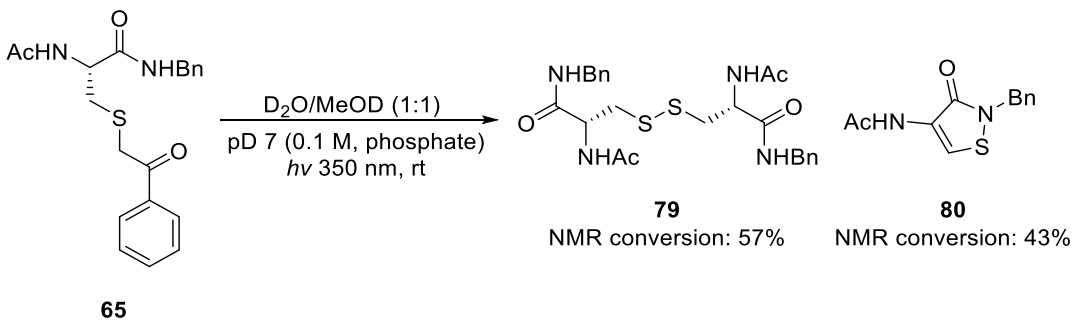

Scheme 1.43: Photolysis of *N*-2-acetyl-*N*-benzyl-*S*-(2-oxo-2-phenylethyl)cysteinamide.

Two major products were observed: disulfide **79** and an isothiazolone, *N*-(2-benzyl-3-oxo-2,3-dihydro-1,2-thiazol-4-yl)acetamide, **80**. NMR analysis of the solution of *N*-2-acetyl-*N*-benzyl-*S*-(2-oxo-2-phenylethyl)cysteinamide **65** during photolysis showed the appearance of a species with a downfield shift of the doublet of doublets corresponding to the diastereotopic methylene protons at the β position of the amino acid derivative (from 2.8/2.9 ppm to 2.9/3.1 ppm) showing conversion into the disulfide **79** (Figure 1.4).

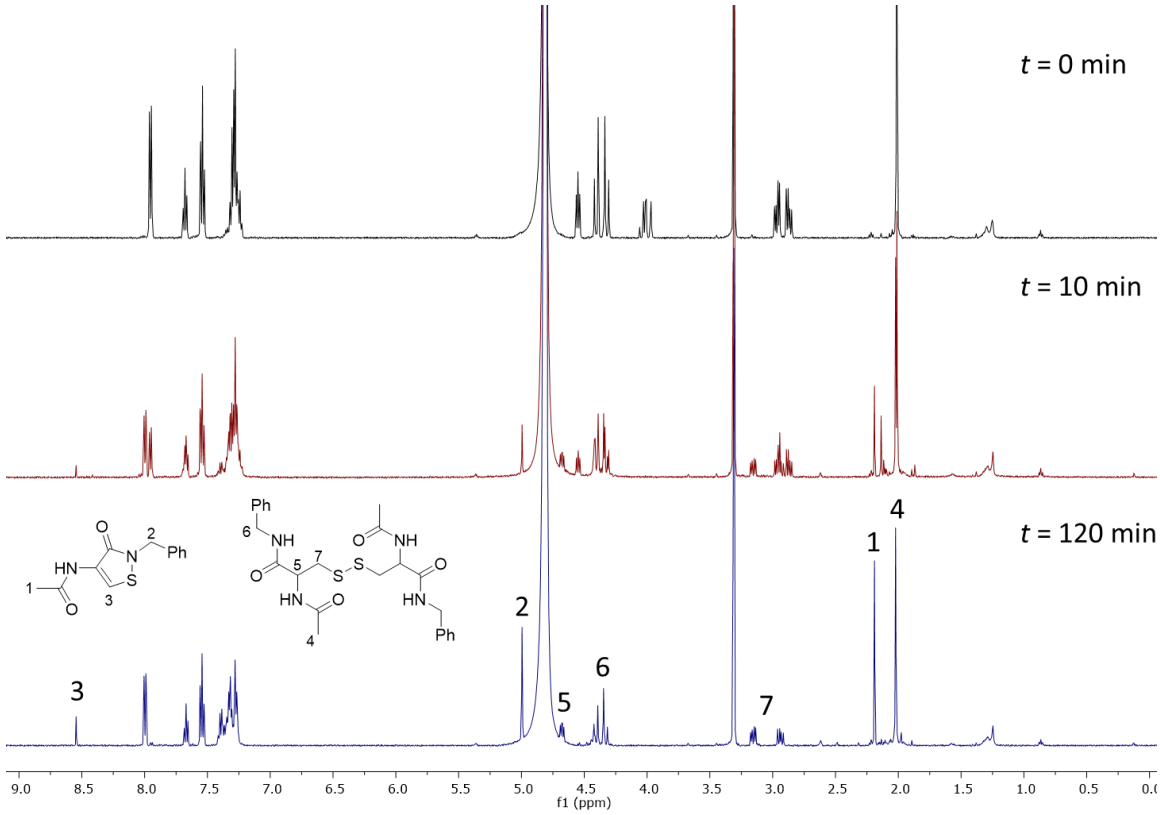

Figure 1.4: ^{1}H NMR spectrum of reaction mixture derived from *N*-2-acetyl-*N*-benzyl-*S*-(2-oxo-2-phenylethyl)cysteinamide at *t* = 0, 10, and 120 minutes of photolysis.

To confirm the assignment, H_2O_2 and sodium iodide mediated oxidation of *N*-2-acetyl-*N*-benzylcysteinamide **61** was carried out. After purification by column chromatography, disulfide **79** was obtained in 80% yield and its structure confirmed by NMR spectroscopy (Scheme 1.44).

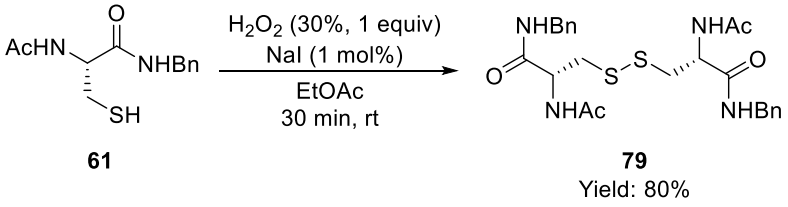

Scheme 1.44: H_2O_2 mediated oxidation of *N*-2-acetyl-*N*-benzylcysteinamide.

Comparison of the NMR spectra confirmed that the doublet of doublets at 2.9 and 3.1 ppm corresponded to disulfide **79** (Figure 1.4). HRMS analysis also supported the presence of disulfide **79**. Interestingly, HRMS also suggested the formation of isothiazolone **80**. NMR analysis of the reaction mixture showed a species with a singlet at 4.9 ppm and a singlet at 8.5 ppm (Figure 1.4). Isothiazolone derivatives have previously been reported. For example, Nadel *et al.*[86] reported the formation of isothiazolone derivative **81** through sulfuryl chloride cyclization of a cystine bis(methylamine). In 1969, Morin *et al.*[87] reported the formation of isothiazolones **82** through S-oxidation and rearrangement of a penicillin derivative. The CH ring proton appeared at 8.05 and 8.72 ppm, respectively (Figure 1.5).

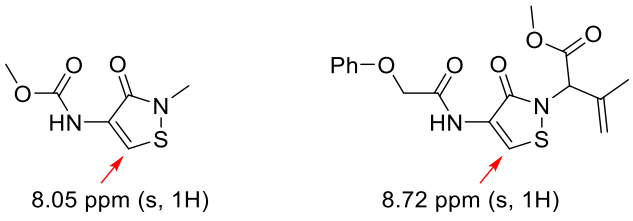

81 **82**

Figure 1.5: Isothiazolones reported by Nadel *et al.*[86] and Morin *et al.*[87]

These pieces of literature suggested that the singlet at 8.5 ppm corresponded to the CH of the isothiazolone ring **80**. The singlet at 4.9 ppm corresponded to the benzylic CH_2 (Figure 1.4).

Isothiazolone **80** was isolated by column chromatography and its structure was confirmed by NMR spectroscopy and X-ray crystallography. Crystallization from slow evaporation of **80** in DCM/petroleum ether afforded the X-ray quality crystals (Figure 1.6).

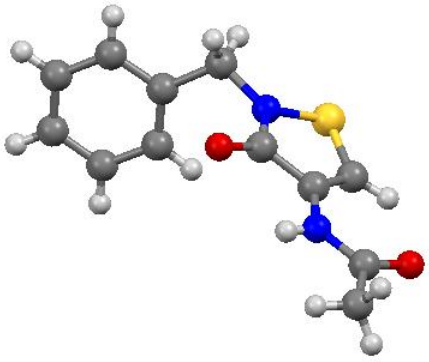

Figure 1.6: X-ray crystal structure for *N*-(2-benzyl-3-oxo-2,3-dihydro-1,2-thiazol-4-yl)acetamide, **80**, crystallized from DCM/petroleum ether and structure obtained by X-ray crystallographer Prof. Patrick McArdle (NUI Galway).

To rationalize the above result, we looked to the literature. Wagner *et al.*[88] studied the photochemistry of ring-substituted phenacyl sulfides **83** (Scheme 1.45). In addition to γ-hydrogen abstraction (Norrish Type II) giving the 1,4-biradical **84**, which fragments to ketone **85** and thioaldehyde **86**, phenacyl sulfides can also undergo two other types of transformations from the triplet state. Charge transfer from sulfur to the carbonyl group in **87** ultimately leads to regeneration of phenacyl sulfide **83**. β-Cleavage of the sulfur–carbon (carbonyl carbon) bond can also occur leading to keto and thiyl radicals **88** and **89**, which can leave the solvent cage and dimerize, forming disulfide **90** and 1,4-dione **91**, or undergo hydrogen abstraction within the solvent cage to form ketone **85** and thioaldehyde **86** (Scheme 1.45). β-Cleavage arises when there is a good radical leaving group on the α-carbon atom and when its rate is comparable to that of the other two transformations.

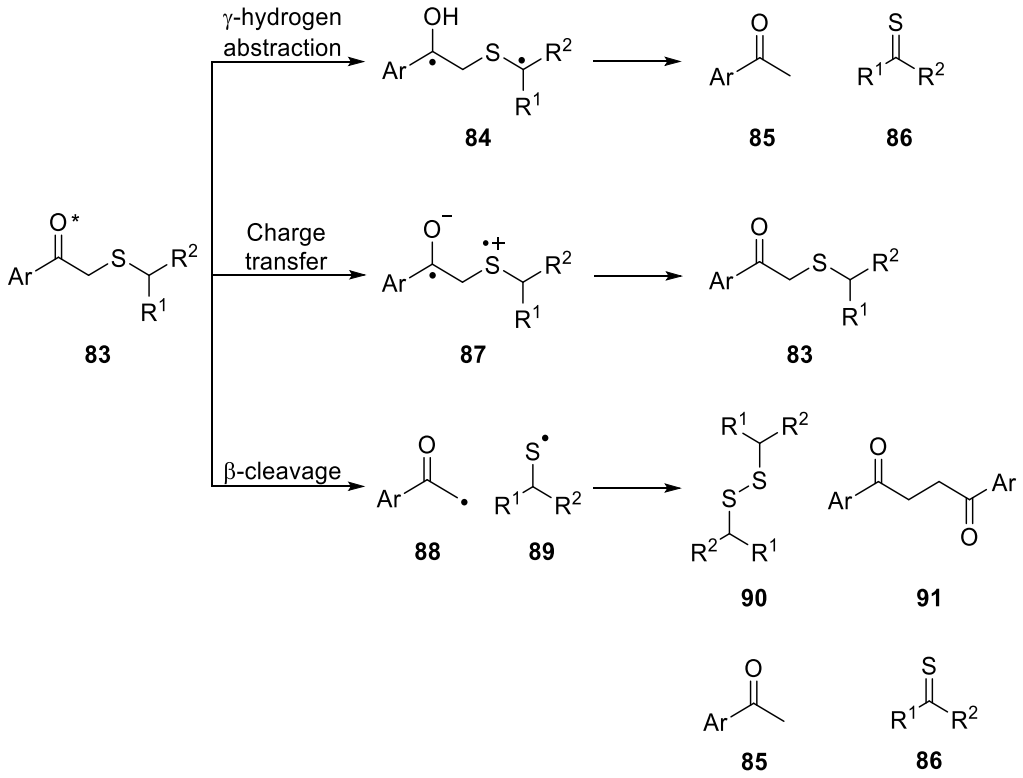

Scheme 1.45: γ-Hydrogen abstraction (Norrish Type II), charge transfer and β-cleavage reactions.[88]

In general, phenacyl sulfides have the n,π* as the lowest triplet state. The sulfur atom has an effect on the n,π* absorption. Specifically, the α-heteroatom (sulfur in this case) substitution is known to both intensify and shift the ketone n,π* transition. It has been proposed that the carbonyl π* and the C–S σ* orbitals mix, with the C–S bond being parallel to the π-orbital of the carbonyl group. The C–S bond becomes a partial electron acceptor of the promoted n

electron. The partial C–S σ character in the n,π* state causes the C–S bond to become weaker and therefore promoting its cleavage. The n,π* state is also stabilized by this mixing of the benzoyl π* and C–S σ* orbital (Figure 1.7).[88]

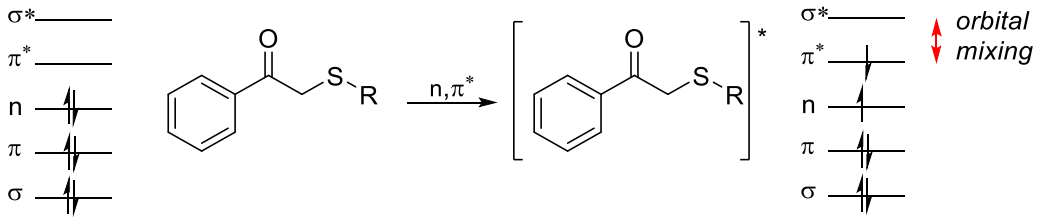

Figure 1.7: n,π* and π,π* transitions of phenacyl sulfides.[88]

Disulfide **79** could arise from two possible pathways (Scheme 1.46). β-Cleavage of the sulfur–carbon (carbonyl carbon) bond of **92** would give thiyl and phenacyl radicals, **93** and **94**, which can leave the solvent cage and dimerize, to form disulfide **79** and 1,4-dione **95**. The thiyl radical **93** could also combine with another molecule of the phenacyl sulfide substrate **65** to give disulfide **78** and phenacyl radical **94**, which could dimerize to form 1,4-dione **95**.

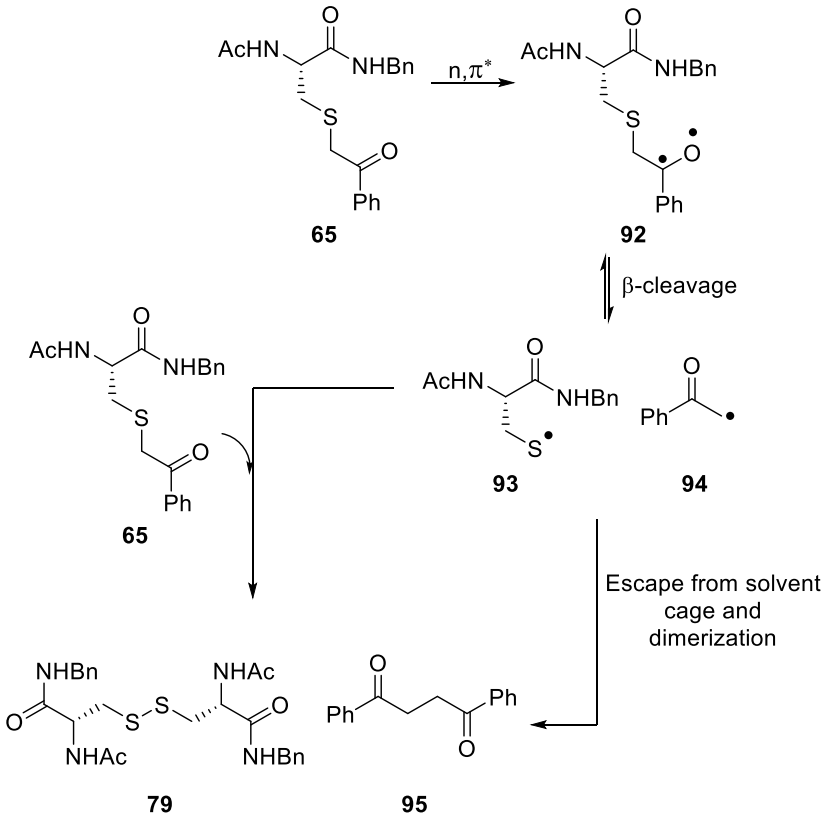

Scheme 1.46: Mechanism of formation of disulfide.

A tentative mechanism is also proposed for the formation of isothiazolone **80** (Scheme 1.47). Two possible pathways exist for the formation of thioaldehyde/enethiolate **71**, which could ultimately lead to isothiazolone **80**. Excitation of phenacyl sulfide **65** would ultimately lead to triplet excited state **92** with 1,2-biradical character. This intermediate could then undergo intramolecular hydrogen abstraction to give thioaldehyde **71** and ketone **72**. Thioaldehyde **71** could also be formed through β-cleavage of the sulfur–carbon (carbonyl carbon) bond to give thiyl and phenacyl radicals, **93** and **94**. The thiyl radical **93** could undergo an intermolecular hydrogen atom abstraction within the solvent cage to form thioaldehyde **71** (which is presumably in the enethiolate form at pH 7.4) and ketone **72**. Oxidation of enethiolate **71** by an electron acceptor, for example thiyl or phenacyl radical, **93** and **94**, forms enethiyl radical **96**. This radical can then combine with another molecule of the substrate **65** to form mixed disulfide **97** and phenacyl radical **94**. Hydrogen atom transfer from the nitrogen atom of mixed disulfide **97** to phenacyl radical **94** would lead to a nitrogen-centred radical **98**. Cyclization forms isothiazolone **80** and thiyl radical **93**, which could combine with another thiyl radical to form disulfide **79**.

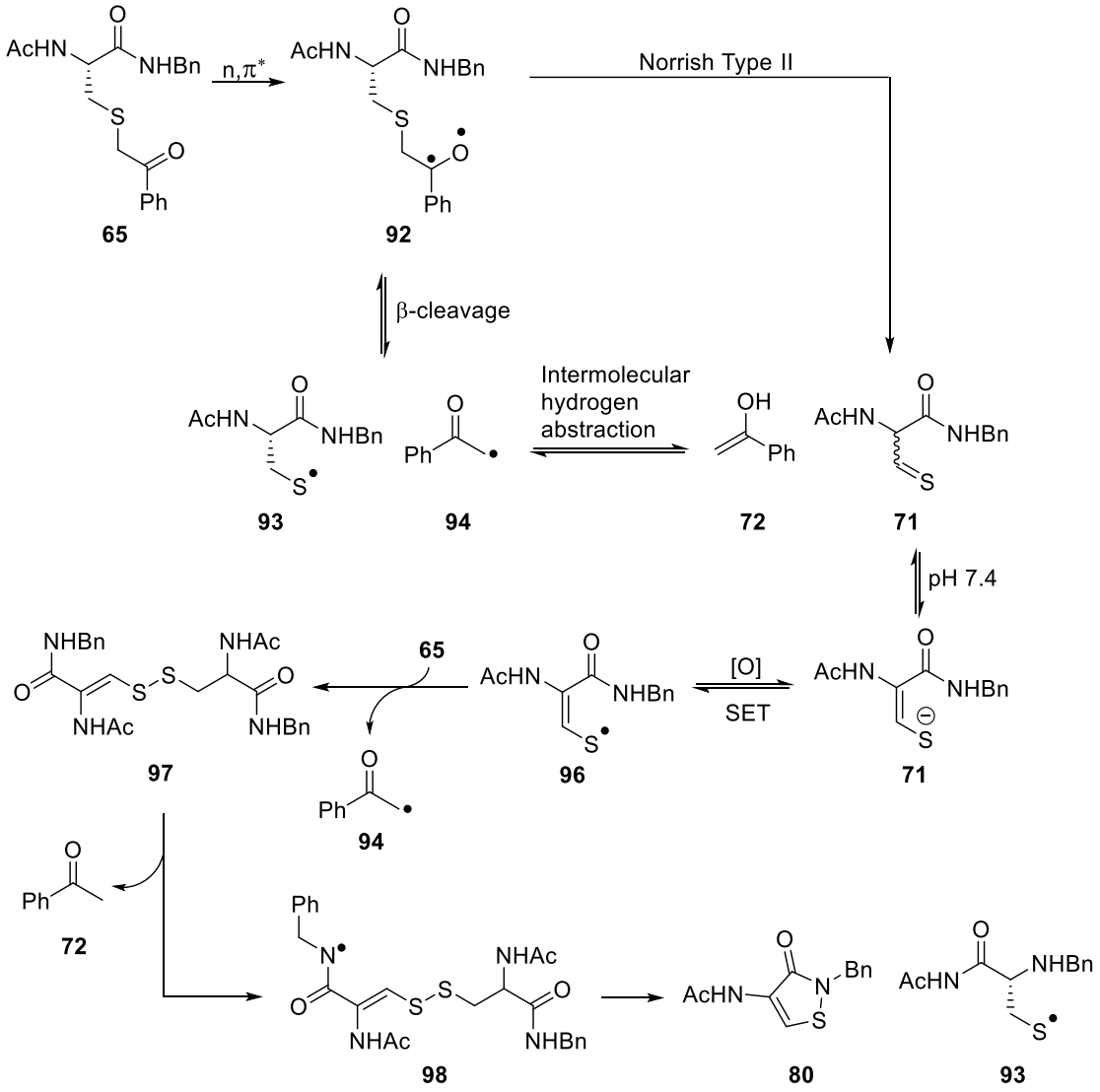

Scheme 1.47: Mechanism of formation of isothiazolone.

1.3.4.1 Significance of Isothiazolones

Having isolated isothiazolone **80**, and upon searching the literature, no isothiazolone derivatives have been found in Nature; however, a reduced derivative has been reported. Salmeen *et al.*[89] reported that redox regulation in protein tyrosine phosphate 1B (PTP1B) **99** is promoted by hydrogen peroxide mediated reversible oxidation of its catalytic cysteine into a sulfenyl-amide intermediate **101** (a saturated version of an isothiazolone) *via* sulfenic acid **100**. This protein modification allows redox regulation by promoting reversible reduction of the protein by thiols. The active-site cysteine is also protected from further irreversible oxidation to sulfonic acid. The catalytic cysteine residue of the PTP1B enzyme is first oxidized by hydrogen peroxide forming sulfenic acid intermediate **100**. Nucleophilic attack by the main chain nitrogen of Ser 216 to the electrophilic sulfur atom of labile sulfenic acid **100** followed

by loss of water was proposed as the mechanism of the sulfenyl-amide formation (Scheme 1.48). To our knowledge, this is the only biologically relevant species related to an isothiazolone.

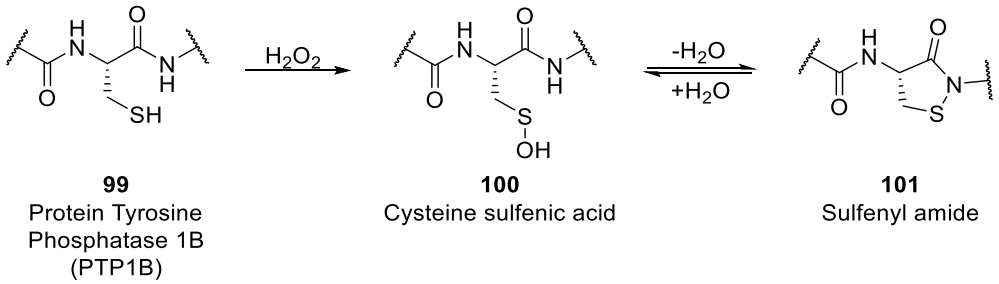

Scheme 1.48: Formation of sulfenyl-amide.

The inhibition of telomerase, an RNA-dependant DNA polymerase enzyme that is associated with cancer cell proliferation, has been identified as a therapeutic approach against cancer. Hayakawa *et al.*[90] screened a library of 16000 synthetic compounds for telomerase inhibition. The isothiazolone, 2-[3-(trifluoromethyl)phenyl]isothiazolin-3-one, **103**, was identified as the most potent inhibitor (Scheme 1.49). Telomerase activity was inhibited by 50% with addition of 1.0 µM of isothiazolone **103**. It was proposed that the isothiazolone undergoes attack by the thiolate group of cysteine residue **102** either near or in the active site of telomerase, leading to disulfide species **104**; this covalent inhibition was supported by the fact that inhibition by the isothiazolone was quenched by dithiothreitol (DTT), which prematurely breaks the N–S bond through a similar ring-opening mechanism (Scheme 1.49).

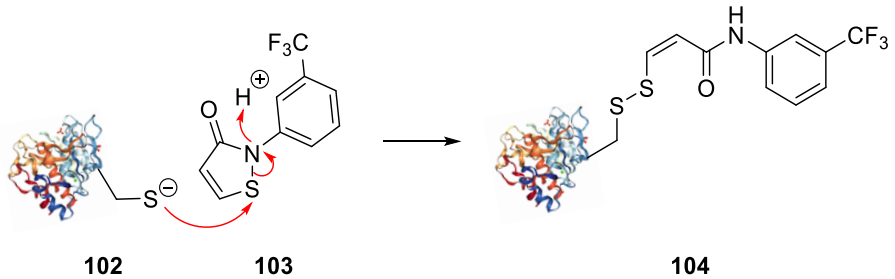

Scheme 1.49: Telomerase inhibitor; 2-[3-(trifluoromethyl)phenyl]isothiazolin-3-one, and its proposed mechanism of action.

1.3.4.2 Reduction of Isothiazolone

Based upon the known reactivity of isothiazolones in the presence of thiols (as mentioned above, Scheme 1.49), we anticipated that our isothiazolone product **80** could be converted into thioaldehyde/enethiolate **71** through reduction with a phosphine (such as the water-soluble tris(2-carboxyethyl)phosphine hydrochloride, TCEP) or a dithiol (such as the commonly used DTT). The reduction of isothiazolone **80** was carried out using tris(2-carboxyethyl)phosphine hydrochloride (TCEP). Isothiazolone **80** was added to a 1:1 mixture of deuterated methanol and D_2O with phosphate buffer at pD 7.0 (Scheme 1.50). TCEP was then added and the reaction was monitored by NMR spectroscopy.

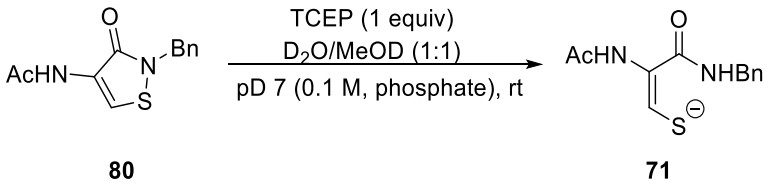

Scheme 1.50: TCEP mediated conversion of isothiazolone into enethiolate.

TCEP is commonly used as a disulfide reducing agent.[91] The proposed mechanism for the reduction of isothiazolone **80** into enethiolate **71** involves the ring-opening of isothiazolone **80** through nucleophilic attack by the phosphorus atom of TCEP generating phosphonium ion intermediate **105**. Hydrolysis of intermediate **105** forms phosphine oxide **106** and thioaldehyde **71**, which, under the reaction conditions, would be in its enethiolate form **71** (Scheme 1.51).

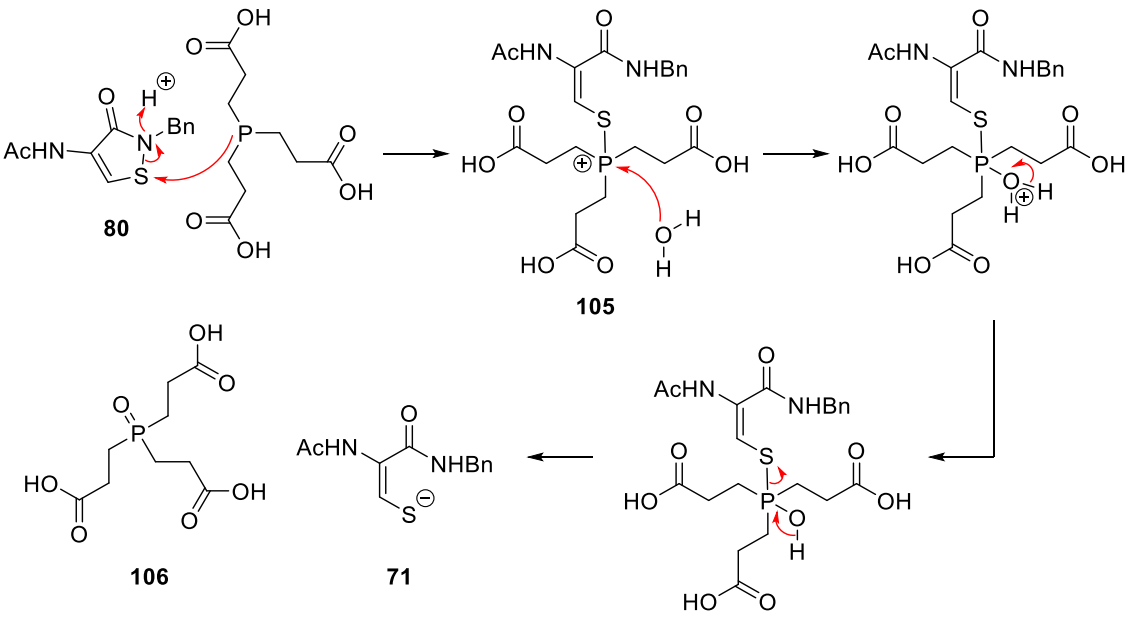

Scheme 1.51: Mechanism of TCEP reduction of isothiazolone into the enethiolate.

HRMS analysis also suggested the formation of enethiolate **71**. (HRMS (ESI) *m/z* (*M*+Na), $C_{12}H_{14}N_2O_2SNa$ calcd. 273.0674, observed 273.0672; (*M*−H), $C_{12}H_{13}N_2O_2S$ calcd. 249.0685, observed 249.0698).

The disappearance of the NMR signals of isothiazolone **80** at 4.9 ppm (benzylic CH_2 ppm) and 8.5 ppm (CH of the isothiazolone ring **80**) and appearance of singlets at 4.4 ppm and 8.0 ppm corresponds to the benzylic CH_2 protons and the proton next to the sulfur atom of enethiolate **71** (Figure 1.8).

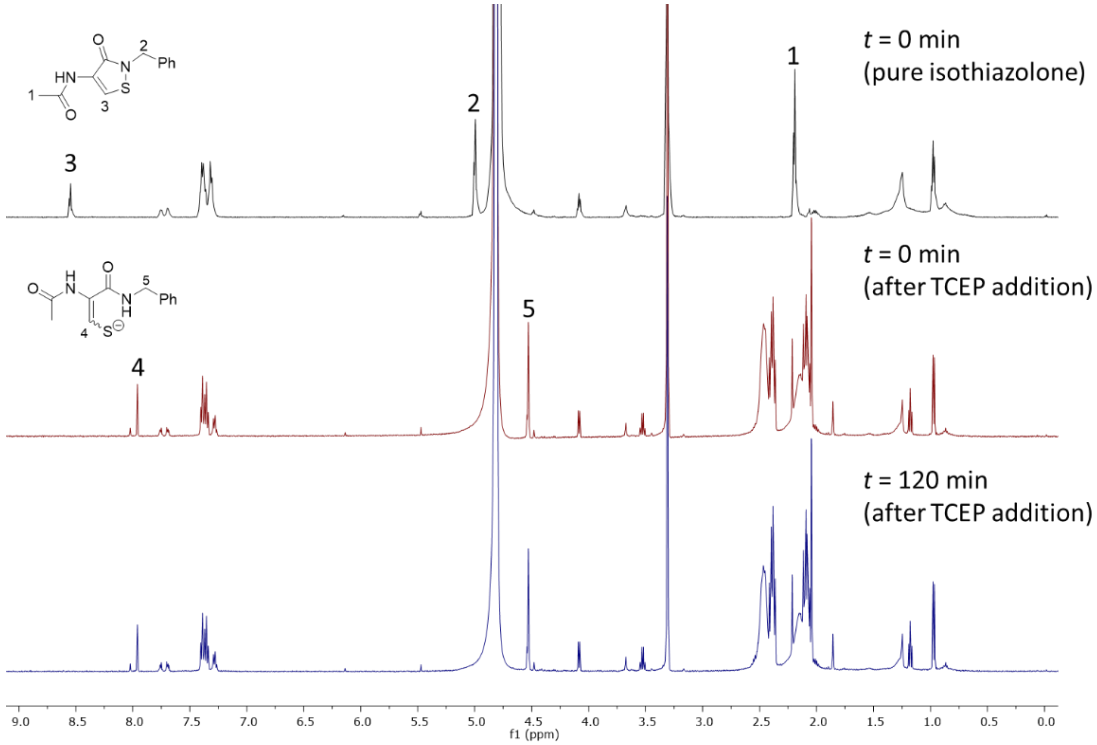

Figure 1.8: ^{1}H NMR spectrum of reaction mixture derived from TCEP reduction of the isothiazolone, *N*-(2-benzyl-3-oxo-2,3-dihydro-1,2-thiazol-4-yl)acetamide at *t* = 0 (pure isothiazolone), 0 (after addition of TCEP to isothiazolone) and 120 minutes (after addition of TCEP to isothiazolone).

1.3.4.3 Selective Disulfide Formation

Wagner *at al.*[88] have previously carried out photolysis of phenacyl sulfides in the presence of thiols such as benzenethiol which traps free phenacyl radicals that have been formed through β-cleavage. Based on this observation, we wondered whether the addition of 1 equivalent of the cysteine thiol **61** would allow the quenching of the phenacyl radicals that are produced after excitation and β-cleavage (Scheme 1.47), thus facilitating the formation of disulfide **79**. NMR analysis was carried out throughout the photolysis (Scheme 1.52 and Figure 1.9).

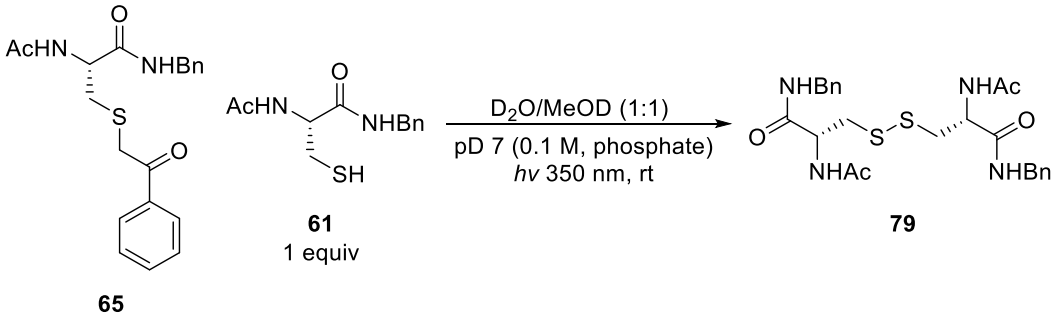

Scheme 1.52: Conversion of *N*-2-acetyl-*N*-benzyl-*S*-(2-oxo-2-phenylethyl)cysteinamide to the disulfide.

It was found that the formation of isothiazolone **80** was supressed by the addition of cysteine free thiol **61**, thus leading to almost exclusive formation of disulfide **79**. There were no signals at 4.9 and 8.5 ppm, which corresponds to isothiazolone **80** (Figure 1.9). The selective formation of disulfide **79** over isothiazolone **80** by trapping of phenacyl radicals supports our mechanism (Scheme 1.47). As isothiazolone **80** is not observed, this suggests that it is derived from a thioaldehyde/enethiolate **71** that arises from β-cleavage, which leads to thiyl radical **93** and ultimately isothiazolone **80** rather than a thioaldehyde/enethiolate **71** that arises from the Norrish Type II process, which we would not expect to be affected by external hydrogen atom donors. Thus, quenching of phenacyl radical **94** with cysteine free thiol **61** would lead to selective formation of disulfide **79** over isothiazolone **80**.

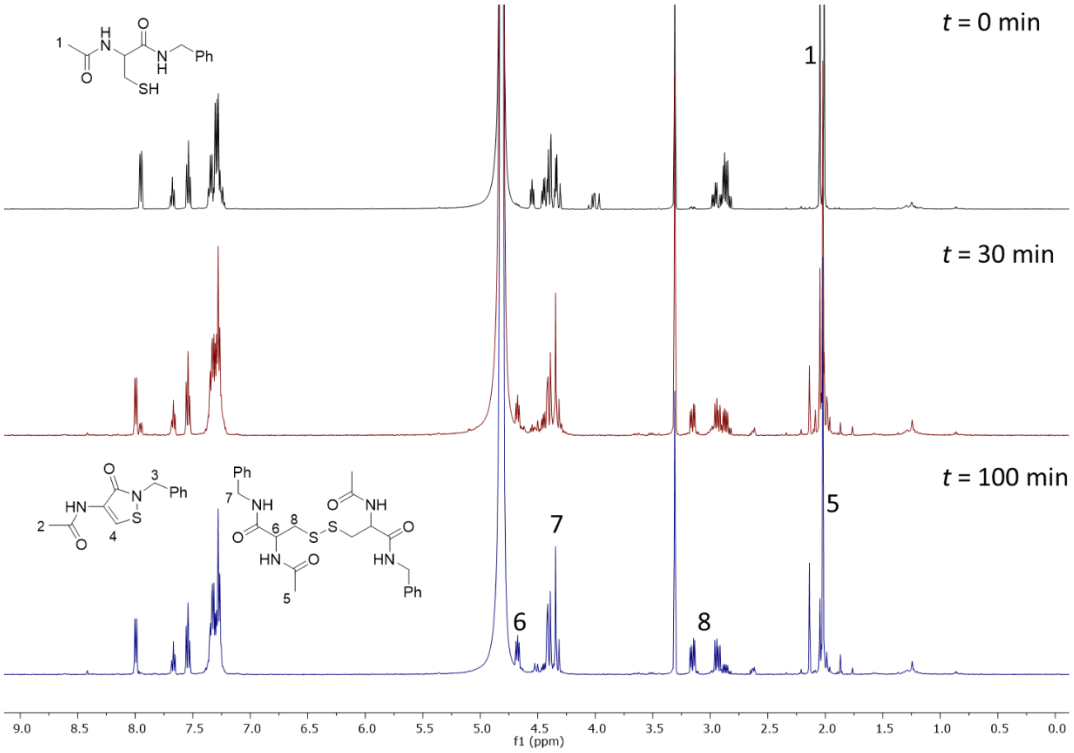

Figure 1.9: ^{1}H NMR spectrum of reaction mixture derived from *N*-2-acetyl-*N*-benzyl-*S*-(2-oxo-2-phenylethyl)cysteinamide and *N*-2-acetyl-*N*-benzylcysteinamide at *t* = 0, 30, and 100 minutes of photolysis.

1.3.5 Photolysis of Model Compounds: Electron-Donating Groups

The effect of electron-donating substituents was investigated using *N*-2-acetyl-*N*-benzyl-*S*-[2-(2,4-dimethoxyphenyl)-2-oxoethyl]cysteinamide **66**, which models Clark and Lowe's[64,65] protein substrate for thioaldehyde/enethiolate generation (Scheme 1.53).

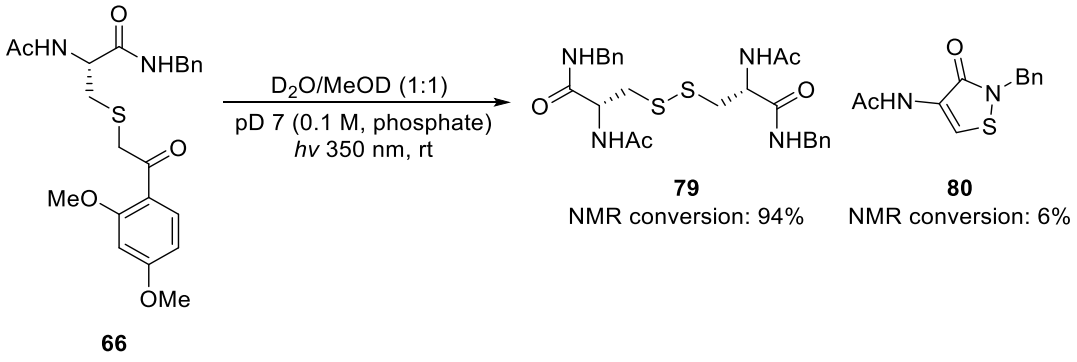

66

79
NMR conversion: 94%

80
NMR conversion: 6%

Scheme 1.53: Photolysis of *N*-2-acetyl-*N*-benzyl-*S*-[2-(2,4-dimethoxyphenyl)-2-oxoethyl]cysteinamide.

NMR analysis of the photolysis (Figure 1.10 and Scheme 1.53) showed the major product to be disulfide **79** (94% conversion) and only small amounts of isothiazolone **80** (6% conversion), compared with parent α-thioketone, **65**, which gave 57% conversion to disulfide **79** and 43% conversion to isothiazolone **80** (Scheme 1.43). This result is consistent with the work of Wagner, as described above in Section 1.3.3.2, who showed that electron-donating groups on the aromatic ring disfavours the formation of Norrish Type II products. It is surprising that Clark and Lowe got some conversion to the thioaldehyde; however, as their transformation was carried out on a protein substrate rather than on a small molecule substrate, it may take more time for the thiyl radicals to leave the solvent cage in a protein. Therefore, the intermolecular hydrogen transfer to form the thioaldehyde/enethiolate would be more favoured in a protein environment. In the case of our small molecule substrate the thiyl radical **93** could leave the solvent cage faster and undergo dimerization to disulfide **79** more efficiently.

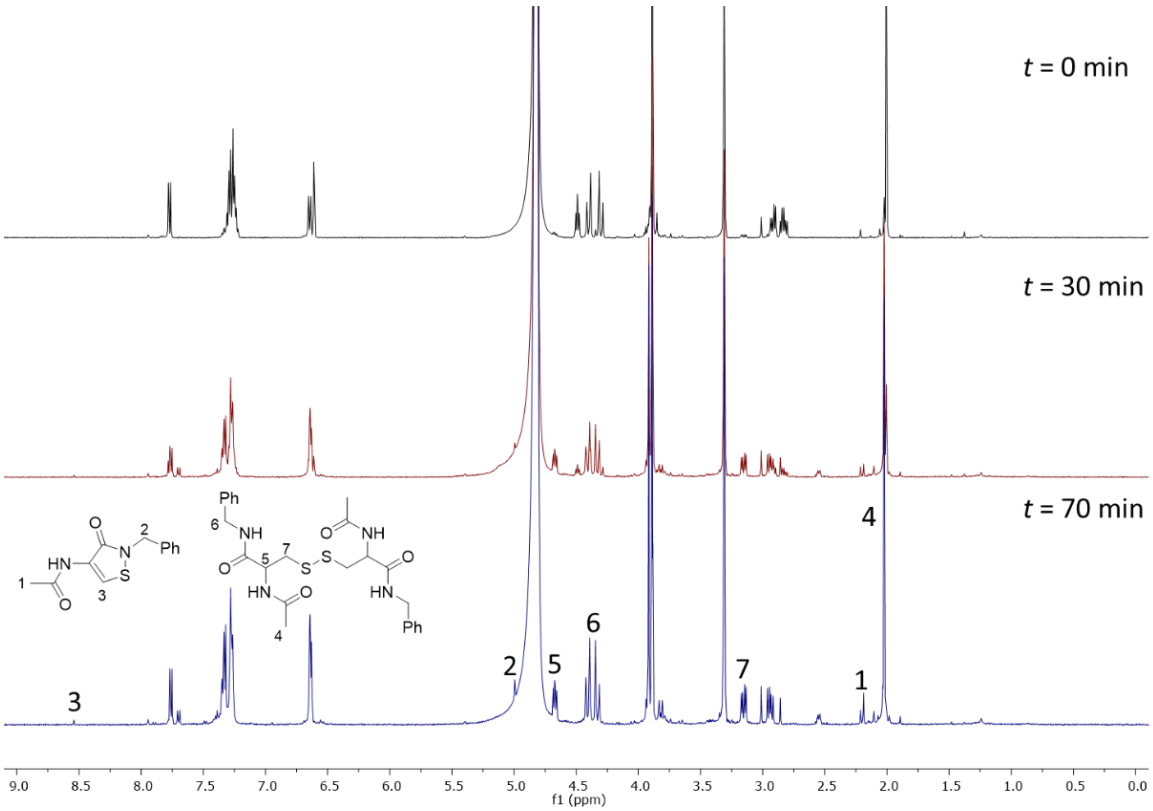

Figure 1.10: ^{1}H NMR spectrum of reaction mixture derived from *N*-2-acetyl-*N*-benzyl-*S*-[2-(2,4-dimethoxyphenyl)-2-oxoethyl]cysteinamide at t = 0, 30, and 70 minutes of photolysis.

1.3.6 Photolysis of Model Compounds: Electron-Withdrawing Groups

The effect of electron-withdrawing groups was also investigated. The cyano group was introduced at the *meta* position of the phenyl ring of parent α-thioketone **65**. Cyano substituents are known to inductively stabilize the n,π* triplet state and increase the electron deficiency of the carbonyl oxygen atom.[72] This inductive electron-withdrawing effect would therefore promote γ-hydrogen abstraction in the Norrish Type II process to form thioaldehyde/enethiolate intermediate **71**, which we believe undergoes intramolecular oxidative cyclization to isothiazolone **80**.

Irradiation of *N*-2-acetyl-*N*-benzyl-*S*-[2-(3-cyanophenyl)-2-oxoethyl]cysteinamide, **67**, led to the formation of both disulfide **79** and isothiazolone **80** products in 30% and 16% conversions respectively, however a new major product, enethiolate **71** (the conjugate base of the stable tautomer of the thioaldehyde), was also observed in 54% conversion (Scheme 1.54).

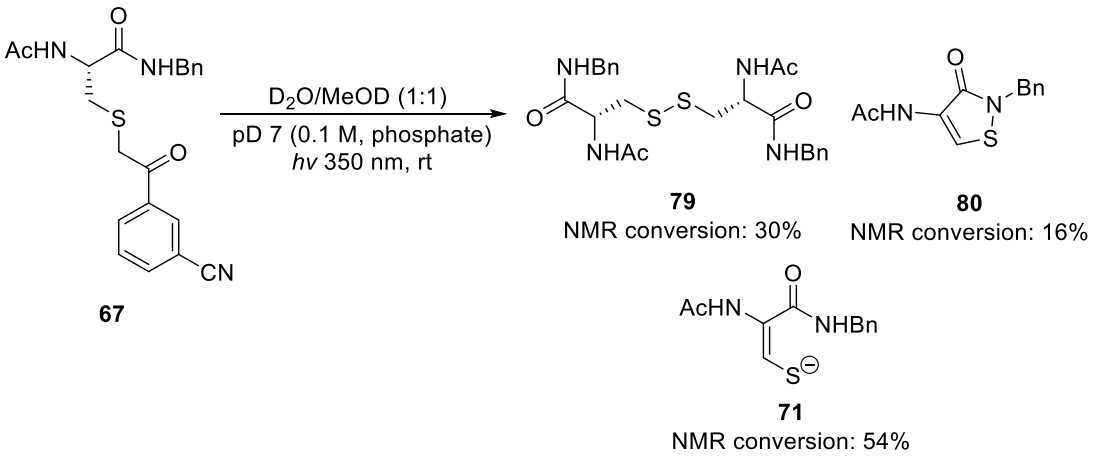

Scheme 1.54: Photolysis of *N*-2-acetyl-*N*-benzyl-*S*-[2-(3-cyanophenyl)-2-oxoethyl]cysteinamide.

HRMS analysis indicated the formation of the enethiolate as the major product. (HRMS (ESI) *m/z* (*M*+Na), $C_{12}H_{14}N_2O_2SNa$ calcd. 273.0674, observed 273.0668; (*M*−H), $C_{12}H_{13}N_2O_2S$ calcd. 249.0703, observed 249.0727). NMR monitoring of the photolysis reaction supported that enethiolate **71** had formed as the signals corresponded to those detected after the TCEP-mediated reduction of isothiazolone **80** to enethiolate **71** (Scheme 1.50 and Figure 1.8). The appearance of a new singlet at 2.14 ppm corresponds to enethiolate **71** methyl protons. The singlet at 4.4 ppm corresponds to enethiolate **71** benzylic CH_2 protons and the singlet at 8.0 ppm corresponds to the alkenyl proton next to the sulfur atom (Figure 1.11).

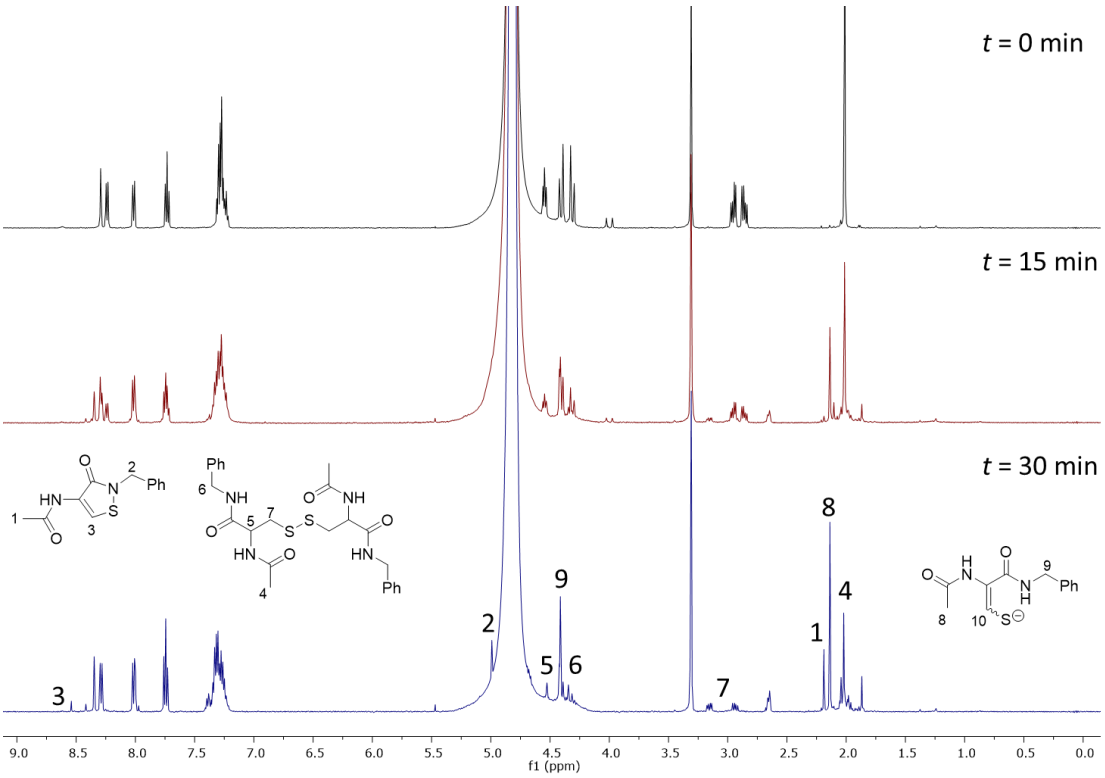

Figure 1.11: ^{1}H NMR spectrum of reaction mixture derived from *N*-2-acetyl-*N*-benzyl-*S*-[2-(3-cyanophenyl)-2-oxoethyl]cysteinamide at *t* = 0, 15, and 30 minutes of photolysis .

1.3.6.1 Thioaldehydes

Based on the above observation of enethiolate/thioaldehyde **71**, we looked to literature reports on thioaldehydes. In 1982, Vedejs *et al.* showed that thioaldehydes directly bearing an electron-withdrawing group (such as CN) could be generated photochemically (sunlamp irradiation) from phenacyl sulfides **107** and are excellent dienophiles. Trapping of these unstable intermediates was achieved by using 2-alkoxybutadienes **108** through a Diels–Alder reaction, which formed enol ether products, **109** and **110** (Scheme 1.55).[92]

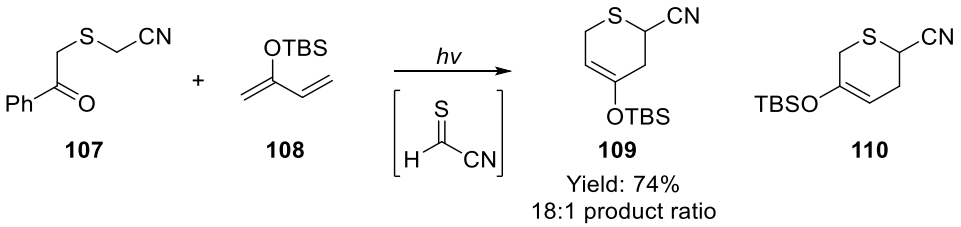

Scheme 1.55: Diels–Alder trapping of thioaldehydes using 2-alkoxybutadiene.[92]

Similarly, in 1984, Vedejs *et al.*[93] trapped thioaldehydes through 1,3-dipolar trapping with *tert*-butyldimethylsilyl nitronate ester to afford the corresponding [2+3] cycloadducts (compounds

111 and **112**). Cleavage of cycloadducts **111** and **112** (mixture of diastereomers) using $Bu_4N^+F^-$ gave the corresponding ketone or aldehyde products (compounds **113** and **114**) (Scheme 1.56). This reduction was proposed to go through a nitroso intermediate.

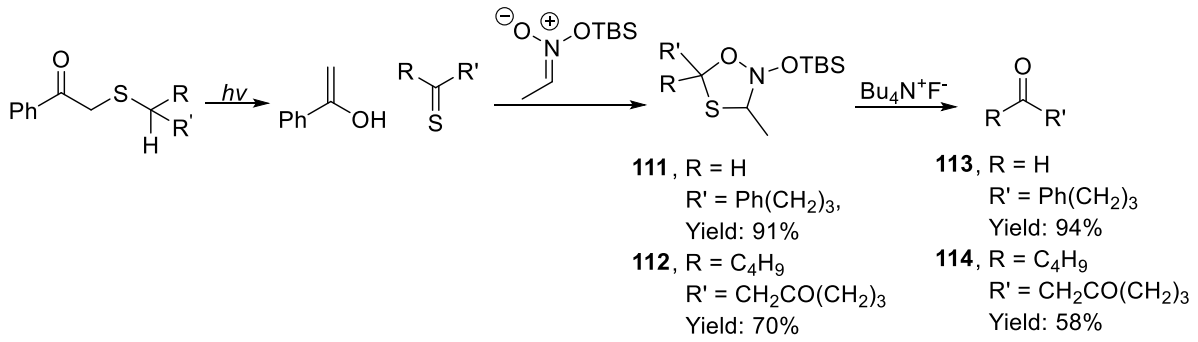

Scheme 1.56: Norrish Type II cleavage of phenacyl sulfides to thiocarbonyl compounds followed by 1,3-dipolar trapping with *tert*-butyldimethylsilyl nitronate ester and reduction to aldehyde/ketone.[93]

Vedejs *et al.*[94] observed and characterized the first aliphatic thioaldehyde, monomeric thiopivaldehyde using a photolytic (rather than thermolysis) procedure (Scheme 1.57). Irradiation of phenacyl sulfide **115** resulted in polymerization of the thioaldehyde. Polymer **116** was depolymerized with heating. Condensation of the volatile products followed by heating in inert solvents such as diethyl ether or chloroform gave thioaldehyde **117** in 40–50% yield and trimer **119**. Thioaldehyde **117** was found to be stable for many hours in inert solvents such as ether and chloroform. Thioaldehyde trapping was also carried out and cycloadducts were obtained in good yields when sufficiently reactive and photostable trapping agents were used such as nitronate esters (for [2+3] cycloaddition) and reactive dienes (for [2+4] cycloaddition); otherwise, thioaldehyde self-condensation and secondary photochemical reaction were observed.

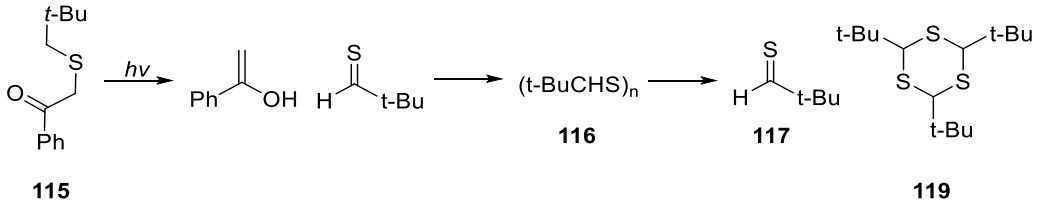

Scheme 1.57: Monomeric thiopivaldehyde formation.[94]

1.3.6. Photolysis of Model Compounds: Electron-Withdrawing Groups (Contd.)

The effect of a *para*-cyano group was investigated through the photolysis of *N*-2-acetyl-*N*-benzyl-*S*-[2-(4-cyanophenyl)-2-oxoethyl]cysteinamide, **68**. Conversions were determined by NMR analysis (Figure 1.12). High conversion (44%) to enethiolate **71** was observed. Conversion to disulfide **79** and isothiazolone **80** was 42% and 14% respectively (Scheme 1.58).

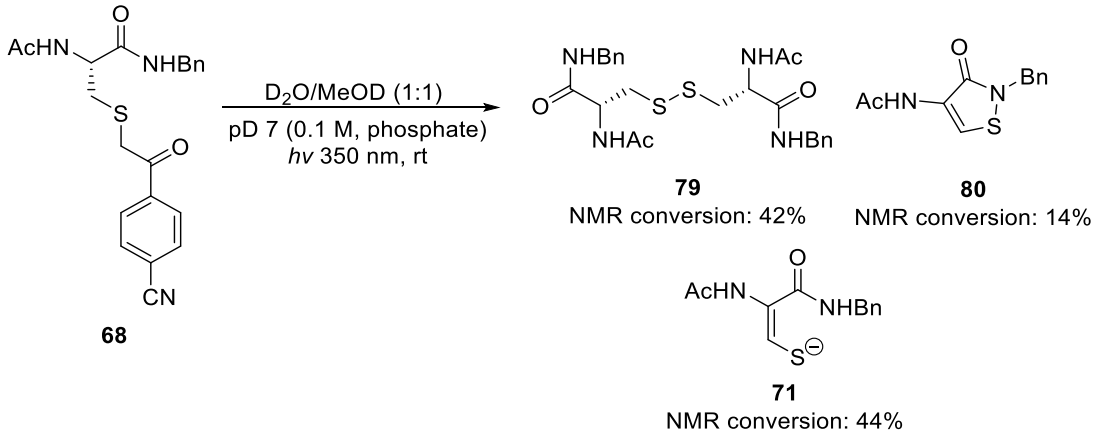

Scheme 1.58: Photolysis of *N*-2-acetyl-*N*-benzyl-*S*-[2-(4-cyanophenyl)-2-oxoethyl]cysteinamide.[93]

Cyano substituents at the *para* position stabilize the π,π* triplets by conjugation more than the n,π* triplets compared with the meta cyano where only the inductive effect applies.[72,75] Therefore this analogue (**68**) was expected to produce less of the thioaldehyde **71** compared with the *meta*-cyano analogue **67**.

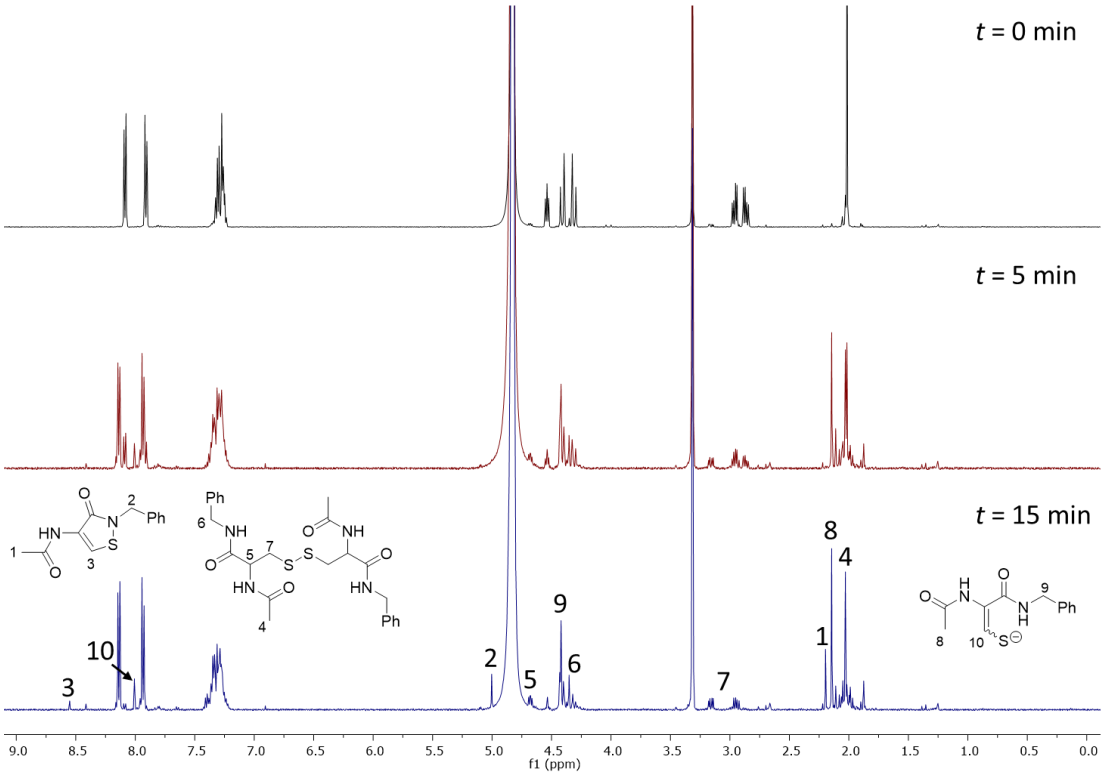

Figure 1.12: ^{1}H NMR spectrum of reaction mixture derived from *N*-2-acetyl-*N*-benzyl-*S*-[2-(4-cyanophenyl)-2-oxoethyl]cysteinamide at *t* = 0, 5, and 15 minutes of photolysis.

The effect of a *meta*-trifluoromethyl substituent on the Norrish Type II process was also investigated. NMR analysis was carried out throughout the photolysis of *N*-2-acetyl-*N*-benzyl-*S*-{2-oxo-2-[3-(trifluoromethyl)phenyl]ethyl}cysteinamide **69** (Scheme 1.59).

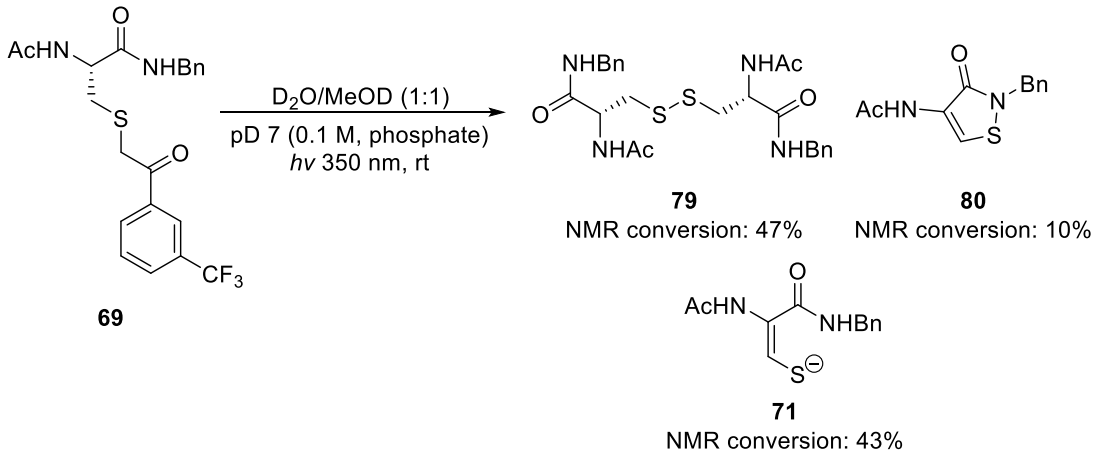

Scheme 1.59: Photolysis of *N*-2-acetyl-*N*-benzyl-*S*-{2-oxo-2-[3-(trifluoromethyl)phenyl]ethyl}cysteinamide.

NMR analysis showed high conversion to enethiolate **71** (43% conversion, Figure 1.13). Isothiazolone **80** and disulfide **79** were also observed with conversions of 10% and 47% respectively (Scheme 1.59 and Scheme 1.33).

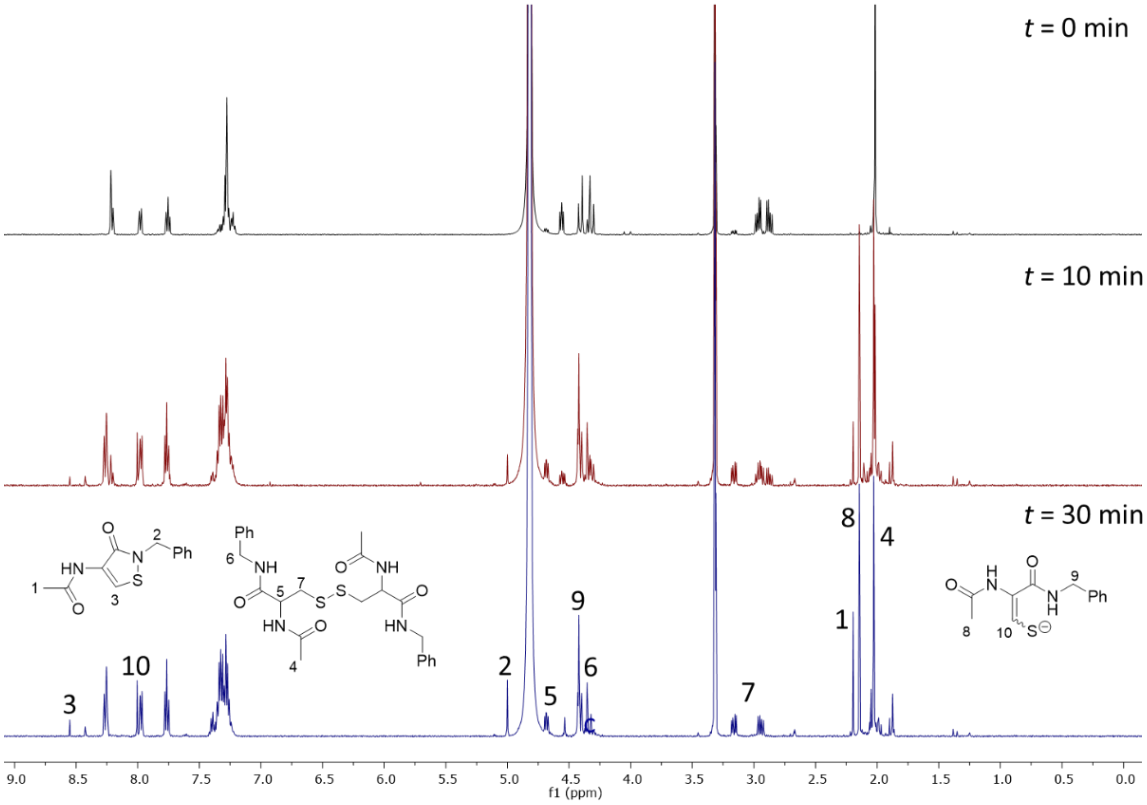

Figure 1.13: ^{1}H NMR spectrum of reaction mixture derived from *N*-2-acetyl-*N*-benzyl-*S*-{2-oxo-2-[3-(trifluoromethyl)phenyl]ethyl}cysteinamide at *t* = 0, 5, and 15 minutes of photolysis.

Based on the positive result obtained from *meta*-trifluoromethyl substitution (compound **69**) in which high conversion to enethiolate **71** was obtained, substrate **70** containing two *meta*-positioned trifluoromethyl groups was investigated to further increase the inductive effect and promote γ-hydrogen abstraction and the formation of enethiolate **71**. Photolysis of *N*-2-acetyl-*N*-benzyl-*S*-{2-oxo-2-[3′5′-(bistrifluoromethyl)phenyl]ethyl}cysteinamide **70** was monitored by NMR spectroscopy (Scheme 1.60).

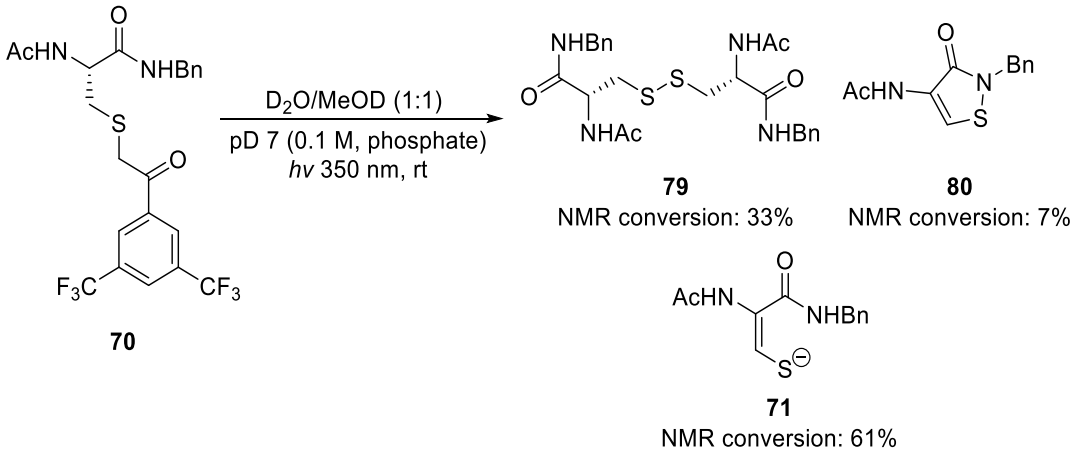

Scheme 1.60: Photolysis of *N*-2-acetyl-*N*-benzyl-*S*-{2-oxo-2-[3′5′-(bistrifluoromethyl)phenyl]ethyl}cysteinamide.

A significant increase in the amount of enethiolate **71** formed was observed, 61% conversion (Scheme 1.60 and Figure 1.14) compared with 43% observed after the photolysis of analogue **69**, which contained a single *meta*-trifluoromethyl substituent (Scheme 1.59). Disulfide **79** and isothiazolone **80** were also observed in 33% and 7% conversion respectively (Figure 1.14).

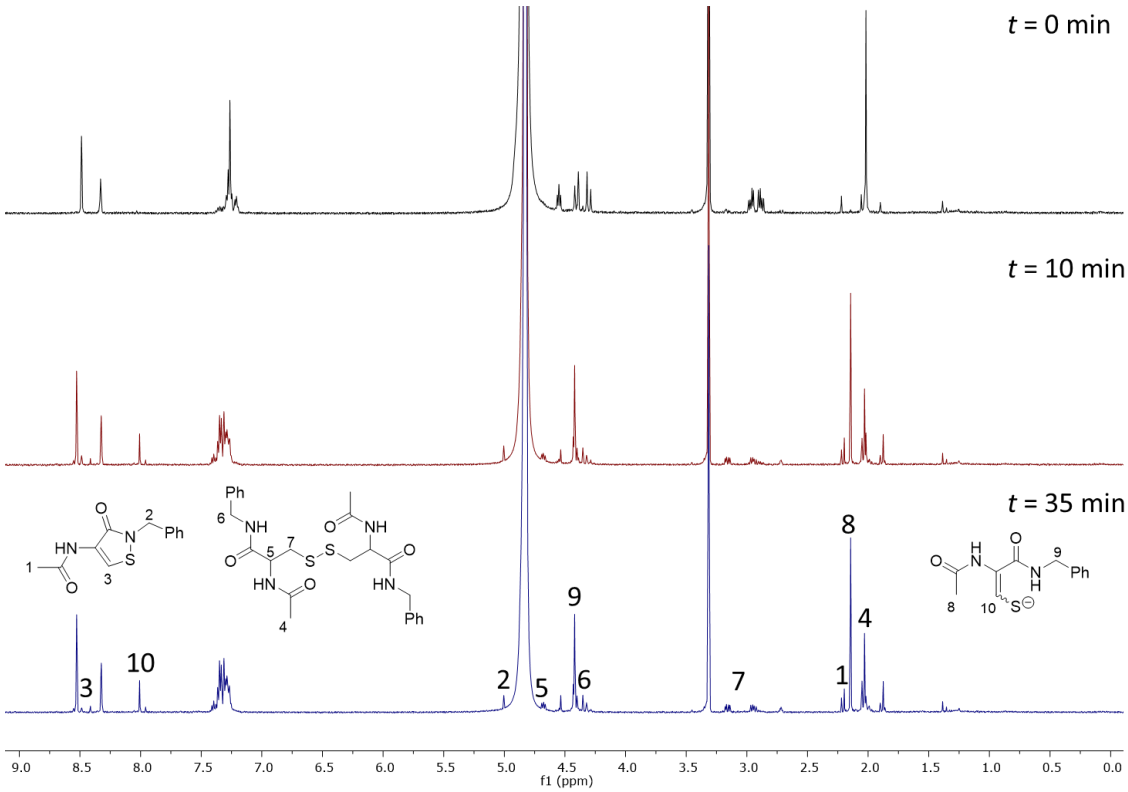

Figure 1.14: ^{1}H NMR spectrum of reaction mixture derived from *N*-2-acetyl-*N*-benzyl-*S*-{2-oxo-2-[3′5′-bis(trifluoromethyl)phenyl]ethyl}cysteinamide at *t* = 0, 10, and 35 minutes of photolysis.

1.3.7 Photolysis of Model Compounds: pH Effect

In addition to ring-substituent effects, the effect of pH was also investigated. Photolysis of parent α-thioketone, **65** was carried out in a 1:1 mixture of deuterated methanol and deuterated phosphate buffer (pD 8.6, 0.1 M) at 350 nm (Scheme 1.61). The photolysis reactions described earlier were carried out at pD 7.0.

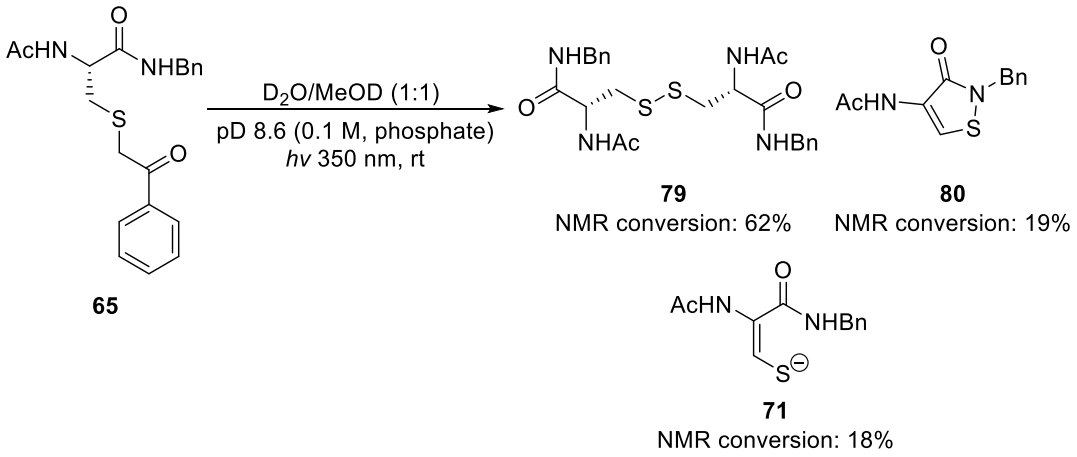

Scheme 1.61: Photolysis of *N*-2-acetyl-*N*-benzyl-*S*-(2-oxo-2-phenylethyl)cysteinamide pD 8.6.

NMR monitoring of the photolysis reaction showed the formation of a significant amount of enethiolate **71**, 18% (Scheme 1.61 and Figure 1.15); photolysis of the same compound, **65**, carried out at pD 7.0, showed no conversion to enethiolate **71** (Scheme 1.43). NMR monitoring of the photolysis of parent α-thioketone **65** at pD 8.6 showed singlets at 2.14, 4.4 and 8.0 ppm that correspond to enethiolate **71** methyl protons, benzylic CH_2 protons and the alkenyl proton next to the sulfur atom, respectively. Disulfide **79** and isothiazolone **80** were also observed in 62% and 18% conversions, respectively (Scheme 1.61 and Figure 1.15). A significant decrease in conversion into isothiazolone **80** (18%) at pD 8.6 was observed compared with 43% conversion at pD 7.0.

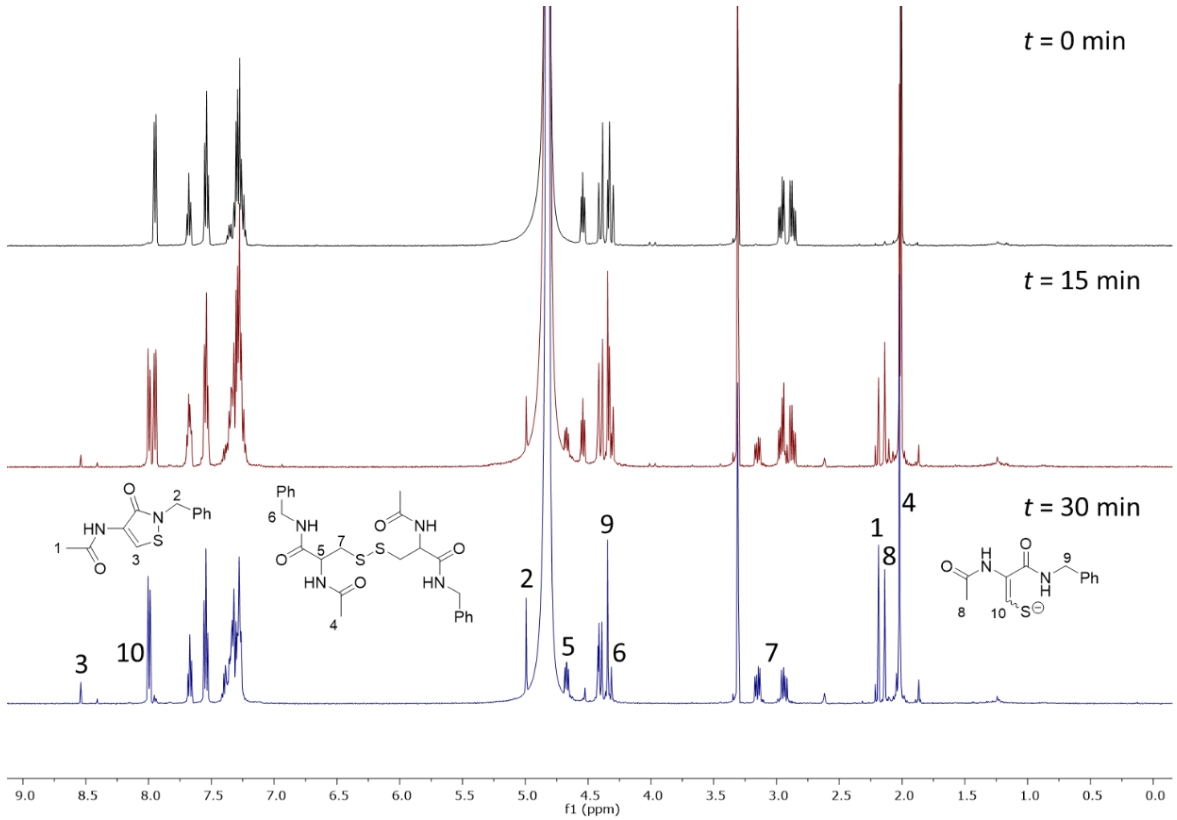

Figure 1.15: ^{1}H NMR spectrum of reaction mixture derived from *N*-2-acetyl-*N*-benzyl-*S*-(2-oxo-2-phenylethyl)cysteinamide at t = 0, 15, and 30 minutes of photolysis.

The higher pH appears to have increased the conversion to enethiolate **71** at the expense of isothiazolone **80**. This suggests that the pK_a value of the enethiol (tautomer of thioaldehyde) **71** may be close to that of cysteine. Enethiyl radical **96**, which we believe is an intermediate for the formation of isothiazolone **80** (Scheme 1.47), could form either through single electron transfer from the enethiolate or through hydrogen atom abstraction from the enethiol. A higher pH would increase the proportion of enethiolate and decrease the proportion of enethiol, therefore suggesting that enethiyl radical **96** is more efficiently generated through hydrogen atom transfer (Scheme 1.62).

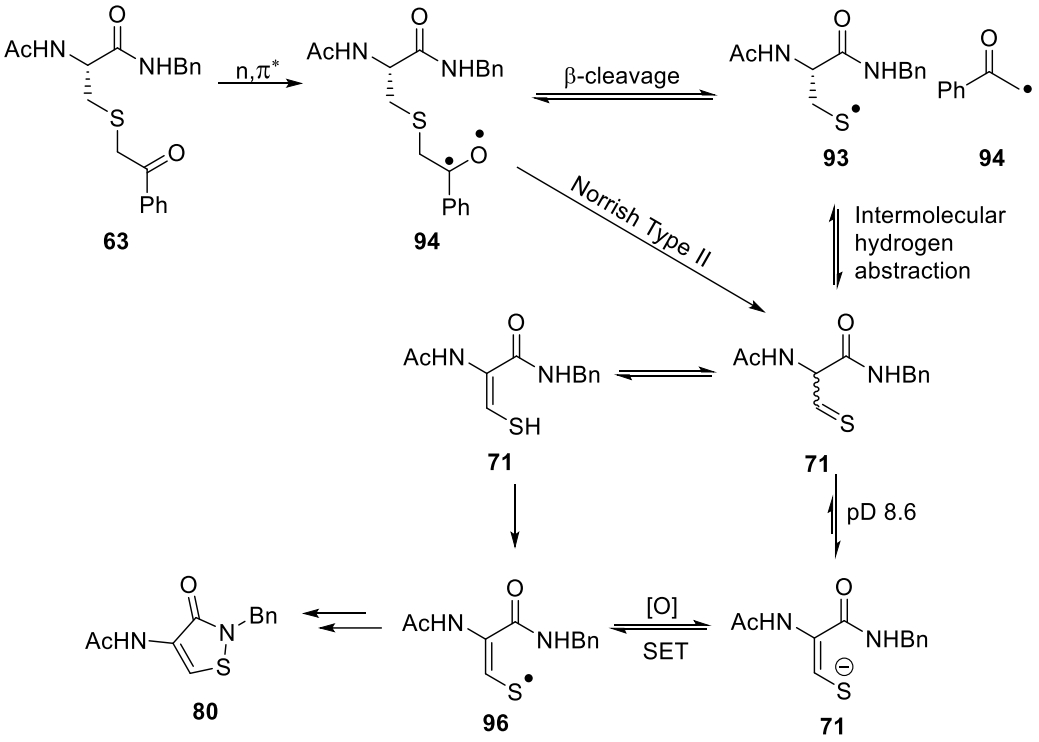

Scheme 1.62: Conversion to the enethiolate at pD 8.6.

Considering the positive result obtained for the photolysis of the parent compound, α-thioketone **65**, at pD 8.6, which gave a higher conversion to enethiolate **71**, compared with the same photolysis at pD 7.0 (Scheme 1.43), the photolysis of the *meta*-cyano analogue **67** was also carried out at pD 8.6 (Scheme 1.63).

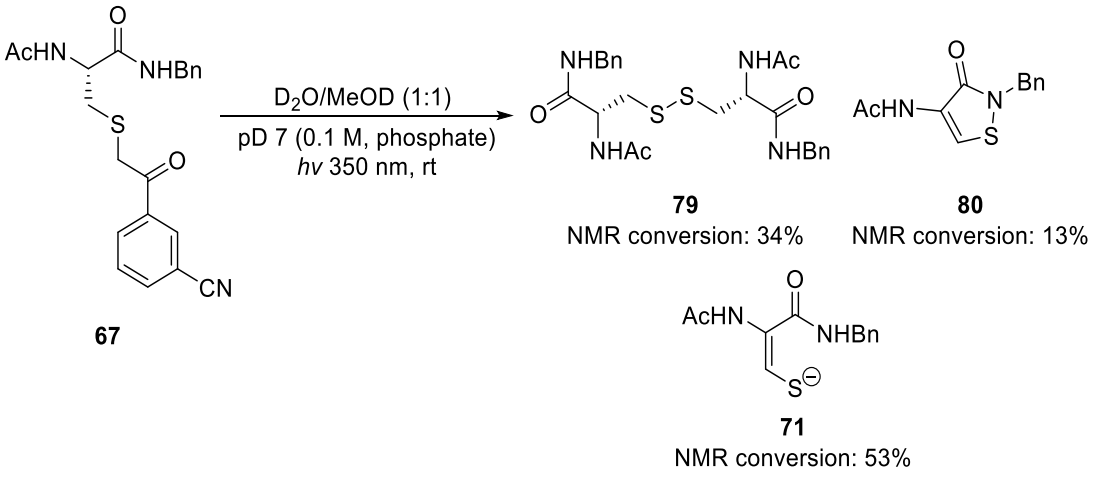

Scheme 1.63: Photolysis of *N*-2-acetyl-*N*-benzyl-*S*-[2-(3-cyanophenyl)-2-oxoethyl]cysteinamide at pD 8.6.

High conversion to enethiolate **71** was observed (53%). However, conversion was similar to that obtained for the photolysis at pD 7.0, which gave 54% conversion (Scheme 1.54 and Figure 1.11). Disulfide **79** and isothiazolone **80** were also observed in 34% and 13% conversion, respectively (Scheme 1.63 and Figure 1.16). This result is not consistent with the hypothesis provided above, suggesting that the increased formation of the isothiazolone at higher pH for the parent compound is due to another effect.

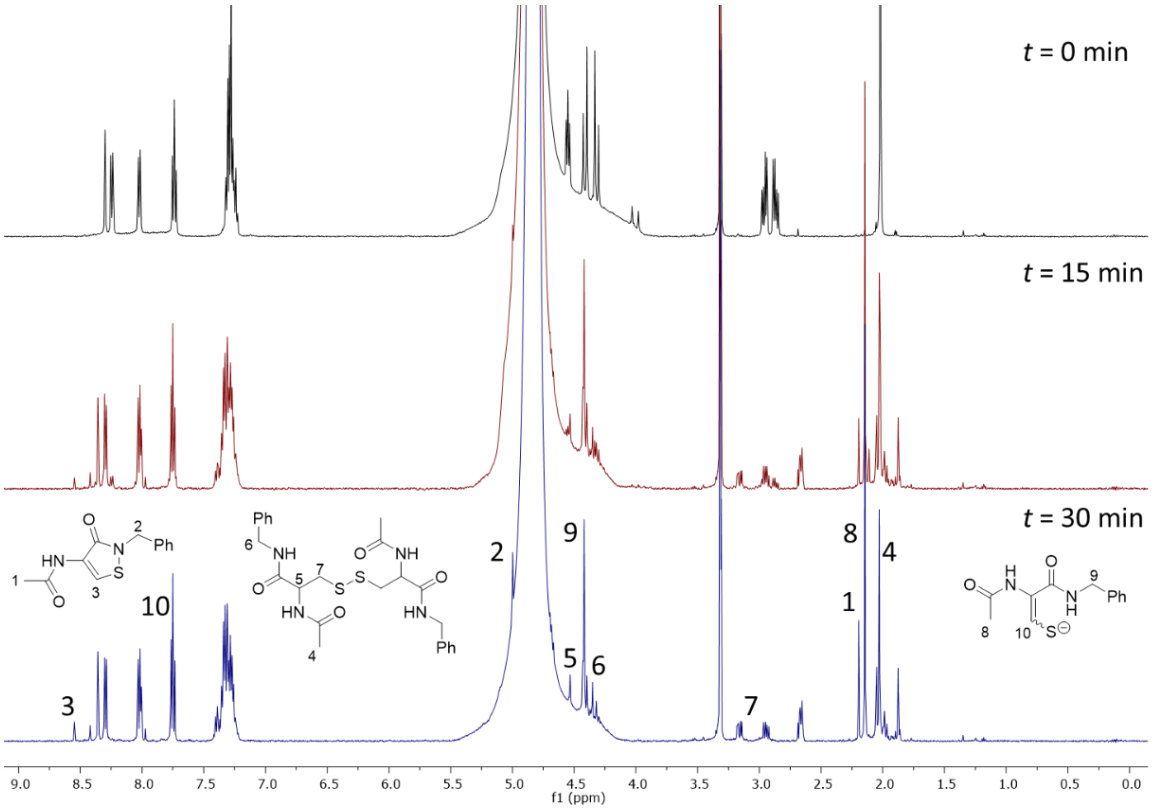

Figure 1.16: ^{1}H NMR spectrum of reaction mixture derived from *N*-2-acetyl-*N*-benzyl-*S*-[2-(3-cyanophenyl)-2-oxoethyl]cysteinamide at t = 0, 5, and 15 minutes of photolysis.

1.3.8 Conversion as Determined by NMR analysis

The conversion was calculated for each of the photolysis reactions of each model compound (compounds **65**–**70**) through integration of the NMR spectra of reaction mixtures (Table 1.3, Figure 1.17). The signal at 3.15 ppm, corresponding to the CH_2 (doublet of doublets) of disulfide **79** was used as a reference. The methyl signals for isothiazolone **80** (2.19 ppm) and enethiolate **69** (2.14 ppm) were integrated with respect to the reference. Each integration value (isothiazolone and enethiolate) was divided by the number of protons it corresponds to and was

expressed as a percentage of the total integral (disulfide reference, isothiazolone and enethiolate), giving the conversion (Table 1.3, Figure 1.17).

Table 1.3: Conversion as determined by NMR analysis.

Compound	Disulfide,**79** (%)	Isothiazolone, **80** (%)	Enethiolate, **71** (%)	Isothiazolone, **80** + Enethiolate, **71** (%)
65 (H)	57.5	42.5	0.0	42.5
66 (OMe)	94.0	6.0	0.0	6.0
67 (*m*-CN)	30.1	15.8	54.2	70.0
68 (*p*-CN)	42.2	13.6	44.3	57.9
69 (*m*-CF_3)	46.7	10.4	42.8	53.2
70 (*m*-$DiCF_3$)	32.8	6.7	60.6	67.3
65 (H, pD 8.6)	62.1	19.5	18.4	37.9
67(*m*-CN, pD 8.6)	34.0	12.9	53.1	66.0

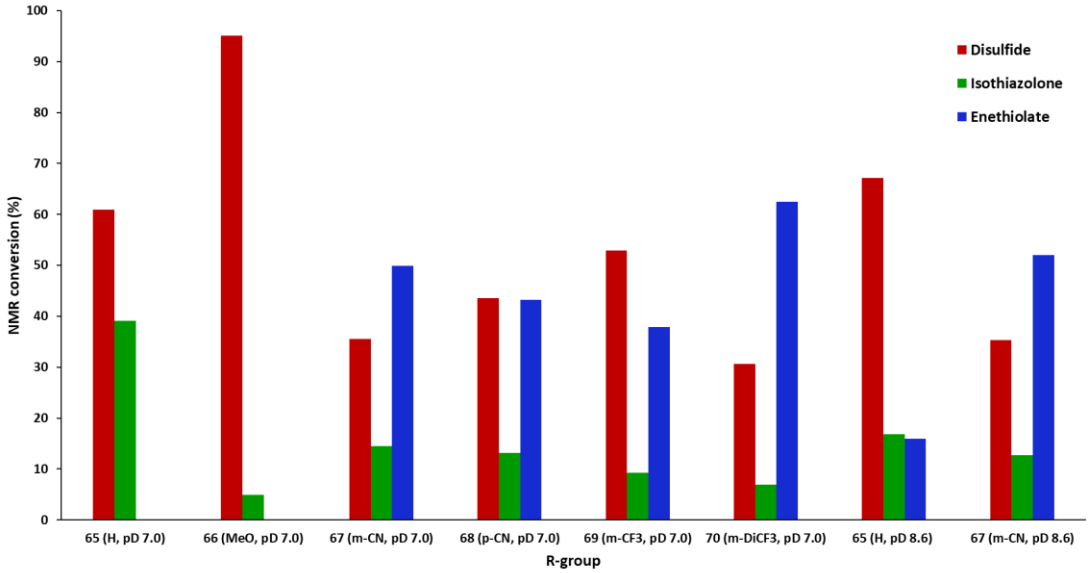

Figure 1.17: Bar chart showing conversions to disulfide, isothiazolone and enethiolate for each cysteine derivative.

Incorporation of electron donating groups (compound **66**) resulted in a significant increase in conversion to disulfide **79** (94%) compared with all α-thioketones (compounds **65**–**70**). Minor conversion to isothiazolone **80** (6%) and no enethiolate **71** was observed.

Incorporation of electron-withdrawing groups allowed a significant increase in conversion into enethiolate **71** as cyano substituents are known to inductively stabilize the n,π* triplet state and increase the electron deficiency of the carbonyl oxygen atom, thereby promoting the Norrish Type II process. The *meta*-cyano analogue **67** resulted in 54% conversion into enethiolate **71**

and the *para*-cyano analogue **68** gave 44% conversion into enethiolate **71**. The α-thioketone containing two *meta*-positioned trifluoromethyl groups (compound **70**) resulted in a significant 20% increase in conversion into the enethiolate **71** (61%) and the highest conversion compared with all other α-thioketones (**65**–**69**).

Photolysis of the parent α-thioketone **65** at pD 8.6 resulted in a significant increase in conversion to enethiolate **71** (18%) compared with the photolysis at pD 7.0, which gave no conversion to enethiolate **71**. The higher pH appears to have increased the conversion to enethiolate **71** at the expense of isothiazolone **80**.

Isothiazolone **80** is suspected to arise from thioaldehyde/enethiolate **71**. Enethiolate **71** could be formed from either the Norrish Type II process or β-cleavage to the thiyl radical **95** followed by intermolecular hydrogen abstraction within the solvent cage. Give the similar formation pathways of both isothiazolone **80** and enethiolate **71** the combined conversion was plotted against the conversion of disulfide **79** (Table 1.3 and Figure 1.18). The highest combined conversions were obtained from the with *meta*-cyano analogue **67** (70% conversion) and *meta*-bistrifluoromethyl analogue **70** (67% conversion).

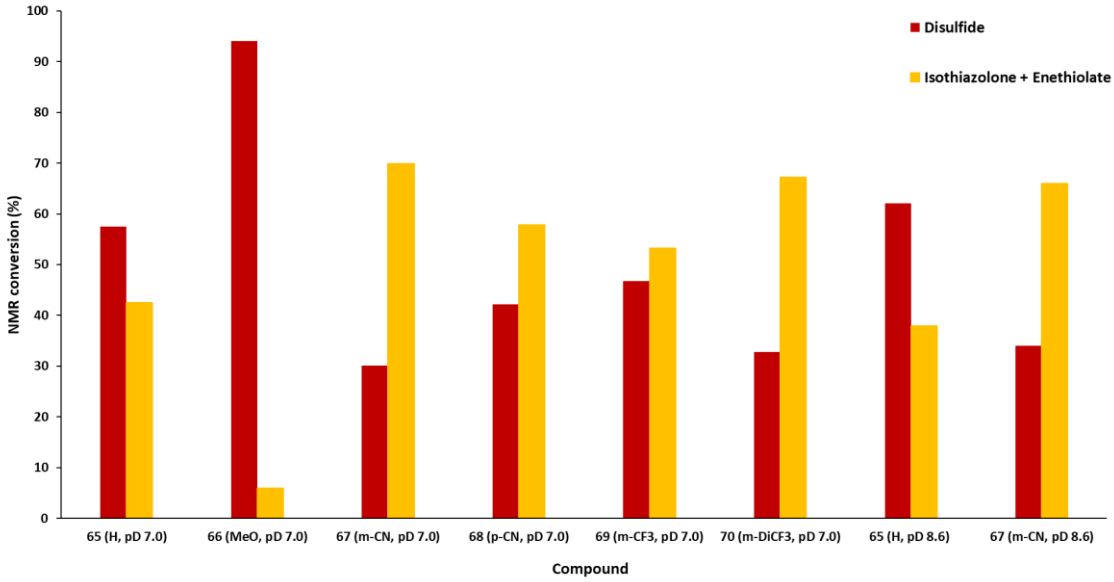

Figure 1.18: Bar chart showing conversions to disulfide **79** versus the combined conversion to isothiazolone **80** and enethiolate **71** for each cysteine derivative.

1.4 Summary and Conclusions

- A cysteine-based peptide model has been synthesized to mimic a cysteine residue embedded within a peptide or protein.
- Alkylation of the cysteine-based peptide model with a series of phenacyl bromide derivatives and under biologically ambient conditions generated a library of phenacyl sulfide derivatives in good yields.
- Exposure of the parent phenacyl sulfide to UV light allowed photofragmentation to occur, producing a disulfide and an isothiazolone. This novel isothiazolone has been fully characterized by NMR spectroscopy with a crystal structure also obtained.
- Reduction of the isothiazolone derivative was performed using TCEP. NMR spectroscopy and HRMS suggested that the expected product, the enethiolate, had formed.
- A mechanism for the formation of the disulfide and isothiazolone products has been proposed which suggests that both products arise from the excitation of the phenacyl sulfide to give an excited state triplet with 1,2-biradical character, followed by β-cleavage to give a thiyl radical. Dimerization of the thiyl radical or combination with a molecule of the phenacyl sulfide substrate are possible pathways suggested for disulfide formation. It has been proposed that the isothiazolone may arise from the thioaldehyde. The thioaldehyde could arise from two pathways; through intermolecular hydrogen abstraction by the phenacyl radical or the Norrish Type II process. The addition of cysteine thiol (cysteine-based peptide model) allowed the selective conversion to the disulfide through quenching of the intermediate phenacyl radicals, thus supressing the production of the isothiazolone.
- Incorporation of methoxy substituents onto the phenacyl sulfide allowed direct comparison with the current state of the art, i.e. the substrate used by Clark and Lowe to convert cysteine into serine through a thioaldehyde intermediate. An increased conversion to the disulfide with significantly less isothiazolone produced was observed. This observation showed that the identity of the biomolecule is important for this type of transformation as significantly more Norrish Type II activity was observed by Clark and Lowe rather than β-cleavage, perhaps owing to the more hindered exit of the thiyl radical from the solvent cage.
- Tuning of the reaction to promote the Norrish Type II process over β-cleavage was affected by the newly identified phenacyl bromide reagents that allowed the

incorporation of electron-withdrawing groups onto the phenacyl sulfide substrate. *Meta*-cyano, *para*-cyano and *meta*-trifluoromethyl substituents led to an approximate 40–50% increase in conversion to the enethiolate. The inductive electron-withdrawing effect was further increased through the incorporation of two *meta*-positioned trifluoromethyl groups onto the phenacyl sulfide substrate, which led to the highest conversion to the enethiolate (61%), i.e. a 20% increase compared with all other substrates.

- There have been no other reports of the use of this approach as a tool for the chemical modification of proteins or a more efficient process since Clark and Lowe[64,65] reported the inefficient conversion of cysteine into serine *via* a suspected thioaldehyde intermediate in the 1970s. Furthermore, given the use of the formylglycine-generating enzyme (FGE) as a currently used protein engineering tool for the oxidative transformation of the thiol group of cysteine (within a specific amino acid sequence) into an electrophilic aldehyde, this photochemical transformation has the potential to allow a bioconjugation handle (aldehyde or thioaldehyde) to be installed without the requirement for a specific amino sequence or extensive protein engineering.

1.5 Future Work

- This novel photoinitiated oxidative approach for the installation of a potential bioconjugation handle, a thioaldehyde, using our newly identified reagents will be directly compared with the formylglycine-generating enzyme (FGE), which is known to convert the thiol group of a cysteine residue (within a specific amino acid sequence) into an electrophilic aldehyde. The ability of the thioaldehyde/enethiolate to act as a bioconjugation handle will be investigated in short peptides and proteins and the reactivity of this handle will be explored using a variety of fluorescent probes. In addition, these reagents will also be investigated for the installation of a bioconjugation handle using proteins that contain cysteines in non-FGE sequences.
- As this approach can also be tuned to give high disulfide conversions, particularly with methoxy substituted phenacyl sulfides there is potential for applications in light-mediated crosslinking of cysteine-based peptides through disulfide bonds for hydrogel formation at physiological pH (pH 7.4) with spatiotemporal control (Scheme 1.64). Thiol-oxidation to a disulfide is a slow process under physiological pH (pH 7.4) and basic conditions or radical initiators, such as hydrogen peroxide, are required.[95]

Hydrogels have found numerous applications, including in tissue engineering, drug delivery and biosensing.[96]

- Targeted covalent inhibition is a potential application of this work through the photoinitiated generation of an isothiazolone (Scheme 1.64). Isothiazolones have been previously shown as a therapeutic approach against cancer through the inhibition of the telomerase enzyme through ring-opening by cysteine thiolates.

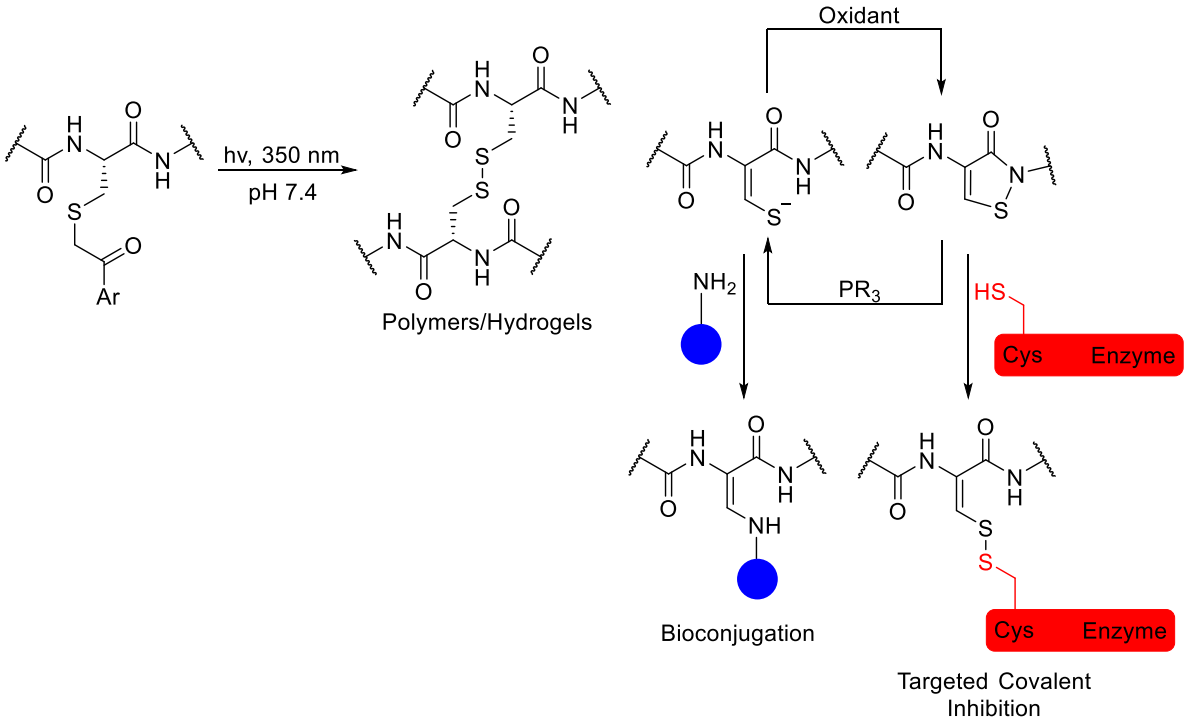

Scheme 1.64: Future applications of the photofragmentation of phenacyl sulfides.

1.6 Experimental

1.6.1 Materials

All reagents and solvents were obtained from Sigma Aldrich and were used without further purification except for 2-bromoacetophenone, 4-(2-bromoacetyl)benzonitrile, 3-(2-bromoacetyl)benzonitrile, 3-(trifluoromethyl)phenacyl bromide, 3′,5′-bis(trifluoromethyl)-2-bromoacetophenone, 2-bromo-1-(2,4-dimethoxyphenyl) ethanone, triethylsilane, methanol-d_4 (> 99.80% D), deuterium oxide (> 99.90% D), trifluoroacetic acid, and ethyl-2-cyano-2-(hydroxyamino)acetate, which were obtained from Fluorochem Ltd. Sodium hydroxide (analytical reagent grade) was obtained from Fischer Scientific. *N*-acetyl-*S*-(triphenylmethyl)cysteine was prepared as reported by Zheng et al.[67] Thin layer chromatography (TLC) was carried out on Merck TLC Silica gel 60 F_{254} plates by using a UV lamp (λ = 254 nm) for visualization. Flash column chromatography was carried out by using silica gel (Sigma Aldrich, technical grade, particle size 40–63 μm).

1.6.2 Measurements

Melting points were measured on a Stuart Scientific melting point apparatus SMP1. High-resolution mass spectrometry (HRMS) was carried out using ESI time-of-flight mass spectrometer (TOFMS) by using a Waters LCT Mass Spectrometry instrument. The precision of all accurate mass measurements was better than 5 ppm. NMR spectra were recorded using a Varian VNMRS 500 MHz spectrometer. The chemical shifts are in ppm relative to $SiMe_4$. ^{13}C NMR spectra were obtained with broadband proton decoupling. NMR assignments are supported by distortionless enhancement by polarization transfer (DEPT) and 2-D ^1H–^1H and ^1H–^{13}C correlation. Data are reported as follows: chemical shift in ppm, integration, multiplicity (s = singlet, d = doublet, t = triplet, q = quartet, sep = septet, m = multiplet, bs = broad singlet) and coupling constant in Hertz (Hz). Single crystal data was collected using an Oxford Diffraction Xcalibur system operated using the CrysAlisPro software and the data collection temperature was controlled at 298 K using a Cryojet system from Rigaku Oxford Diffraction. The crystal structures were solved using ShelxT version 2014/5[97] and refined using ShelxL version 2017/1[98] both of which were operated within the Oscail software package.[99] Photolysis was performed using a quartz NMR tube and a Rayonet photochemical reactor and 350 nm ultraviolet lamps.

1.6.3 Synthetic Procedures and Characterization

1.6.3.1 Preparation of Cysteine-Based Peptide Model

Preparation of 1-carboxy-2-sulfanylethan-1-aminium 4-methylbenzene-1-sulfonate (53)

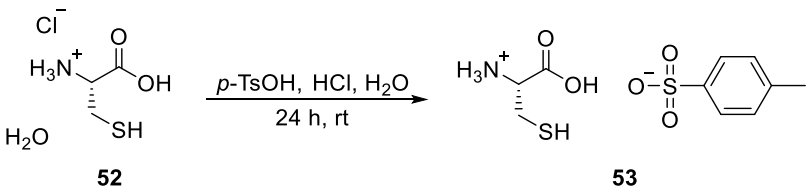

52 **53**

A solution of cysteine hydrochloride hydrate **52** (10 g, 0.056 mol) and concentrated HCl (36%, 2.54 mL) in water (20 mL) was added dropwise to a stirred solution of *p*-toluenesulfonic acid monohydrate (14.49 g, 0.076 mol) in water (6.35 mL) at room temperature. A white precipitate formed during the addition and a further 20 mL of water was added to facilitate stirring. The solution was stirred at room temperature for 24 h. The reaction mixture was filtered and the product was washed with a 10% solution of *p*-toluenesulfonic acid in water (30 mL). The product was dried under vacuum to give **53 as** a white solid (12.84 g, 77%) with spectral data (only ^{1}H NMR previously reported) consistent with the literature;[67] mp 228–230 ºC (lit. mp[100] 225–227 ºC); ν_{max} (neat, cm^{-1}) 3001, 1747, 1519, 1408, 1167, 1039, 1010; ^{1}H NMR (D_2O, 500 MHz) δ_H 2.24 (3H, s), 2.96 (1H, dd, J = 15.2, 4.3 Hz), 3.03 (1H, dd, J = 15.2, 5.6 Hz), 4.19 (1H, dd, J = 5.6, 4.3 Hz), 7.21 (2H, d, J = 8.1 Hz), 7.54 (2H, d, J = 8.1 Hz); ^{13}C NMR (D_2O, 125 MHz) δ_C 20.4 (CH_3), 23.8 (CH_2), 54.4 (CH), 125.3 (CH), 129.4 (CH), 139.3 (C), 142.4 (C), 170.1 (C=O).

Preparation of *S*-(triphenylmethyl)-L-cysteine 54

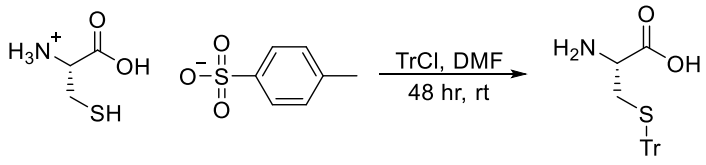

53 **54**

1-Carboxy-2-sulfanylethan-1-aminium 4-methylbenzene-1-sulfonate **53** (12.84 g, 0.043 mol) was dissolved in anhydrous DMF (44 mL). Trityl chloride (18.43 g, 0.066 mol) was added and the reaction mixture was stirred at room temperature under argon for 48 hours. Sodium acetate solution (10%, 220 mL) was added, forming a white precipitate, which was filtered. The

product was washed with water (30 mL), diethyl ether (50 mL) and dried under vacuum to give **54** as a white solid (13.57 g, 87%) with spectral data consistent with the literature;[67,101,102] mp 180–181 ºC (lit. mp[103] 201–202 ºC); ν_{max} (neat, cm^{-1}) 3055, 1594, 1489, 1442, 1391, 1337, 1299; ^{1}H NMR (DMSO-d_6, 500 MHz) δ_H 2.39 (1H, dd, J = 12.6, 9.1 Hz), 2.56 (1H, dd, J = 12.6, 4.3 Hz), 2.91 (1H, dd, J = 9.1, 4.3 Hz,), 7.21–7.24 (3H m,), 7.29–7.33 (12H, m); ^{13}C NMR (DMSO-d_6, 125 MHz) δ_C 33.9 (CH_2), 53.8 (CH), 66.5 (C), 127.2 (CH), 128.0 (C), 128.5 (CH), 129.6 (CH), 144.7 (C), 168.7 (C=O).

Preparation of *N*-acetyl-*S*-(triphenylmethyl)cysteine 55

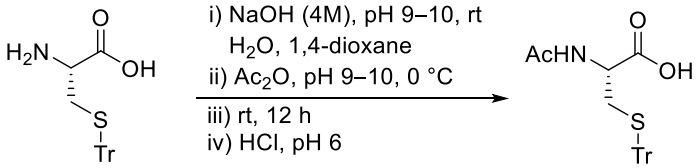

54 **55**

S-(triphenylmethyl)cysteine **54** (5.36 g, 0.015 mol) was added to 1,4-dioxane (30 mL) and water (30 mL) at room temperature. The pH of the solution was adjusted to 9–10 with aqueous NaOH (4 M). Acetic anhydride (2.80 mL, 0.029 mol) was added dropwise at 0 °C and the pH was maintained at 9–10 by the simultaneous addition of aqueous NaOH (4 M). The reaction mixture was stirred at room temperature for 12 hours. After 12 hours, the reaction mixture was acidified with aqueous HCl (2 M) to pH 6. The solvent was removed and the product was purified by flash column chromatography (EtOAc:MeOH:H_2O, 4:1:1) to give **55** as a pale yellow solid (5.80 g, 97%) with spectral data consistent with the literature;[67] mp 115–118 ºC (lit. mp[104] 108–110ºC); R_f 0.68 (EtOAc:MeOH:H_2O, 4:1:1); ν_{max} (neat, cm^{-1}) 3462, 3061, 1489, 1444, 1156, 1009; ^{1}H NMR (500 MHz, DMSO-d_6) δ_H 1.81 (3H, s), 2.34–2.43 (2H, m), 4.10–4.14 (1H, m), 7.19–7.31 (15H, m), 7.92 (1H, d, J = 8.0 Hz); ^{13}C NMR (DMSO-d_6, 125 MHz): δ_C 23.0 (CH_3), 34.6 (CH_2), 52.4 (CH), 66.1 (C), 127.1 (CH), 128.4 (CH), 129.5 (CH), 144.9 (C), 169.2 (C=O), 172.5 (C=O).

Preparation of N^2-acetyl-*N*-benzyl-*S*-(triphenylmethyl)cysteinamide 56

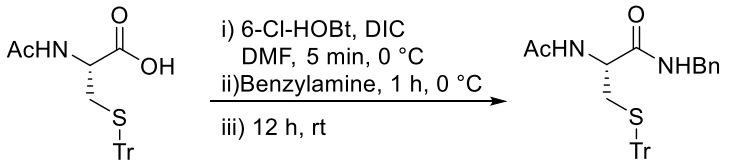

55 **56**

N-acetyl-*S*-(triphenylmethyl)cysteine **55** (2.83 g, 6.99 mmol), 6-Cl-HOBt (1.30 g, 7.68 mmol), DIC (1.17 mL, 7.68 mmol) were added to anhydrous DMF (57 mL, 0.89 mol) at 0 °C. The reaction mixture was stirred for 5 min to preactivate the acid and generate the active ester. Benzylamine (0.63 mL, 5.92 mmol) was added dropwise. The reaction was stirred at 0 °C for 1 hour and at room temperature overnight. The reaction mixture was filtered to remove the dicyclohexylurea side-product. The filtrate was diluted with ethyl acetate (50 mL) and washed with HCl (1 N, 2 × 20 mL), Na_2CO_3 (10%, 2 × 20 mL) and sat. NaCl (2 × 20 mL). The combined organic layers were dried ($MgSO_4$) and evaporated. The product was purified by flash column chromatography (EtOAc/MeOH/H_2O, 5:2:1) and obtained as a mixture containing diisopropylurea (1.69 g, 49%, 3.5:1 ratio); mp 140–141 ºC; R_f 0.55 (EtOAc/MeOH/H_2O, 5:2:1); ν_{max} (neat, cm^{-1}) 3339, 3263, 3029, 3058, 2968, 2926, 1631, 1555, 1489, 1443, 1245; ^{1}H NMR (500 MHz, $CDCl_3$) δ_H 1.85 (3H, s), 2.56 (1H, dd, J = 13.0, 6.0 Hz), 2.73 (1H, dd, J = 13.0, 7.0 Hz), 4.09–4.17 (1H, m), 4.36 (1H, dd, J = 14.9, 5.9 Hz), 4.28 (1H, dd, J = 14.9, 5.6 Hz), 6.11 (1H, d, J = 7.7 Hz), 6.52 (1H, app. t, J = 5.4 Hz), 7.18–7.27 (11H, m), 7.41 (4H, m); ^{13}C NMR (125 MHz, $CDCl_3$) δ_C 23.1 (CH_3), 33.4 (CH_2) 43.6 (CH_2), 52.3 (CH), 67.2 (C), 126.9 (CH), 127.5 (CH), 127.7 (CH), 128.1 (CH), 128.6 (CH), 129.5 (CH), 137.6 (C), 144.4 (C), 169.9 (C=O), 170.1 (C=O). HRMS (ESI) *m/z* $(M+H)^+$, $C_{31}H_{31}N_2O_2S$ calcd. 495.2106, observed 495.2120; $(M-H)$, $C_{31}H_{29}N_2O_2S$ calcd. 493.1950, observed 493.1949.

Preparation of N^2-acetyl-*N*-benzylcysteinamide 61

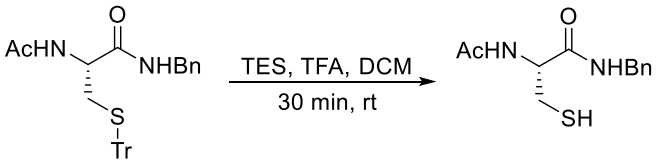

56 **61**

To a solution of N^2-acetyl-*N*-benzyl-*S*-(triphenylmethyl)cysteinamide **56** (4.67 g, 9.45 mmol) in anhydrous DCM (24 mL), trifluoroacetic acid (7.23 mL, 0.095 mol) was added dropwise at room temperature. The colour of the solution changed from colourless to yellow. Triethylsilane (3.77 mL, 0.024 mol) was added dropwise and the colour changed from yellow to colourless. The reaction mixture was stirred at room temperature for 30 mins. After 30 mins, the reaction mixture was concentrated under vacuum and purified using flash column chromatography (EtOAc/pet. ether, 5:1) to give the product as a white solid (1.19 g, 50%); mp 180–181 ºC (lit. mp[105] 164–166 ºC); R_f 0.36; ν_{max} (neat, cm^{-1}) 3282, 3086, 2930, 1541, 1736, 1630, 1535, 1452, 1369, 1242, 1225; ^{1}H NMR (500 MHz, $CDCl_3$) δ_H 1.63 (1H, dd, J = 10.0, 7.8 Hz), 2.00 (3H, s), 2.76 (1H, ddd, J = 13.8, 10.0, 7.0 Hz), 3.03 (1H, ddd, J = 13.8, 7.8, 4.6 Hz), 4.39–4.48 (2H, m), 4.61–4.65 (1H, m), 6.58 (1H, d, J = 7.5 Hz), 6.91 (1H, bs), 7.25–7.34 (5H, m); ^{13}C NMR (125 MHz, $CDCl_3$) δ_C 23.1 (CH_3), 26.7 (CH_2), 43.7 (CH_2), 54.3 (CH), 127.6 (CH), 127.7 (CH), 128.7, (CH), 137.6 (C), 169.7 (C=O), 170.4 (C=O); HRMS (ESI) *m/z* (M+H)$^+$, $C_{12}H_{17}N_2O_2S$ calcd. 253.1005, observed 253.1011; (M−H), $C_{12}H_{15}N_2O_2S$ calcd. 251.0854, observed 251.0859.

Preparation of *N*,*N′*-diacetyl-*N*,*N′*-dibenzylcystinamide (L-cystine) 79

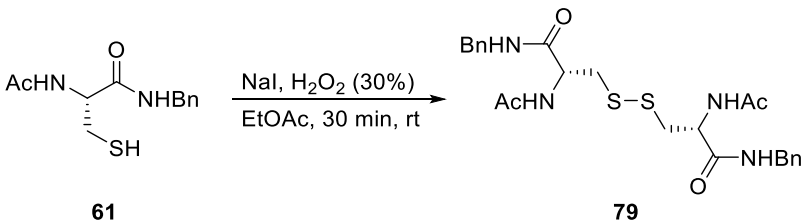

61 **79**

To a stirred solution of N^2-acetyl-*N*-benzylcysteinamide **61** (0.100 g, 0.396 mmol) in EtOAc (0.45 mL), sodium iodide (36 mg, 0.240 mmol) and 30% H_2O_2 (27 µL, 0.119 mmol) was added. The reaction mixture was stirred at room temperature for 30 min. The reaction mixture was diluted with DCM (10 mL) and washed with sat. Na_2CO_3 (2 × 10 mL). The combined organic

extracts were dried ($MgSO_4$), evaporated to dryness and purified by flash column chromatography (80:20 EtOAc/pet. ether) to give **79** (0.159 g, 80%) as a white solid; mp 230–233 ºC (mp[106] 216–220 ºC); R_f 0.125 (80:20 EtOAc/pet. ether); ν_{max} (neat, cm^{-1}) 3288, 3065, 2918, 1738, 1634, 1578, 1454, 1432, 1370, 1245, 1032; ^1H NMR (500 MHz, $CDCl_3$) δ_H 1.95 (6H, s), 2.89 (2H, dd, J = 14.8, 11.0 Hz), 3.01 (2H, dd, J = 14.8, 3.3 Hz), 4.41 (2H, dd, J = 14.8, 5.4 Hz), 4.47 (2H, dd, J = 14.8, 5.7 Hz), 5.34–5.39 (2H, m), 6.47 (2H, d, J = 9.3 Hz), 7.26–7.27 (5H, m), 7.32–7.33 (5H, m), 8.54 (2H, bs); ^{13}C NMR (125 MHz, $CDCl_3$) δ_C 23.3 (CH_3), 29.7 (CH_2), 43.7 (CH_2), 46.6 (CH_2), 53.4 (CH), 127.3 (CH), 127.8 (CH), 128.5 (CH), 137.7 (C), 170.0 (C=O), 170.3 (C=O). HRMS (ESI) *m/z* (M+H)$^+$, $C_{24}H_{31}N_4O_4S_2$ calcd. 503.1787, observed 503.1790; (M+Na), $C_{24}H_{31}N_4O_4S_2Na$ calcd. 525.1606, observed 525.1612.

1.6.3.2 Alkylation of Cysteine-Based Peptide Model

General Procedure for Alkylation of N^2-acetyl-*N*-benzylcysteinamide 61

To a solution of N^2-acetyl-*N*-benzylcysteinamide **61** (0.1 g, 0.40 mmol) in DMF (0.2 mL) and phosphate buffer (0.1 M, 1.6 mL, pH 9) at room temperature the bromoacetophenone (0.44 mmol, 1.1 equiv) was added. The reaction mixture was stirred at room temperature for 12 h. After 12 h, the reaction mixture was diluted with water (10 mL) and extracted with DCM (3 × 10 mL). The combined organic extracts were washed with aqueous lithium chloride solution (5%, 3 × 10 mL) and dried ($MgSO_4$). The solvent was evaporated and all residues of products were purified with flash column chromatography with isocratic elution of EtOAc and pet. ether.

Compound Data

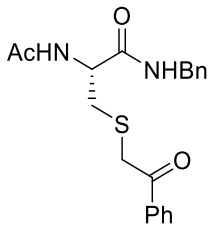

***N^2*-acetyl-*N*-benzyl-*S*-(2-oxo-2-phenylethyl)cysteinamide 65**: (In accordance with the general alkylation procedure, section 1.6.3.2, using 2-bromoacetophenone, 0.09 g, 0.44 mmol) 0.090 g, 62%; white solid; mp 148–149 °C; R_f 0.26 (80:20 EtOAc/pet. ether); ν_{max} (neat, cm^{-1}) 3269, 3064, 2927, 1739, 1675, 1630, 1543, 1445, 1368, 1277, 1235, 1015; ^1H NMR (500 MHz,

$CDCl_3$) δ_H 1.98 (s, 3H), 2.79 (1H, dd, J = 14.1, 7.0, Hz), 3.02 (1H, dd, J = 14.1, 5.7 Hz,), 4.04 (2H, s), 4.39–4.47 (2H, m), 4.64 (1H, m), 6.98 (1H, d, J = 7.2 Hz), 7.22–7.31 (5H, m), 7.44–7.47 (3H, m), 7.58 (1H, app. t, J = 7.4 Hz), 7.93 (2H, d, J = 7.5 Hz); ^{13}C NMR (125 MHz, $CDCl_3$) δ_C 23.1 (CH_3), 35.3 (CH_2), 39.0 (CH_2), 43.7 (CH_2), 52.3 (CH), 127.4 (CH), 127.6 (CH), 128.6 (CH), 128.6 (CH), 128.8 (CH), 133.9 (CH), 135.2 (C), 137.7 (C), 170.0 (C=O), 170.4 (C=O), 196.9 (C=O); HRMS (ESI) *m/z* (M+H)$^+$, $C_{20}H_{23}N_2O_3S$ calcd. 371.1429, observed 371.1415.

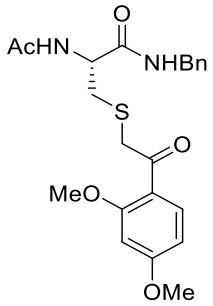

***N*^{2}-acetyl-*N*-benzyl-*S*-[2-(2,4-dimethoxyphenyl)-2-oxoethyl]cysteinamide 66**: (In accordance with the general alkylation procedure, section 1.6.3.2, using 2-bromo-1-(2,4-dimethoxyphenyl)-ethanone, 0.113 g, 0.437 mmol) 0.133 g, 78%; white solid; mp 210–211 °C; R_f 0.11 (80:20 EtOAc/pet. ether); ν_{max} (neat, cm^{-1}) 3267, 3067, 2920, 1735, 1663, 1630, 1602, 1544, 1498, 1455, 1415, 1368, 1291, 1213, 1160, 1128, 1025; ^{1}H NMR (500 MHz, $CDCl_3$) δ_H 2.01 (3H, s), 2.74 (1H, dd, J = 14.1, 7.1 Hz), 3.04 (1H, dd, J = 14.1, 5.6 Hz), 3.85 (3H, s), 3.89 (3H, s), 4.01 (1H, d, J = 16.1 Hz), 4.09 (1H, d, J = 16.1 Hz), 4.45–4.46 (2H, m), 4.58–4.62 (1H, m), 6.44 (1H, d, J = 2.1 Hz), 6.53 (1H, dd, J = 8.8, 2.1 Hz), 7.12 (1H, d, J = 7.1 Hz), 7.24–7.32 (5H, m), 7.53 (1H, m), 7.86 (1H, d, J = 8.8 Hz); ^{13}C NMR (125 MHz, $CDCl_3$) δ_C 23.1 (CH_3), 35.2 (CH_2), 43.6 (CH_2), 44.0 (CH_2), 52.7 (CH), 55.6 (OMe), 55.6 (OMe), 98.3 (CH), 105.8 (CH), 118.8 (C), 127.3 (CH), 127.5 (CH), 128.6 (CH), 133.5 (CH), 137.9 (C), 161.2 (C), 165.3 (C), 170.2 (C=O), 170.4 (C=O), 195.3 (C=O); HRMS (ESI) *m/z* (M+H)$^+$, $C_{22}H_{25}N_2O_5S$ calcd. 431.1641, observed 431.1634.

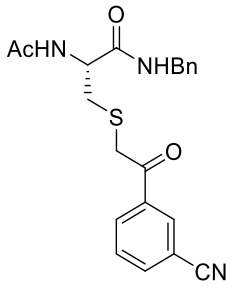

***N*²-acetyl-*N*-benzyl-*S*-[2-(3-cyanophenyl)-2-oxoethyl]cysteinamide 67**: (In accordance with the general alkylation procedure, section 1.6.3.2, using 3-(2-bromoaceytl)benzonitrile, 0.1 g, 0.436 mmol) 0.092 g, 60%; white solid; mp 113–115 °C; R_f 0.12 (80:20 EtOAc/pet. ether); ν_{max} (neat, cm^{-1}) 3011, 2989, 2596, 1716, 1625, 1580, 1561, 1462, 1415, 1282, 1214, 1130, 1100, 1028; ^{1}H NMR (500 MHz, $CDCl_3$) δ_H 2.01 (3H, s), 2.80 (1H, dd, *J* = 14.2, 7.1 Hz), 2.99 (1H, dd, *J* = 14.2, 5.7 Hz), 4.04 (2H, s), 4.40–4.50 (2H, m), 4.61–4.66 (1H, m), 6.78 (1H, d, *J* = 7.5 Hz), 7.28–7.34 (6H, m), 7.61 (1H, app. t, *J* = 7.8 Hz), 7.86 (1H, d, *J* = 7.7 Hz), 8.15 (1H, d, *J* = 8.0 Hz), 8.22 (1H, s); ^{13}C NMR (125 MHz, $CDCl_3$) δ_C 23.1 (CH_3), 35.1 (CH_2), 38.5 (CH_2), 43.7 (CH_2), 52.1 (CH), 113.4 (C), 117.7 (C), 127.6 (CH), 127.6 (CH), 128.7 (CH), 129.8 (CH), 132.3 (CH), 132.5 (CH), 136.0 (C), 136.5 (CH), 137.6 (C), 169.8 (C=O), 170.4 (C=O), 193.5 (C=O); HRMS (ESI) *m/z* (*M*−H), $C_{21}H_{20}N_3O_3S$ calcd. 394.1225, observed 394.1221.

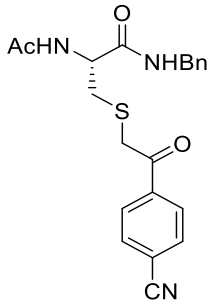

***N*²-acetyl-*N*-benzyl-S-[2-(4-cyanophenyl)-2-oxoethyl]cysteinamide 68**: (In accordance with the general alkylation procedure, section 1.6.3.2, using 4-(2-bromoaceytl)benzonitrile, 0.1 g, 0.437 mmol) 0.074 g, 47%; white solid; mp 150–151 °C; R_f 0.18 (80:20 EtOAc/pet. ether); ν_{max} (neat, cm^{-1}) 3272, 3065, 2232, 1738, 1631,1537, 1454, 1370, 1275, 1201, 1107; ^{1}H NMR (500 MHz, $CDCl_3$) δ_H 2.04 (3H, s), 2.79 (1H, dd, *J* = 14.3, 7.3, Hz), 3.02 (1H, dd, *J* = 14.3, 5.3 Hz), 4.07 (1H, d, *J* = 16.0 Hz), 4.11 (1H, d, *J* = 16.0 Hz), 4.44–4.51 (2H, m), 4.58 (1H, m), 6.71 (1H, d, *J* = 7.4 Hz), 7.15 (1H, bs), 7.27–7.36 (5H, m), 7.78 (2H, d, *J* = 8.2 Hz), 8.04 (2H, d, *J* = 8.2 Hz); ^{13}C NMR (125 MHz, $CDCl_3$) δ_C 23.2 (CH_3), 35.2 (CH_2), 38.9 (CH_2), 43.7 (CH_2),

52.1 (CH), 117.0 (C), 117.7 (C), 127.6 (CH), 127.6 (CH), 128.7 (CH), 129.0 (CH), 132.6 (CH), 137.6 (C), 138.3 (C), 169.8 (C=O), 170.3 (C=O), 194.4 (C=O); HRMS (ESI) *m/z* (*M*+H)$^+$, $C_{21}H_{22}N_3O_3S$ calcd. 396.1382, observed 396.1401.

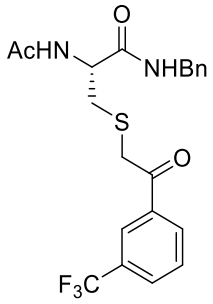

***N*^{2}-acetyl-*N*-benzyl-*S*-{2-oxo-2-[3-(trifluoromethyl)phenyl]ethyl} cysteinamide 69**: (In accordance with the general alkylation procedure, section 1.6.3.2, using 3-(2-trifluoromethyl)phenacyl bromide, 0.12 g, 0.436 mmol) 0.10 g, 60%; white solid; mp 128–129 °C; R_f 0.36 (80:20 EtOAc/pet. ether); ν_{max} (neat, cm^{-1}) 3279, 3090, 2928, 1738, 1693, 1632, 1535, 1497, 1373, 1330, 1166, 1120, 1071; ^{1}H NMR (500 MHz, $CDCl_3$) δ_H 1.94 (3H, s), 2.85 (1H, dd, *J* = 14.1, 6.9 Hz), 2.97 (1H, dd, *J* = 14.1, 6.1 Hz), 4.01 (2H, s), 4.37 (1H, dd, *J* = 15.0, 5.7 Hz), 4.43 (1H, dd, *J* = 15.0, 5.8 Hz), 4.75 (1H, m), 7.07 (1H, d, *J* = 7.7 Hz), 7.21–7.30 (5H, m), 7.59 (2H, m), 7.82 (1H, d, *J* = 7.8), 8.09 (1H, d, *J* = 1H, 7.8 Hz), 8.18 (1H, s); ^{13}C NMR (125 MHz, $CDCl_3$) δ_C 22.9 (CH_3), 35.0 (CH_2), 38.2 (CH_2), 43.6 (CH_2), 52.1 (CH), 123.5 (q, *J* = 271.1 Hz, CF_3), 124.6 (C), 125.4 (q, *J* = 3.7 Hz, CHCCF$_3$), 126.8 (C), 127.4 (CH), 127.5 (CH), 128.6 (CH), 129.4 (CH), 130.0 (q, *J* = 3.7 Hz, CHCCF$_3$), 131.4 (q, *J* = 32.9 Hz, CCF$_3$), 131.8 (CH), 170.2 (C=O), 170.6 (C=O), 194.0 (C=O); HRMS (ESI) *m/z* (*M*+Na), C21H21$N_2O_3F_3S$ calcd. 461.1123, observed 461.1132.

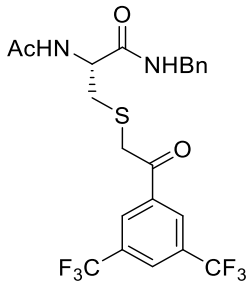

***N*^{2}-acetyl-*N*-benzyl-*S*-{2-[3,5-bis(trifluoromethyl)phenyl]-2-oxoethyl} cysteinamide 70**: (In accordance with the general alkylation procedure, section 1.6.3.2, using 3′5-

bis(trifluoromethyl)-2-bromoacetophenone, 0.146 g, 0.437 mmol) 0.125 g, 62%; white solid; mp 146–147 °C; R_f 0.41 (80:20 EtOAc/pet. ether); ν_{max} (neat, cm^{-1}) 3273, 3091, 2934, 1688, 1631, 1537, 1380, 1276, 1254, 1171, 1120, 1109; ^{1}H NMR (500 MHz, $CDCl_3$) δ_H 1.95 (3H, s), 2.86 (1H, dd, J = 14.1, 7.0 Hz), 2.96 (1H, dd, J = 14.1, 6.0 Hz), 4.03 (2H, s), 4.38 (1H, dd, J = 14.9, 5.7 Hz), 4.44 (1H, dd, J = 14.9, 5.8 Hz), 4.76 (1H, m), 6.93 (1H, d, J = 7.9 Hz), 7.22–7.31 (5H, m), 7.46 (1H, app. t, J = 5.6 Hz), 8.08 (1H, s), 8.36 (2H, s); ^{13}C NMR (125 MHz, $CDCl_3$) δ_C 23.0 (CH_3), 34.9 (CH_2), 38.0 (CH_2), 43.7 (CH_2), 52.0 (CH), 122.8 (q, J = 271.5 Hz, CF_3), 126.7 (sep, J = 3.5 Hz, $\underline{C}HCCF_3$), 127.5 (CH), 127.6 (CH), 128.7 (CH), 128.7 (CH), 132.5 (q, J = 33.9 Hz, $\underline{C}CF_3$), 136.7 (C), 137.5 (C), 170.0 (C=O), 170.5 (C=O), 192.4 (C=O); HRMS (ESI) m/z $(M+H)^+$, $C_{22}H_{21}N_2O_3F_6S$ calcd. 507.1177, observed 507.1198.

1.6.4 Photolysis of Model Compounds

Preparation of *N*-(2-benzyl-3-oxo-2,3-dihydro-1,2-thizol-4-yl)acetamide 80

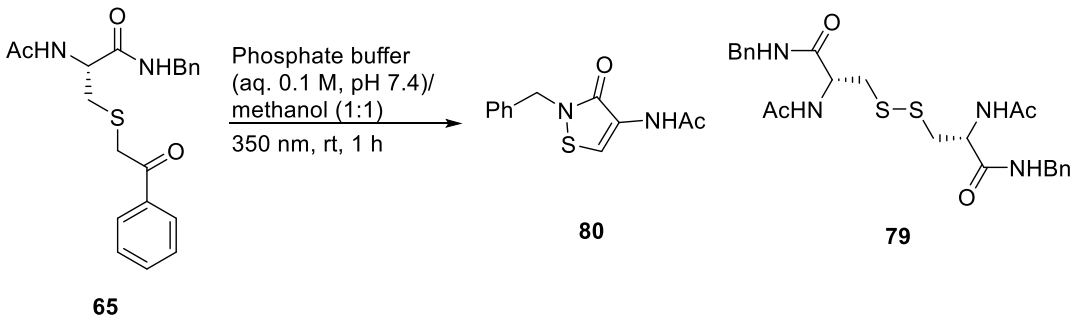

65 **80** **79**

N^2-acetyl-*N*-benzyl-*S*-(2-oxo-2-phenylethyl)cysteinamide **65** (0.200 g, 0.540 mmol) was added to methanol (42 mL) and aqueous phosphate buffer (0.1 M, 48 mL, pH 7.4). The solution was degassed with argon for 30 min and irradiated with UV light (350 nm) for 1 h. The reaction mixture was extracted with DCM (3 × 20 mL) dried ($MgSO_4$) and the solvent evaporated. Purification by flash column chromatography (80:20 EtOAc/pet. ether) gave the product **80** as a white solid; mp 216–218 ºC; R_f 0.50 (80:20 EtOAc/pet. ether); ν_{max} (neat, cm^{-1}) 3238, 3192, 3123, 3034, 2919, 2850, 1728, 1684, 1621, 1581, 1537, 1495, 1374, 1349, 1239, 1149, 1031, 1006; Initial ^{1}H NMR in methanol-d_4 confirmed the product as observed from the original photolysis reactions. Full characterization was carried out in $CDCl_3$; ^{1}H NMR (500 MHz, methanol-d_4) δ_H 2.21 (3H, s), 5.00 (2H, s), 7.31–7.33 (2H, m), 7.38–7.42 (3H, m), 8.54 (1H, s); ^{1}H NMR (500 MHz, $CDCl_3$) δ_H 2.19 (3H, s), 4.97 (2H, s), 7.27–7.37 (5H, m), 8.44 (1H, s); ^{13}C NMR (125 MHz, $CDCl_3$) δ_C 23.6 (CH_3), 48.1 (CH_2), 118.4 (CH), 120.5 (C), 128.3 (CH),

128.5 (CH), 128.9 (CH), 135.4 (C), 162.7 (C=O), 168.3 (C=O); HRMS (ESI) *m/z* (*M*+H)$^+$, $C_{12}H_{13}N_2O_2S$ calcd. 249.0698, observed 249.0654.

1.6.4.1 General Photolysis Procedure

The α-thioketone (1.2 mg) was dissolved in methanol-d_4 (0.25 mL). D_2O (0.1 M phosphate buffer 0.25 mL, pD 7.0) was added to the solution. The solution was degassed with argon for 15 min. Photolysis was performed using a Rayonet photochemical reactor and 350 nm ultraviolet lamps (Figure 1.19). The reaction was monitored by NMR spectroscopy.

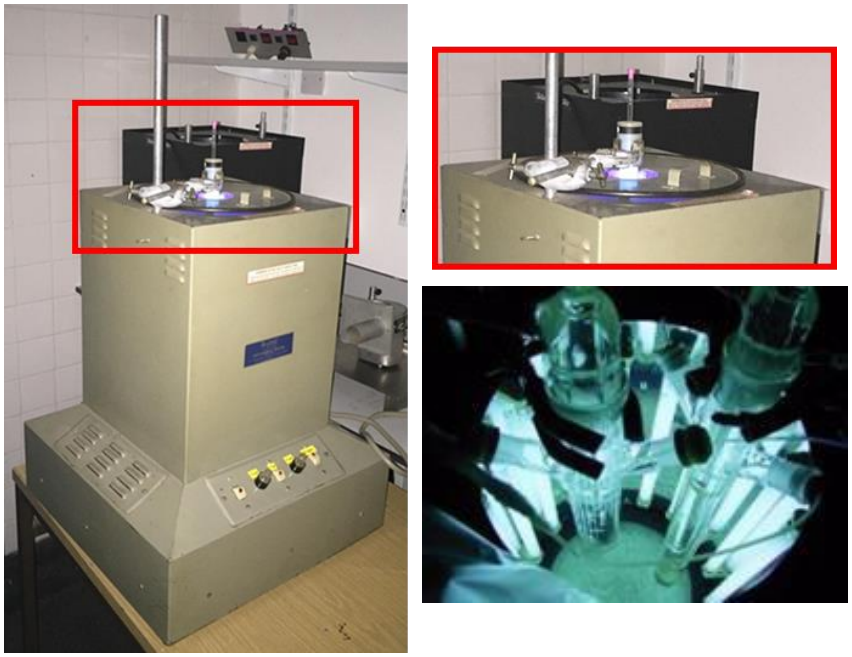

Figure 1.19: Rayonet photochemical reactor with quartz NMR tube.

Compound Data

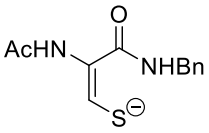

(1*E*)-2-acetamido-3-(benzylamino)-3-oxoprop-1-ene-1-thiolate 71: (In accordance with the general photolysis procedure, section 1.6.4.1, using N^2-acetyl-*N*-benzyl-*S*-{2-oxo-2-[3-(trifluoromethyl) phenyl]ethyl}cysteinamide (**69**), 1.2 mg); ^{1}H NMR (500 MHz, methanol-d_4) δ_H 2.14 (3H, s), 4.42 (2H, s), 7.26–7.35 (5H, m), 8.00 (1H, s); HRMS (ESI) *m/z* (*M*+Na), $C_{12}H_{14}N_2O_2SNa$ calcd. 273.0674, observed 273.0668; (*M*−H), $C_{12}H_{13}N_2O_2S$ calcd. 249.0703, observed 249.0727.

1.6.5 NMR Spectra

^{1}H NMR (500 MHz) of 1-carboxy-2-sulfanylethan-1-aminium 4-methylbenzene-1-sulfonate (53) in D_2O

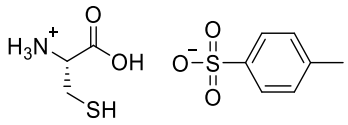

53

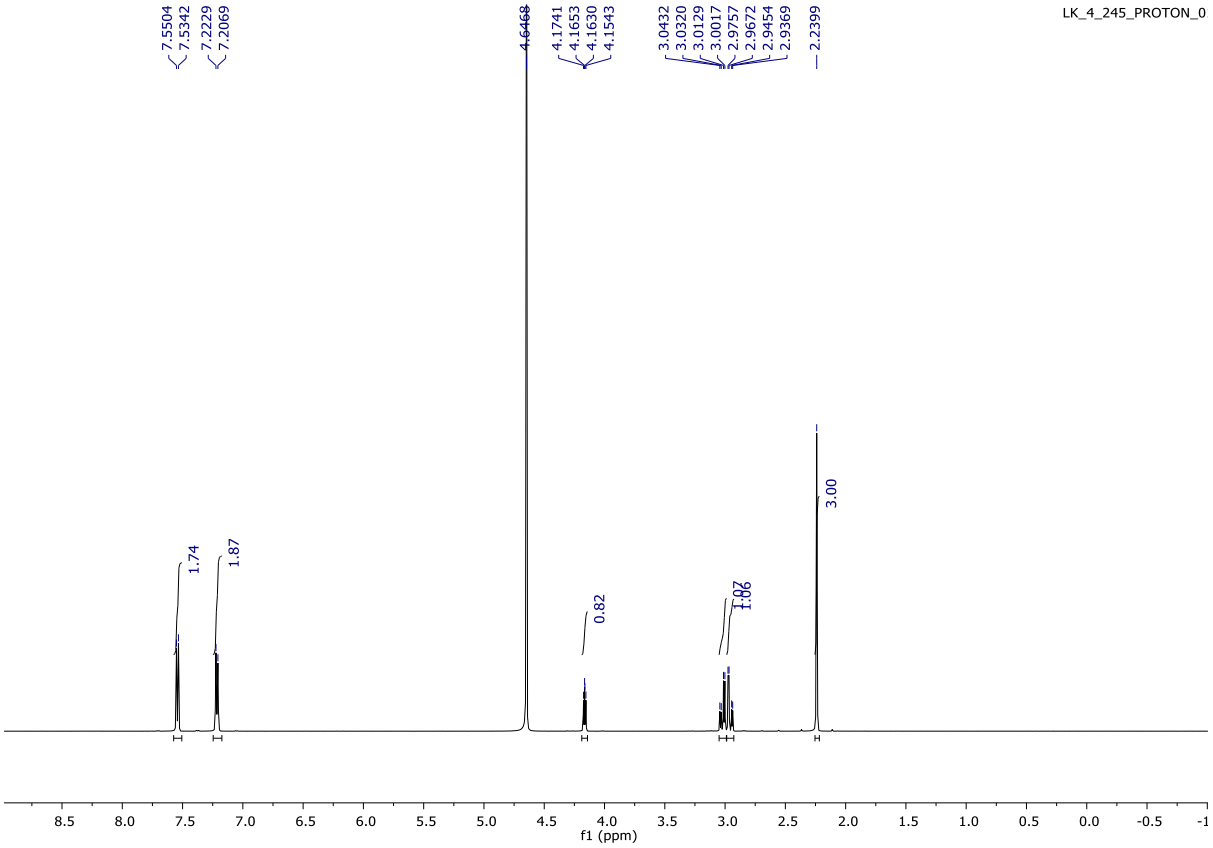

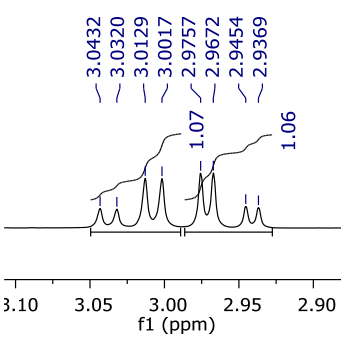

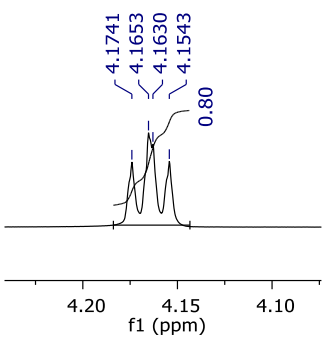

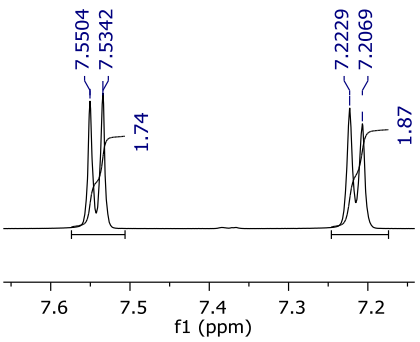

^{13}C NMR (125 MHz) of 1-carboxy-2-sulfanylethan-1-aminium 4-methylbenzene-1-sulfonate (53) in D_2O

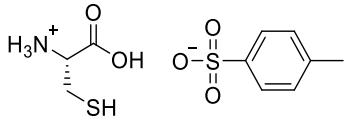

53

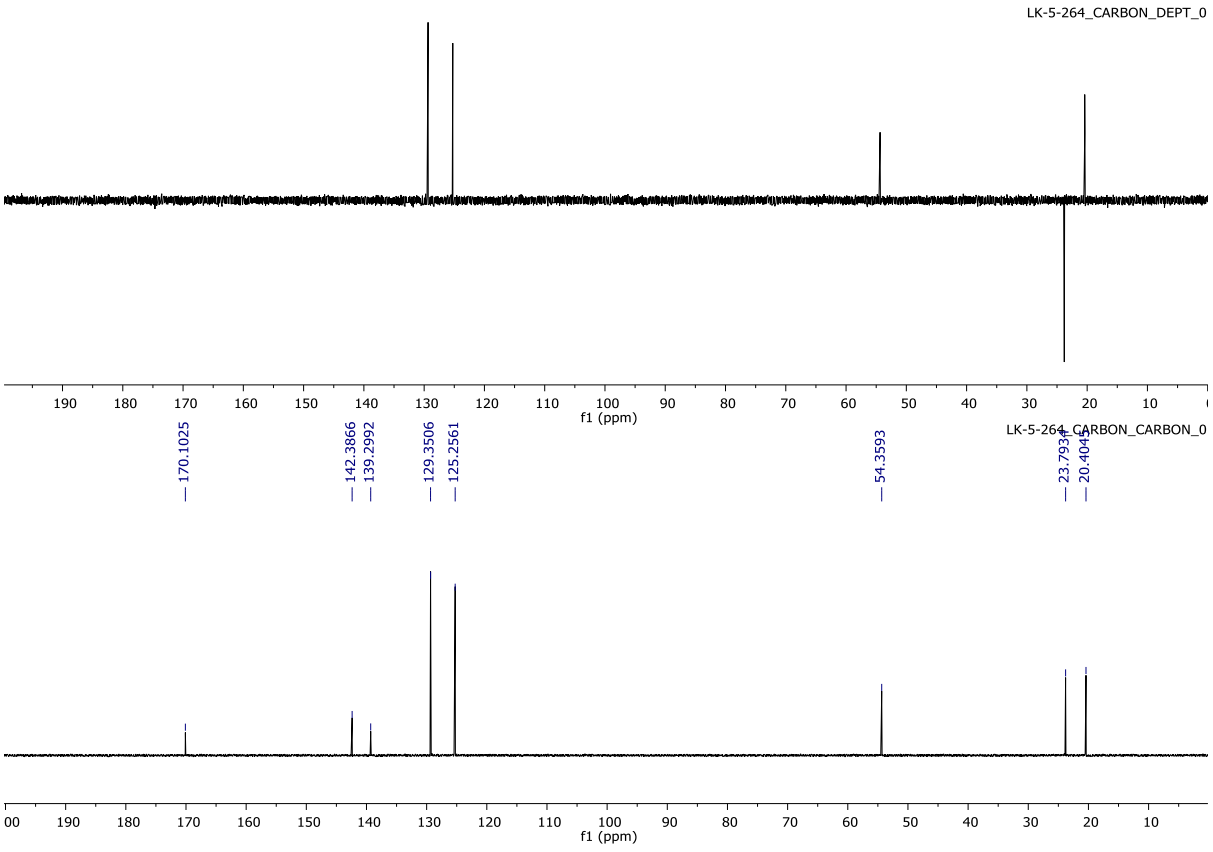

^{1}H NMR (400 MHz) of *S*-(triphenylmethyl)cysteine (54) in DMSO-d_6

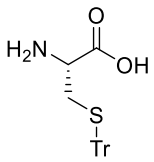

54

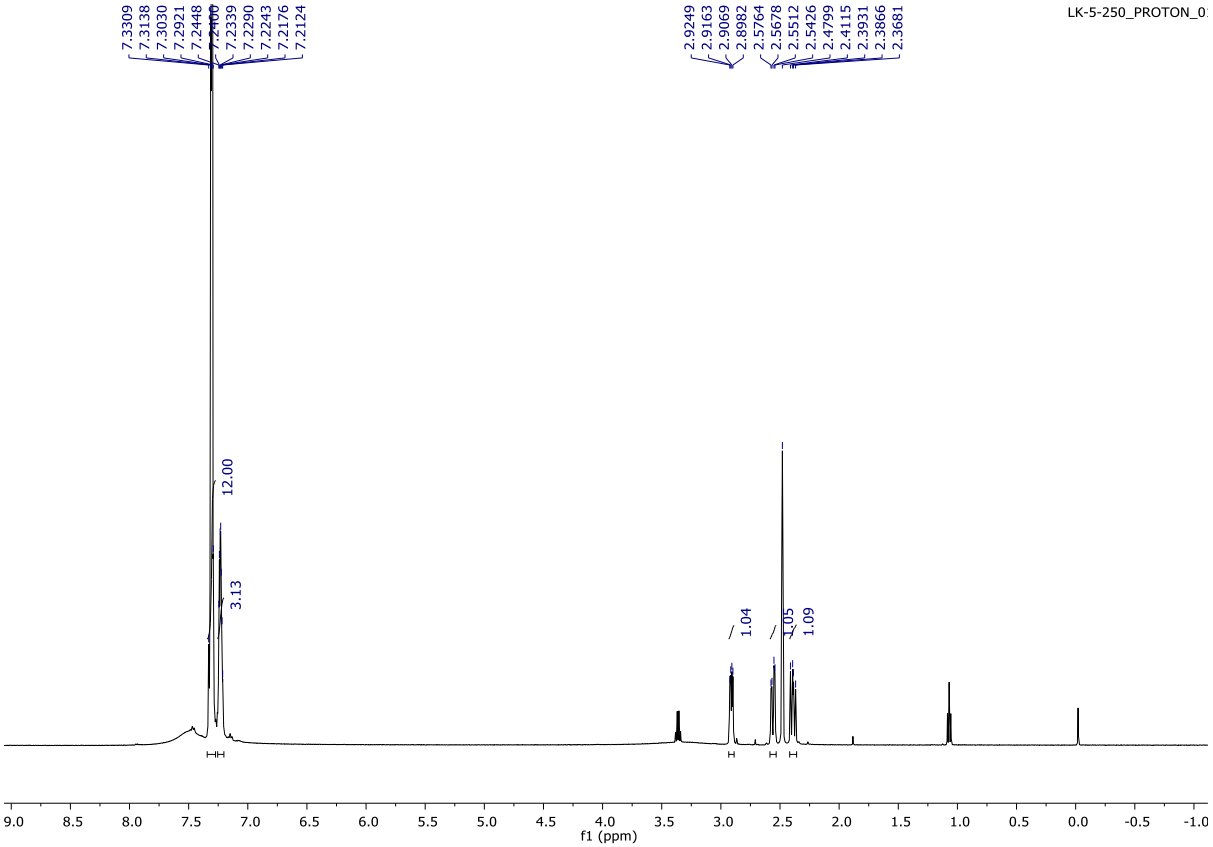

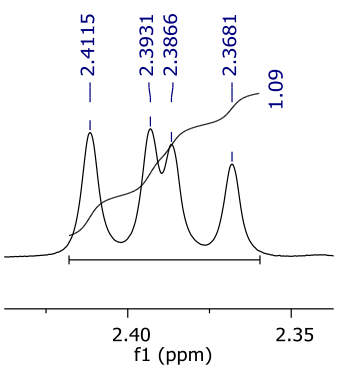

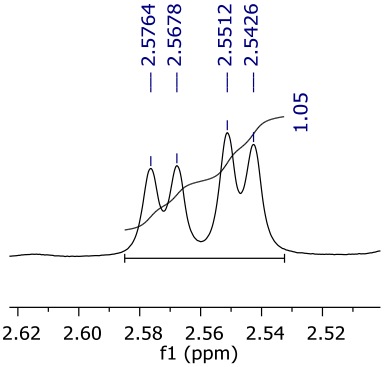

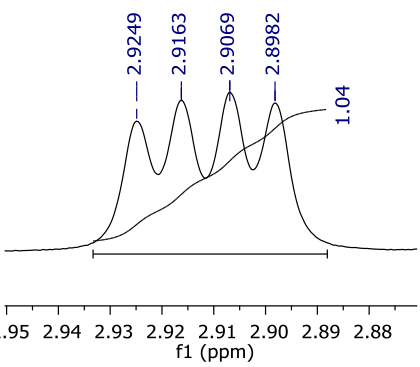

^{13}C NMR (125 MHz) of *S*-(triphenylmethyl)cysteine (54) in DMSO-d_6

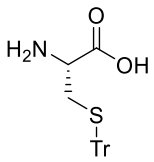

54

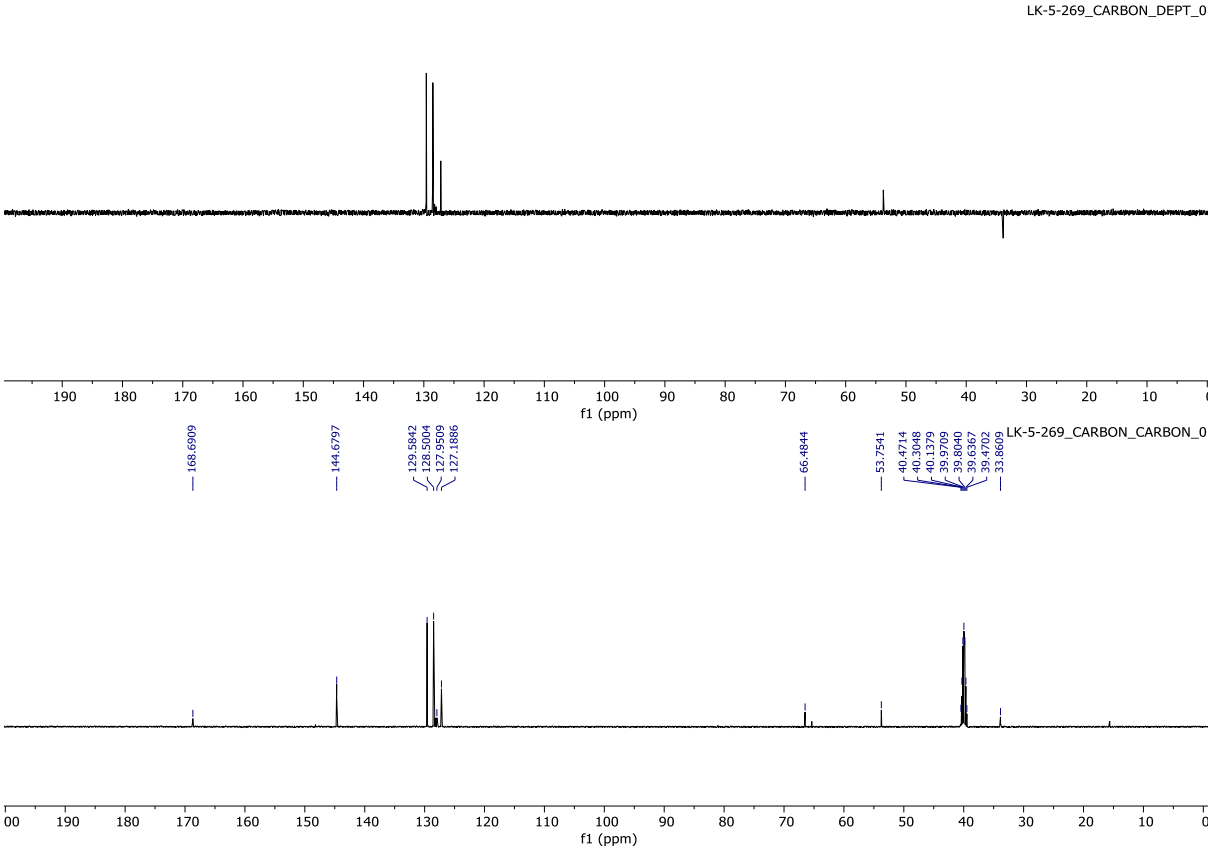

^{1}H NMR (500 MHz) of *N*-acetyl-*S*-(triphenylmethyl)cysteine (55) in DMSO-d_6

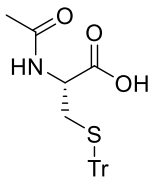

55

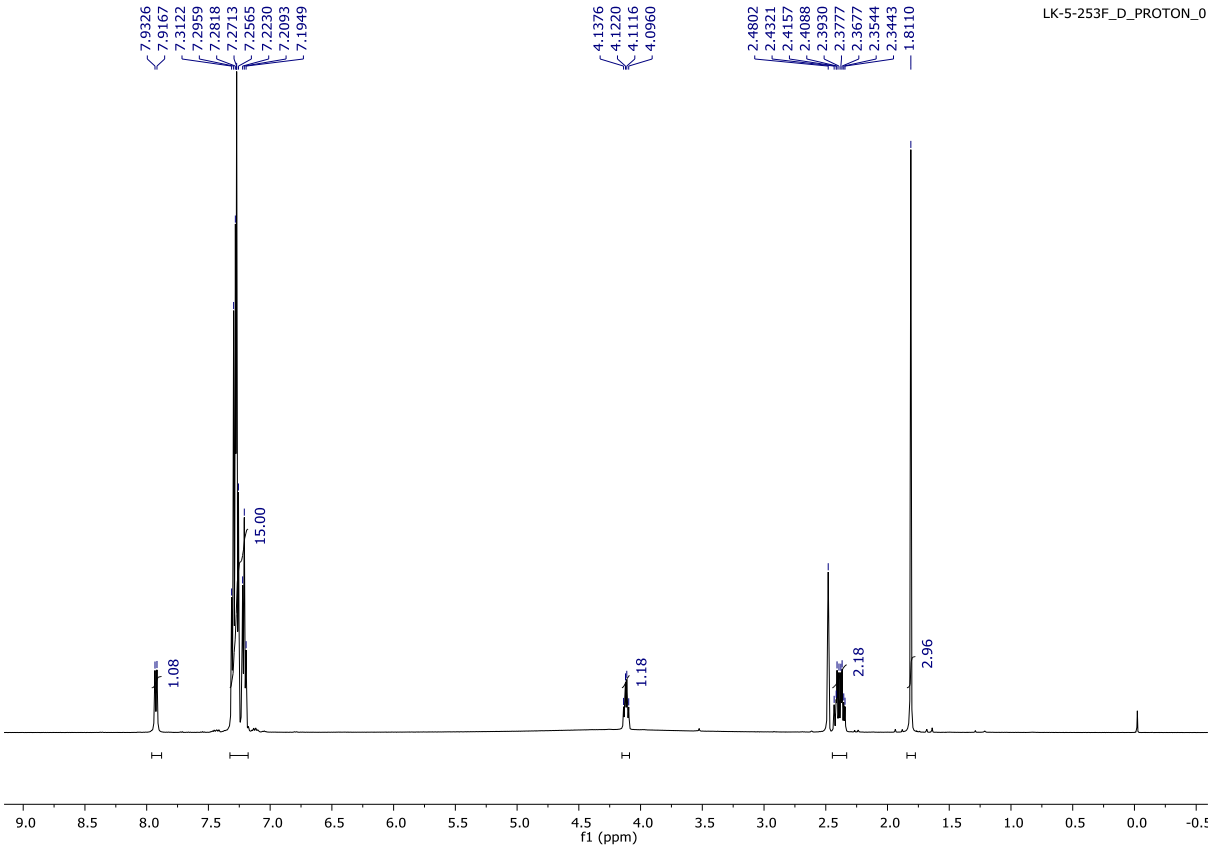

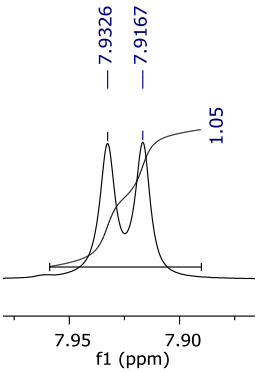

^{13}C NMR (125 MHz) of *N*-acetyl-*S*-(triphenylmethyl)cysteine in DMSO-d_6

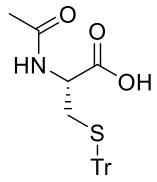

55

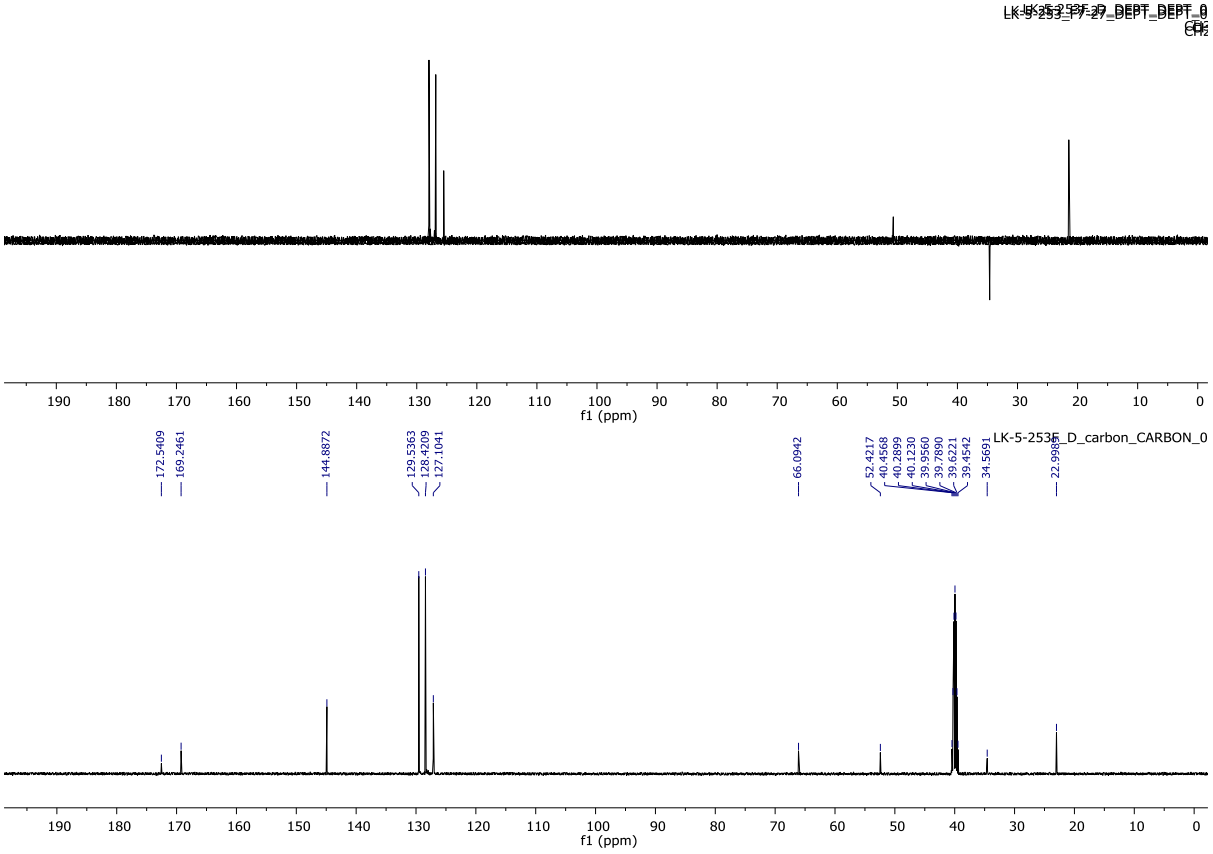

^{1}H NMR (500 MHz) of N^2-acetyl-*N*-benzyl-*S*-(triphenylmethyl)cysteinamide (56) in $CDCl_3$

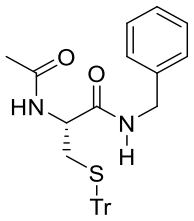

56

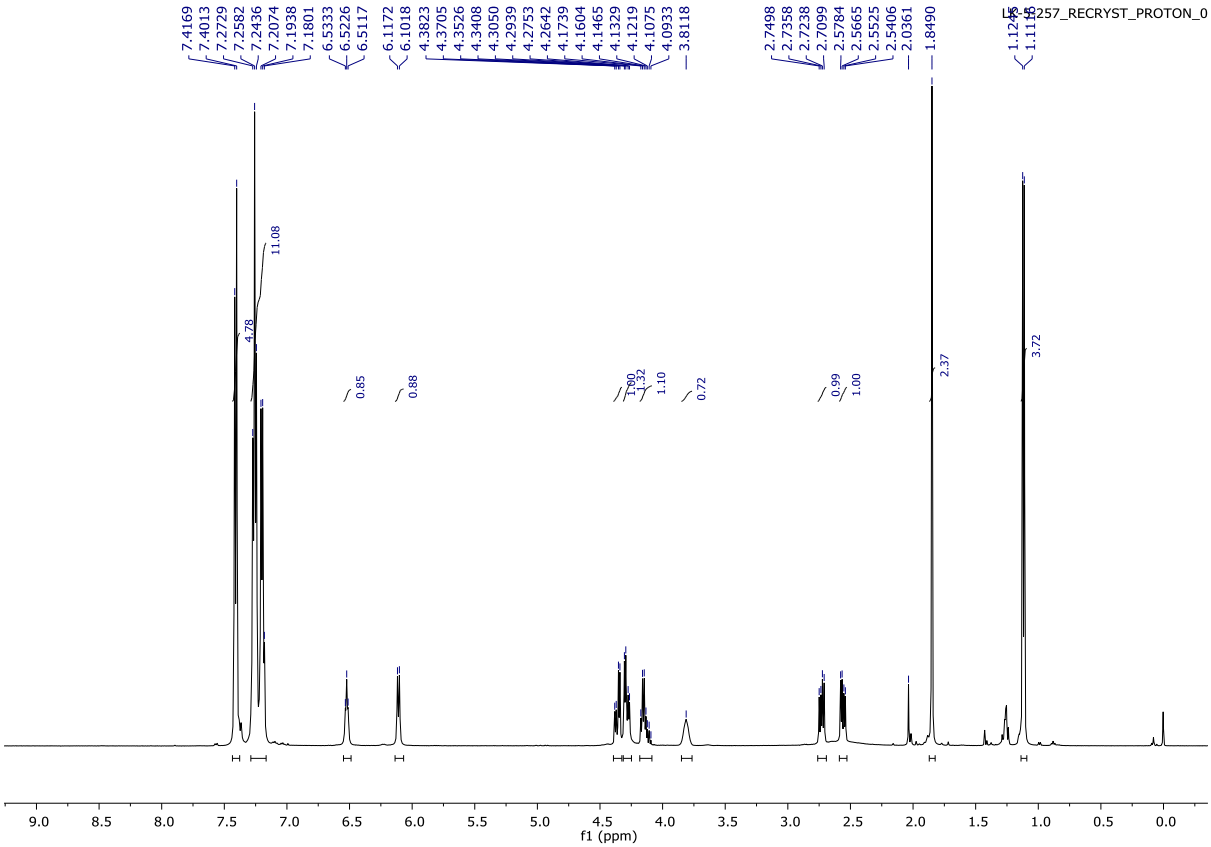

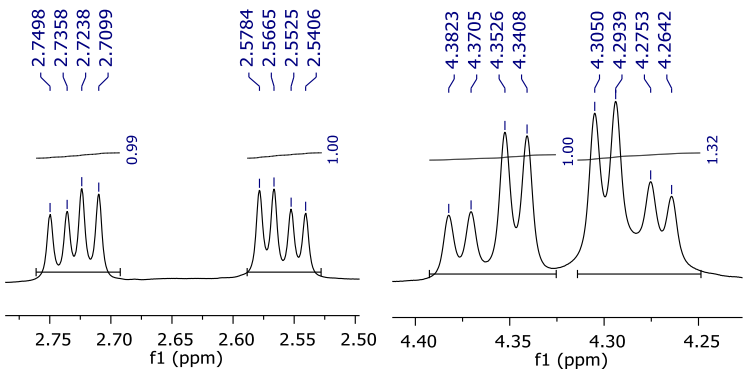

^{13}C NMR (125 MHz) of *N*^{2}-acetyl-*N*-benzyl-*S*-(triphenylmethyl)cysteinamide (56) in $CDCl_3$

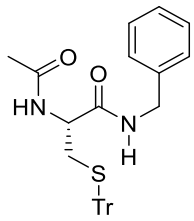

56

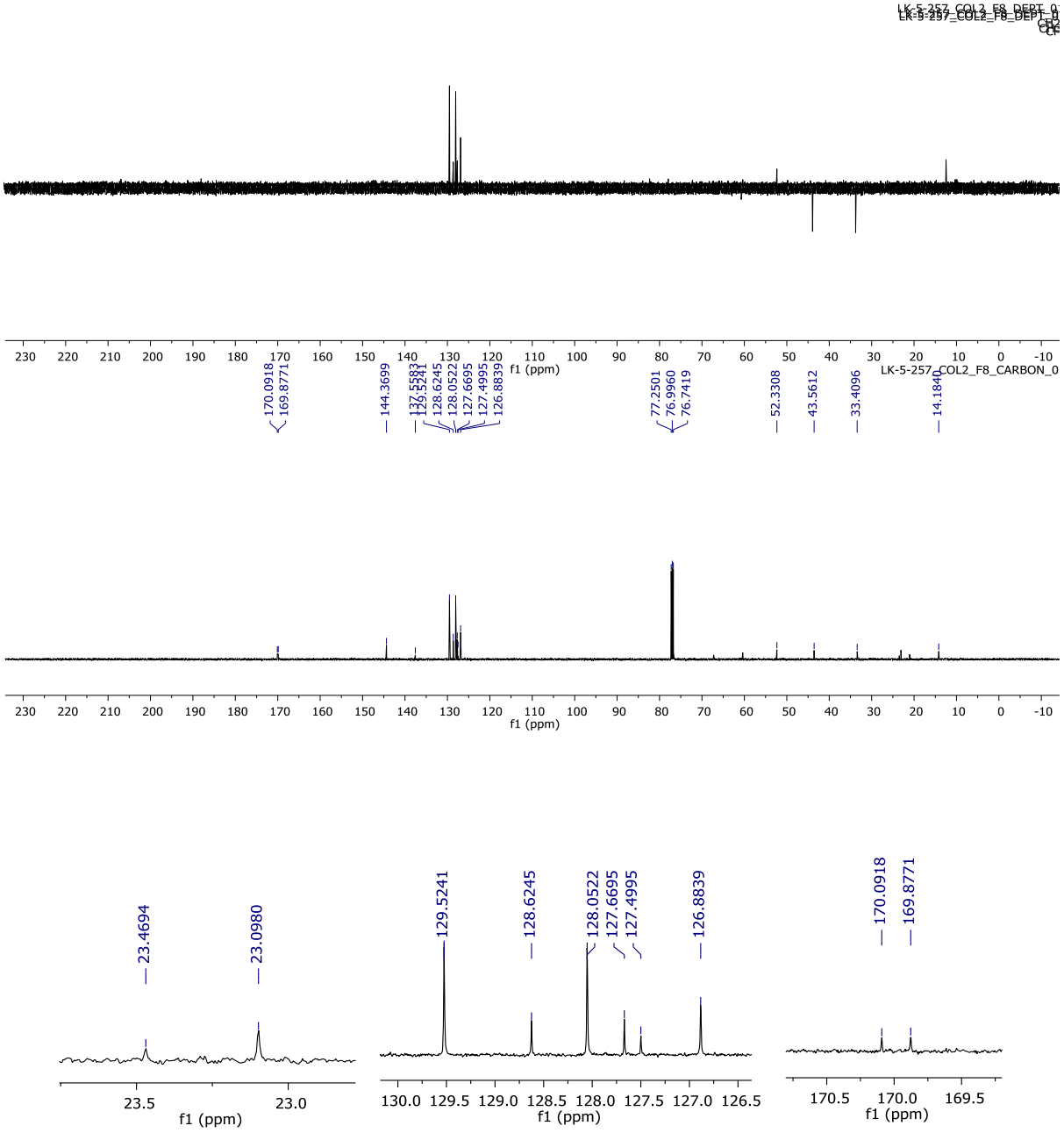

^{1}H NMR (500 MHz) of N^{2}-acetyl-*N*-benzylcysteinamide (61) in $CDCl_3$

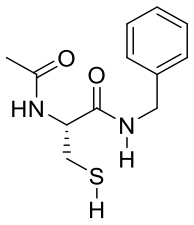

61

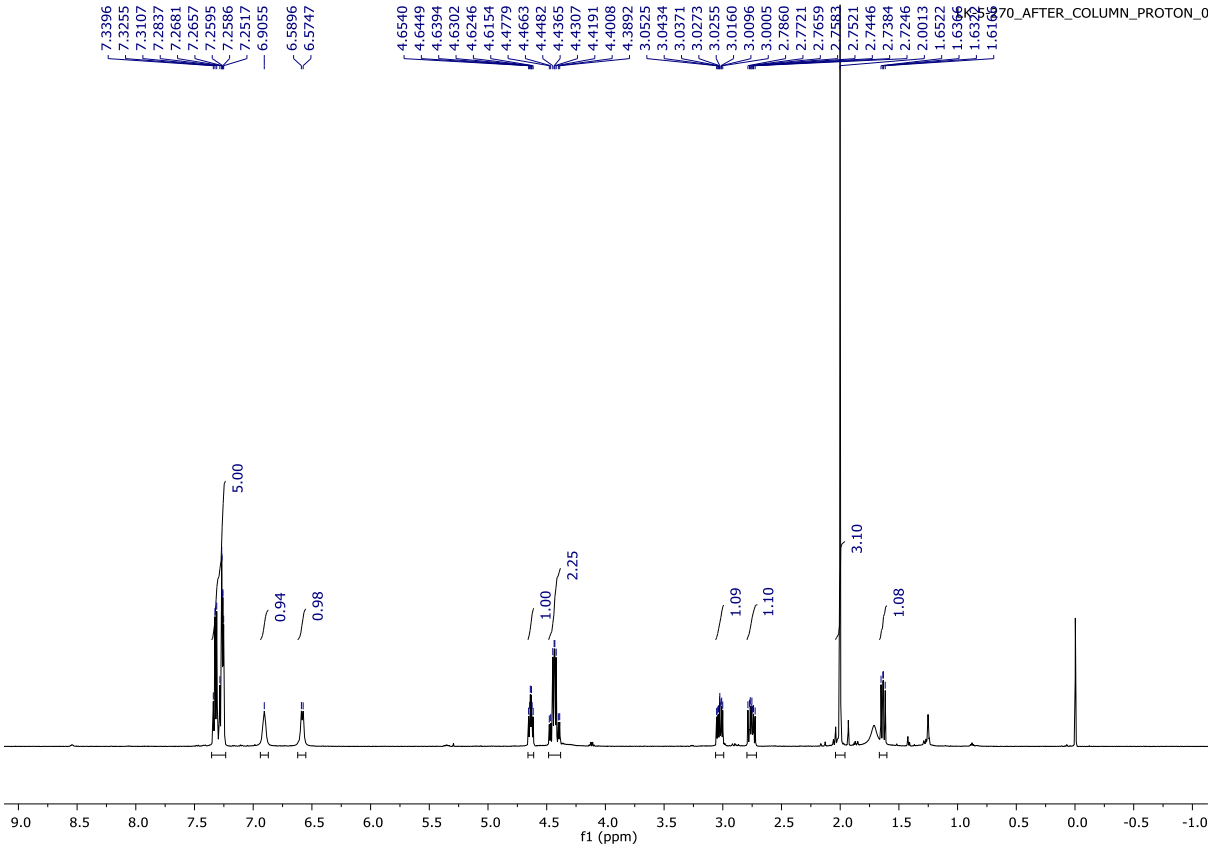

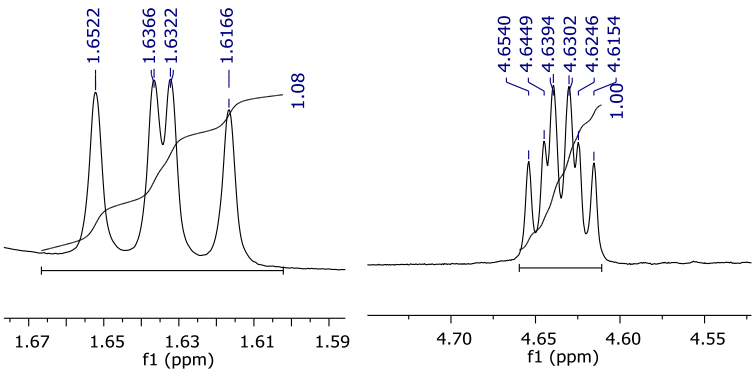

^{13}C NMR (125 MHz) of N^2-acetyl-*N*-benzylcysteinamide (61) in $CDCl_3$

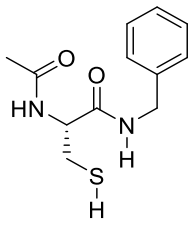

61

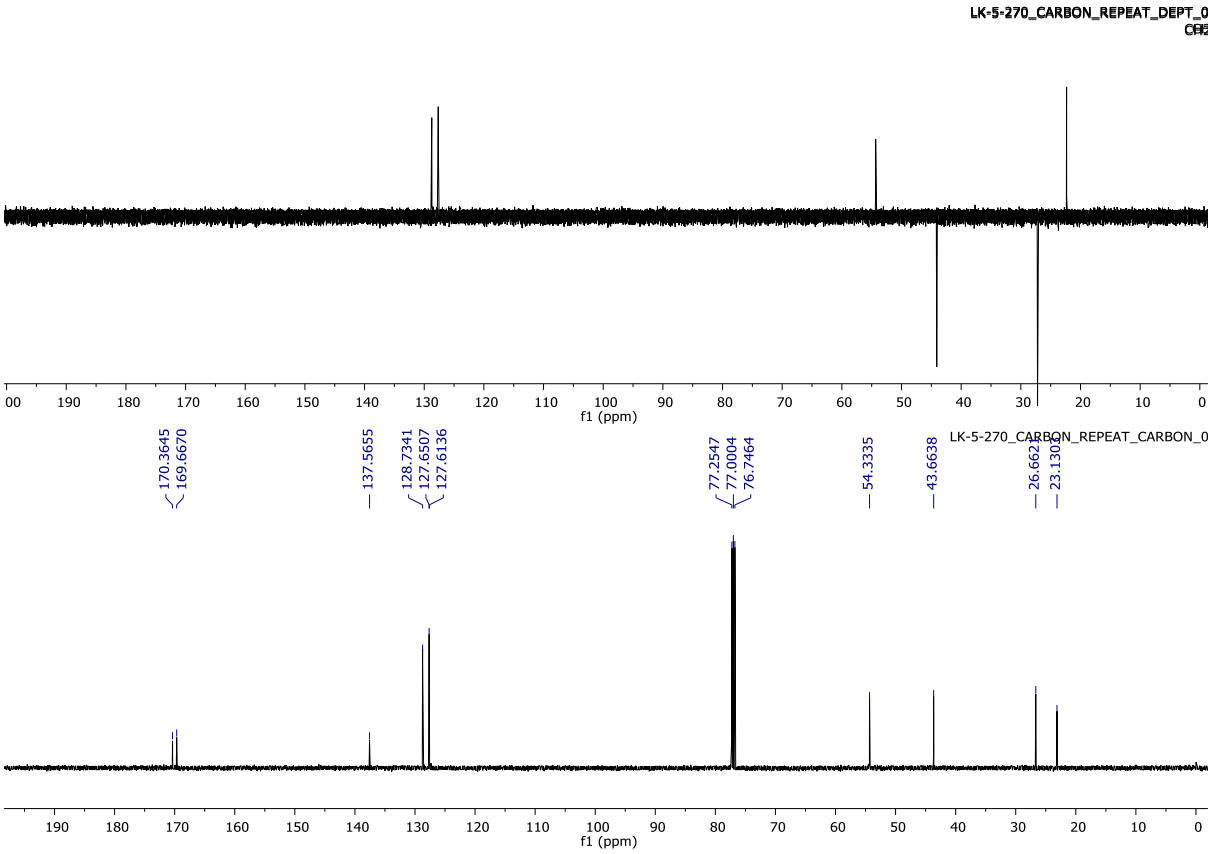

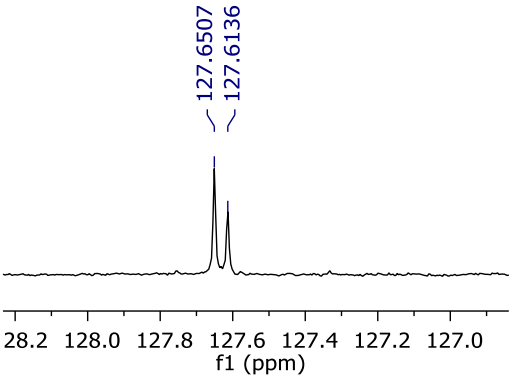

^{1}H NMR (500 MHz) of *N*^{2}-acetyl-*N*-benzyl-*S*-(2-oxo-2-phenylethyl)cysteinamide (65) in $CDCl_3$

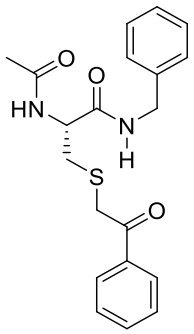

65

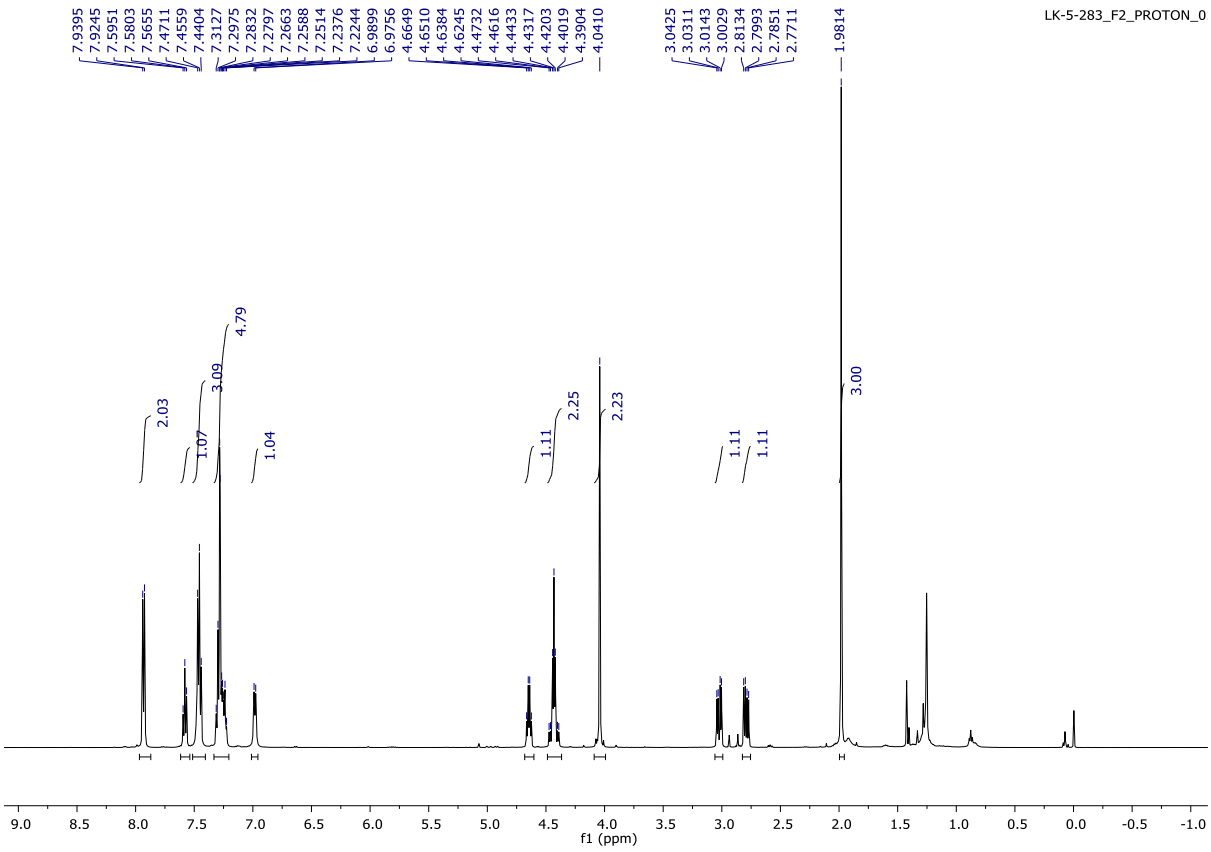

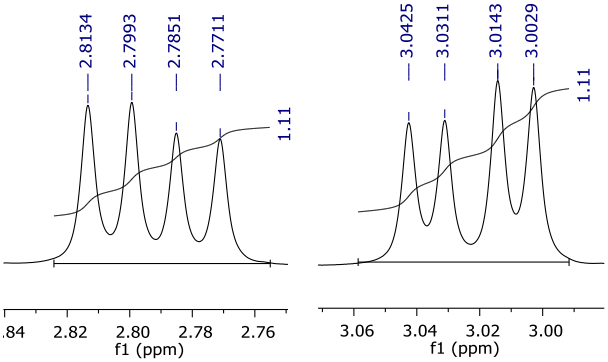

^{13}C NMR (125 MHz) of *N*^{2}-acetyl-*N*-benzyl-*S*-(2-oxo-2-phenylethyl)cysteinamide (65) in $CDCl_3$

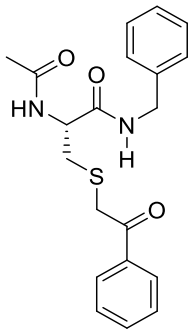

65

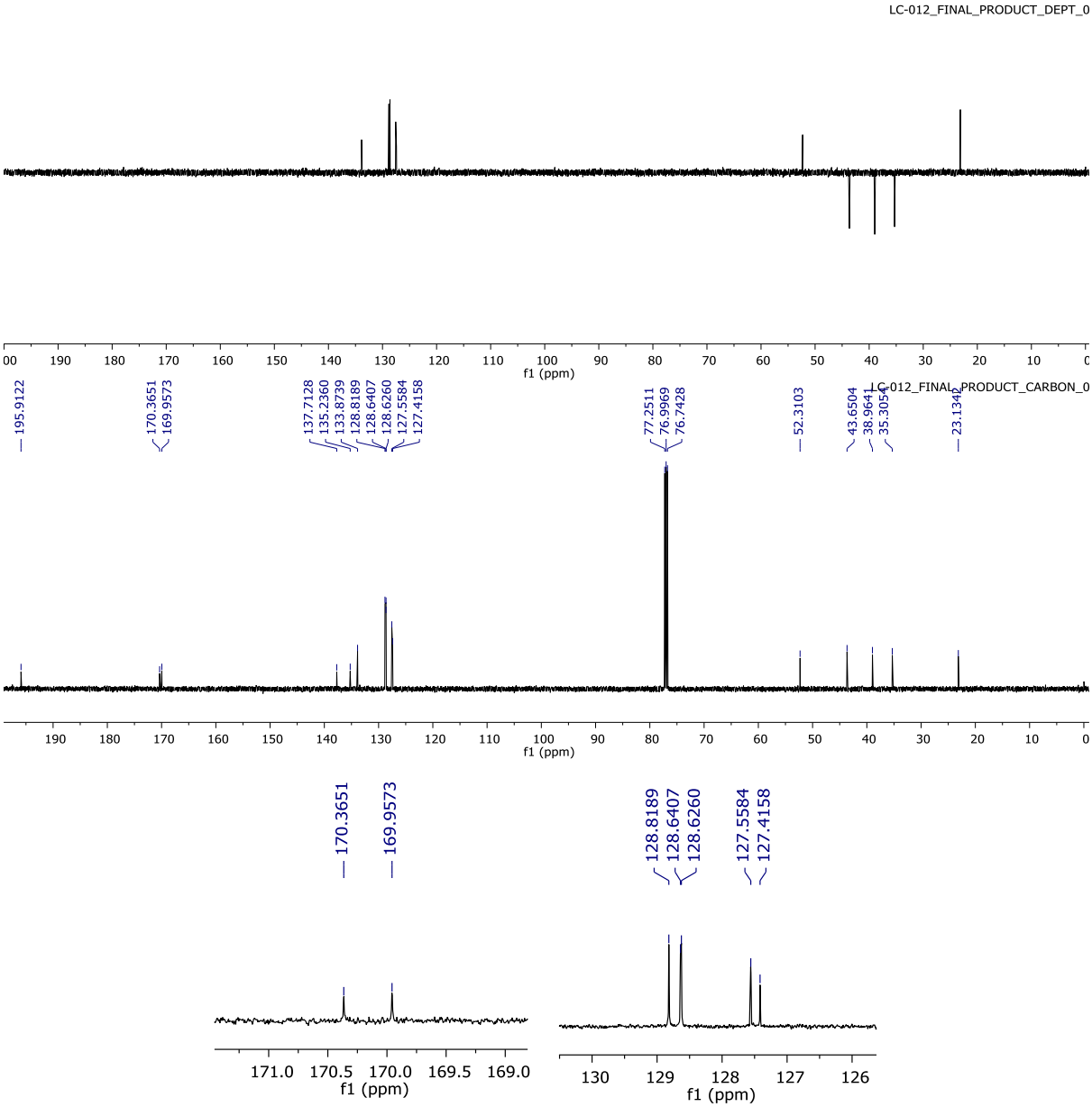

^{1}H NMR (500 MHz) of N^2-acetyl-*N*-benzyl-*S*-[2-(2,4-dimethoxyphenyl)-2-oxoethyl] cysteinamide (66) in $CDCl_3$

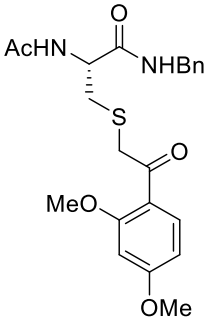

66

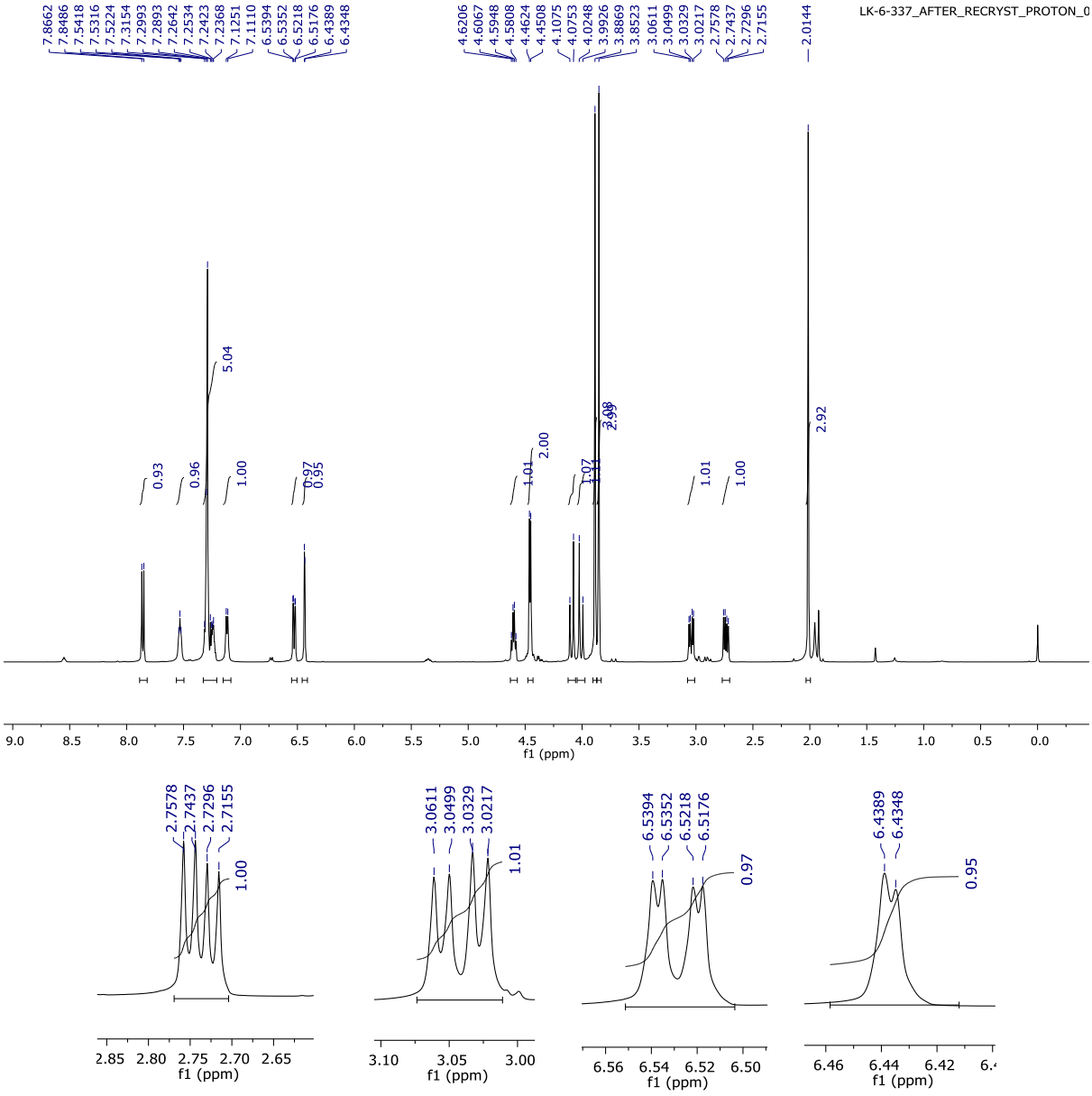

^{13}C NMR (125 MHz) of *N*^{2}-acetyl-*N*-benzyl-*S*-[2-(2,4-dimethoxyphenyl)-2-oxoethyl] cysteinamide (66) in $CDCl_3$

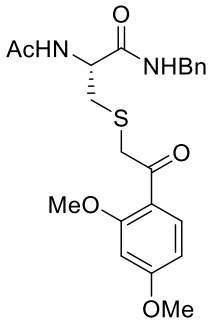

66

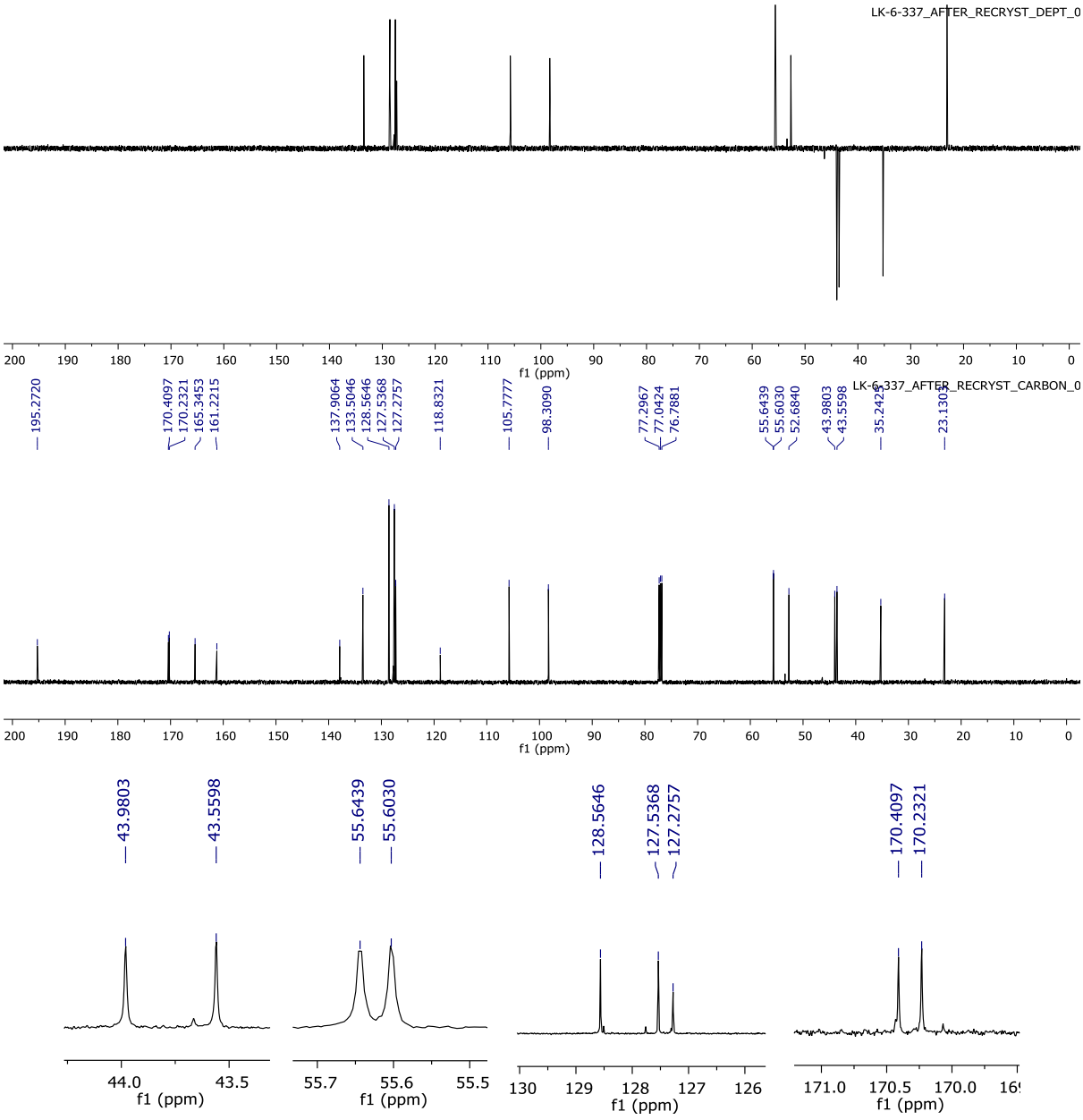

^{1}H NMR (500 MHz) of N^2-acetyl-*N*-benzyl-*S*-[2-(3-cyanophenyl)-2-oxoethyl]cysteinamide (67) in $CDCl_3$

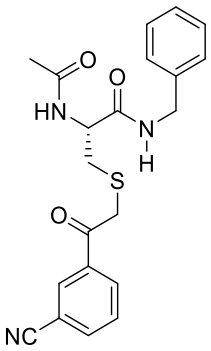

67

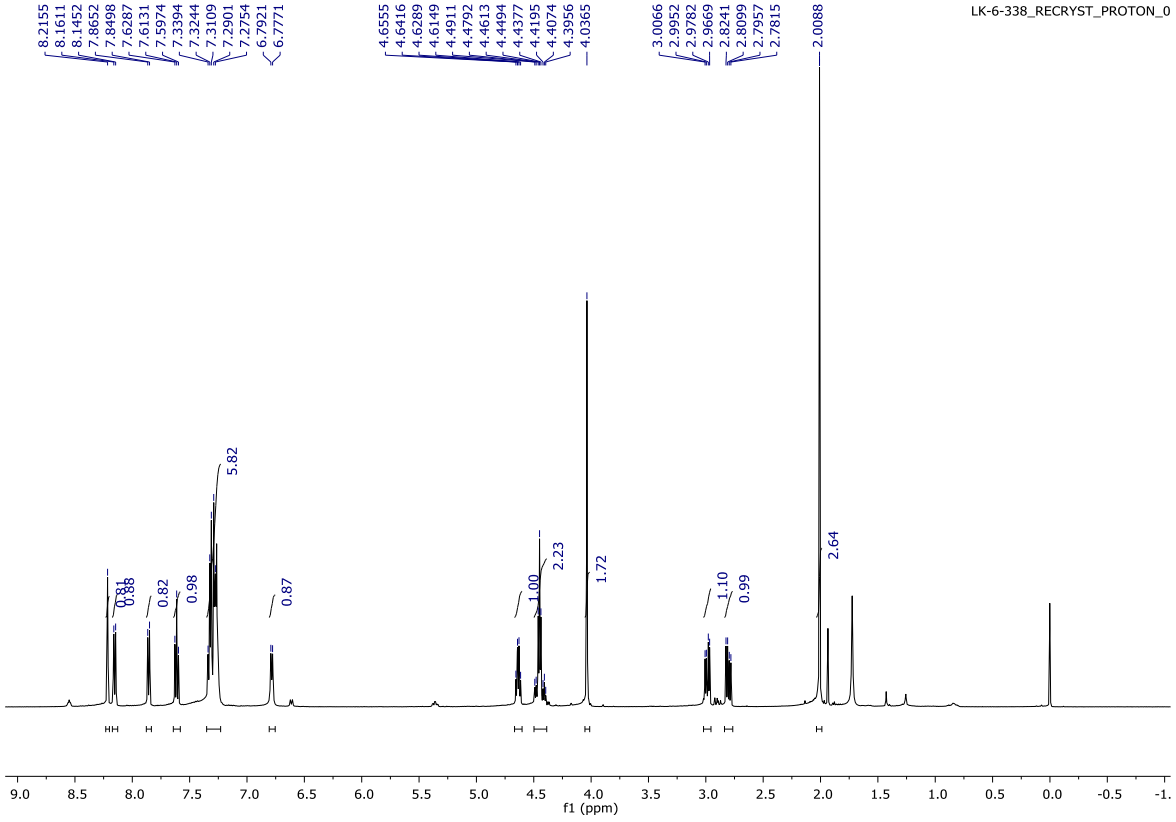

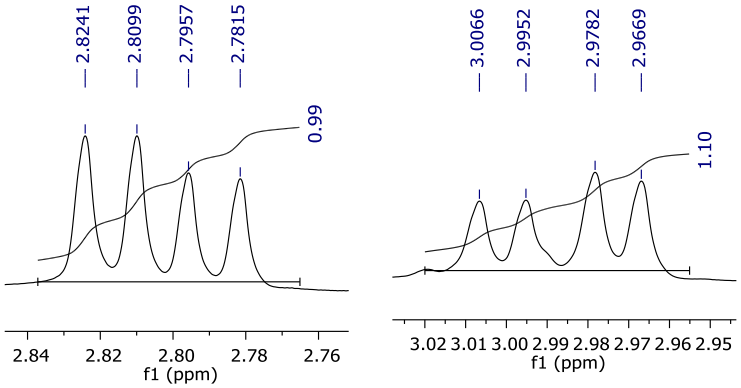

^{13}C NMR (125 MHz) of *N*^{2}-acetyl-*N*-benzyl-*S*-[2-(3-cyanophenyl)-2-oxoethyl]cysteinamide (67) in $CDCl_3$

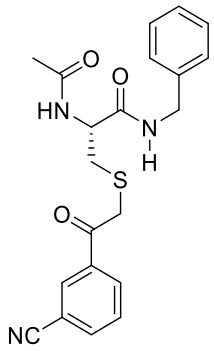

67

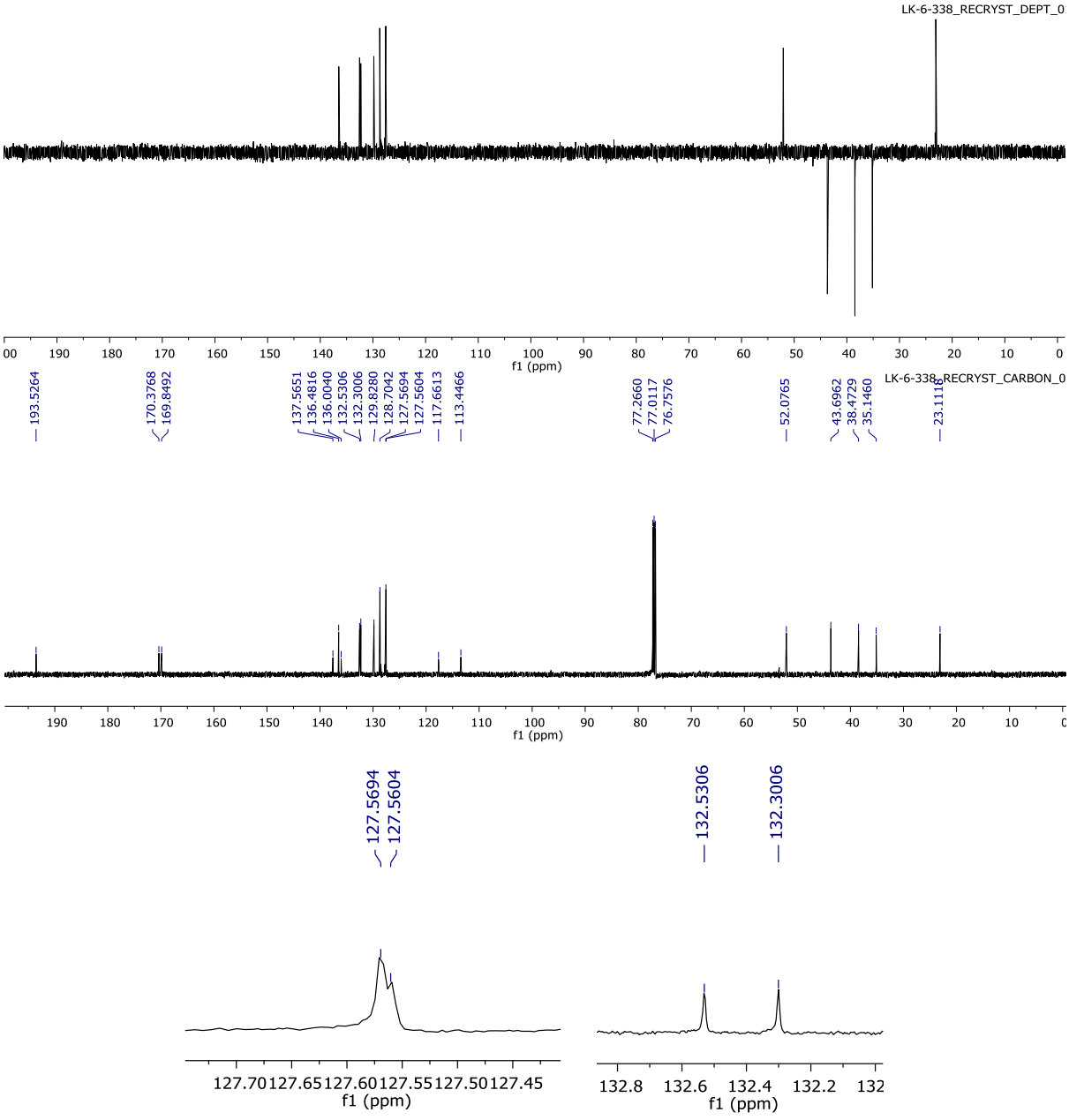

^{1}H NMR (500 MHz) of N^2-acetyl-*N*-benzyl-*S*-[2-(4-cyanophenyl)-2-oxoethyl] cysteinamide (68) in $CDCl_3$

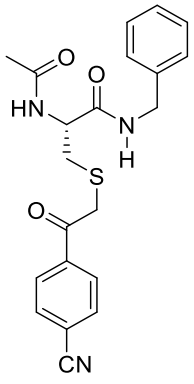

68

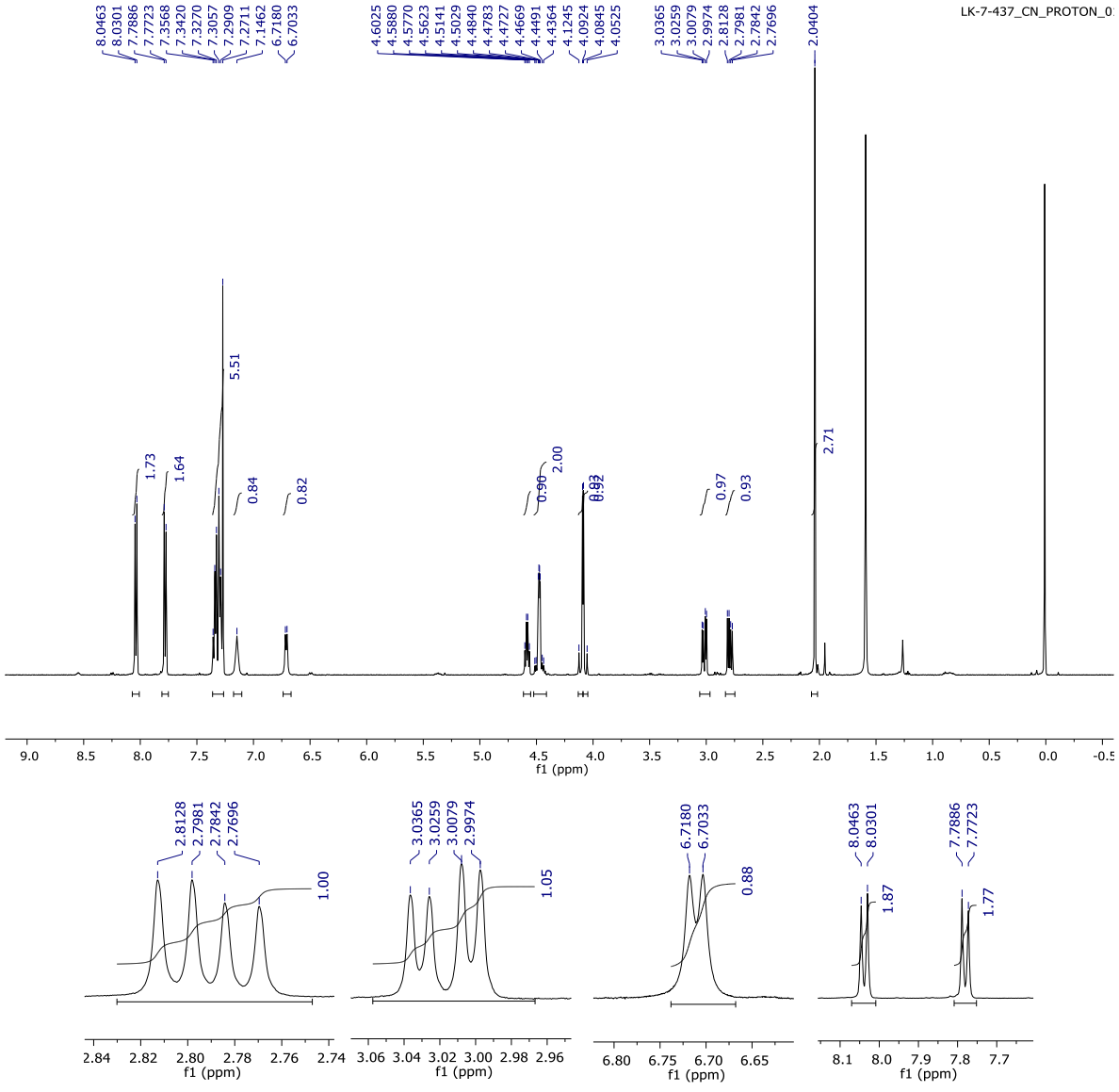

^{13}C NMR (125 MHz) of *N*^{2}-acetyl-*N*-benzyl-*S*-[2-(4-cyanophenyl)-2-oxoethyl] cysteinamide (68) in $CDCl_3$

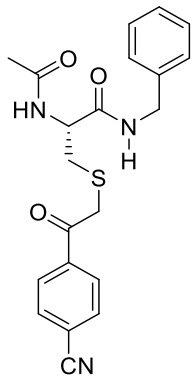

68

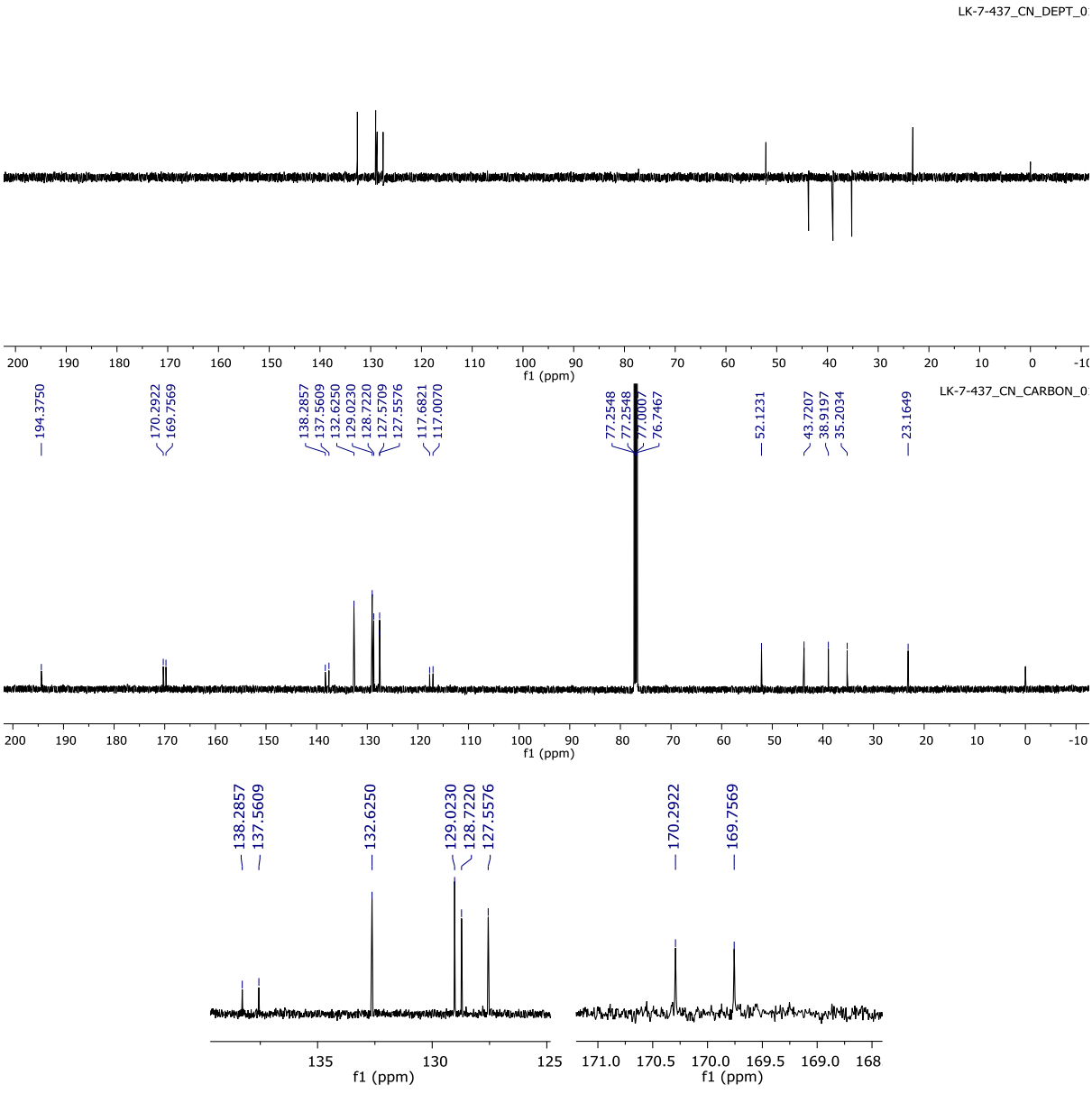

^{1}H NMR (500 MHz) of N^2-acetyl-*N*-benzyl-*S*-{2-oxo-2-[3-(trifluoromethyl) phenyl]ethyl}cysteinamide (69) in $CDCl_3$

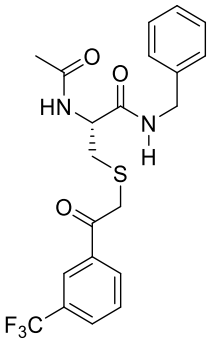

69

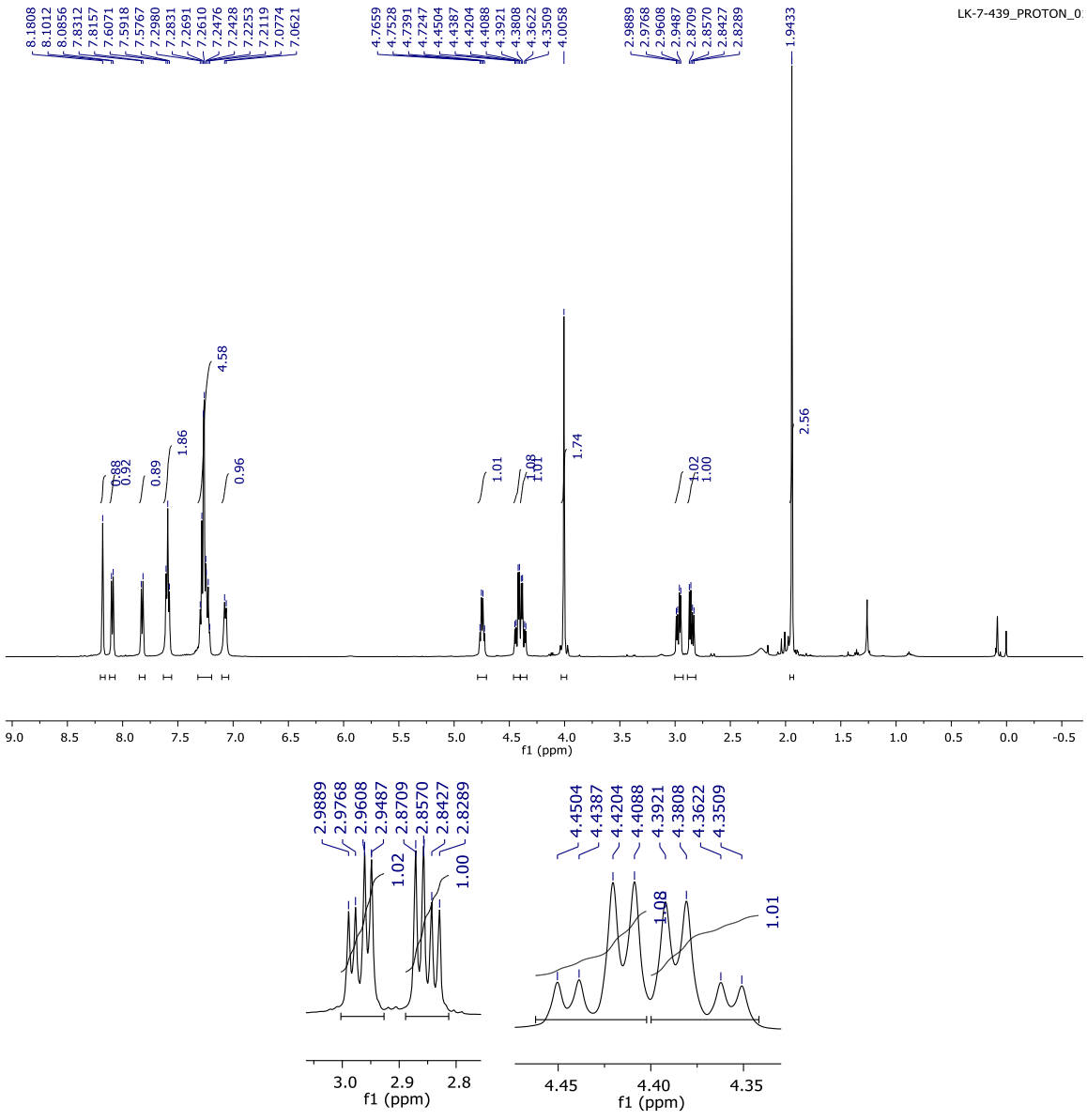

^{13}C NMR (125 MHz) of *N*^{2}-acetyl-*N*-benzyl-*S*-{2-oxo-2-[3-(trifluoromethyl) phenyl]ethyl}cysteinamide (69) in $CDCl_3$

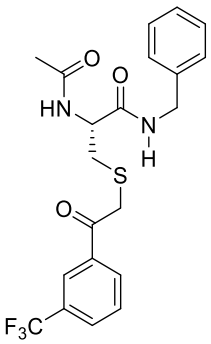

69

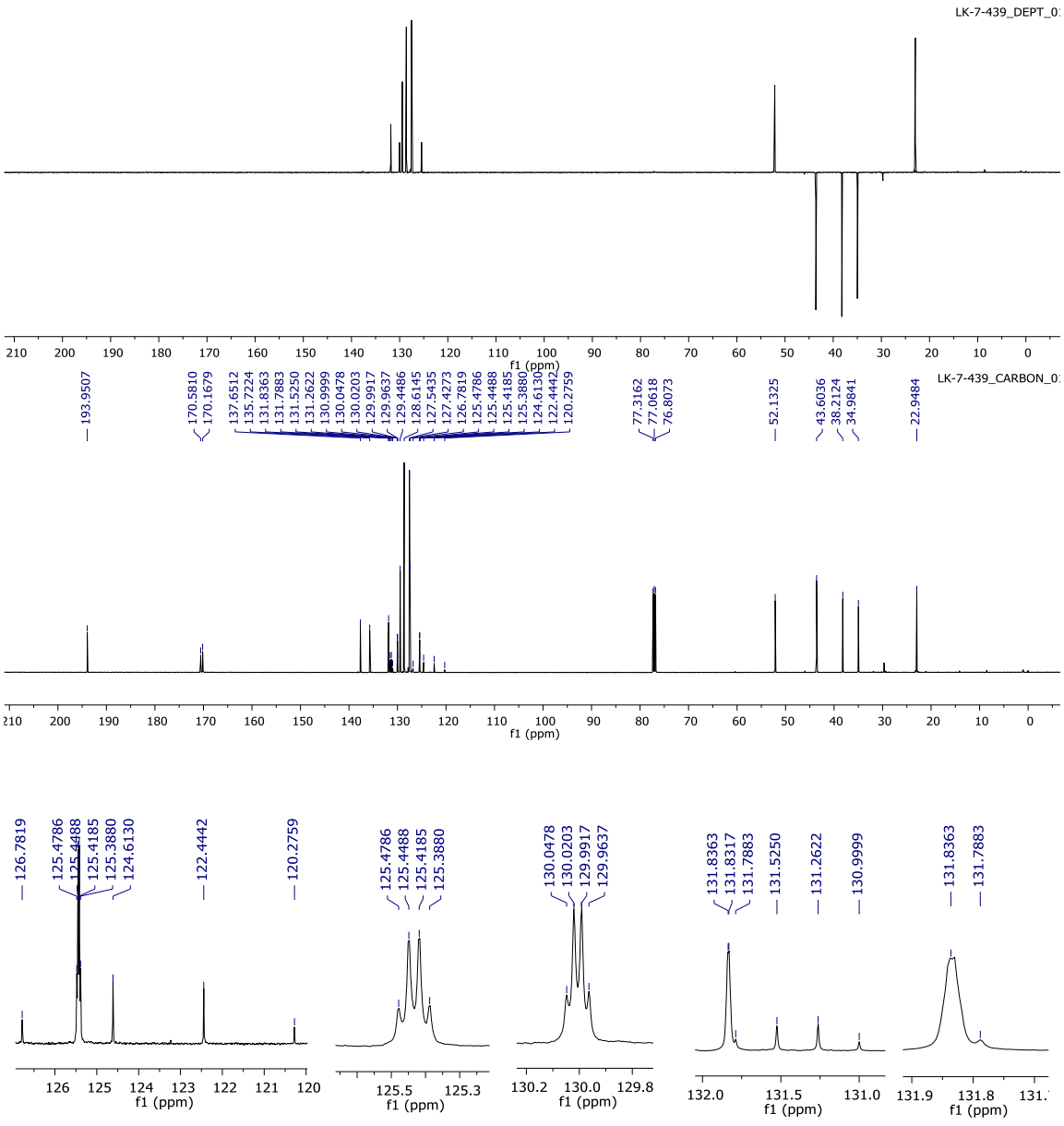

^{1}H NMR (500 MHz) of N^2-acetyl-*N*-benzyl-*S*-{2-[3,5-bis(trifluoromethyl)phenyl]-2-oxoethyl}cysteinamide (70) in $CDCl_3$

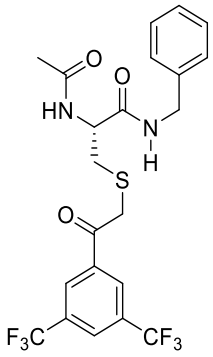

70

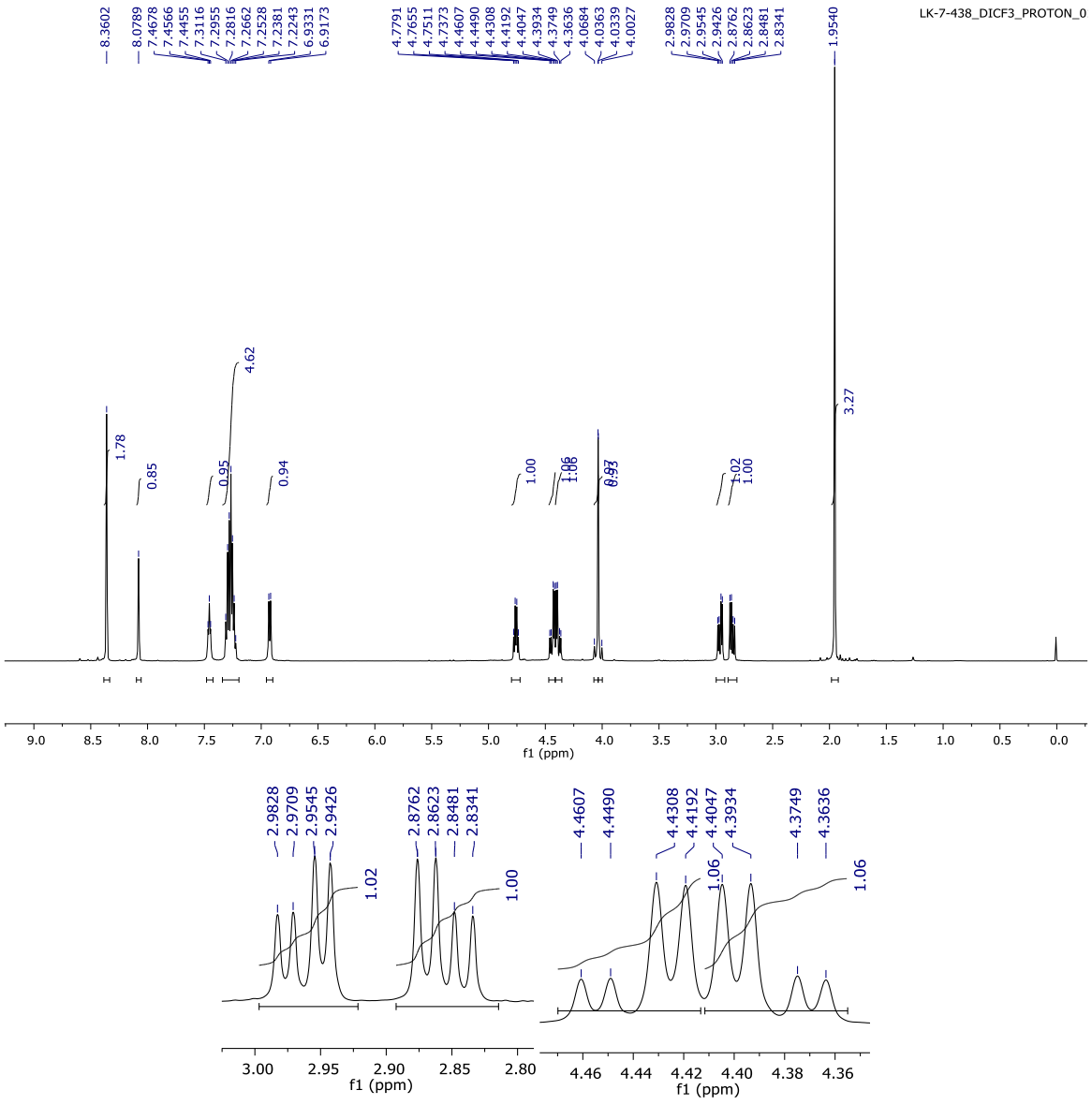

^{13}C NMR (125 MHz) of N^2-acetyl-*N*-benzyl-*S*-{2-[3,5-bis(trifluoromethyl)phenyl]-2-oxoethyl}cysteinamide (70) in $CDCl_3$

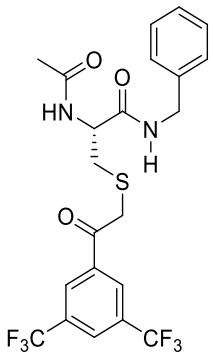

70

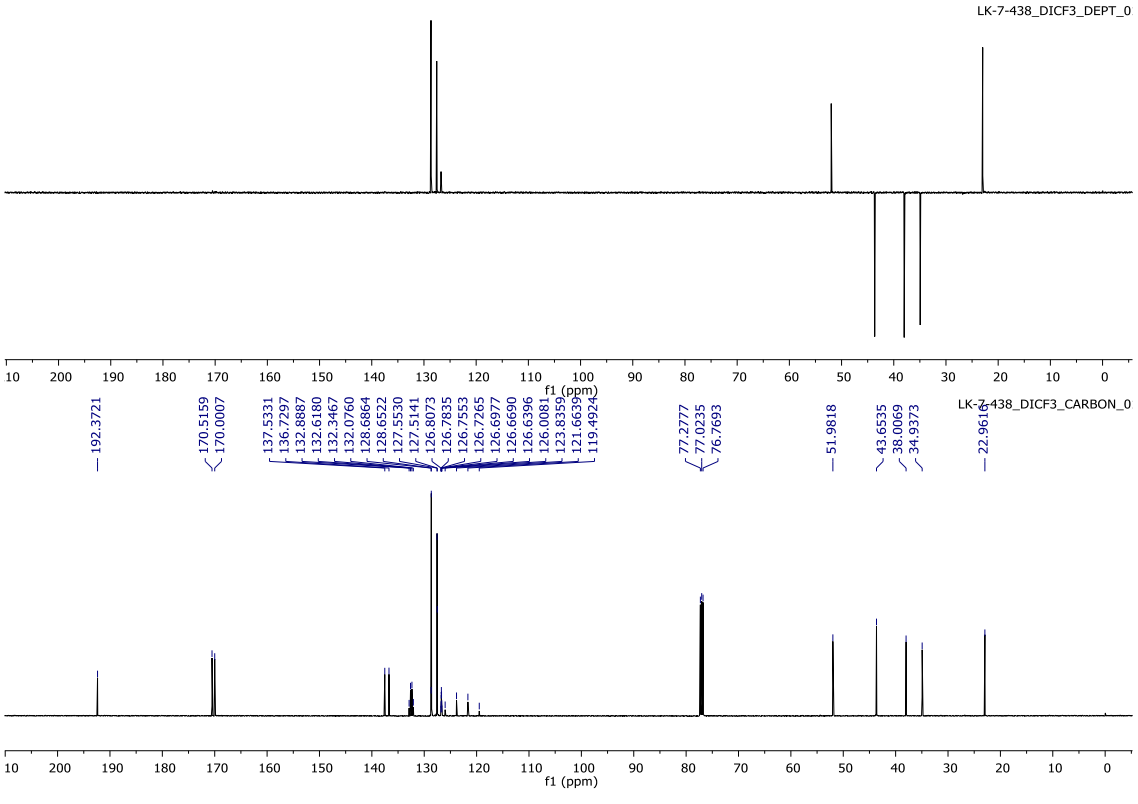

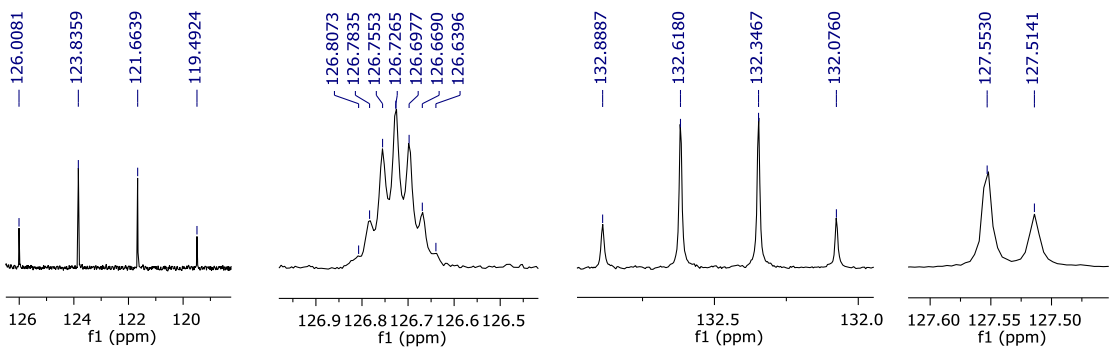

^{1}H NMR (500 MHz) of *N*,*N*′-diacetyl-*N*,*N*′-dibenzylcystinamide (L-cystine) (79) in $CDCl_3$

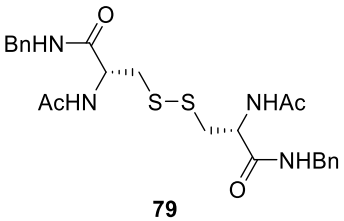

79

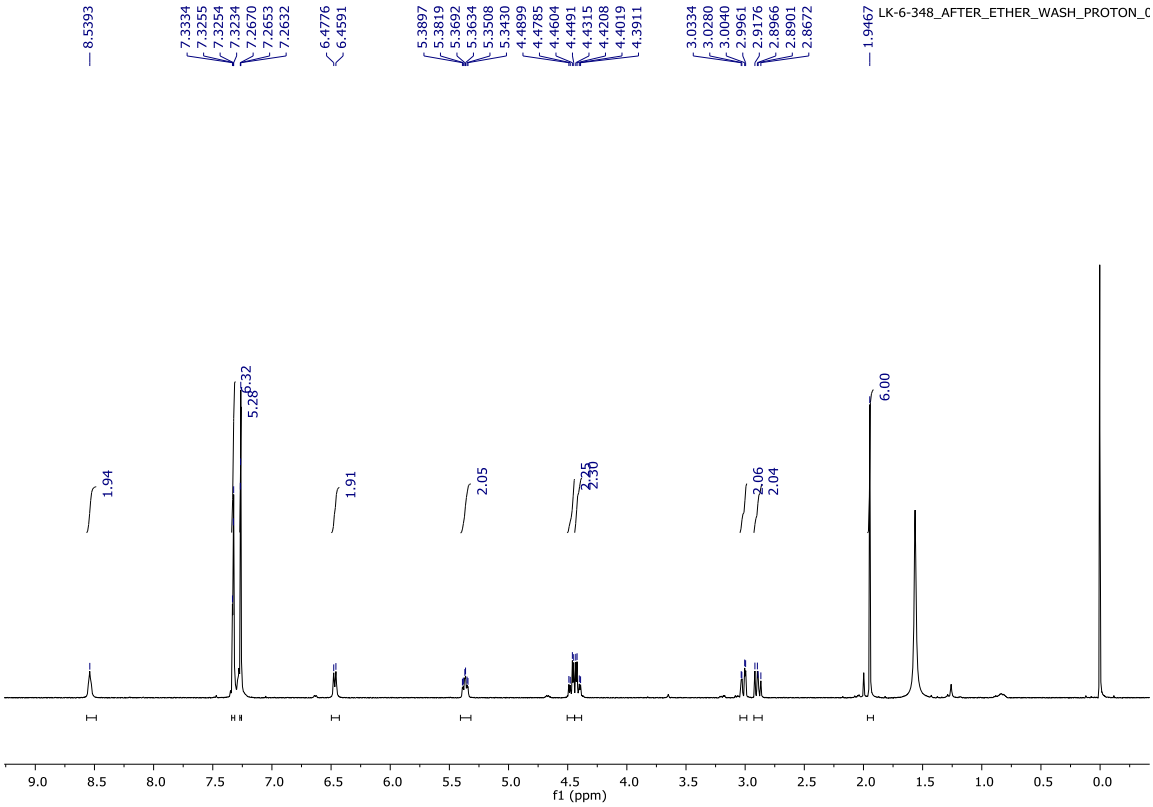

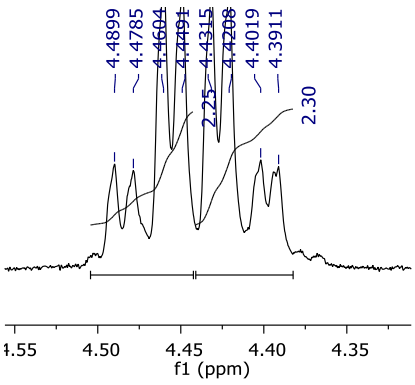

^{13}C NMR (125 MHz) of *N*,*N*′-diacetyl-*N*,*N*′-dibenzylcystinamide (L-cystine) (79) in $CDCl_3$

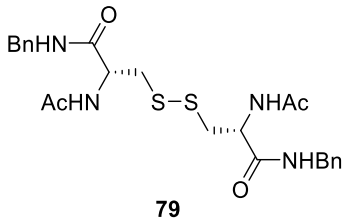

79

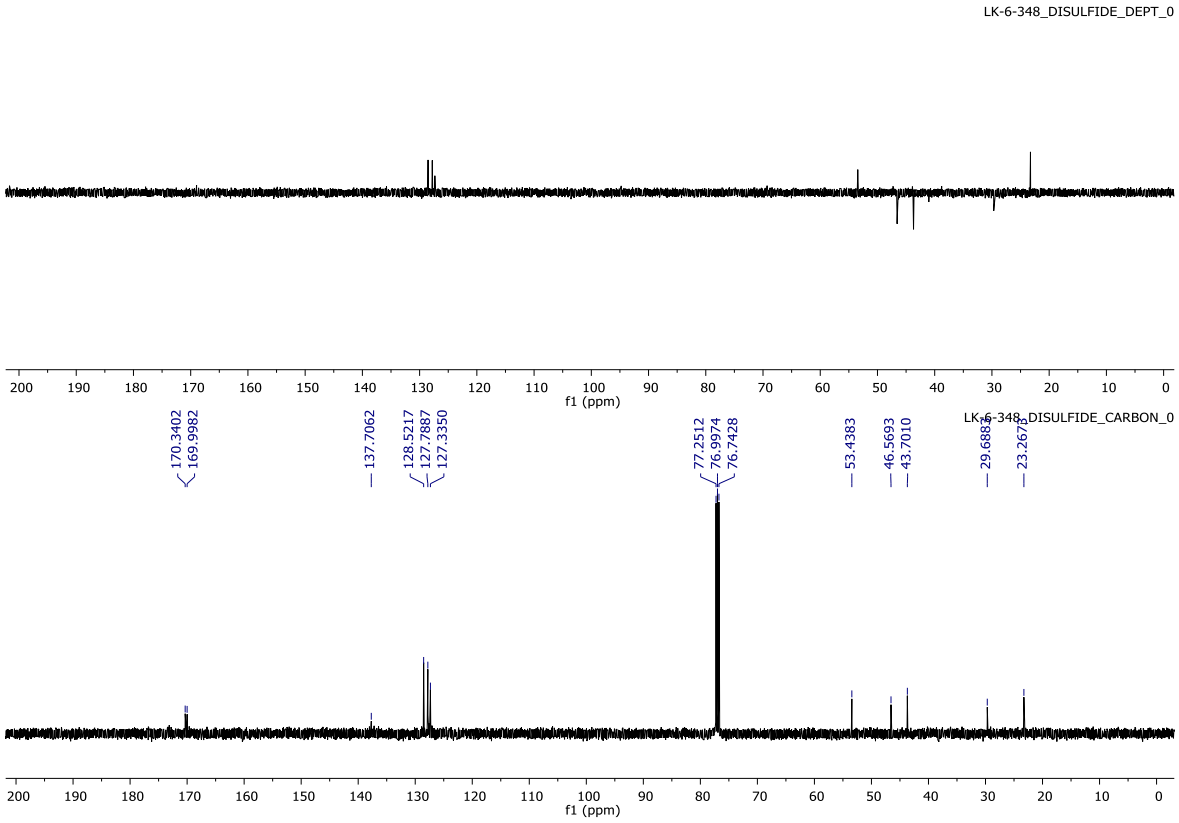

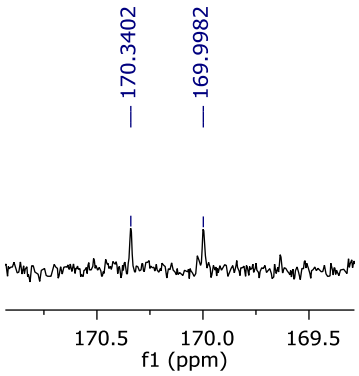

^{1}H NMR (500 MHz) of *N*-(2-benzyl-3-oxo-2,3-dihydro-1,2-thizol-4-yl)acetamide (80) in methanol-d_4/D_2O

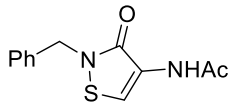

80

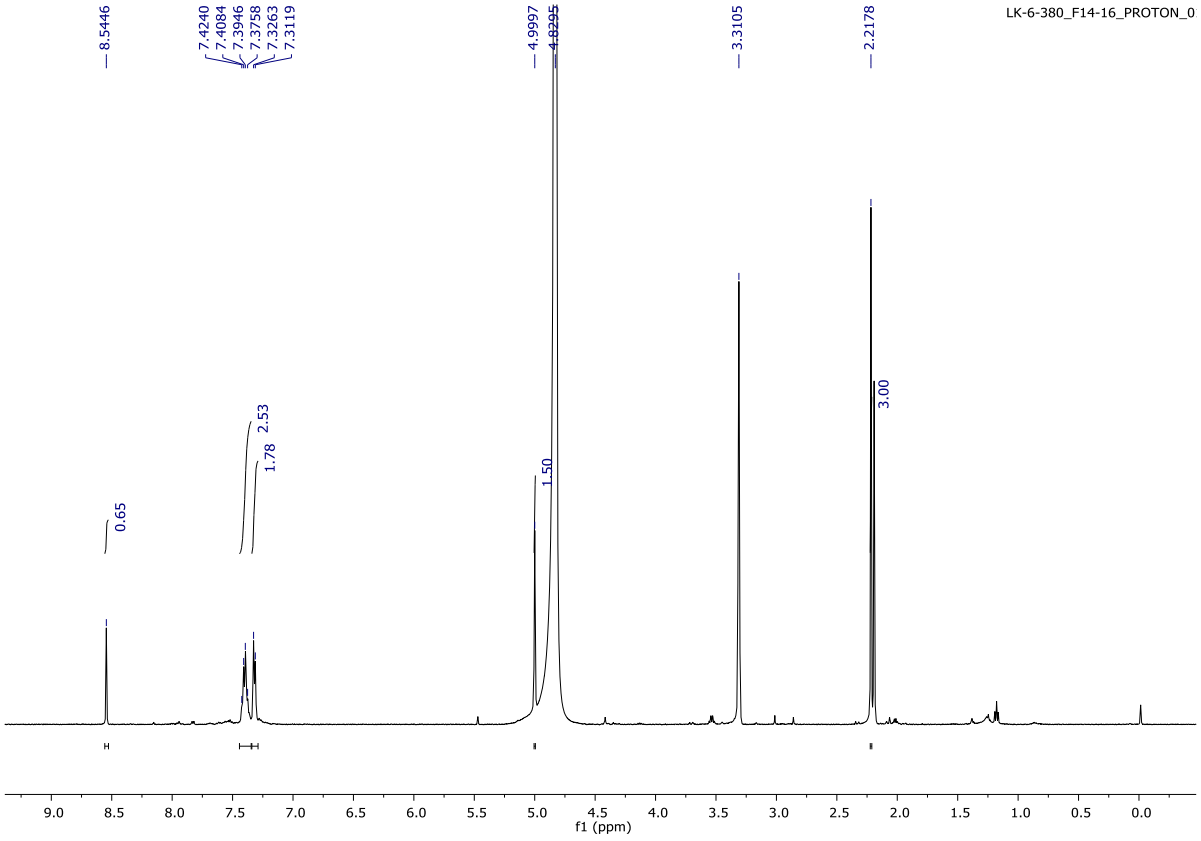

^{1}H NMR (500 MHz) of *N*-(2-benzyl-3-oxo-2,3-dihydro-1,2-thizol-4-yl)acetamide (80) in $CDCl_3$

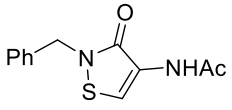

80

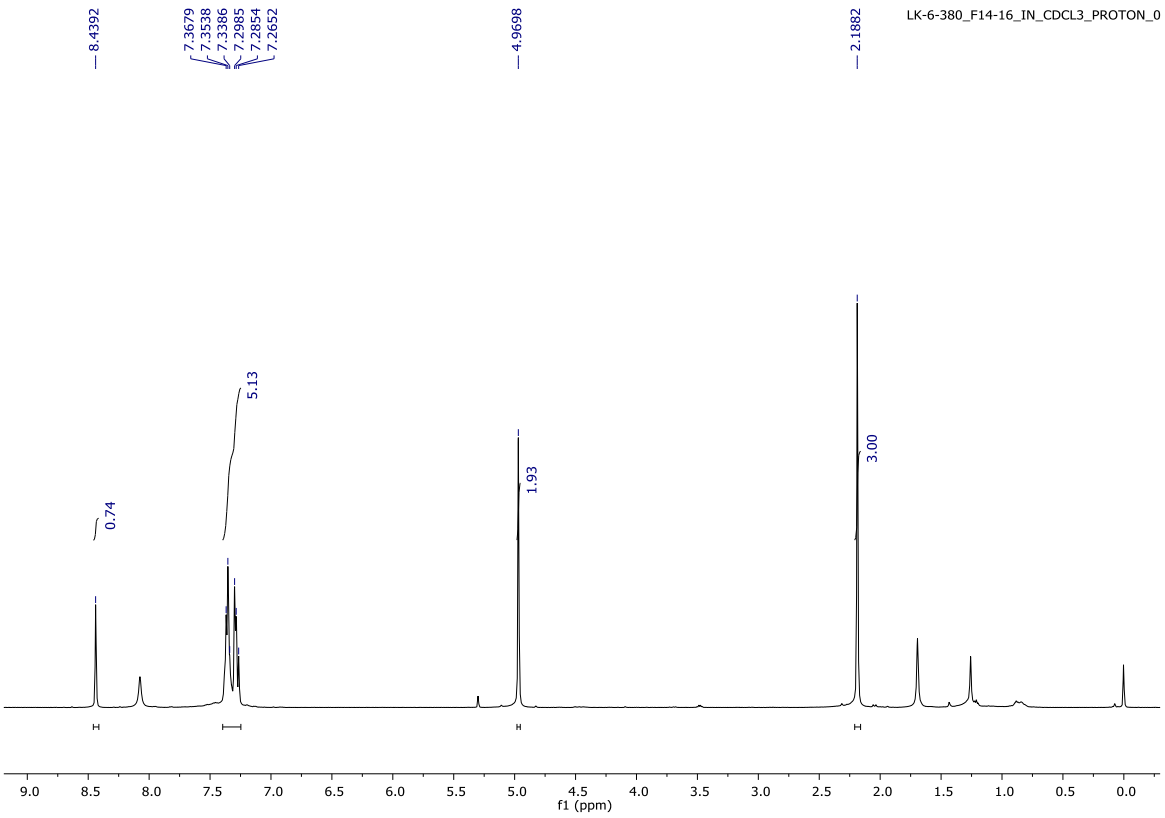

^{13}C NMR (125 MHz) of *N*-(2-benzyl-3-oxo-2,3-dihydro-1,2-thizol-4-yl)acetamide (80) in $CDCl_3$

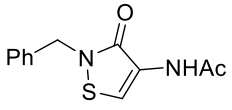

80

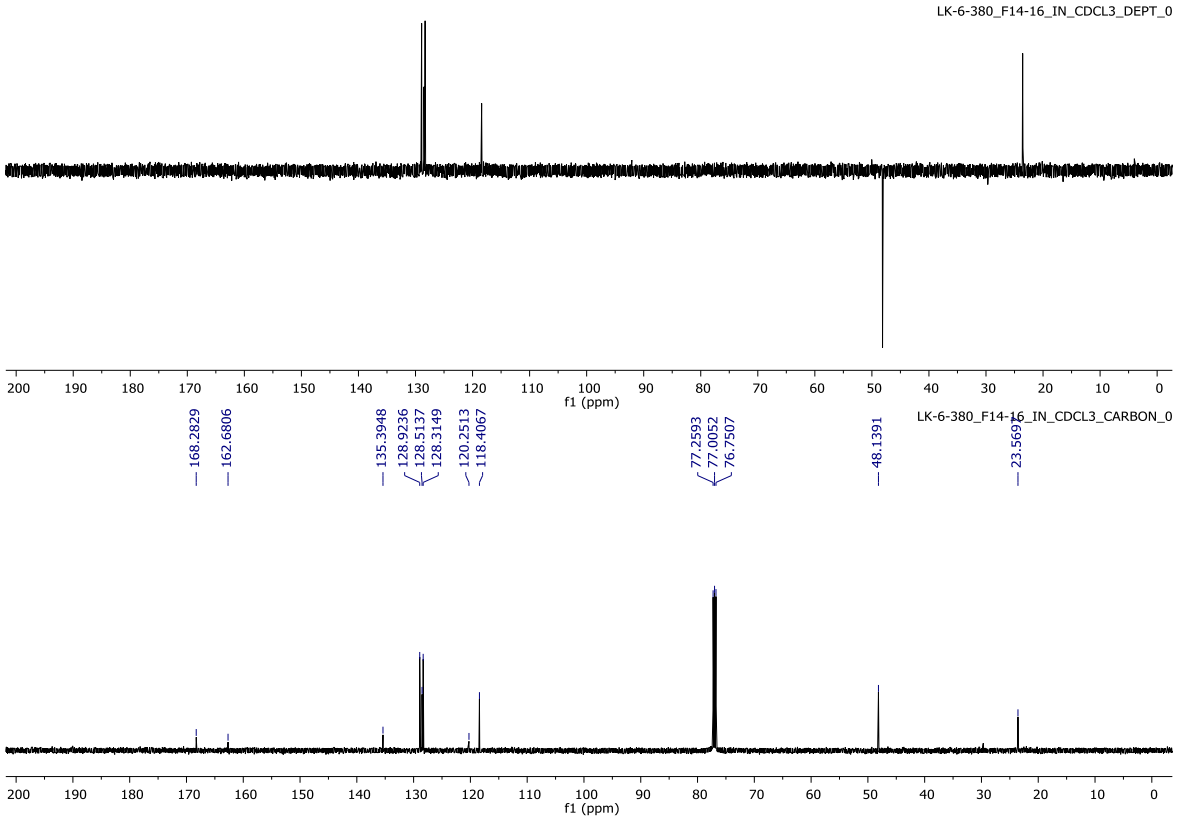

^{1}H-^{13}C HSQC (125 MHz) of *N*-(2-benzyl-3-oxo-2,3-dihydro-1,2-thizol-4-yl)acetamide (80) in $CDCl_3$

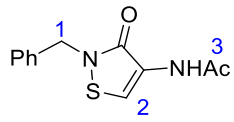

80

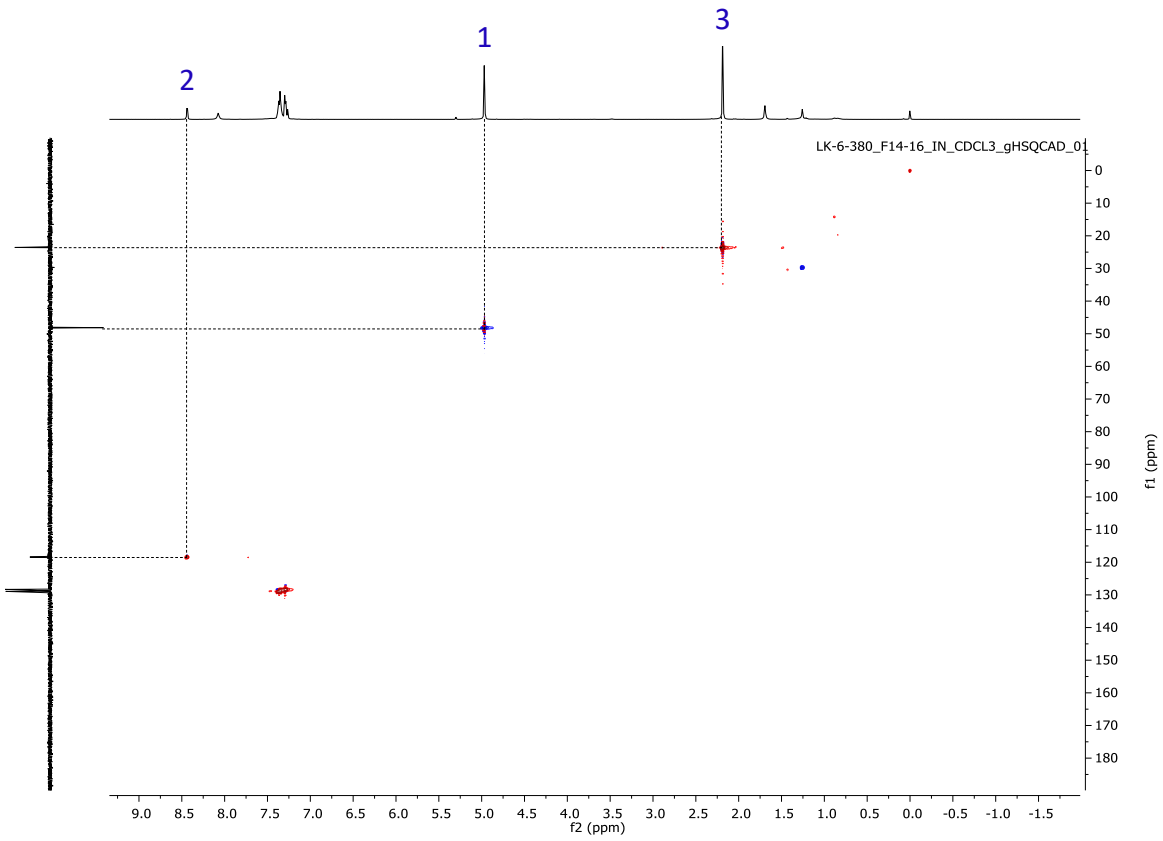

^{1}H NMR (500 MHz) of photolysis mixture containing (1*E*)-2-acetamido-3-(benzylamino)-3-oxoprop-1-ene-1-thiolate (71) in methanol-d_4/D_2O

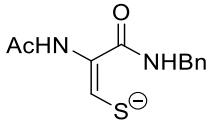

71

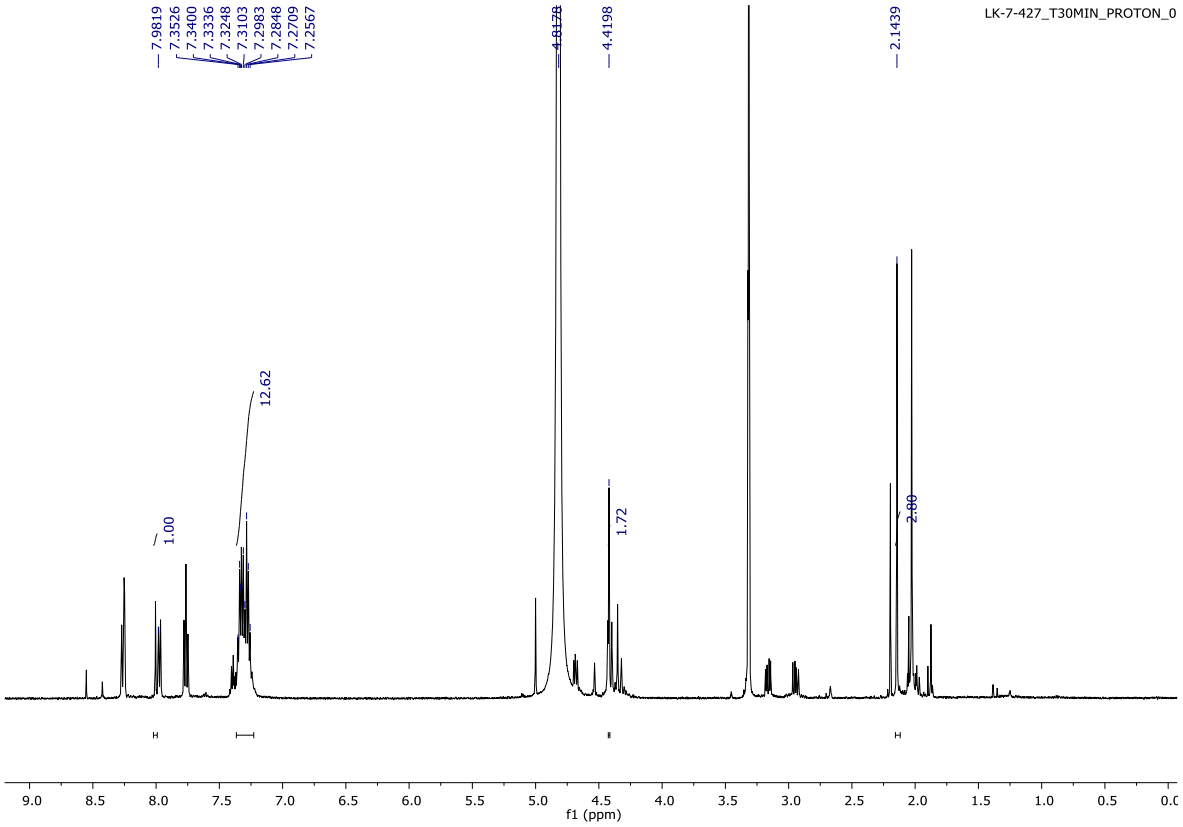

1.6.6 X-Ray Crystallography Data

Table 1.4: X-ray crystallography data and structure refinement for N-(2-benzyl-3-oxo-2,3-dihydro-1,2-thiazol-4-yl)acetamide (**80**).

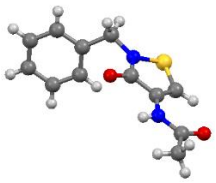

Empirical formula	$C_{12}H_{12}N_2O_2S$
Formula weight	248.30
Temperature	299.0(1) K
Wavelength	0.71073 Å
Crystal system	Monoclinic
Space group	$P2_1/n$
Unit cell dimensions	a = 10.9773(7) Å b = 5.8082(4) Å c = 18.7529(15) Å
Volume	1192.80(15) $Å^3$
Z	4
Density (calculated)	1.383 Mg/m^3
Absorption coefficient	0.262 mm^{-1}
F(000)	520
Crystal size	0.50 x 0.40 x 0.20 mm^3
Theta range for data collection	3.647 to 29.150°.
Index ranges	$-13 \leq h \leq 14, -7 \leq k \leq 7, -24 \leq l \leq 25$
Reflections collected	10229
Independent reflections	2899 [R(int) = 0.0269]
Completeness to theta = 25.242°	99.9 %
Absorption correction	Semi-empirical from equivalents
Max. and min. transmission	1.00000 and 0.70368
Refinement method	Full-matrix least-squares on F^2
Data / restraints / parameters	2899 / 121 / 159
Goodness-of-fit on F^2	1.030
Final R indices [I>2sigma(I)]	R1 = 0.0475, wR2 = 0.1123
R indices (all data)	R1 = 0.0666, wR2 = 0.1243
Extinction coefficient	n/a
Largest diff. peak and hole	0.197 and −0.361 $e.Å^{-3}$
Empirical formula	$C_{12}H_{12}N_2O_2S$

1.6.7 UV-Vis Data

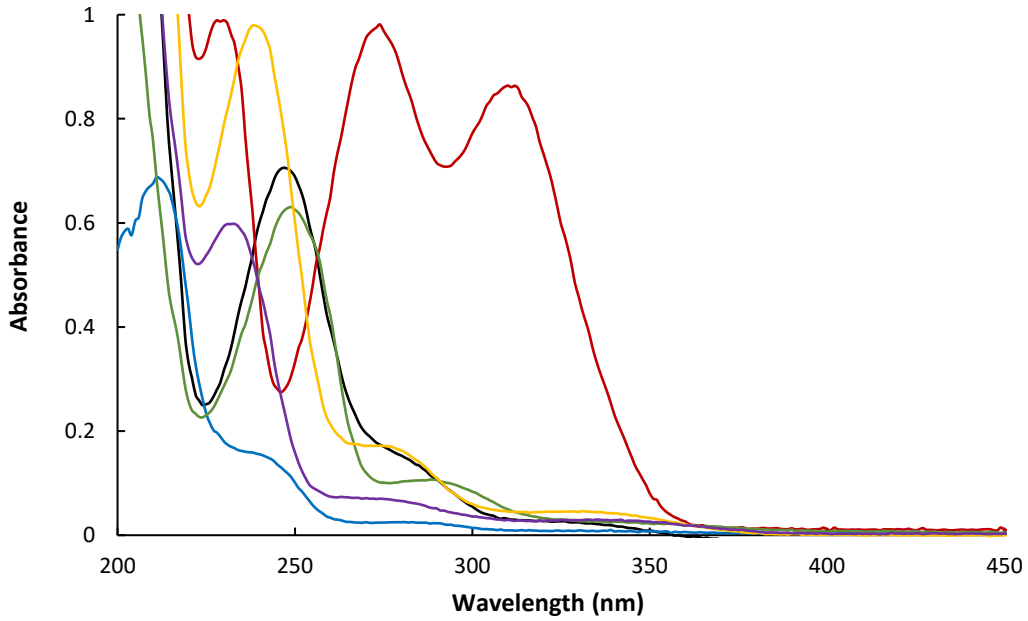

Figure 1.20: UV-vis absorption spectrum of N^2-acetyl-*N*-benzyl-*S*-(2-oxo-2-phenylethyl)cysteinamide **65** (—), N^2-acetyl-*N*-benzyl-*S*-[2-(2,4-dimethoxyphenyl)-2-oxoethyl] cysteinamide **66** (—), N^2-acetyl-*N*-benzyl-*S*-[2-(3-cyanophenyl)-2-oxoethyl]cysteinamide **67** (—), N^2-acetyl-*N*-benzyl-*S*-[2-(4-cyanophenyl)-2-oxoethyl] cysteinamide **68** (—), N^2-acetyl-*N*-benzyl-*S*-{2-oxo-2-[3-(trifluoromethyl) phenyl]ethyl}cysteinamide **69** (—) and N^2-acetyl-*N*-benzyl-*S*-{2-[3,5-bis(trifluoromethyl)phenyl]-2-oxoethyl}cysteinamide **70** (—) in methanol/aq. phosphate buffer (1:1, pH 7.4).

Chapter 2
Anti-Cancer Activity of Phenyl and Pyrid-2-yl 1,3-Substituted Benzo[1,2,4]triazin-7-ones and Stable Free Radical Precursors

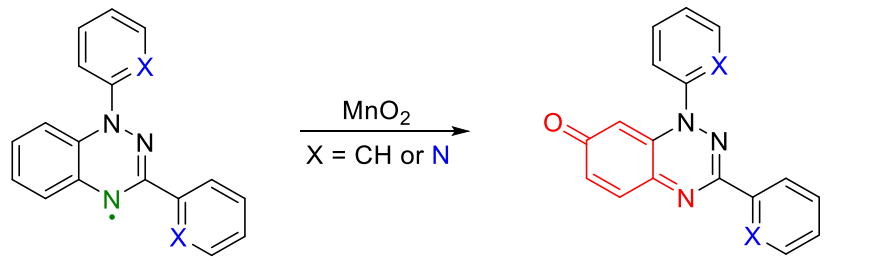

Blatter-type Radical
(less cytotoxic)

Anti-cancer Agents (Cytotoxic)
Very Good Correlation to Pleurotin

Parts of this chapter are published in:

Anti-Cancer Activity of Phenyl and Pyrid-2-yl 1,3-Substituted Benzo[1,2,4]triazin-7-ones and Stable Free Radical Precursors, **Lee-Ann J. Keane**, Styliana I. Mirallai, Martin Sweeney, Michael P. Carty, Georgia A. Zissimou, Andrey A. Berezin, Panayiotis A. Koutentis, and Fawaz Aldabbagh, *Molecules*, **2018**, 23, 574–581.

Invited contribution to the Medicinal Chemistry section of Molecules.

Author contributions will be stated at relevant points of mention and this article is included in the appendix.

2.1 Introduction

2.1.1 The Thioredoxin – Thioredoxin Reductase System

Most cysteine residues of extracellular proteins are involved in disulfide bonds. However, a reducing environment exists inside cells, where most cysteine residues are in the reduced thiol form.[107] The thioredoxin system consists of thioredoxin (Trx), thioredoxin reductase (TrxR) and nicotinamide adenine dinucleotide phosphate (NADPH) and its primary function is the regulation of the cellular redox balance[108] through catalytic reversible reduction of disulfide bonds in target proteins.[109] Trx is a protein that contains two cysteine residues in its active site with the amino acid sequence: -Cys-Gly-Pro-Cys-. Trx can exist in the oxidised form with an intramolecular disulfide bridge or in the reduced dithiol form.[110] TrxR is the only known enzyme that reduces Trx. TrxR is a selenoflavoprotein homodimer in which each monomer contains a flavin adenine dinucleotide (FAD) group, an NADPH binding site and an active site containing a redox-active selenium–sulfur bond. The active site amino acid sequence of TrxR is -Gly-Cys-SeCys-Gly-.[110,111]

The catalytic cycle (Figure 2.1) involves NADPH binding to the NADPH-binding domain of TrxR. Electrons transfer from NADPH through FAD and then to the active site of the TrxR, which reduces its selenylsulfide, thus forming a selenolate anion. The selenolate anion attacks the disulfide of Trx forming an enzyme–Trx-mixed selenylsulfide intermediate. This intermediate is attacked by its neighbouring cysteine residue to regenerate the selenylsulfide of TrxR and reducing the Trx to the dithiol form. The reduced Trx then reduces the disulfide of a substrate protein and the disulfide of Trx is reformed (Figure 2.1).[110–113]

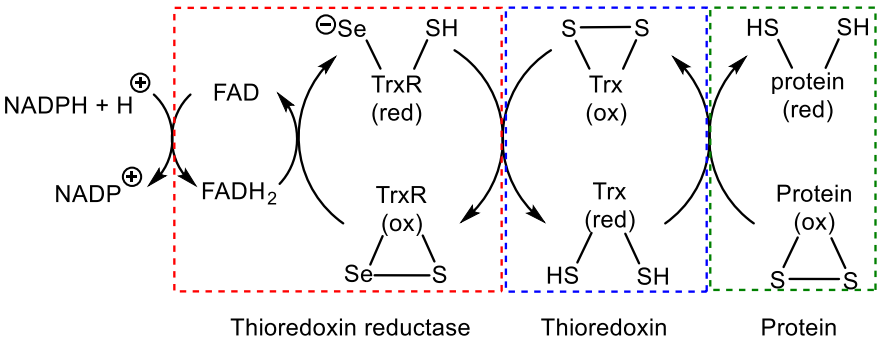

Figure 2.1: Mechanism of protein disulfide reduction in the Trx–TrxR catalytic cycle.[110]

Trx is known to be overexpressed in many cancers such as lung[114], cervical,[115] prostate[116] and breast cancers[117] and studies have shown a relationship between the over-expression of Trx and enhanced cancer cell growth.[118–120] High levels of Trx have also been correlated with resistance

to chemotherapeutic agents such as cisplatin.[121] Therefore Trx and other members of the Trx system are significant targets in the development of anti-cancer strategies.

Negative regulation of Trx through the inhibition of TrxR is a known anti-cancer strategy. As tumour cells often produce excessive amounts of reactive oxygen species (ROS), due to their high metabolic rate, high levels of oxygen scavenging enzymes, such as TrxR are produced. These enzymes counteract excessive ROS production, thereby preventing ROS–induced cell death. The inhibition of TrxR results in an increase in the level of oxidized Trx and a decrease in the level of reduced Trx, therefore altering the entire Trx–TrxR system. Reduced Trx catalyses the reduction of disulfides of many proteins which have been oxidized by ROS and Trx can then be reduced by TrxR. Therefore, the inhibition of TrxR is a promising strategy for the development of anti-cancer drugs.[108,116] A number of TrxR inhibitors have been approved by the FDA, for example, arsenic trioxide binds to TrxR resulting in irreversible inactivation and inhibition of the growth of breast cancer cells (MCF-7).[116,119]

2.1.2 Pleurotin – A Known TrxR Inhibitor

Pleurotin, a naturally occurring *para*-quinone antibiotic was first isolated in the 1940s from the basidiomycete, *Pleurotus griseus* (Figure 2.2).[122] It is known to exhibit antibacterial,[122] antifungal[123] and anti-cancer activities through the inhibition of the hypoxia-induced factor (HIF-1α), a transcription factor associated with tumour growth.[124] Pleurotin's carbocyclic nucleus is uncommon in natural products; however, the trans-fused perhydroindan is common to many terpenoids, and quinones that are substituted with two benzylic leaving groups appear in many antitumour agents, which are classified as bioreductive bisalkylating agents.[125]

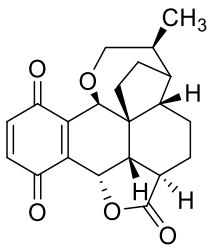

Figure 2.2: Structure of pleurotin.

Pleurotin is also a known potent inhibitor (IC_{50} 0.17 μM) of the Trx–TrxR system and this is the underlying pathway of much of the biological activity associated with pleurotin.[126] It has previously been suggested that the bioactivation of pleurotin **1** may occur through reduction to hydroquinone **2** followed by elimination giving quinone methide **3**. This quinone methide **3**

could behave as an alkylating agent or it could undergo elimination to give alcohol **4** followed by alkylation with biologically active nucleophiles such as cysteine of Trx to give crosslink **5** (Scheme 2.1).[127,128] Interruption of biologically important events by crosslinking may be responsible for cell damage.[128]

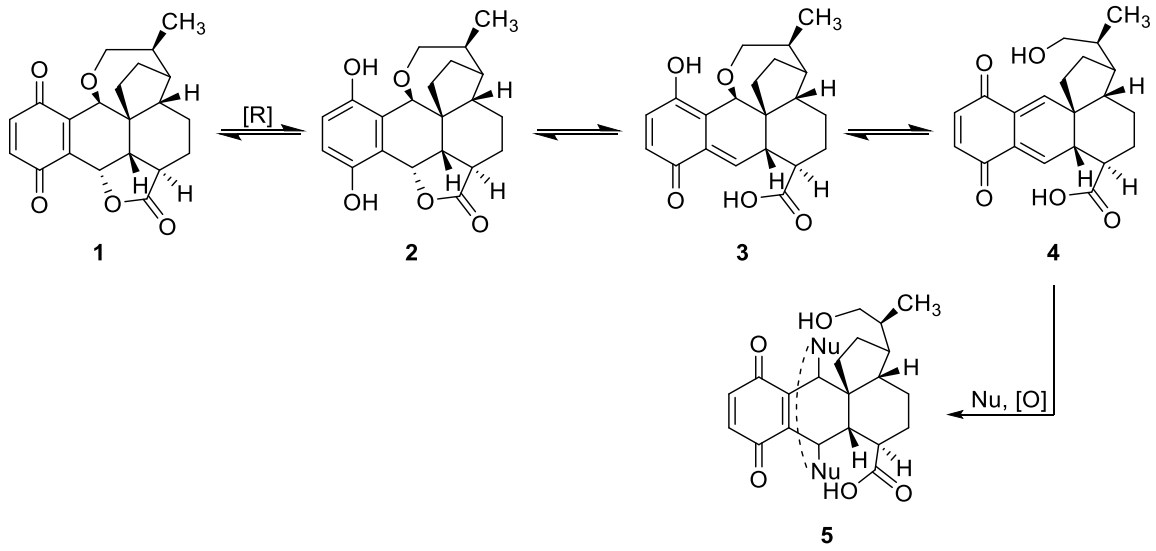

Scheme 2.1: Suggested bioactivation of pleurotin.[128]

Pleurotin irreversibly inhibits TrxR, as identified by the National Cancer Institute's (NCI) COMPARE algorithm. It was discovered to have growth inhibitory activity similar to PX-12, a substituted 2-imidazolyl disulfide (Figure 2.3) and known Trx inhibitor, against the NCI human cancer cell line panel. Similar to PX-12, pleurotin inhibited the growth of both MCF-7 (breast cancer) and HT-29 (colon cancer) cells (IC_{50} 0.9 μM).[129,130] The disulfide of PX-12 interacts with Trx through a thiol–disulfide exchange/thioalkylation with a cysteine residue in the catalytic site of Trx with the release mercaptoimidazole.[130]

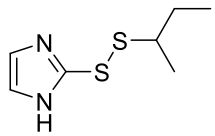

Figure 2.3: Structure of PX-12.

2.1.3 Cytotoxicity of Benzo[1,2,4]triazin-7-ones

Benzo[1,2,4]triazin-7-one derivatives are well known TrxR inhibitors. Sweeney *et al.*[131] investigated the structural requirements for cytotoxicity of several benzo[1,2,4]triazin-7-ones (Figure 2.4), which contain a highly conjugated iminoquinone motif. Substitution at the 6-position and 3-position was investigated so that the derivatives could be tested for both

inhibitory activity towards TrxR and cytotoxicity against a number of cancer cell lines (breast cancer (MCF-7), prostate cancer (DU-145) and normal skin fibroblast (GM00637) cell lines).

The parent structure, 1,3-diphenylbenzo-[*e*][1,2,4]-triazine-7-(1*H*)one **6** (Figure 2.4 and Table 2.1) displayed submicromolar toxicities towards all cancer cell lines, the resulting IC_{50} values being comparable to those of pleurotin. Substitution with the electron-donating methoxy and ethoxy groups at the 6 position (compounds **7** and **8**) decreased cytotoxicity to negligible values. This result was correlated to a reduced electron affinity owing to the presence of the electron-donating group. 1-Phenyl-3-(trifluoromethyl)benzo[1,2,4]triazin-7-one (Figure 2.4, Table 2.1, compound **9**), which was substituted with a CF_3 group at the 3-position showed greater specificity towards tumour cell lines.[131]

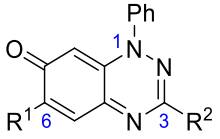

6, R^1 = H, R^2 = Ph
7, R^1 = OMe, R^2 = Ph
8, R^1 = OEt, R^2 = Ph
9, R^1 = H, R^2 = CF_3

Figure 2.4: Benzo[1,2,4]triazin-7-ones.

Table 2.1: Cytotoxicity evaluation of pleurotin and compounds **6**–**9**.[131]

Compound	R-group		Cell lines (IC_{50} values in µM)		
	R^1	**R^2**	**GM00637**	**DU-145**	**MCF-7**
	Pleurotin		0.51 ± 0.12	0.43 ± 0.06	0.28 ± 0.03
6	H	Ph	0.23 ± 0.01	0.23 ± 0.03	0.81 ± 0.08
7	OMe	Ph	> 5.0	> 5.0	> 5.0
8	OEt	Ph	>5.0	> 5.0	> 5.0
9	H	CF_3	1.61 ± 0.21	0.85 ± 0.04	0.60 ± 0.13

Both benzo[1,2,4]triazin-7-ones **6** and **9** (Figure 2.5) show strong correlations to pleurotin (Pearson correlation coefficients ~0.8) as shown by NCI COMPARE analysis. Both **6** and **9**, like pleurotin, are thus TrxR inhibitors (as shown by a TrxR inhibition assay) although the mode of inhibition was found to be reversible rather than irreversible inhibition as in the case of pleurotin. NCI one dose (10 µM) data of **6** showed significant cytotoxicity against the

DU-145 and MCF-7 cancer cell lines while **9** exhibited cytotoxicity against the MCF-7 cancer cell line.[131]

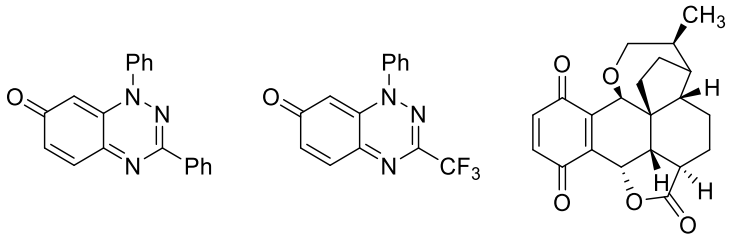

6
Pearson correlation coefficient: 0.842

9
Pearson correlation coefficient: 0.793

Pleurotin

Figure 2.5: 1,3-Diphenylbenzo-[*e*][1,2,4]-triazine-7-(1*H*)one **6**, 1-phenyl-3-(trifluoromethyl)benzo [1,2,4]triazin-7-one **7**, and pleurotin.

2.1.4 Synthetic Routes to Benzo[1,2,4]triazin-7-ones

Koutentis and co-workers[132] developed a high-yielding synthesis of **6** through a manganese dioxide (MnO_2) mediated oxidation of Blatter's radical **10** (1,3-diphenyl-1,4-dihydro-1,2,4-benzotriazin-4-yl). Similarly **6** can be obtained through a potassium permanganate ($KMnO_4$) mediated oxidation of an amidrazone precursor **11** (Scheme 2.2).[133]

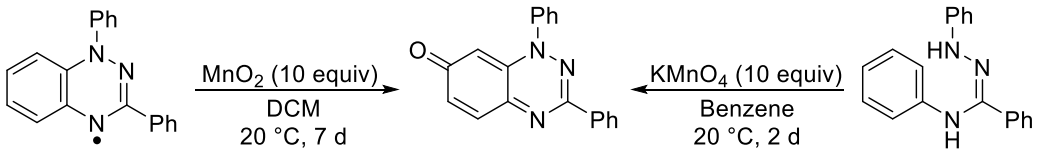

10

6
Yield: 84%

11
Yield: 62%

Scheme 2.2: MnO_2/ $KMnO_4$ mediated oxidation of Blatter's radical **10** or amidrazone **11** to give 1,3-diphenylbenzo[1,2,4]triazin-7-one **6**.

2.1.5 Blatter's Radical

Blatter's radical, 1,3-diphenyl-1,4-dihydro-1,2,4-benzotriazin-4-yl (**10**) which was first synthesized by Blatter *et al.* in 1968,[134] is electron rich and is known to be a stable neutral organic radical.[134,135] Blatter's radical undergoes two fully reversible one electron redox reactions[136] to give anion $\mathbf{10}^-$ and cation $\mathbf{10}^+$ (Scheme 2.3).

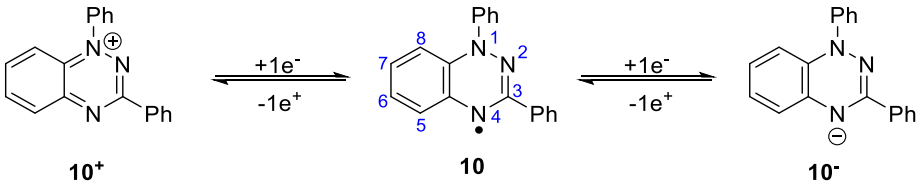

Scheme 2.3: Redox behaviour of Blatter's radical **10**.[136]

Blatter's radical **10** can be stored for months under ambient conditions while some derivatives such as one that incorporates a highly electron-withdrawing trifluoromethyl group at the C7 position (Figure 2.6) is known to exhibit even more oxidative stability than the parent radical. This was shown by treatment of Blatter's radical **10** with the oxidant, MnO_2 in DCM at 20 °C for 7 d. Oxidation to the corresponding benzo[1,2,4]triazin-7-one **6** was observed (Scheme 2.2); however when the 7-trifluoromethylbenzotriazinyl (Figure 2.6) was treated with the same conditions, no new products were formed and the starting radical was recovered. This added stability is due to the C7 position being blocked against further oxidation.[132,137]

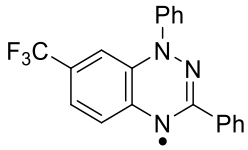

Figure 2.6: 7-Trifluoromethylbenzotriazinyl radical.

Blatter's radical **10** owes its air, moisture and thermal stability to extensive delocalization of spin density on both the endocyclic nitrogen atoms and the fused arene.[138,139] The unpaired electron is thus not confined to one nitrogen atom (N4), as in its normal depiction; rather, it is delocalized across both the triazinyl ring and the fused benzene.[137] EPR studies carried out by Koutentis and co-workers on Blatter's radical have shown that the spin density was primarily delocalized on the 1,2,4-amidrazonyl moiety (**10**, Scheme 2.3). The largest hyperfine coupling constant was observed on N1 (7.5 G) whereas the coupling constants are smaller for N2 and N4 and are approximately equal (5.1 G each).[132]

Blatter's radical **10** has been previously synthesized by Koutentis and co-workers[133] through a mild and high-yielding catalytic oxidation of its amidrazone precursor **11** (*N*-phenylamidrazone) by using diazabicyclo[5.4.0]undec-7-ene (DBU) and palladium on carbon under an atmosphere of air (Scheme 2.4).

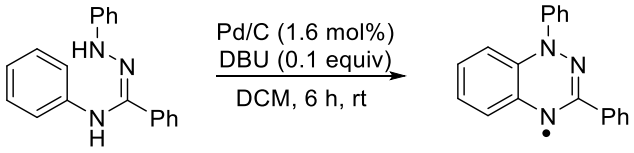

11 **10**
Yield: 98%

Scheme 2.4: Synthesis of Blatter's radical.[133]

2.1.6 Nitroxides

Nitroxides or nitroxyl radicals are a class of stable, organic radicals[140] that incorporate an *N*,*N*-disubstituted N-O group containing one unpaired electron. A number of factors contribute to the stability of nitroxides. The high delocalization energy of the unpaired electron over the nitrogen-oxygen bond provides thermodynamic stability to the radical (Figure 2.7).[141]

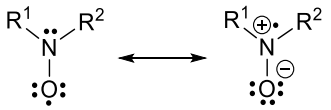

Figure 2.7: Nitroxide resonance structures.[141]

Dimerization would result in the formation of a weak O–O bond, which would not compensate for the loss of delocalization energy of the two nitroxide groups.[142] Steric hindrance of the radical centre, caused by the presence of bulky substituents on the α carbon atoms inhibits bimolecular reactions of nitroxides. The presence of bis(*tert*-alkyl) substituents, which do not contain β-hydrogen atoms, prevent nitroxides undergoing disproportionation reactions.[141]

TEMPO (2,2,6,6-tetramethyl-piperidin-1-oxyl, Figure 2.8) is a well-known stable nitroxyl radical, which exhibits antioxidant properties owing to its ability to act as a radical scavenger.[143] The non-conjugated, stable radical nature of TEMPO is attributed to the kinetic stability that is imparted by the presence of bulky α-methyl substituents,[144] making it sterically difficult for the radical to combine with other molecules, thus leading to unproductive quenching.[145]

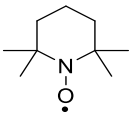

Figure 2.8: TEMPO.

Suy *et al.* found TEMPO to be cytotoxic against the breast cancer MDA-MB 231 cell line (IC_{50} 10 mM). Treatment of prostate cancer cells with TEMPO resulted in an IC_{50} value of

2.5 mM.[146] TEMPO is an uncharged nitroxide at physiological pH. It can readily cross the cell membrane and accumulate in the cell due to its lipophilic character and low molecular weight.[147]

2.1.7 Influence of Pyridine on Cytotoxicity

Moriarty *et al.*[148] reported a pyridyl-fused benzimidamidazole-4,7-dione (**12**; Figure 2.9) which exhibited cytotoxicity against DU-145 cancer cells. Quinone **12** was found to be more cytotoxic towards the DU-145 cell line compared to the fused aryl ring analogue. It was proposed that the highly conjugated structure would promote bioreduction owing to more stable reduced intermediates and result in selective cytotoxicity towards cancer cells that have high levels of reductase enzymes such as NAD(P)H:quinone oxido-reductase (NQO1), which is known to be expressed in high levels in the prostate cancer cell line (DU-145) and the cervical cancer cell line (HeLa).

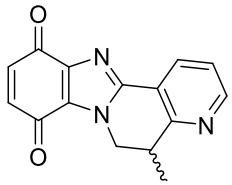

12

IC_{50} (DU-145): 0.7 μM

Figure 2.9: Cytotoxicity of pyridyl-fused and 2-pyridyl substituted benzimidamidazole-4,7-diones.

2.2 Aims and Objectives

Benzo[1,2,4]triazin-7-one **6** (Figure 2.4), substituted at the 3-position has previously been shown to exhibit submicromolar cytotoxicity against breast and prostate cancer cell lines as well as strong correlations to the naturally occurring anti-cancer agent pleurotin. The incorporation of pyridine into cytotoxic compounds has also been shown to significantly alter cytotoxicity against cancer cell lines. Based on these findings, this chapter is focused on the cytotoxicity evaluation of the benzo[1,2,4]triazin-7-ones, 3-phenyl-1-(pyrid-2-yl)benzo[*e*][1,2,4]triazin-7(*H*)-one (**13**) and 1-phenyl-3-(pyrid-2-yl)benzo[*e*][1,2,4]triazin-7(*H*)-one (**14**) (Figure 2.10) which incorporate a pyridine ring at the N1 or C3 position, respectively. In addition, as the stable free radical TEMPO is known to exhibit cytotoxicity (against the breast cancer cell line, MDA-MB 231) the benzotriazin-4-yl radical precursors (Blatter-type), **15** and **16**, of benzo[1,2,4]triazin-7-ones **13** and **14** will also be evaluated for cytotoxicity against breast and prostate cancer cell lines with contrast to the oxidation products **13** and **14** (Figure 2.10). The cytotoxicity of all compounds (**13**–**16**) will be measured using the MTT (3-(4,5-dimethylthiazol-2-yl)-2,5-diphenyltetrazolium bromide) colorimetric assay using the breast (MCF-7) and prostate (DU-145) cancer cell lines.

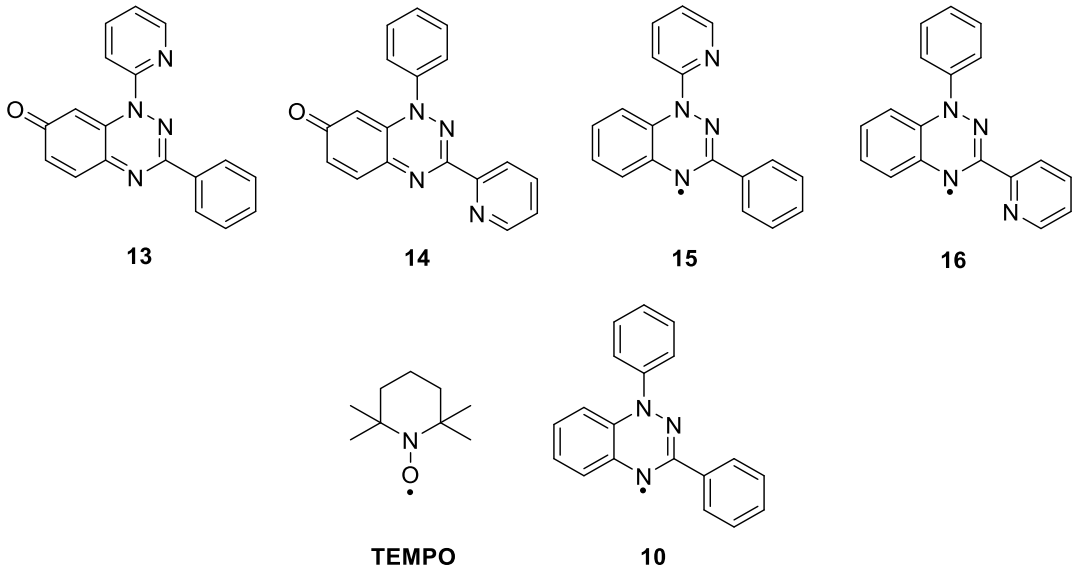

Figure 2.10: Benzo[1,2,4]triazin-7-ones **13** and **14**, benzotriazin-4-yl radical precursors **15** and **16**, TEMPO and Blatter's radical **10** were biologically evaluated against two human cancer cell lines, MCF-7 and DU-145.

2.3 Results and Discussion

2.3.1 The Effect of Variation of Aromatic Substituents at N1 and C3 Positions of Benzo[1,2,4]-triazin-7-ones on cytotoxicity

New pyridyl-substituted benzo[1,2,4]triazin-7-ones, **13** and **14** were prepared by our collaborators Koutentis and co-workers[136] through the MnO_2-mediated oxidation of benzotriazin-4-yl radicals, **15** and **16** in 90 and 46% yields, respectively (Scheme 2.5).

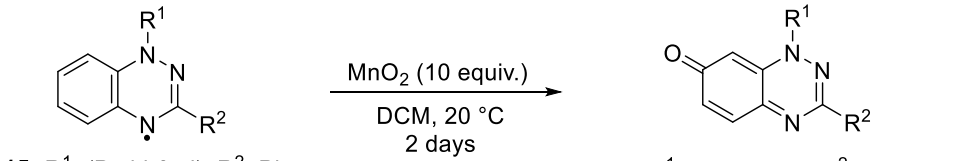

15: R^1=(Pyrid-2-yl), R^2=Ph
16: R^1=Ph, R^2=(Pyrid-2-yl)

13: R^1=(Pyrid-2-yl), R^2=Ph, 90%
14: R^1=Ph, R^2=(Pyrid-2-yl), 46%

Scheme 2.5: Synthetic route to benzo[1,2,4]triazin-7-one.[136]

The MCF-7 (breast cancer) and DU-145 (prostate cancer) cell lines were used to determine the IC_{50} values of benzo[1,2,4]triazin-7-ones, **13** and **14**. The MTT colorimetric assay was used to determine the IC_{50} values. The IC_{50} value represents the concentration required for the reduction of the mean cell viability to 50% of the control cells after incubation for 72 h at 37 °C as determined by the MTT assay. Both **13** and **14** displayed submicromolar cytotoxicities towards MCF-7 and DU-145 cancer cell lines as shown by MTT assay (Figure 2.11 and Table 2.2). Greater cytotoxicity was exhibited by both **13** and **14** towards the DU-145 cancer cell line. These cytotoxicities were comparable with the parent structure **6** in the case of the DU-145 cancer cell line and significantly more cytotoxic (over a 2-fold increase) towards the MCF-7 cancer cell line (Figure 2.11 and Table 2.2).

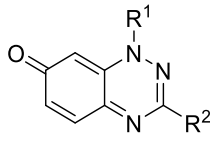

6, R^1=Ph, R^2=Ph
13, R^1=(Pyrid-2-yl), R^2=Ph
14, R^1=Ph, R^2=(Pyrid-2-yl)

Figure 2.11: General benzo[1,2,4]triazin-7-one structure to represent the parent structure **6** and the evaluated compounds **13** and **14**.

Table 2.2: The effect of a variation of aromatic substituents at the N1 and C3 positions of the benzo[1,2,4]triazin-7-one scaffold on cytotoxicity against DU-145 and MCF-7 cancer cell lines.

Compound	R^1	R^3	IC_{50} DU-145 (µM)	IC_{50} MCF-7 (µM)
6	Ph	Ph	0.230 ± 0.03	0.810 ± 0.08
13	Pyrid-2-yl	Ph	0.245 ± 0.003	0.303 ± 0.009
14	Ph	Pyrid-2-yl	0.241 ± 0.011	0.277 ± 0.002

2.3.2 The effect of Blatter-type (Benzotrizin-4-yl) Radical Precursors on Cytotoxicity versus Benzo[1,2,4]-triazin-7-ones

Benzotriazin-4-yl radicals **15** and **16** were prepared by our collaborators Koutentis and co-workers through a one-pot reduction and cyclodehydration of the corresponding *N*′-(2-nitrophenyl)-*N*′-phenyl-benzohydrazide precursors, **17** and **18** using Sn powder in AcOH followed by an alkali work-up. This protocol gave 3-phenyl-1-(pyrid-2-yl)-1,4-dihydrobenzo[*e*][1,2,4]-benzotriazin-4-yl **15** and 1-phenyl-3-(pyrid-2-yl)-1,4-dihydrobenzo[*e*][1,2,4]triazine-4-yl **16** in 77% and 82% yield, respectively (Scheme 2.6).[149]

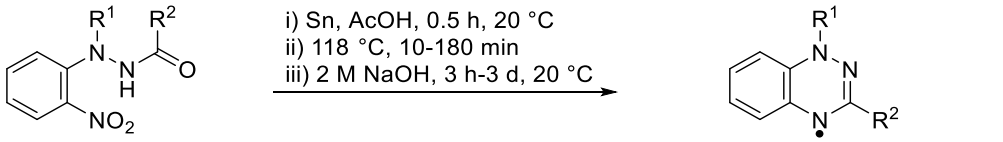

17, R^1=(Pyrid-2-yl), R^2=Ph
18, R^1=Ph, R^2=(Pyrid-2-yl)

15, R^1=(Pyrid-2-yl), R^2=Ph, 77%
16, R^1=Ph, R^2=(Pyrid-2-yl), 82%

Scheme 2.6: Synthetic route to benzo[1,2,4]-triazin-7-ones.[149]

Both benzotriazin-4-yl radicals **15** and **16** showed selectivity towards the DU-145 cancer cell line and were approximately 10 times more cytotoxic towards this cell line compared with the MCF-7 cancer cell line (Figure 2.12 and Table 2.3). These radicals were approximately 13 and 105 times less cytotoxic towards the DU-145 and MCF-7 cancer cell lines, respectively, compared with their corresponding benzo[1,2,4]triazin-7-one oxidation products, **13** and **14**. TEMPO was found to be relatively non-toxic, a result that was expected as it has previously been reported that high concentrations (2.5 mM for 24 h) are required to induce a 3.4-fold increase in both early apoptotic cells and late apoptotic/necrotic cells compared with untreated DU-145 cell controls.[146] High concentrations of TEMPO were also required to obtain a therapeutic dose against various prostate and breast cancer cell lines.[146,147]

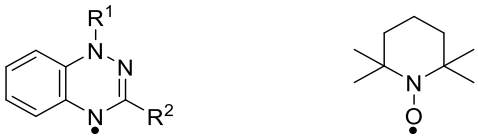

15, R^1=(Pyrid-2-yl), R^2=Ph
16, R^1=Ph, R^2=(Pyrid-2-yl)

TEMPO

Figure 2.12: Benzotrizin-4-yl radicals and TEMPO.

Table 2.3: Cytotoxicity of benzotrizin-4-yl radical precursors on DU-145 and MCF-7 cell lines.

Compound	R^1	R^2	IC_{50} DU-145 (µM)	IC_{50} MCF-7 (µM)
TEMPO			151.400 ± 7.480	>999
15	Pyrid-2-yl	Ph	3.140 ± 0.179	34.740 ± 6.236
16	Ph	Pyrid-2-yl	3.177 ± 0.154	26.415 ± 2.538

2.3.3 National Cancer Institute (NCI) – 60 Tumour Cell Line Screen

Since the early 1990s, over 100,000 compounds and over 50,000 natural products have been screened for their effects on cell viability by the NCI under the Development Therapeutics Program (DTP).[150] A panel of 60 tumour cell lines, derived from nine tumour types is used, including cells from leukaemia, lung, melanoma, colon, ovarian, prostate, breast, renal and central nervous system (CNS) tumours to identify potential anti-tumour candidates. Cells placed in 96-well plates are first exposed to a single concentration (10 µM) of the test compound for 48 h. The sulforhodamine B assay is then used to determine cell viability.[151] If the test compound shows activity, five concentrations of the test compound are used against all cell lines. The toxicity of test compounds is expressed by the GI_{50} (the concentration of the test compound required for 50% growth inhibition relative to control cells that have not been exposed to the test compound), LC_{50} (the concentration of the test compound required to kill 50% of the cells that were present at the time the test compound was added) and TGI (the concentration of the compound required for no net growth of cells to occur during the course of the assay). Using these parameters, the NCI COMPARE algorithm can determine the degree of similarity of the cytotoxicity profiles of test compounds with those of known compounds in the NCI database. This program uses a commercially available SAS statistical package to calculate Pearson correlation coefficients to show the similarity between two cytotoxicity profiles and is expressed as a value between −1 and +1. A coefficient of 0 indicates no correlation, a +1 coefficient indicates direct correlation and a −1 coefficient indicates direct

inverse correlation. Coefficients in the range of ±0.3 to ±0.5 are medium strength. Coefficients above ±0.5 are strong. Therefore it is possible for the mode of action of test compounds to be determined if the cytotoxic response is similar to that of compounds where the mode of action is known.[131,152]

The benzotriazin-4-yl radicals **15** and **16** were not selected by the NCI for cytotoxicity evaluation. The benzo[1,2,4]triazin-7-one **13** and **14** were selected for the initial one-dose (10 μM) screening against the NCI's 60 cell line panel (Figure 2.13 and Figure 2.14). The one-dose data is reported as a mean graph of the growth percent of each cancer cell line (Figure 2.14). The growth percent value that is reported for each cell line is calculated with respect to untreated cells and the number of cells at time zero. A growth percent value of 100 indicates normal cell growth and values from 0–100 represents growth inhibition. Growth percent values that are less than 0 represent lethality. A growth percent value of 0 represents no net growth during the experiment. For example, a growth percent value of −56 corresponds to 56% lethality and a growth percent value of −100 means that all cells are dead. Both **13** and **14** showed similar cytotoxicity profiles for the one-dose test. Based on the one-dose data (Figure 2.14), the cytotoxicity values of **13** and **14** were greater compared with the parent structure **6** against the majority of the cell lines. Strong growth inhibition was observed against cell lines including COLO 205, SW-620, HT29 (colon cancers) NCI-H522 (non-small cell lung cancer), TK10, ACHN (renal cancers) and MDA-MB-468, MCF-7, T-47D (breast cancers).

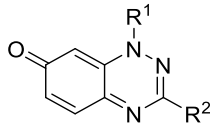

6, R^1=Ph, R^2=Ph
13, R^1=(Pyrid-2-yl), R^2=Ph
14, R^1=Ph, R^2=(Pyrid-2-yl)

Figure 2.13: General benzo[1,2,4]triazin-7-one structure to represent the parent structure **6** and the NCI evaluated compounds **13** and **14**.

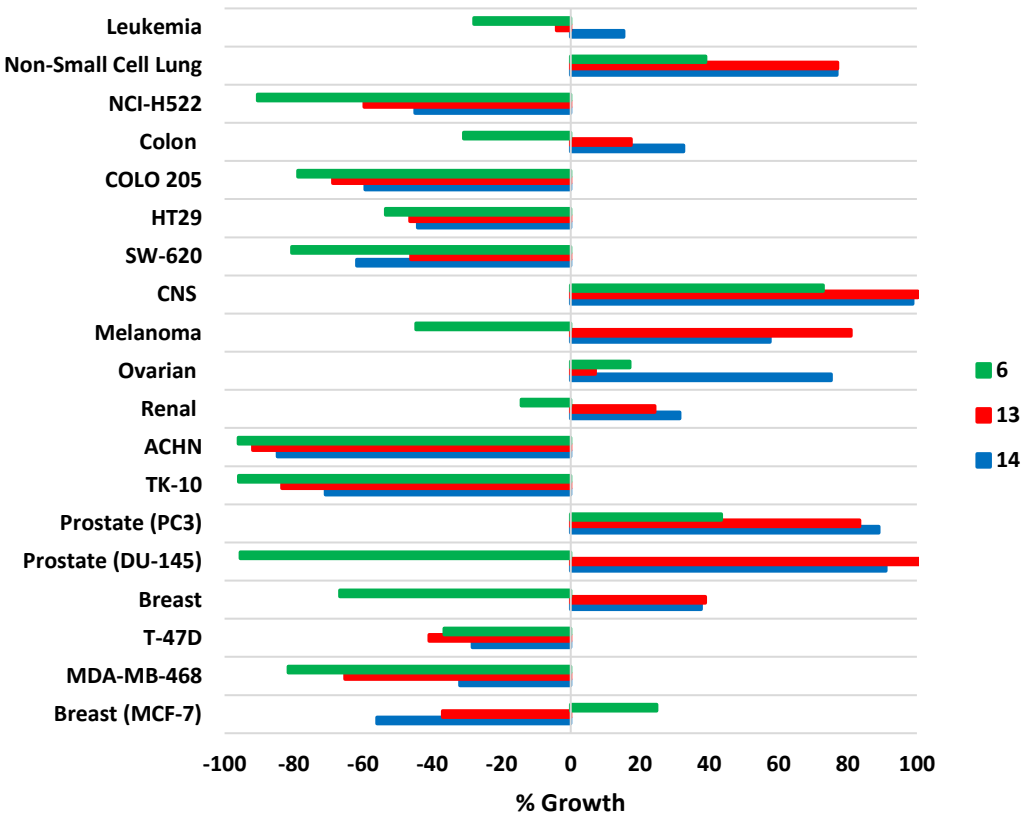

Figure 2.14: Summary of NCI-single dose (10 μM) screening results for the parent benzo[1,2,4]triazin-7-one **6** (green), **13** (red) and **14** (blue) expressed as an average percentage growth of a certain cancer cell line or of each cancer cell type relative to untreated control cancer cells.

After the one-dose test, little growth inhibition of the DU-145 cell line (prostate cancer) was exhibited by either **13** or **14**, compared with the parent structure **6**. However, the NCI five-dose test (in which five concentrations of each compound are tested against a range of cancer cell lines) gave IC_{50} values (Figure 2.15 and Table 2.4) that showed that **14** exhibited comparable cytotoxicity and **13** was over eight times less cytotoxic compared with the parent structure **6** against the DU-145 cell line (Table 2.4). The discrepancies between the IC_{50} values obtained from the NCI compared with the values obtained by our in-house evaluations were expected given the longer exposure time of cancer cells to the test compound in the MTT assay (72 h versus 48 h at the NCI). The fundamental differences in the assays would also contribute the discrepancy.[153–155] The NCI uses the SRB assay to measure the amount of dye (sulforhodamine B) bound onto the cellular protein and this assay is reported to be more sensitive than the MTT assay.[154,155] In contrast, the MTT assay relies on the ability of the

mitochondria of viable cells to reduce the tetrazolium dye MTT (3-(4,5-dimethylthiazol-2-yl)-2,5-diphenyltetrazolium bromide) to measure the number of living cells.[153]

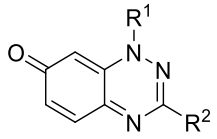

6, R^1=Ph, R^2=Ph
13, R^1=(Pyrid-2-yl), R^2=Ph
14, R^1=Ph, R^2=(Pyrid-2-yl)

Figure 2.15: General benzo[1,2,4]-triazin-7-one structure to represent the parent structure **6** and the NCI evaluated compounds **13** and **14**.

Table 2.4: NCI IC_{50} data after five-dose testing: DMSO solution of compound (100 µM) was added to 96-well plates which were incubated for 48 h at 37 °C using 5% CO_2 (humidified atmosphere). Cytotoxicity was evaluated using the SRB assay.

Compound	**IC_{50} DU-145 (µM)**	**IC_{50} MCF-7 (µM)**
6	3.388	0.295
13	27.542	3.388
14	5.248	1.348

2.3.4 COMPARE Analysis

The NCI selected **13** and **14** for further five-dose testing. This test would allow the key parameters for the NCI COMPARE algorithm to be established to determine any closely matching cytotoxicity profiles. Our compounds were compared with the over 250,000 synthetic compounds in the NCI's database. Both **13** and **14** showed strong correlations to pleurotin with Pearson correlation coefficients of 0.842 and 0.730 respectively. These coefficients were comparable with the coefficient reported by Sweeney *et al.*[131] for the parent structure **6** (Figure 2.16 and Table 2.5). Altering the substitution at the N1 and C3 positions from phenyl to pyrid-2-yl in the benzo[1,2,4]triazin-7-one scaffold did not suggest a change in the compounds' mechanism of action as the cytotoxicity profiles closely matched that of pleurotin, an irreversible TrxR inhibitor.

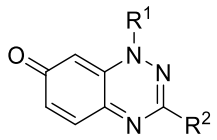

6, R^1=Ph, R^2=Ph
13, R^1=(Pyrid-2-yl), R^2=Ph
14, R^1=Ph, R^2=(Pyrid-2-yl)

Figure 2.16: General benzo[1,2,4]-triazin-7-one structure to represent the parent structure **6** and the NCI evaluated compounds **13** and **14**.

Table 2.5: Pearson correlation coefficients of the parent benzo[1,2,4]triazin-7-one **6** and pyrid-2-yl substituted benzo[1,2,4]triazin-7-ones **13** and **14** to pleurotin obtained by NCI COMPARE analysis.

Compound	Pearson correlation coefficient
6	0.841
13	0.842
14	0.730

2.4 Summary and Conclusions

The benzotriazin-4-yl radicals **15** and **16** were found to be significantly more cytotoxic towards the DU-145 cancer cell line compared with the MCF-7 cell line, however they were significantly less cytotoxic that their corresponding oxidation products, benzo[1,2,4]triazin-7-ones **13** and **14**. The pyridyl-substituted benzo[1,2,4]triazin-7-ones **13** and **14** exhibited submicromolar cytotoxicity towards both the DU-145 and MCF-7 cancer cell lines using the MTT assay. These cytotoxicities were on par with the parent benzo[1,2,4]triazin-7-one **6**. The DTP-NCI one-dose testing cytotoxicity profiles of **13** and **14** led to their selection for five-dose testing. The NCI COMPARE analysis showed that both compounds **13** and **14** had strong correlations to pleurotin.

2.5 Experimental

2.5.1 Cell Lines

The DU-145 (prostate cancer) and MCF-7 (breast cancer) cell lines were obtained from Dr. Stephen Rea, NUI Galway. All cell culture reagents were obtained from Sigma-Aldrich and all disposable sterile plastic ware was obtained from Sarstedt AG (Numbrecht, Germany). The MCF-7 cells were cultured in dulbecco's modified eagle's medium (DMEM) which contained high glucose (4.5 g/mL). This media was supplemented with 10% heat-inactivated fetal bovine serum (FBS) and 1% penicillin-streptomycin. The DU-145 cells were cultured in RPMI-1640 medium. This medium was supplemented with 1% penicillin-streptomycin, 1% of 2 mM L-glutamine and 10% of non heat-inactivated fetal bovine serum (FBS). All cells grew as adherent cultures in 75 cm^3 flasks in 20 mL of medium and incubated in an autoflow CO_2 (5%) water-jacket incubator at 37 °C. All surfaces were sprayed with 70% ethanol prior to carrying out all procedures. Cells were subcultured when they were approximately 80% confluent. DU-145 cells were treated with 2X trypsin-EDTA in Hanks balance salt solution and MCF-7 cells were treated with 5X trypsin-EDTA in Hanks balance salt solution for five minutes. All cells were centrifuged at 1200 rpm in a Rotanta 300 centrifuge. The cell pellet was then re-suspended in fresh cell culture medium. When cells need to be counted (before carrying out the MTT assay) a Kova® Glasstic® slide 10 combination coverslip-microslip slide was used to determine the cell number. When cells did not need to be counted before subculturing, the MCF-7 stock suspension was seeded with 1/5 and DU-145 at 1/4 and this volume was added to 20 mL of pre-warmed medium in a sterile 75 cm^3 flask followed by incubation at 37 °C and 5% CO_2. The cell culture medium was replaced every two–three days.

2.5.2 Cell Resuscitation

Both the DU-145 and MCF-7 cell lines were resuscitated though rapid thawing at 37 °C. The thawed cell suspension was added to the culture medium (1 mL) which was pre-heated to 37 °C and this mixture was added to a sterile culture flask (25 cm^3). A further 4 mL of the pre-heated culture medium was added and the cells were then incubated (37 °C and 5% CO_2). The cell culture medium was replaced after 24 h.

2.5.3 Cytotoxicity Measurements

Cytotoxicity evaluations were carried out on the MCF-7 breast cancer cell line and DU-145 prostate cancer cell line. The MTT (3-(4,5-dimethylthiazol-2-yl)-2,5-diphenyltetrazolium bromide) colorimetric assay was used to determine the IC_{50} values of all compounds. Cells were added to 96-well plates at a cell density of 2000 cells per well for the DU-145 cell line (200 µL per well) and 1000 cells per well for the MCF-7 cell line (200 µL per well). The cells were allowed to adhere to the culture flask over 24 hours. Test compound solutions were added in DMSO after 24 hours (1% v/v final concentration in well). Control cells were exposed to the same concentration of DMSO without the test compound. All cells were incubated at 37 ºC and 5% CO_2 for 72 hours. After 72 h, MTT (20 µL, 5 mg/mL solution) was added. The cells were then incubated for a further 3 hours after which the supernatant was then removed from each well. The MTT formazan crystals were dissolved using DMSO (100 µL). The absorbance was determined using a plate reader at 550 nm with a reference at 690 nm. Cell viability is expressed as a percentage of the vehicle-only treated control (DMSO). Non-linear regression analysis was used to analyse the obtained dose-response curves. The IC_{50} values were determined using GraphPad Prism software, v 8.0 (GraphPad Inc., San Diego, CA, USA).

2.5.4 MTT Assay

The MTT colorimetric assay is used to determine cell viability as it detects living but not dead cells. This assay is rapid and precise with no washing steps required and has been employed for cytotoxicity studies on a wide range of cell types. Living cells reductively cleave the tetrazolium ring of the water-soluble yellow 3-(4,5-dimethylthiazol-2-yl)-2,5-diphenyltetrazolium bromide **19** (MTT) in the mitochondria, forming formazan **20**, which is water insoluble and purple (Figure 2.17).[153]

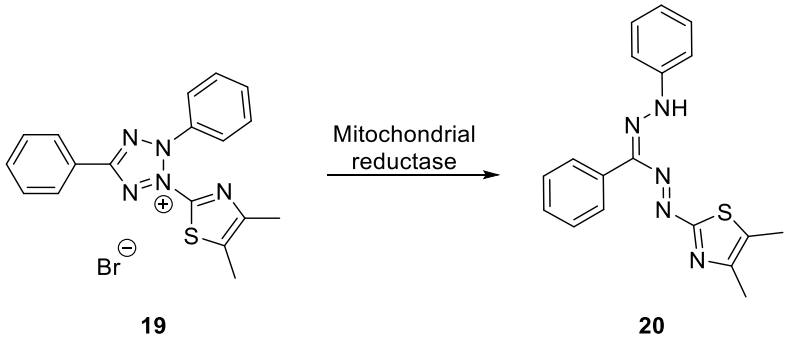

Figure 2.17: Reduction of MTT to formazan.

Some disadvantages associated with the MTT assay include non-linearity with cell number at high cell densities and cell lines can sometimes differ in the ability to reduce 3-(4,5-dimethylthiazol-2-yl)-2,5-diphenyltetrazolium bromide.

2.5.5 Sulforhodamine B Assay (SRB)

The SRB assay (Figure 2.18) is known to be more sensitive than the MTT assay and has higher reproducibility, better linearity with cell number and lower variation between cell lines.[155] This assay determines the cell density and SRB binds to cellular protein that has been fixed to tissue culture plates using trichloroacetic acid (TCA). SRB is a pink aminoxanthene, fluorescent dye consisting of two sulfonic acid groups (Figure 2.18). These groups bind to basic amino acid residues under acidic conditions and dissociate under basic conditions. The amount of the aminoxanthene dye that is extracted from the cells is directly proportional to the cell mass.[156]

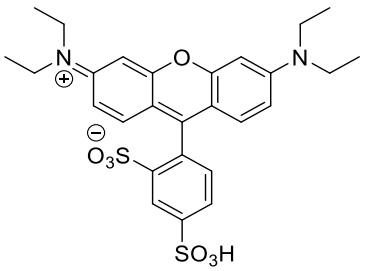

Figure 2.18: Structure of sulforhodamine B.

2.5.6 Cytotoxicity Profiles

The dose-response curves for each compound (**13**–**16** and TEMPO) are shown below. These curves are based on the cytotoxicity evaluations carried out using the MTT assay.

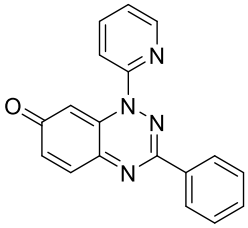

13

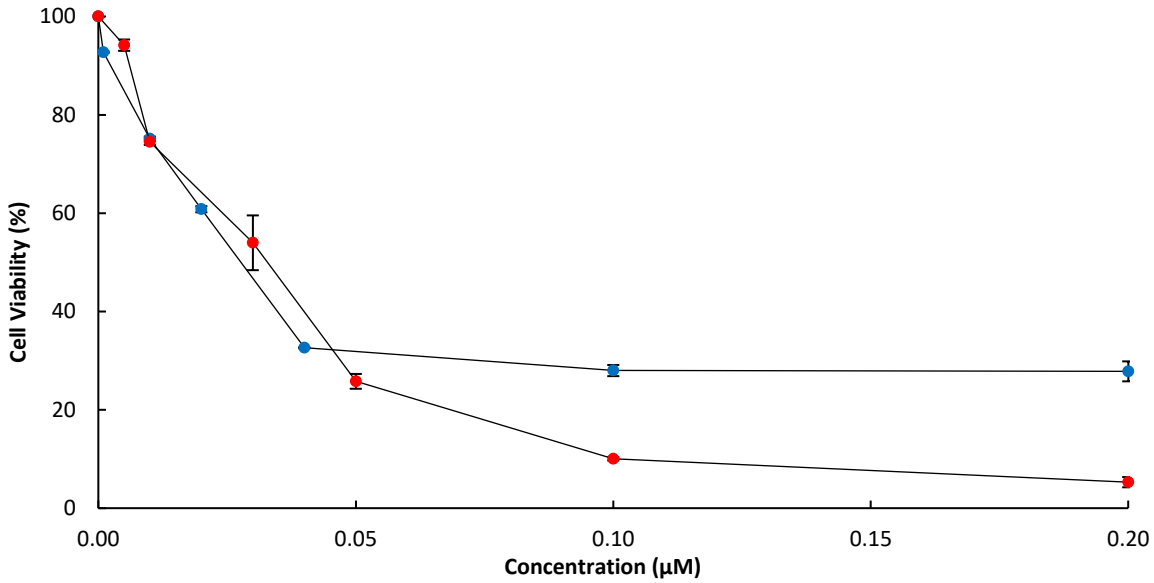

Figure 2.19: Viability of DU-145 (●) and MCF-7 (●) cell lines determined using MTT assay following treatment with 3-phenyl-1-(pyridine-2-yl)-1,2,4-benzotriazin-7(1*H*)-one (**13**) under aerobic conditions for 72 h at 37 ºC. Each data point is the mean of at least two independent experiments. The lines shown are trend lines.

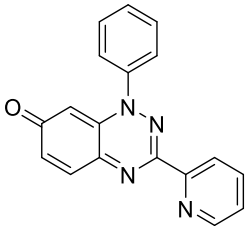

14

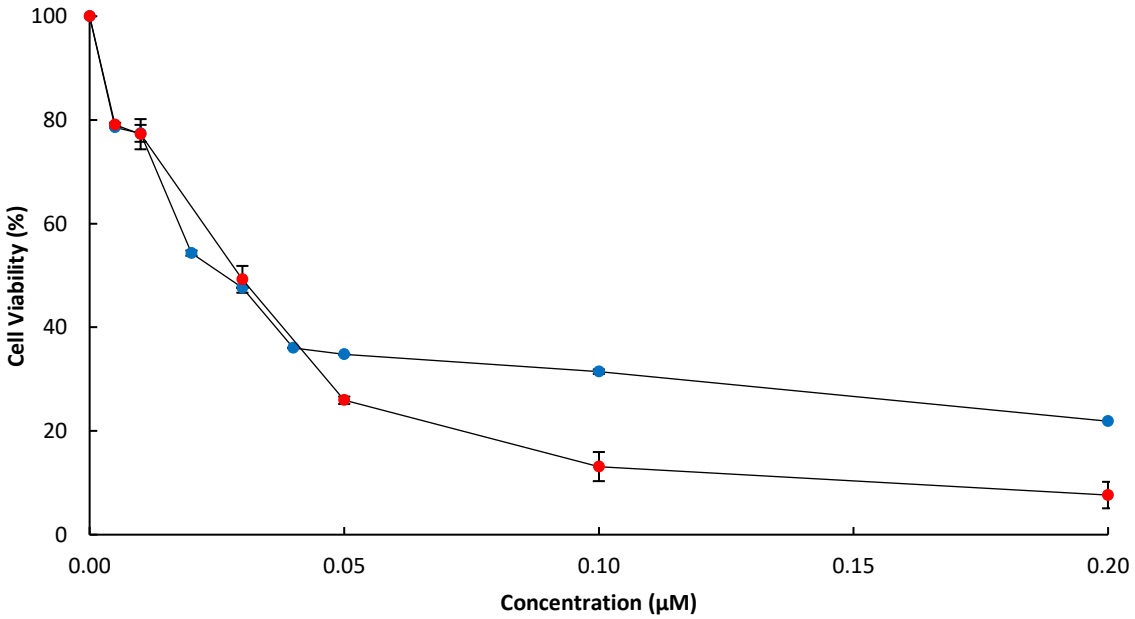

Figure 2.20: Viability of DU-145 (●) and MCF-7 (●) cell lines determined using MTT assay following treatment with 1-phenyl-3-(pyridine-2-yl)-1,2,4-benzotriazin-7(1*H*)-one (**14**) under aerobic conditions for 72 h at 37 ºC. Each data point is the mean of at least two independent experiments. The lines shown are trend lines.

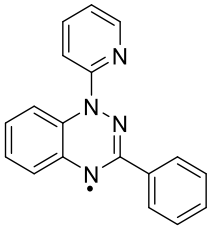

15

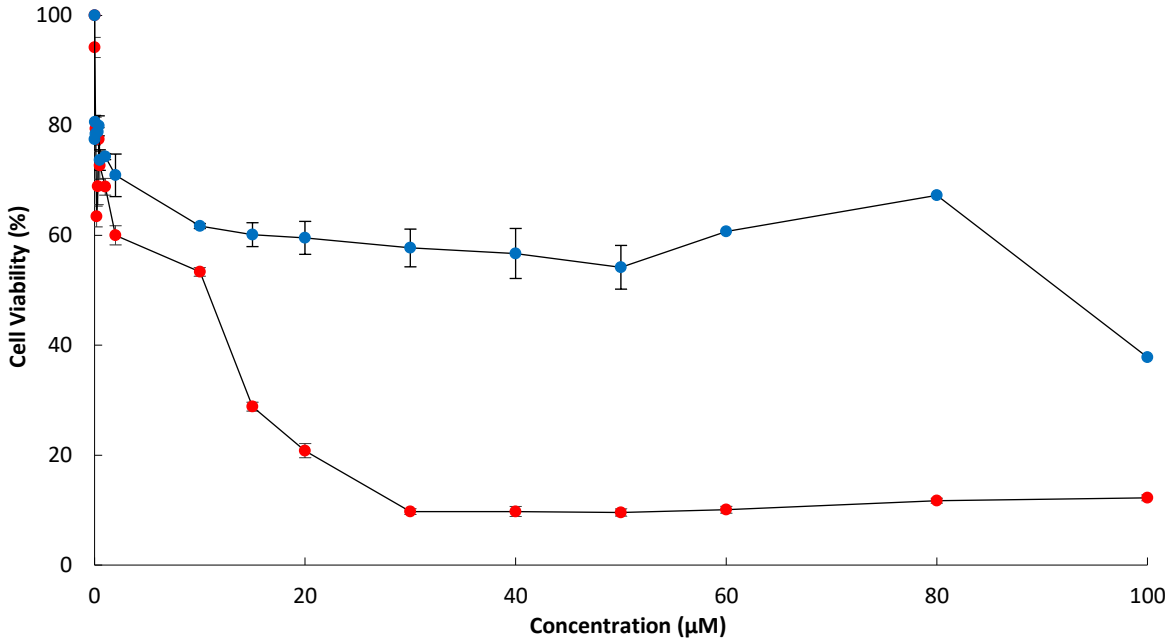

Figure 2.21: Viability of DU-145 (●) and MCF-7 (●) cell lines determined using MTT assay following treatment with 3-phenyl-1-(pyrid-2-yl)-1,4-dihydrobenzo[*e*][1,2,4]-benzotriazin-4-yl (**15**) under aerobic conditions for 72 h at 37 ºC. Each data point is the mean of at least three independent experiments. The lines shown are trend lines.

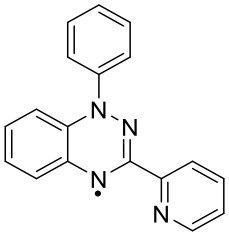

16

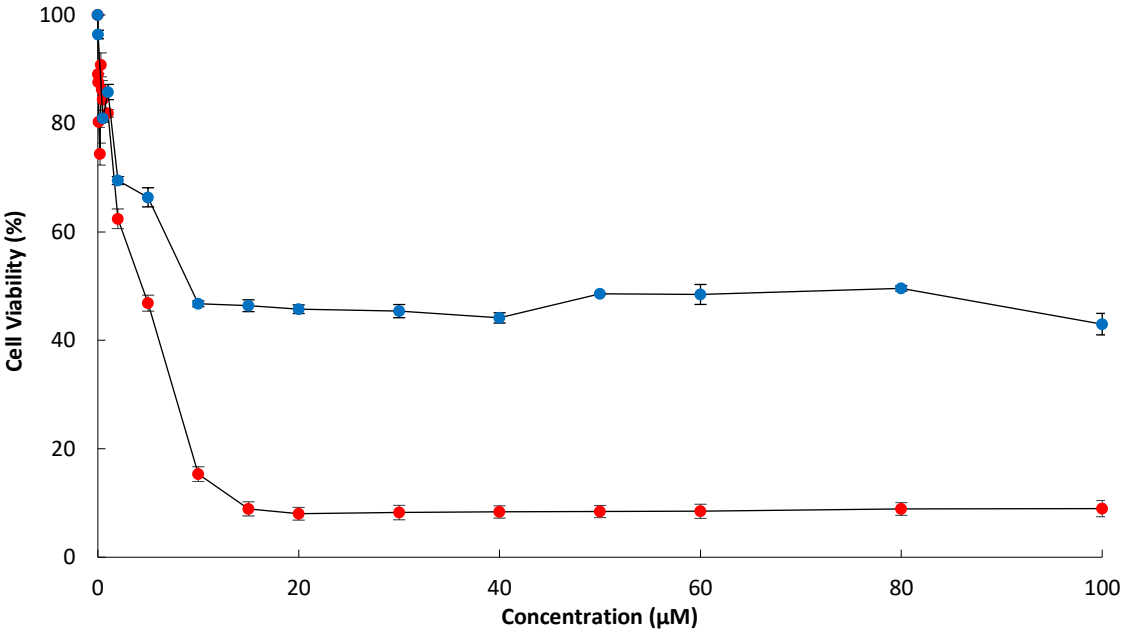

Figure 2.22: Viability of DU-145 (●) and MCF-7 (●) cell lines determined using MTT assay following treatment with 1-phenyl-3-(pyrid-2-yl)-1,4-dihydrobenzo[*e*][1,2,4]triazin-4-yl (**16**) under aerobic conditions for 72 h at 37 ºC. Each data point is the mean of at least three independent experiments. The lines shown are trend lines.

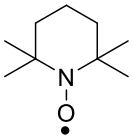

TEMPO

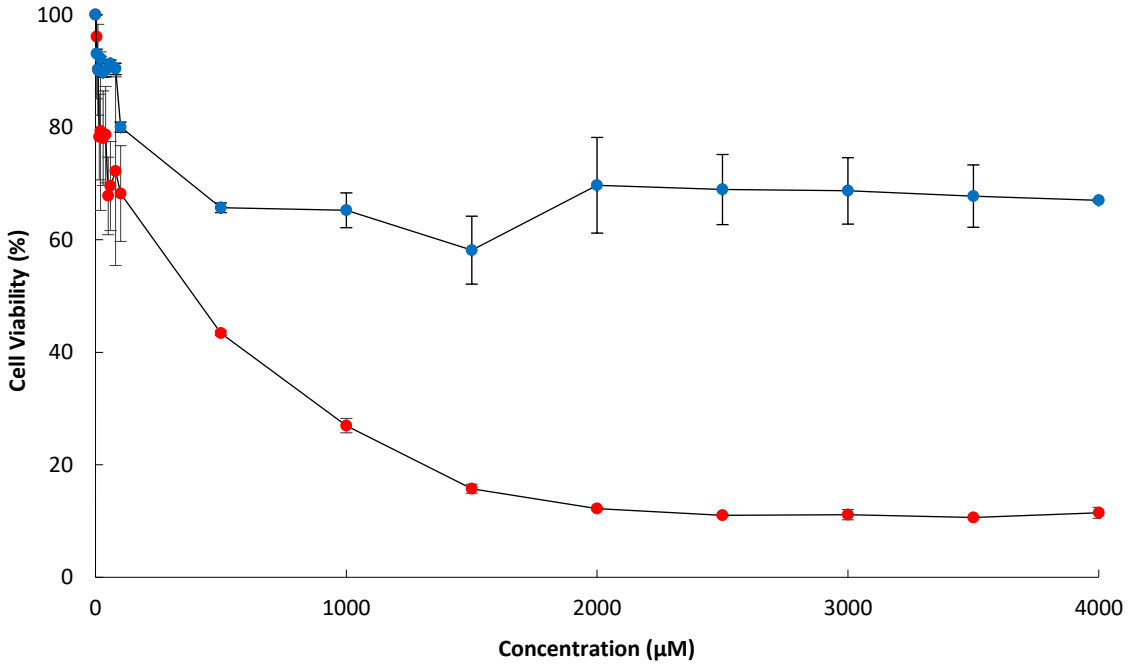

Figure 2.23: Viability of DU-145 (●) and MCF-7 (●) cell lines determined using MTT assay following treatment with TEMPO under aerobic conditions for 72 h at 37 ºC. Each data point is the mean of at least three independent experiments. The lines shown are trend lines.

2.5.7 NCI One-dose Data

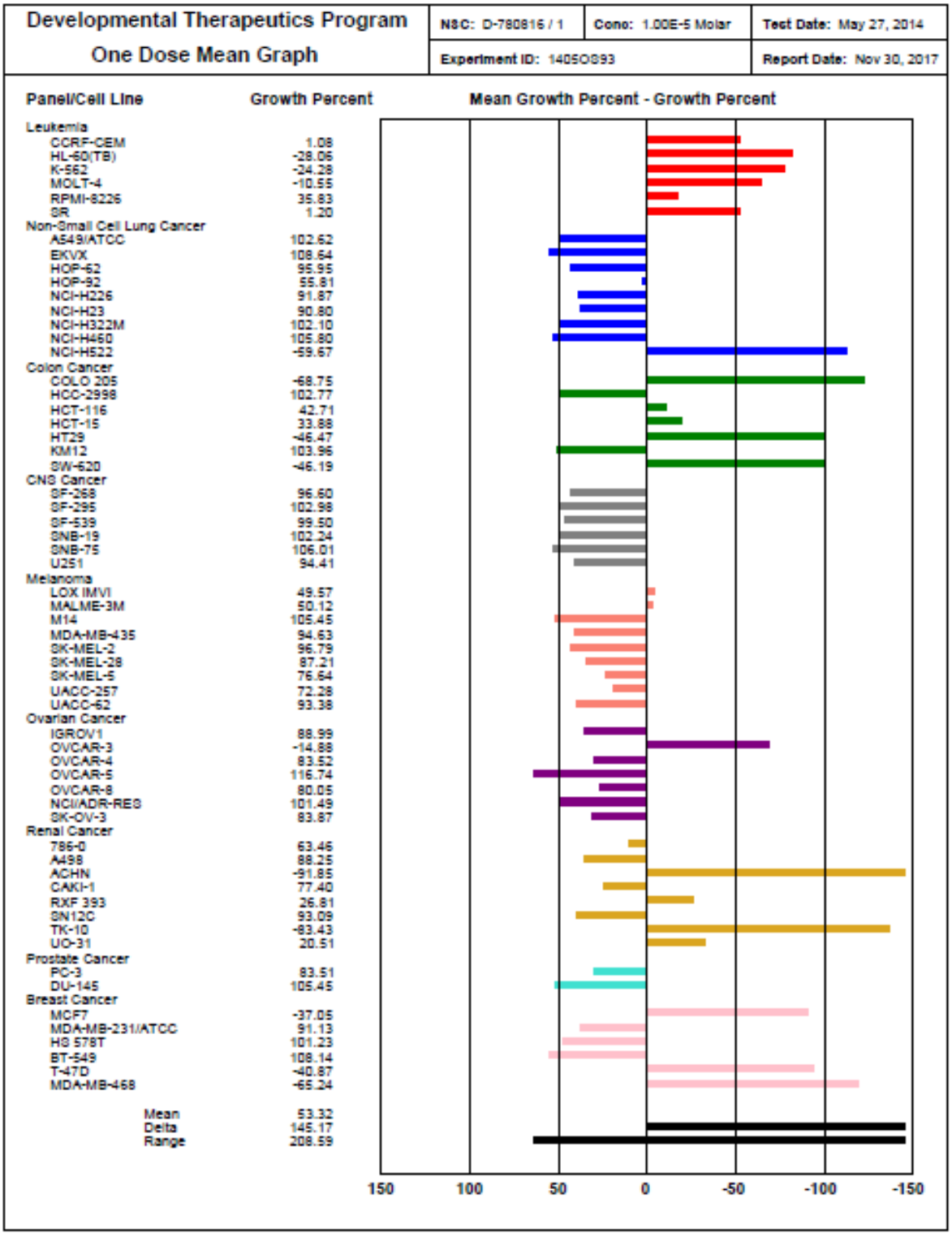

Figure 2.24: Activity of 3-phenyl-1-(pyridin-2-yl)-1,2,4-benzotriazin-7(1*H*)-one (**13**) towards the NCI 60 cancer cell line panel, one-dose test (This figure is courtesy of the NCI-DTP program).

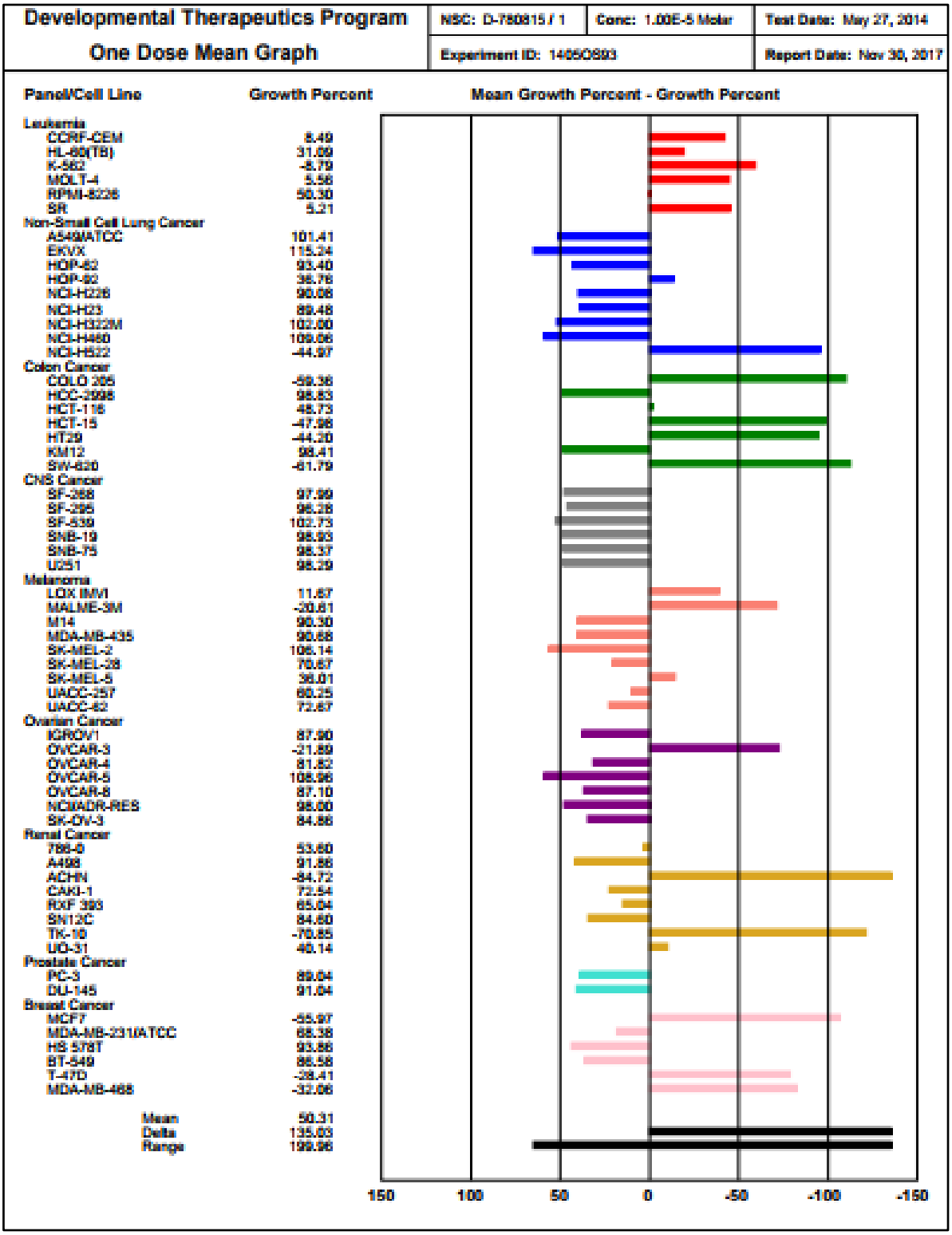

Figure 2.25: Activity of 1-phenyl-3-(pyridin-2-yl)-1,2,4-benzotriazin-7(1*H*)-one (**14**) towards the NCI 60 cancer cell line panel, one-dose test (This figure is courtesy of the NCI-DTP program).

Chapter 3
Synthesis of Azocane-fused Benzimidazole(quinones) and Cytotoxicity Evaluation towards Breast and Prostate Cancer Cells Lines

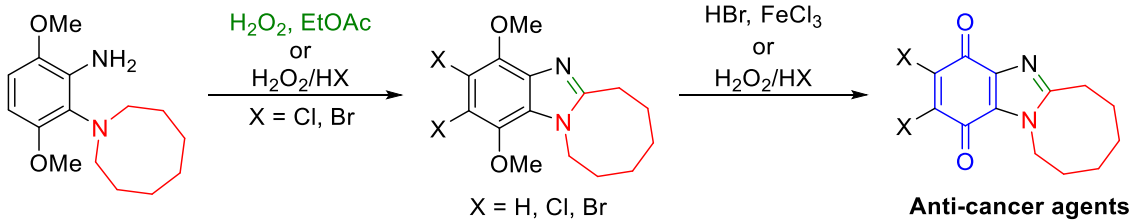

Parts of this chapter are published in:

Greener synthesis using hydrogen peroxide in ethyl acetate of alicyclic ring-fused benzimidazoles and anti-tumour benzimidazolequinones, Martin Sweeney, Michael Gurry, **Lee-Ann J. Keane** and Fawaz Aldabbagh, *Tetrahedron Lett.*, **2017**, 58, 3565–3567.

One-Pot Synthesis of Dihalogenated Ring-Fused Benzimidazolequinones from 3,6-Dimethoxy-2-(cycloamino)anilines Using Hydrogen Peroxide and Hydrohalic Acid, Martin Sweeney, **Lee-Ann J. Keane**, Michael Gurry, Patrick McArdle, Fawaz Aldabbagh. *Org. Lett.* **2018**, 20, 6970–6974.

This chapter is based on collaborative projects. Author contributions will be stated at relevant points of mention and articles are included in an appendix.

3.1 Introduction

3.1.1 Quinones as Bioreductive Prodrugs

The development of bioreductive prodrugs that require activation through reductive metabolism, thereby giving a cytotoxic species, is a significant approach to anti-cancer treatment. Quinones have been employed as bioreductive prodrugs.[157,158] Bioreduction of a quinone moiety is a strategy that may offer selective cytotoxicity and reduced side effects if bioreductive activation can occur through a specific property associated with tumour cells.[159,160] For example, selective cytotoxicity can be obtained through enzymatic reduction of quinones, through either one- or two- electron reductase enzymes.[160] Following bioreductive activation of the quinone moiety, there are a variety of mechanisms in which cytotoxicity can be exerted. Some of the known mechanisms include the alkylation of biomolecules, DNA intercalation and phosphatase inhibition.[161,162] The indolequinone, mitomycin C (MMC, Figure 3.1) is a naturally occurring, clinically used antitumour agent that was isolated from *Streptomyces caespitous* and exerts its cytotoxicity through DNA alkylation.[160,163] MMC is relatively non-toxic and must be reductively activated before DNA alkylation can occur so as to exert its cytotoxic effect.[164] It has been used in the treatment of non-small-cell lung cancer and bladder cancer.[161,162] Bioreduction of the quinone moiety, such as that of MMC, can occur through either a one-electron reduction to form a semiquinone radical anion or a two-electron reduction to form a hydroquinone. [160,165] These approaches are described below.

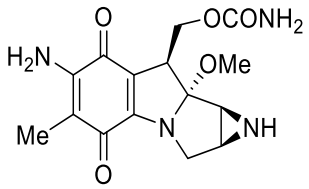

Figure 3.1: Structure of mitomycin C.

3.1.1.1 One-Electron Reduction

One-electron reduction of MMC is catalysed by single-electron reductase enzymes such as NADPH cytochrome c (P450) reductase and leads to a reactive semiquinone radical anion that can be protonated to form semiquinone radical **1** (Scheme 3.1). This radical can rapidly undergo oxidation by molecular oxygen in well-oxygenated cells (aerobic conditions) to regenerate MMC. Re-oxidation prevents semiquinone radical **1** from undergoing significant DNA alkylation under aerobic conditions. In solid tumours, where hypoxic conditions are

prevalent (regions of solid tumours in which cells have a low concentration of oxygen) re-oxidation is less efficient, thus allowing semiquinone radical **1** to undergo DNA alkylation. Once semiquinone radical **1** is formed (Scheme 3.1), the elimination of methanol followed by protonation of the nitrogen atom of the aziridine ring, which promotes ring opening of the aziridine ring giving free amine **3**. Alkylation of DNA, followed by elimination of the carbamate group gives alkene **4**, which can undergo further DNA alkylation at the C10 position to give DNA crosslinked species **5**. Oxidation of **5** gives the DNA crosslinked adduct **6**.[163,166]

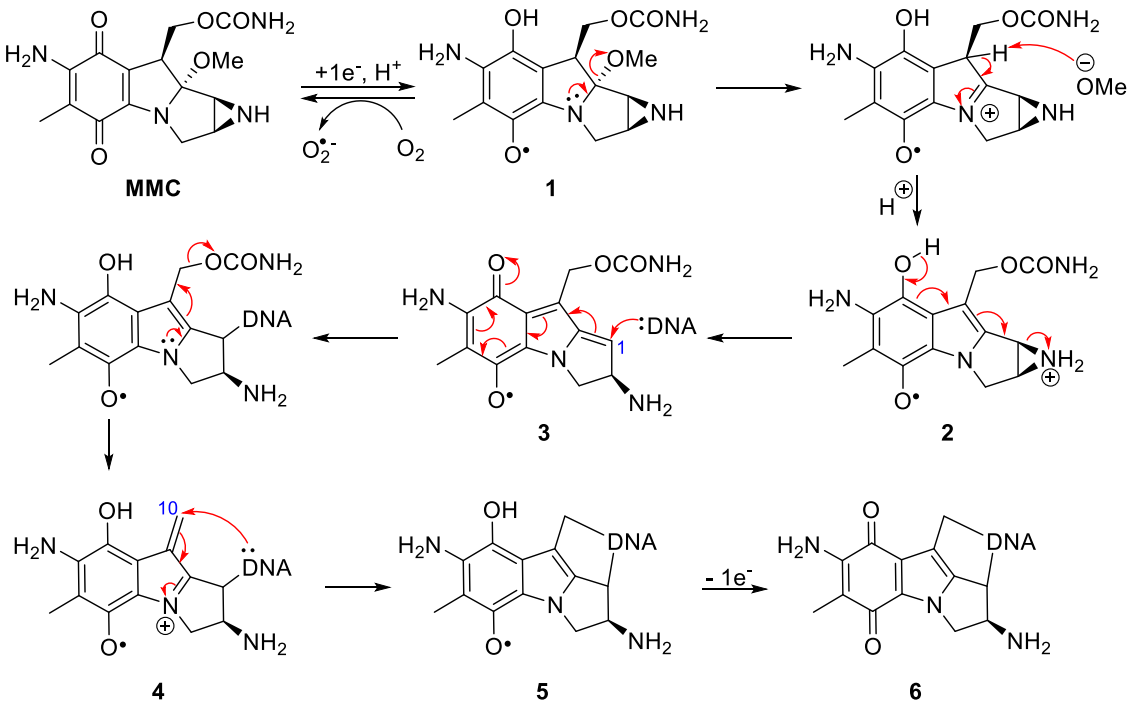

Scheme 3.1: One-electron reduction of MMC.[166]

3.1.1.2 Two-Electron Reduction

MMC can also undergo a two-electron reduction to hydroquinone **7** (Scheme 3.2) by two-electron reductase enzymes such as NAD(P)H: quinone oxidoreductase 1 (NQO1), which is known to be over-expressed in certain cancer cell lines (such as breast, colon and lung cancers[167]) relative to healthy cells. The hydroquinone intermediate can be formed under normal and hypoxic conditions. Loss of the methoxy group gives iminium ion **8**, which undergoes aromatization with loss of a proton to give leuco-aziridinomitosene species **9**. Protonation of the aziridine nitrogen of **9** is followed by ring opening of the aziridine to give quinone methide **10** with an electrophilic C1 position. This electrophilicity allows for DNA alkylation to give alkylated product **11**. After elimination of the carbamate group to give alkene

12 another electrophilic position is generated at the C10 position. From here, DNA crosslinked adduct **13** can form upon alkylation at the C10 position or water can add to the alkene to form a dicarbamoyl DNA mono-adduct **14** (Scheme 3.2). Alkylation of MMC with DNA has previously been shown to occur with specificity at the N2 position of guanine.[168–170]

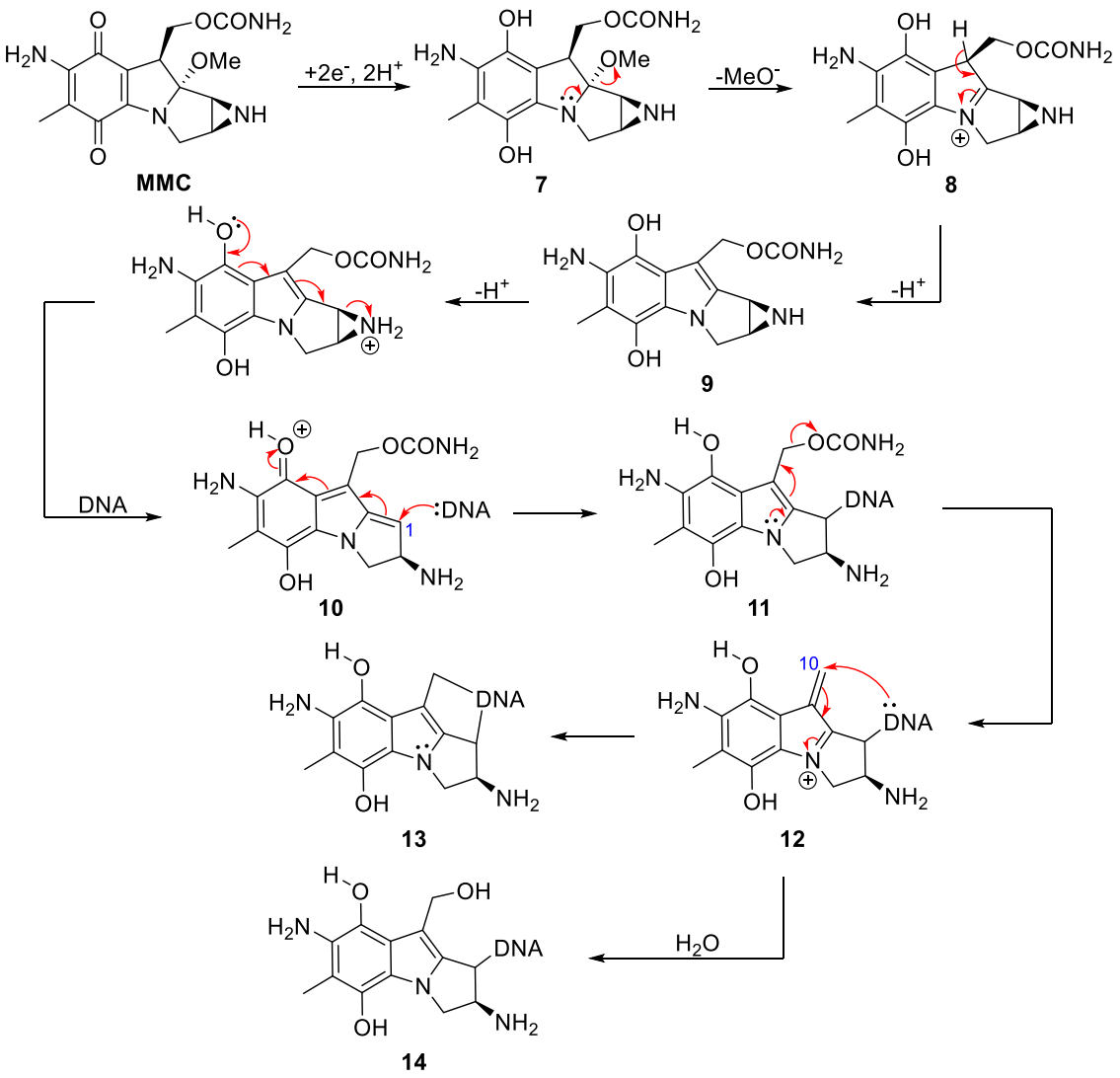

Scheme 3.2: Mechanism for the two-electron reductive activation and DNA alkylation by MMC.[168]

The two-electron reduction of the quinone, MMC, as described above, is catalysed by reductase enzymes such as NQO1. The over-expression of NQO1 in certain types of cancer cells relative to healthy cells results in selective cytotoxicity. NQO1 is a flavoenzyme. It is a homodimer of a monomer, which consist of 274 amino acids, each subunit containing a molecule of flavin adenine dinucleotide (FAD), which is non-covalently bound. The mechanism of action associated with NQO1 is described as a ping-pong mechanism as both the quinone and NAD(P)H must independently occupy the same binding site (Scheme 3.3). The NAD(P)H

occupies the NQO1 binding site and transfers hydride to FAD leading to NAD(P)$^+$ and FADH. The NAD(P)$^+$ leaves the binding site and is replaced by the quinone substrate. A hydride transfer from FADH to the quinone reduces the quinone to the hydroquinone and regenerates FAD (Scheme 3.3)[171]. NQO1 is expressed at high levels in many solid tumours such as breast, colon, bladder, ovarian and lung cancers, compared with healthy tissues.[167] Therefore, selective cytotoxicity can occur due to the difference in the levels of enzymes that catalyse bioreduction.[160]

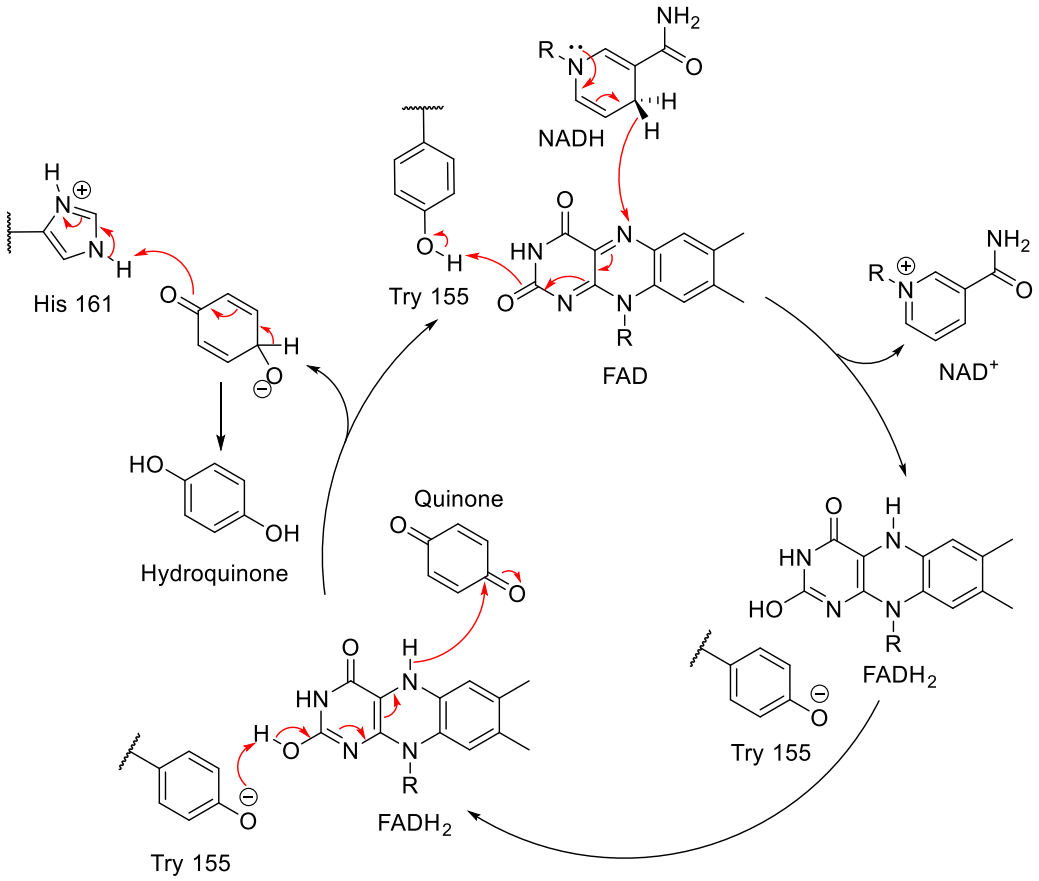

Scheme 3.3: NQO1 mechanism of action.[171]

3.1.2 Benzimidazolequinones

Skibo *et al.*[172,173] reported a new class of bioreductive anti-tumour agents, 6-aziridinyl-pyrrolidino[1,2-*a*]benzimidazolequinones (Figure 3.2), which are cytotoxic against a range of cancer cell lines, such as melanoma, non-small cell lung cancer and renal cancer cell lines (R = OAc).[172]

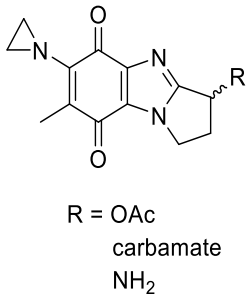

Figure 3.2: 6-Aziridinyl- pyrrolidino[1,2-*a*]benzimidazole quinones.

These types of quinones undergo two-electron reduction by NQO1 to give a reactive hydroquinone species **15** and then cause cleavage of DNA upon alkylation of the phosphate backbone **16**. It was proposed that the alkylation of the phosphate oxygen atom through nucleophilic attack at the activated aziridine gives a hydrolytically labile phosphotriester **17**. The oxygen anion of the phosphate backbone is the target of these quinones because of the positively charged pyrrolidino benzimidazole. Hydrolysis of phosphotriester **17** leads to DNA cleavage (Scheme 3.4).[160,173]

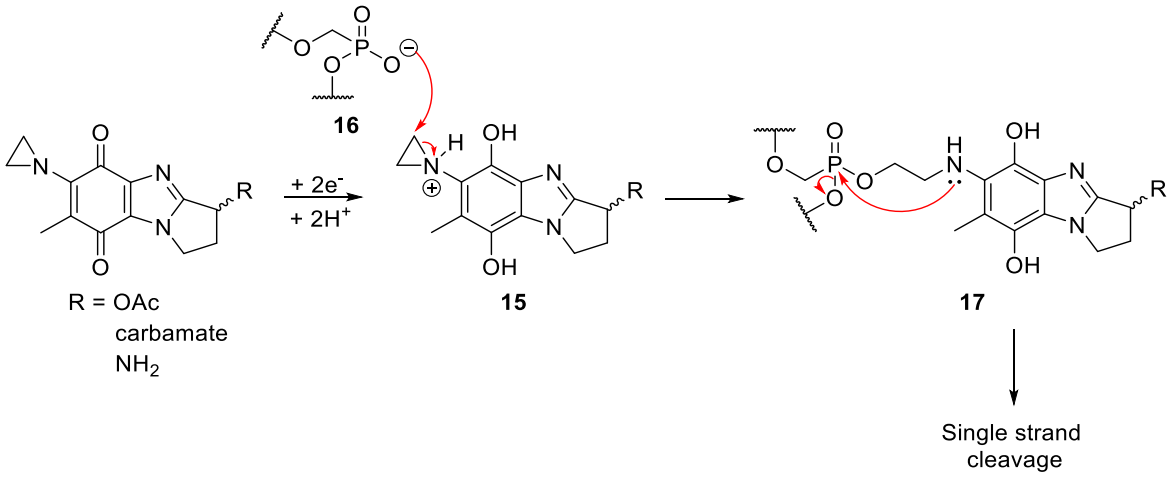

Scheme 3.4: Phosphate alkylation.[160]

In the Aldabbagh group, Lynch *et al.*[174] reported the radical cyclization mediated synthesis and cytotoxicity evaluation of six-membered alicyclic ring-fused [1,2-*a*]benzimidazolequinone anti-tumour agents (Figure 3.3, compounds **18** and **19**). A cytotoxicity evaluation of both quinones, **18** and **19** against the human skin fibroblast cell line (GM00637) under hypoxic conditions (associated with solid tumours) showed IC_{50} values in the nanomolar range. Both quinones, **18** and **19** exhibited similar cytotoxicity under aerobic conditions; however, quinone **18** was 1.6 times more cytotoxic under hypoxic conditions compared with methyl-substituted

quinone **19** (Figure 3.3). Quinone **18** was determined to be over 300 times more cytotoxic than the indolequinone, mitomycin C towards the GM00637 cell line under hypoxic conditions (MMC IC_{50} 0.5 µM).

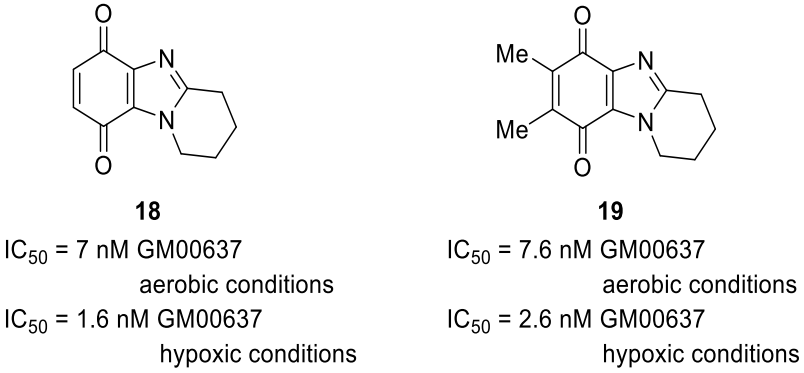

18

IC_{50} = 7 nM GM00637 aerobic conditions

IC_{50} = 1.6 nM GM00637 hypoxic conditions

19

IC_{50} = 7.6 nM GM00637 aerobic conditions

IC_{50} = 2.6 nM GM00637 hypoxic conditions

Figure 3.3: Alicyclic-ring-fused [1,2-*a*]benzimidazolequinones.

Both benzimidazolequinones **18** and **19** lack a moiety for DNA alkylation (such as an aziridine ring); however, it was proposed that cytotoxicity was due to redox cycling in the presence of oxygen[174] (Scheme 3.5). Bioreduction of the quinone moiety produces a semiquinone radical or hydroquinone. Under aerobic conditions, the semiquinone radical can be reoxidized back to the original quinone by molecular oxygen. This process yields superoxide anion radicals ($O_2^{\bullet -}$). This oxygen-dependent process continues until the system is anaerobic. Superoxide radical anions are unstable in an aqueous environment and spontaneously react to form molecular oxygen and hydrogen peroxide. Hydrogen peroxide reacts with iron (Fenton reaction) to produce toxic hydroxyl radicals ($HO^{\bullet}$). These reactive oxygen species (ROS) are also produced during normal aerobic metabolism. The antioxidative defence system of cells, consisting of radical scavengers such as ascorbic acid and antioxidant enzymes such as superoxide dismutase protects the cell against these ROS. Excessive production of ROS leads to an imbalance of antioxidants and oxidants, which leads to pathological effects. For example, the hydroxyl radical can spontaneously oxidize guanine residues in DNA to form 8-oxo-2-deoxyguanine. Mispairing of 8-oxo-2-deoxyguanine with adenine during DNA replication leads to G→T transversions and are frequently found in tumour genes.[157,160]

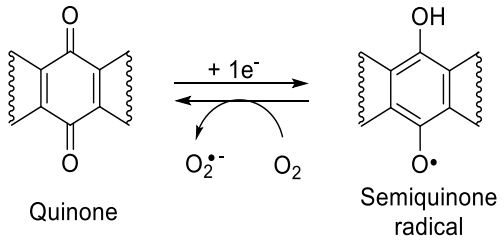

Scheme 3.5: Quinone redox cycling.[160]

3.1.3 Influence of Halogenation on Quinone Cytotoxicity

Siraki *et al.*[175] investigated the cytotoxicity of various chlorinated and non-chlorinated *p*-benzoquinones against PC12 cells (tumour cells from the adrenal medulla of a rat) by using the MTT assay. Tetrachloro-1,4-*p*-benzoquinone (**21**) was found to be two times more cytotoxic than *p*-benzoquinone **20** (Figure 3.4). Chlorinated quinone analogues are more hydrophobic, thus facilitating their passage through cell membranes. Halogen atoms exert an inductive electron-withdrawing effect, thus making the quinone moiety in tetrachloro-1,4-*p*-benzoquinone (**21**) more electrophilic compared with that of *p*-benzoquinone (**20**). This difference would cause tetrachloro-1,4-*p*-benzoquinone (**21**) to undergo nucleophilic attack more easily.

20
LD_{50}: 20.8 μM

21
LD_{50}: 10.1 μM

Figure 3.4: Cytotoxicity of tetrachloro-1,4-*p*-benzoquinone and *p*-benzoquinone evaluated against PC12 cells.

Scherz *et al.*[175] prepared a dibromo-*p*-benzoquinone containing two amino oligo(ethylene glycol) groups (Scheme 3.6, compound **24**). The double 1,4-addition of amino oligo(ethylene glycol) (**23**) to tetrabromo-*p*-benzoquinone (**22**), followed by elimination of HBr gave the 2,5-bis(2,5,9,12-tetraoxatridecan-7-ylamino)-3,6-dibromocyclohexa-2,5-diene-1,4-dione (**24**) (Scheme 3.6). Tetrabromo-*p*-benzoquinone (**22**) is known to have poor solubility in water (18 mg/L), thus limiting its biological application (MCF-7 IC_{50} = > 100 μM). The known reactivity with amines, as described above, allows conjugation with water-soluble moieties such as oligo(ethylene glycol) (**23**) to give product **24**, which has an aqueous solubility of

1.752 g/L. The cytotoxicity of amino oligo(ethylene glycol) derivative **24** against the MCF-7 breast cancer cell line and the human normal skin fibroblast cell line was investigated. Low cytotoxicity was exhibited towards the human normal skin fibroblast cell line (IC_{50} value not given). A significant increase in cytotoxicity was observed against MCF-7 cells and the IC_{50} value of was found to be 0.8 μM. The enhanced potency of this compound against the MCF-7 cancer cell line versus human normal skin fibroblast cell line suggested a bioreductive mechanism of action as selectivity could be due to a difference in enzyme expression between solid tumours and normal tissue. NQO1 is known to be overexpressed in most solid tumours, including MCF-7. The two-electron bioreduction of the quinone by NQO1 generates a hydroquinone, which can undergo DNA alkylation resulting in a cytotoxic effect.[176]

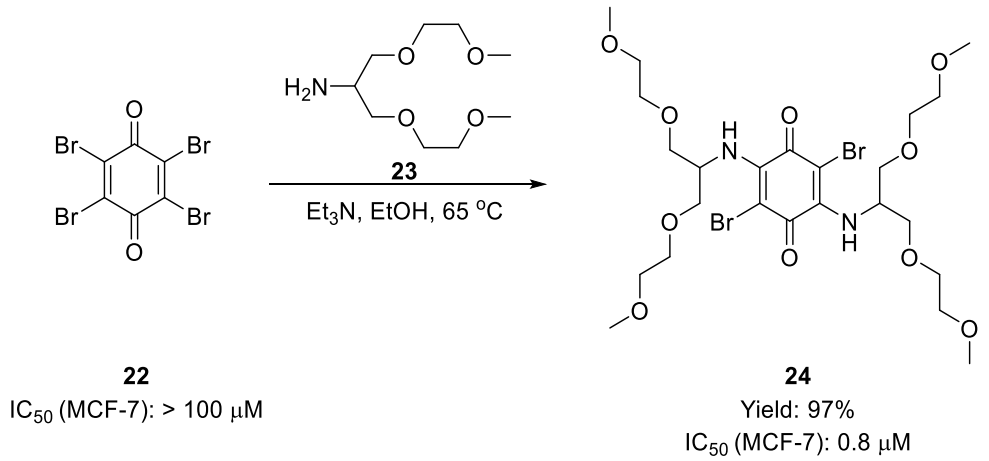

Scheme 3.6: Synthesis and cytotoxicity of 2,5-bis(2,5,9,12-tetraoxatridecan-7-ylamino)-3,6-dibromocyclohexa-2,5-diene-1,4-dione.[176]

3.1.4 Influence of Alicyclic Ring-Size on Quinone Cytotoxicity

In the Aldabbagh group, it has previously been reported by Fahey *et al*.[177] that the size of the fused alicyclic ring influences cytotoxicity of methoxy substituted benzimidazolequinones. Increasing the size of the alicyclic ring led to a decrease in cytotoxicity against human normal skin fibroblast cell line, GM00637 with the five-membered ring-fused benzimidazolequinone **25** being more cytotoxic that the six- and seven-membered ring-fused benzimidazolequinone analogues, **26** and **27** respectively (Figure 3.5).

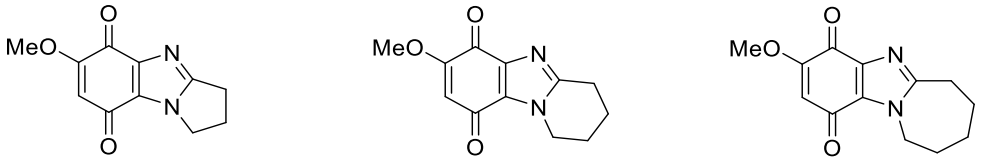

25
IC_{50} = 0.36 μM

26
IC_{50} > 1.5 μM

27
IC_{50} > 1.5 μM

Figure 3.5: Cytotoxicity evaluation of quinones **25**, **26**, and **27** against the human normal skin fibroblast cell line (GM00637).

Aldabbagh and co-workers have previously investigated the effect of the fused alicyclic ring size on the cytotoxicity of imidazo[5,4-*f*]benzimidazolequinones (Figure 3.6).[178] Diazepino-fused imidazo[5,4-*f*]benzimidazolequinone **28** exhibited enhanced cytotoxicity towards both HeLa (IC_{50} 1.78 μM) and DU-145 (IC_{50} 4.46 μM) cancer cell lines. Piperidine-fused imidazo[5,4-*f*]benzimidazolequinone **29** was more cytotoxic towards both HeLa (IC_{50} 1.67 μM) and DU-145 (IC_{50} 1.99 μM) cancer cell lines compared with quinone **28**. Variation of one of the fused piperidine rings to a morpholine ring (quinone **30**) led to enhanced cytotoxicity towards both cancer cell lines (HeLa, IC_{50} 0.58 μM and DU-145, IC_{50} 0.66 μM) compared with both quinones **28** and **29**.[178]

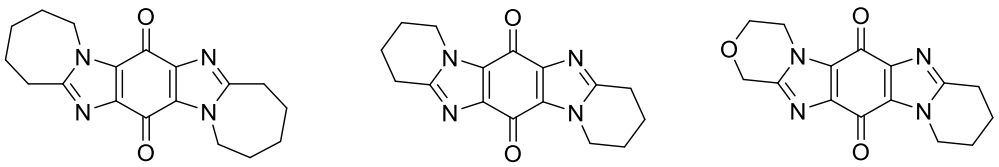

28
IC_{50} (HeLa): 1.78 μM
IC_{50} (DU-145): 4.46 μM

29
IC_{50} (HeLa): 1.67 μM
IC_{50} (DU-145): 1.99 μM

30
IC_{50} (HeLa): 0.58 μM
IC_{50} (DU-145): 0.66 μM

Figure 3.6: Cytotoxicity of alicyclic ring-fused imidazo[5,4-*f*]benzimidazolequinones.

3.1.5 Synthetic Routes to Alicyclic Ring-Fused [1,2-*a*]benzimidazoles

Alicyclic ring-fused [1,2-*a*]benzimidazoles have attracted attention as valuable precursors to potent anti-tumour benzimidazolequinones.[174,179,180] In the Aldabbagh group, Lynch *et al.*[174] synthesized [1,2-*a*]benzimidazoles containing five, six and seven-membered alicyclic rings through a radical cyclization of nucleophilic N-alkyl radicals (Scheme 3.7). The piperidino[1,2-*a*]benzimidazole analogue **33** was prepared by alkylation of 4,7-dimethoxy-1*H*-benzimidazole (**31**) with a phenylselenide to give radical precursor **32** and sodium hydride was used to generate the required N-centred anion. The radical cyclization was initiated using 1,1′-azobis(cyclohexanecarbonitrile) (ACN) to give a tertiary carbon-centred radical that undergoes

hydrogen abstraction with tributyltin hydride (Bu_3SnH) to generate the stannyl radical. Propagation of the reaction through the abstraction the phenylselenide group by the stannyl radical generates carbon-centred radical **34**. Camphorsulfonic acid (CSA) was used to quaternise the basic N3 atom of benzimidazole **34**, thus activating the C2 position for intramolecular radical cyclization to give a nitrogen-centred radical cation **35**. Hydrogen abstraction by the azo-initiator (ACN) or its corresponding radical allows the regeneration of aromaticity to give protonated benzimidazole **36**, which upon basic work-up generates benzimidazole **33** (Scheme 3.7). The requirement for radical cyclization precursors to be prepared and the use of excess azo-initiator are drawbacks associated with this transformation.

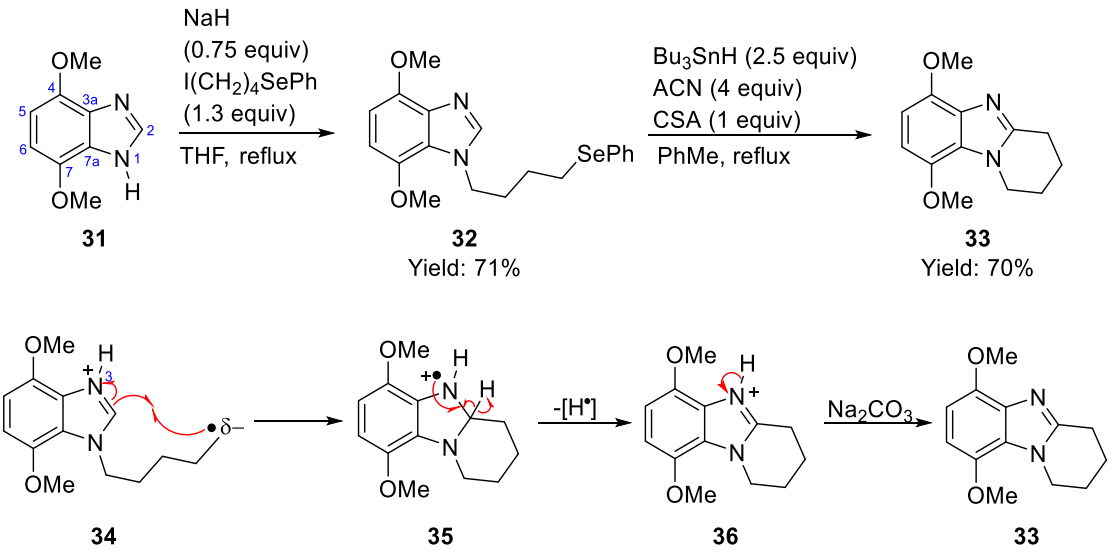

Scheme 3.7: Preparation of 6,6-dimethoxy-1,2,3,4-tetrahydropyrido[1,2-*a*]benzimidazole and intramolecular radical cyclization mechanism.[174]

Routes to benzimidazoles that involve transition-metal catalysis have been explored by Anastasiou *et al.*[181] A rhodium (II) acetate ($[Rh(OAc)_2]_2$) catalysed hydroformylation reaction of *N*-alkyl-1,2-diaminobenzene **37** in the presence of a triphenylphosphine (PPh_3), carbon monoxide and hydrogen gave access to both five and six-membered alicyclic ring-fused benzimidazoles **40** and **41** with high regioselectivity (Scheme 3.8). PPh_3 was used for catalyst stability. It was proposed that *N*-alkyl-1,2-diaminobenzene **37** undergoes a regioselective hydroformylation reaction to give terminal aldehyde **38**. Aldehyde **38** cyclizes to give imine **39** and subsequent oxidation gives the benzimidazole products **40** and **41** (Scheme 3.8).

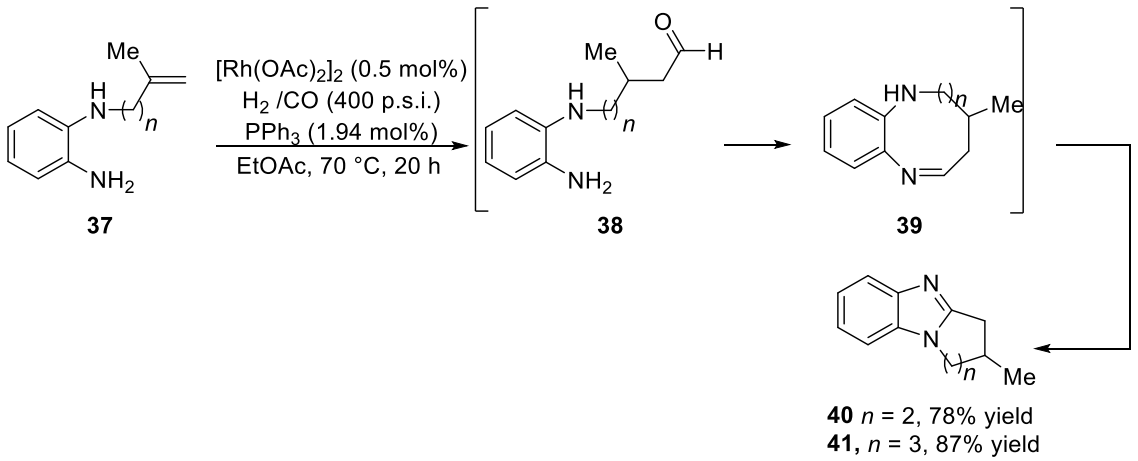

Scheme 3.8: Synthesis of alicyclic ring-fused benzimidazoles through a hydroformylation reaction of *N*-alkyl-1,2-diaminobenzenes.[181]

High molar mass hypervalent iodine reagents such as phenyliodine(III) diacetate (PIDA) in the presence of base (Cs_2CO_3) have been used to synthesize 2-substituted benzimidazole **43** through an intramolecular oxidative imidation of the aromatic C–H bond of *N*-arylamidine **42** (Scheme 3.9)[182]. It was proposed that through the reaction of *N*-phenylbenzamidine and PIDA an N-iodoimido species is produced with release of acetic acid. Homolysis of the N–I bond generates a nitrogen-centred radical and a hypervalent iodine-(III)-centred radical. Addition of the nitrogen-centred radical onto the aromatic ring ultimately leads to 2-phenyl-1-*H*-benzimidazole **43**.

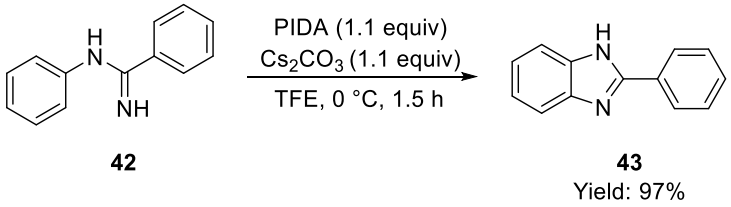

Scheme 3.9: Synthesis of 2-phenyl-1-H-benzimidazole.[182]

Synthesis of five-, six- and seven-membered ring-fused [1,2-*a*]benzimidazoles (**47**–**49**) by cyclization of amidine precursors (**44**–**46**) *via* a benzyne intermediate using an excess of strong base, *t*-BuLi (3.3 equiv) at −75 to −30 °C was reported by Caroon *et al* (Scheme 3.10).[183] Addition of *t*-BuLi gave a cyclized lithio species. Electrophilic trapping of this species with water gave the benzimidazole products (**47**–**49**).

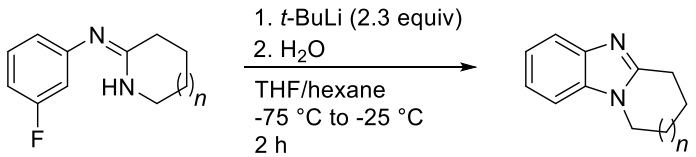

44, *n* = 0
45, *n* = 1
46, *n* = 2

47, *n* = 0 = 65%
48, *n* = 1 = 85%
49, *n* = 2 = 30%

Scheme 3.10: Synthesis of five, six and seven-membered ring-fused [1,2-*a*]benzimidazoles.[183]

Another oxidative cyclization method for preparing ring-fused [1,2-*a*]benzimidazoles was reported by Nair and Adams[184] in the 1960s (Scheme 3.11). *Ortho*-amino anilines **50** were converted into alicyclic ring-fused [1,2-*a*]benzimidazoles **51** by using a combination of hydrogen peroxide and trifluoroacetic acid, thus generating peroxytrifluoroacetic acid *in-situ*. The *o*-amino aniline precursors **50** were substituted at the 5 position with both electron-withdrawing groups (such as NO_2) and electron-donating groups (such as CH_3) (Scheme 3.11).

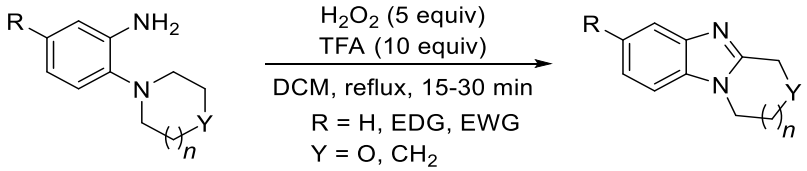

50

51
Yield: 58-91%

Scheme 3.11: Synthesis of alicyclic ring-fused [1,2-*a*]benzimidazoles by using hydrogen peroxide and TFA.[184]

Nair and Adams suggested that this reaction could either proceed through a nitroso or an *N*-oxide intermediate. Later Aldabbagh and co-workers[174] isolated an amine *N*-oxide intermediate of an *o*-*tert*-aminoacetanilide, which led to a new proposed mechanism for the formation of ring-fused benzimidazoles (Scheme 3.12). It was proposed that *o*-amino aniline **51** is first oxidized to the protonated amine *N*-oxide **52**. This functionalization causes the NCH_2 of the alicyclic ring to become acidic, thus promoting the elimination of water and forming iminium ion **53**. Nucleophilic addition of the primary amine onto the iminium ion gives hydrobenzimidazole **54**. Further oxidation by hydrogen peroxide followed by elimination of water gives iminium ion **55**, which can re-aromatize to give benzimidazole **56**.

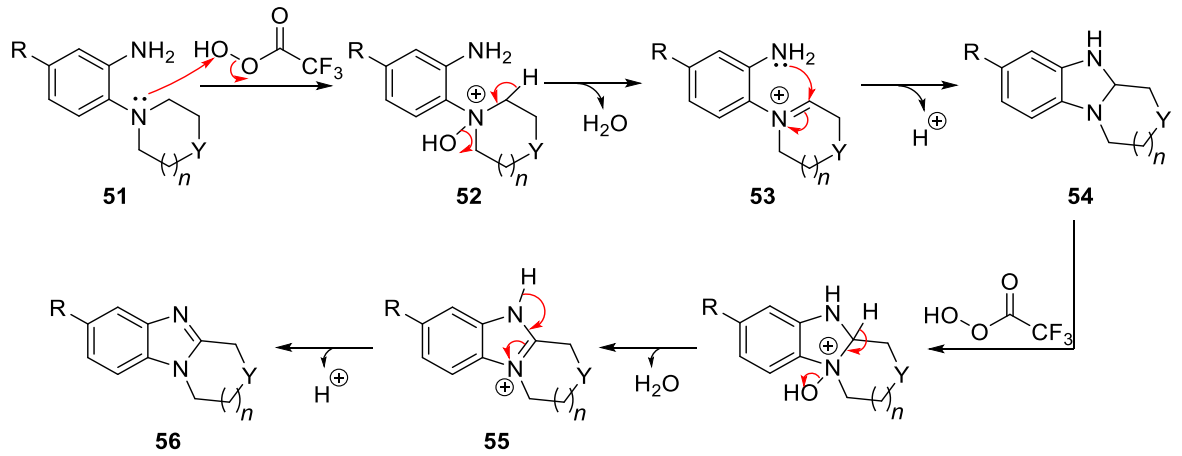

Scheme 3.12: Proposed mechanism for the synthesis of ring-fused [1,2-*a*]benzimidazoles *via* an *N*-oxide intermediate.

Recently, in the Aldabbagh group, Gurry *et al.*[185] prepared a series of halogenated five–eight membered ring-fused [1,2-*a*]benzimidazoles **58** containing both electron-withdrawing and electron-donating groups (C3 position) in high yields through a one-pot oxidative cyclization with selective dichloroination/dibromination of commercial *o*-cyclic amine substituted anilines **57**. This transformation was mediated by hydrogen peroxide and hydrohalic acid (Scheme 3.13).

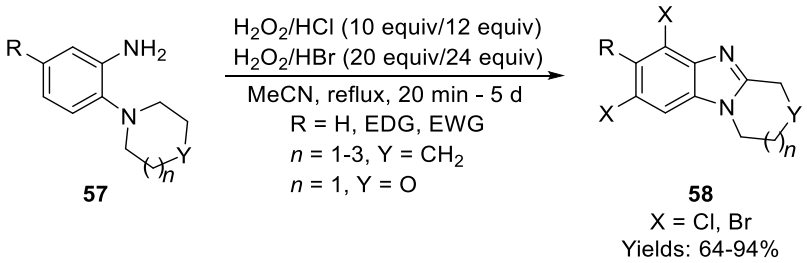

Scheme 3.13: Hydrogen peroxide/hydrohalic acid mediated oxidative cyclization and selective halogenation giving dichlorinated and dibrominated alicyclic ring-fused benzimidazoles.[185]

The *in-situ* generation of elemental chlorine and bromine by using hydrogen peroxide and hydrochloric and hydrobromic acid, respectively, facilitates electrophilic aromatic halogenation. This reaction is known to proceed through a hypohalous acid intermediate (HOX). HOX in an acidic solution is in equilibrium with the molecular halogen, X_2 (Figure 3.7).[186–189]

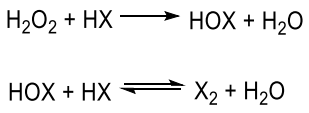

Figure 3.7: Generation of X_2 from H_2O_2/HX.[190]

3.1.6 Synthesis of Alicyclic Ring-Fused [1,2-*a*]benzimidazolequinones

Since 2010, when Skibo *et al.*[172] introduced pyrrolidino[1,2-*a*]benzimidazolequinone derivatives as bioreductive anti-cancer agents, there have been a number of reports for the synthesis of benzimidazolequinone derivatives. The conversion of *para*-dimethoxybenzimidazoles into benzimidazolequinones is a well-known method for the synthesis of benzimidazolequinones. Moriarty *et al.*[191] converted dimethoxybenzimidazole containing a fused pyridine ring **59** into the corresponding benzimidazolequinone **60** (Scheme 3.14). This two-step method involved a HBr-mediated deprotection of the methoxy-ether groups to give a dihydroquinone intermediate. Subsequent oxidation of the dihydroquinone intermediate to the *para*-quinone by using ferric chloride gave the benzimidazolequinone **60** in 78% yield.

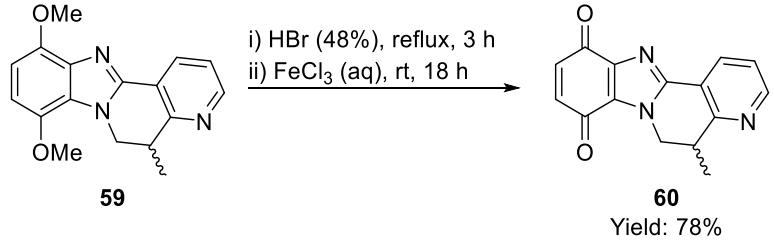

Scheme 3.14: Two step synthesis of 5-methyl-5,6-dihydrobenzimidazo[2,1-*f*][1,6]naphthyridine-8,11-dione.[191]

One-step procedures are also known for the conversion of *para*-dimethoxybenzimidazoles into benzimidazolequinones. Antonini *et al.*[192] used cerium ammonium nitrate (CAN) to convert 5-(chloromethyl)-4,7-dimethoxybenzimidazole **61** into 5-(chloromethyl)-1*H*-benzimidazole-4,7-dione **62** (Scheme 3.15).

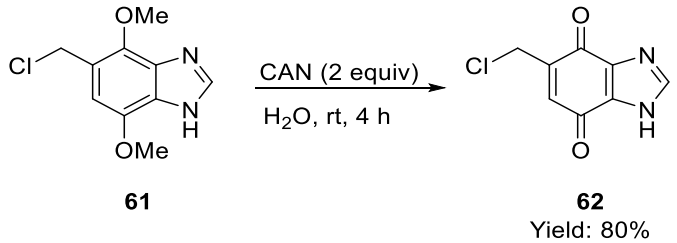

Scheme 3.15: One-step synthesis of 5-(chloromethyl)-1*H*-benzimidazole-4,7-dione.[192]

3.2 Aims and Objectives

Aldabbagh and co-workers have previously observed that the size of fused-alicyclic ring of benzimidazolequinones influences cytotoxicity (Sections 3.1.3 and 3.1.4). This chapter is focused on the synthesis of an azocane-fused[1,2-*a*]benzimidazolequinone. A hydrogen peroxide mediated cyclization of an *o*-cyclic amine-substituted aniline will be used to give the corresponding benzimidazole, followed by hydrobromic acid (HBr)-induced demethylation and oxidation using ferric chloride to give the benzimidazolequinone (Scheme 3.16).

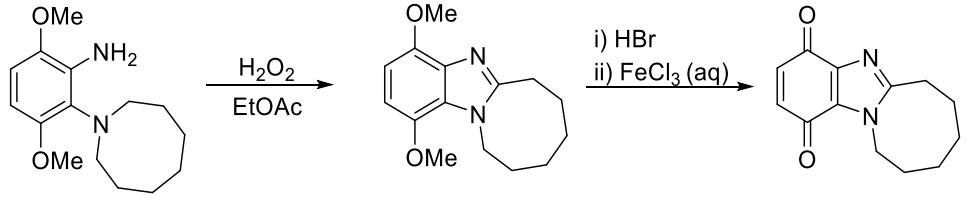

63 **64** **65**

Scheme 3.16: Synthesis of azocino[1,2-*a*]benzimidazoles and benzimidazolequinones.

The incorporation of halogen atoms onto the quinone moiety has previously been used to enhance cytotoxicity (Section 3.1.3). Halogenated quinones have also been shown to be synthetically useful intermediates for further functionalization (Section 3.1.4). Hypohalous acid has been reported for electrophilic halogenation of many aromatics and the combination of hydrogen peroxide and trifluoroacetic acid has previously been employed for the synthesis of ring-fused benzimidazoles from *o*-cyclic amine substituted anilines. Building on these methods, the H_2O_2–HX system will be used to carry out a one-pot oxidative cyclization, aromatic halogenation and demethylation of *o*-cyclic amine-substituted anilines **63** to form dihalogenated azocino[1,2-*a*]benzimidazoles, **66** and **67** and benzimidazolequinones, **68** and **69** (Scheme 3.17).

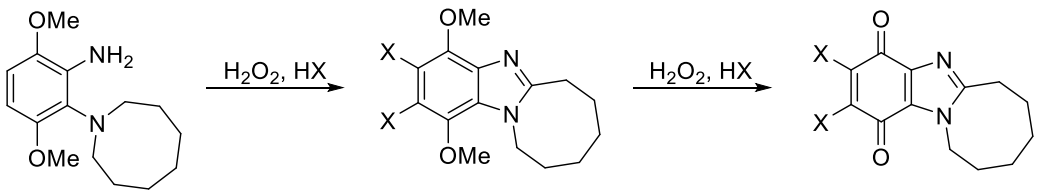

63 **66**, X = Cl **67**, X = Br **68**, X = Cl **69**, X = Br

Scheme 3.17: One-pot conversion of 3,6-dimethoxy-2-(cycloamino)aniline into dihalogenated ring-fused benzimidazoles and benzimidazolequinones.

The cytotoxicity of the azocino[1,2-*a*]benzimidazolequinone **65** (Figure 3.8) will be investigated. In addition, the cytotoxicity of a series of halogenated and non-halogenated piperidino[1,2-*a*]benzimidazolequinones (**70**–**72**) will be evaluated as well as a series of alicyclic ring-fused benzimidazolequinones (**73**–**75**) (Figure 3.8). Two human cancer cell lines, prostate cancer (DU-145) and breast cancer (MCF-7) will be used for these cytotoxicity evaluations, which will be carried out using the MTT colorimetric assay.

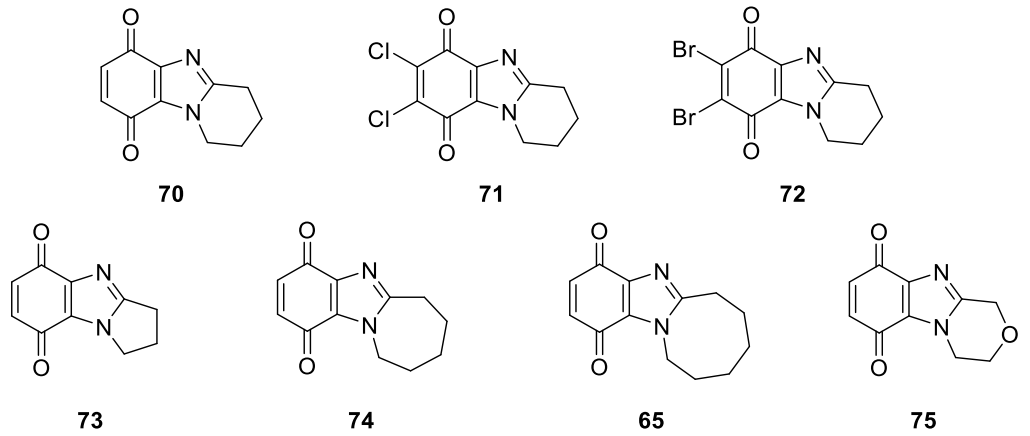

Figure 3.8: Alicyclic ring-fused [1,2-*a*]benzimidazolequinones evaluated against two human cancer cell lines; DU-145 and MCF-7.

From this cytotoxicity evaluation, the following structure–activity relationships will be determined:

1. The effect of halogenation of the piperidine fused [1,2-*a*]benzimidazolequinone moiety on cytotoxicity (comparing **70**, **71** and **72**, Figure 3.8).
2. The effect of the size of the fused alicyclic ring onto the benzimidazolequinone moiety on cytotoxicity (comparing **70**, **73**, **74,** and **65**, Figure 3.8).
3. The effect of an oxygen atom within the fused alicyclic ring of piperidine fused [1,2-*a*]benzimidazolequinone moiety (comparing **70** and **75**) on cytotoxicity (Figure 3.8).

3.3 Results and Discussion

The retrosynthetic analysis of the azocane-fused[1,2-*a*]benzimidazolequinones is outlined (Scheme 3.18). 1,4-Dimethoxybenzene will be used as the starting precursor.

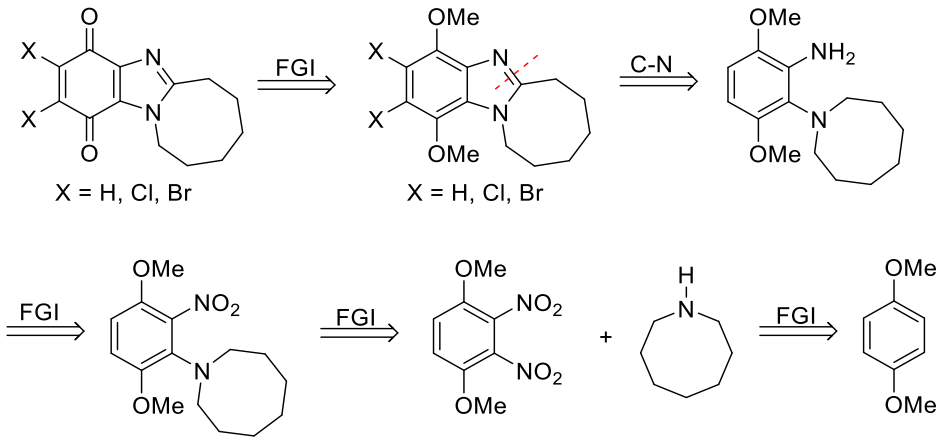

Scheme 3.18: Retrosynthesis of halogenated and non-halogenated azocane-fused[1,2-*a*]benzimidazolequinones.

3.3.1 Synthesis of 2-(Azocan-1-yl)-3,6-dimethoxyaniline

Based on the procedure by Hammershoj *et al.*,[193] nitration of 1,4-dimethoxybenzene (**76**) was carried out by using concentrated nitric acid to give a mixture of isomers, 1,4-dimethoxy-2,3-dinitrobenzene (**77**) and 1,4-dimethoxy-2,5-dinitrobenzene (**78**) in 75% yield, 7:1 ratio (Scheme 3.19). The desired major isomer, 1,4-dimethoxy-2,3-dinitrobenzene (**77**) was not isolated, owing to difficulty in separation by flash column chromatography; the mixture was thus carried forward to the next step with the aim of purification at a later stage.

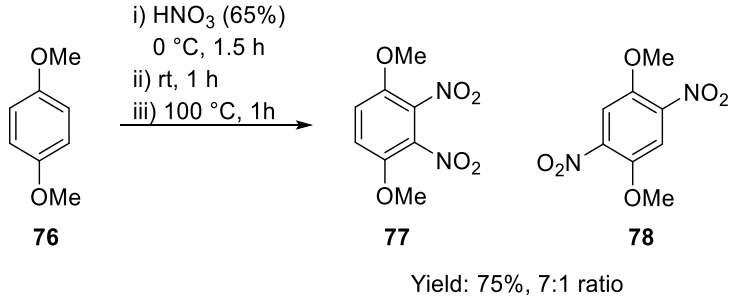

Scheme 3.19: Preparation of 1,4-dimethoxy-2,3-dinitrobenzene and 1,4-dimethoxy-2,5-dinitrobenzene.

Based on a similar procedure described by Mustroph and Haedder[194] for the preparation of 1-(3,6-dimethoxy-2-nitrophenyl)pyrrolidine, hexamethyleneimine (**79**) was added to the mixture

of the isomers, 1,4-dimethoxy-2,3-dinitrobenzene (**77**) and 1,4-dimethoxy-2,5-dinitrobenzene (**78**) in acetonitrile and potassium carbonate so as to affect a nucleophilic aromatic substitution of one of the nitro groups (Scheme 3.20). The reaction mixture was stirred at reflux for 22 hours. Nucleophilic substitution of nitro group at the 3 position of 1,4-dimethoxy-2,3-dinitrobenzene (**77**) and the 5-position of 1,4-dimethoxy-2,5-dinitrobenzene (**78**) with hexamethyleneimine (**79**) occurred. Both isomers (**80** and **81**) were separated by flash column chromatography, thus allowing the desired product, 1-(3,6-dimethoxy-2-nitrophenyl)azocane (**80**) to be isolated in 48% yield (Scheme 3.20).

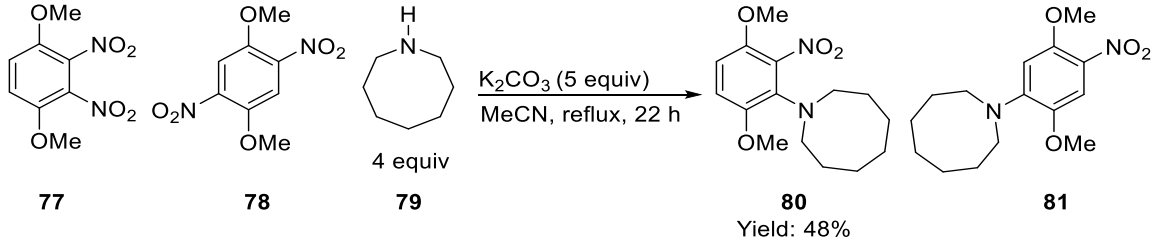

Scheme 3.20: Preparation of 1-(3,6-dimethoxy-2-nitrophenyl)azocane.

Following a similar protocol reported by Zhang *et al.*[195] for the reduction of 2-phenoxynitrobenzenes, reduction of the remaining nitro group of 1-(3,6-dimethoxy-2-nitrophenyl)azocane (**80**) using iron powder and aqueous ammonium chloride in refluxing ethanol for eight hours led to the desired *o*-cyclic amine substituted aniline **63** in 55% yield (Scheme 3.21). Flash column chromatography purification was required to remove dimethoxy[1,2-*a*]benzimidazole **64** (Scheme 3.21).

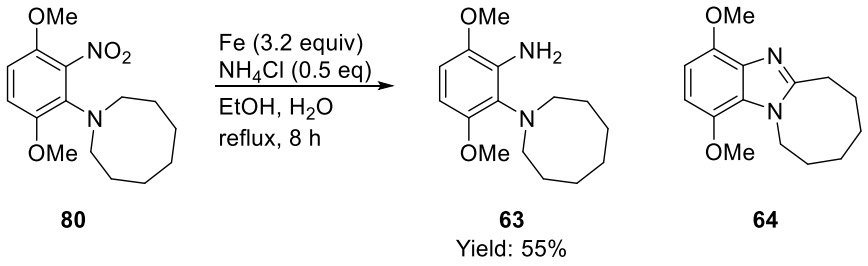

Scheme 3.21: Preparation of 2-(azocan-1-yl)-3,6-dimethoxyaniline.

3.3.2 Synthesis of Azocane-Fused [1,2-*a*]Benzimidazole

The oxidative cyclization of 2-(azocan-1-yl)-3,6-dimethoxyaniline (**63**) was initially carried out using hydrogen peroxide in refluxing ethyl acetate. After 36 hours of reflux, benzimidazole product **64** was isolated in 35% yield; the remaining material was unreacted starting material

63. The reaction was repeated with the addition of one equivalent of methanesulfonic acid (MSA). This change led to the isolation of the product in 60% yield and a reduced reaction time of 7 hours (Scheme 3.22).

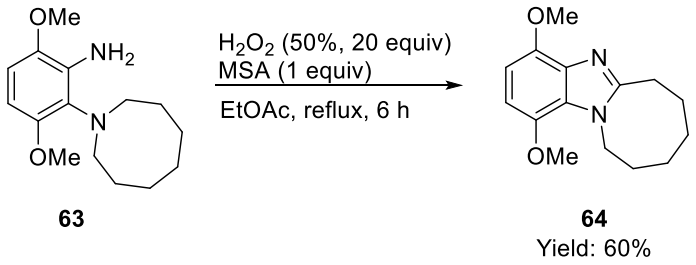

63 **64**
Yield: 60%

Scheme 3.22: Preparation of 1,4-dimethoxy-6,7,8,9,10,11-hexahydroazocino[1,2-*a*]benzimidazole using hydrogen peroxide.

The combination of MSA and hydrogen peroxide is known to generate a peroxy acid *in-situ* (Figure 3.9)[196], which is similar to the procedure reported by Nair and Adams,[171] could then produce an *N*-oxide intermediate of **63**.

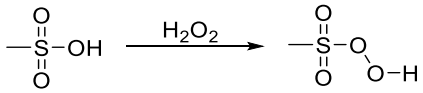

Figure 3.9: Generation of peroxy acid from MSA and hydrogen peroxide.[196]

It was proposed that intermediate *N*-oxide[197] of the azocane ring tertiary amine of **63** is stabilized through hydrogen bonding and therefore acidic conditions are required for the oxidative cyclization. This conclusion was based on previous work carried out in the Aldabbagh group in which ring-fused benzimidazole **87** was synthesized through an Oxone and formic acid mediated cyclization of *o*-*tert*-aminoacetanilide **82** (Scheme 3.23).[197] Investigation into the cyclization mechanism through the oxidation of *o*-*tert*-aminoacetanilide **82** with *m*-chloroperoxybenzoic acid (*m*-CPBA) allowed the isolation of the *N*-oxide product **83**. An X-ray crystal structure showed that the orientation of the amide of **83** was influenced by hydrogen bonding between the amide NH and the *N*-oxide residues (**83**). It was proposed that oxidation of *o*-*tert*-aminoacetanilide **82** to the *N*-oxide is followed by protonation of the *N*-oxide under the acidic conditions giving **83**. This leads to the methylene group next the *N*-oxide nitrogen to become more acidic and water is eliminated forming species **84**, which contains an iminium ion and an imidol moiety. Nucleophilic addition of the imidol onto the iminium ion forms *N*-acetyldihydrobenzimidazole **85**. Oxidation by Oxone leads to

imidazolium formate **86**, which upon hydrolysis and neutralization forms benzimidazole **87** (Scheme 3.23).[197]

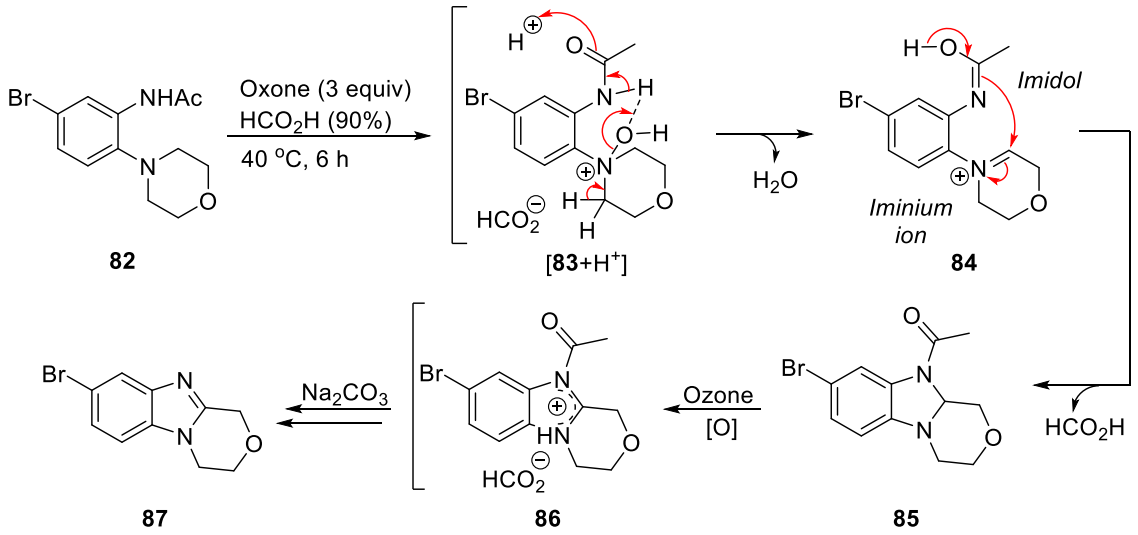

Scheme 3.23: Mechanism for the formation of ring-fused benzimidazole showing hydrogen bonding between *N*-oxide and amide.[197]

When the morpholine *N*-oxide **83** was treated with formic acid, a 1:1 mixture of starting material, *o*-*tert*-aminoacetanilide **82** and benzimidazole product **87** was obtained (Scheme 3.24). Therefore, it was proposed that an acid-catalysed cyclization occurred forming *N*-acetyldihydrobenzimidazole intermediate **85**. When no oxidant is present, such as Oxone, intermediate *N*-acetyldihydrobenzimidazole **85** is oxidized by morpholine *N*-oxide **83**, which forms the mixture of acetanilide **82** and benzimidazole **87**.[197]

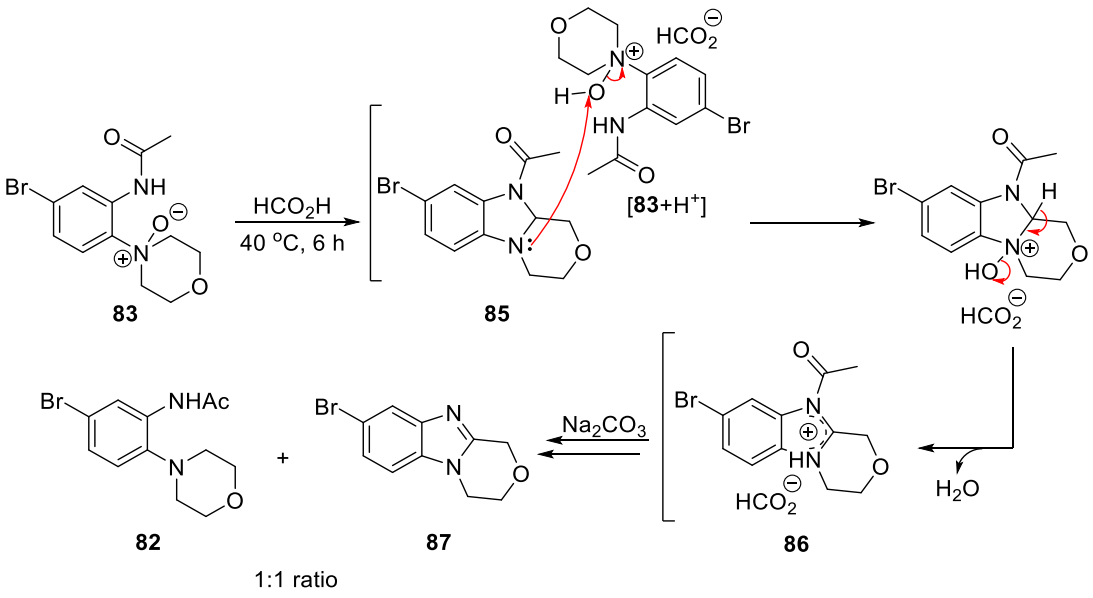

Scheme 3.24: Intermolecular oxidation by morpholine *N*-oxide.[197]

3.3.3 Synthesis of Dihalogenated Azocane-Fused[1,2-*a*]Benzimidazoles

The oxidative cyclization and chlorination of 2-(azocan-1-yl)-3,6-dimethoxyaniline (**63**) by using hydrogen peroxide and hydrochloric acid in acetonitrile at reflux gave the desired dichlorinated [1,2-*a*]benzimidazole **66** in 35% yield (Table 3.1, Scheme 3.25). When this reaction was carried out at room temperature, a longer reaction time of 34 hours was required to reach full conversion; under these milder conditions, the product was isolated in 89% yield (Table 3.1). When the reaction was repeated at the slightly higher temperature of 40 ºC, the desired product was obtained in 90% yield after 5 hours; the material was sufficiently pure and chromatography was not required (Scheme 3.25, Table 3.1).

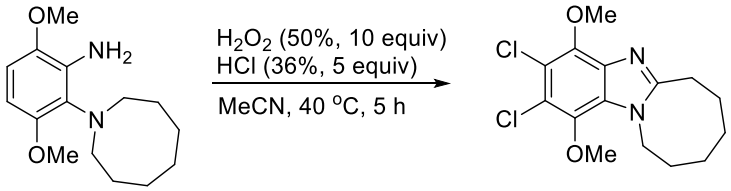

63 **66**
Yield: 90%

Scheme 3.25: Preparation of 2,3-dichloro-1,4-dimethoxy-6,7,8,9,10,11-hexahydro[1,2-*a*]benzimidazole.

Table 3.1: Optimization of the oxidative cyclization and chlorination of 2-(azocan-1-yl)-3,6-dimethoxyaniline **63**. Conditions: 2-(azocan-1-yl)-3,6-dimethoxyaniline (1 mmol), H_2O_2 (10 mmol), HCl (5 mmol), MeCN (10 mL).

Entry	Temp (ºC)	Time (h)	Yield (%)
1	Reflux	0.5	35
2	Room temperature	34	89
3	40	5	90

Dichlorinated [1,2-*a*]benzimidazole **66** was isolated and its structure confirmed by NMR spectroscopy and X-ray crystallography. Crystallization by slow evaporation of the product from DCM/diethyl ether afforded the X-ray quality crystals (Figure 3.10).

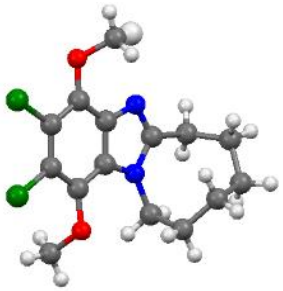

Figure 3.10: X-ray crystal structure of 2,3-dichloro-1,4-dimethoxy-6,7,8,9,10,11-hexahydro[1,2-*a*]benzimidazole (**66**), crystallized from DCM/diethyl ether and structure obtained by X-ray crystallographer Prof. Patrick McArdle (NUI Galway).

The oxidative cyclization and bromination of 2-(azocan-1-yl)-3,6-dimethoxyaniline (**63**) by using hydrogen peroxide and hydrobromic acid in refluxing acetonitrile gave dibrominated [1,2-*a*]benzimidazole **67** in 95% yield after 5.5 hours (Scheme 3.26).

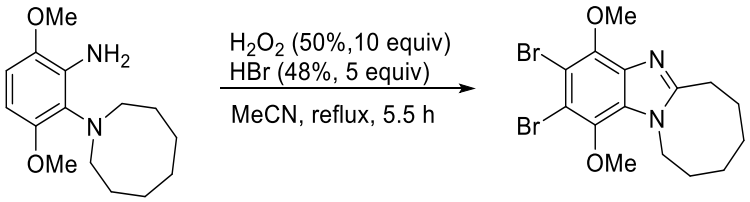

63 **67**
Yield: 95%

Scheme 3.26: Preparation of 2,3-dibromo-1,4-dimethoxy-6,7,8,9,10,11-hexahydro[1,2-*a*]benzimidazole.

Dibrominated [1,2-*a*]benzimidazole **67** was isolated and its structure confirmed by NMR spectroscopy and X-ray crystallography. Crystallization by slow evaporation of the product from DCM/diethyl ether afforded the X-ray quality crystals (Figure 3.11).

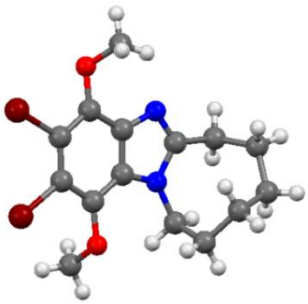

Figure 3.11: X-ray crystal structure of 2,3-dibromo-1,4-dimethoxy-6,7,8,9,10,11-hexahydro[1,2-*a*]benzimidazole, crystallized from DCM/diethyl ether and structure obtained by X-ray crystallographer Prof. Patrick McArdle (NUI Galway).

Reaction profiling by HPLC and mass spectrometry, carried out by my colleague Martin Sweeney,[190] on the conversion of tetrahydroisoquinoline substituted aniline **88** into the corresponding benzimidazolequinone **90** showed the presence of chlorinated aniline intermediate **89** (Scheme 3.27). X-ray crystallography was used to confirm the structure of this intermediate. This observation suggested that chlorination of the 3,6-dimethoxy-2-(cycloamino)aniline **63** occurs before the oxidative cyclization.

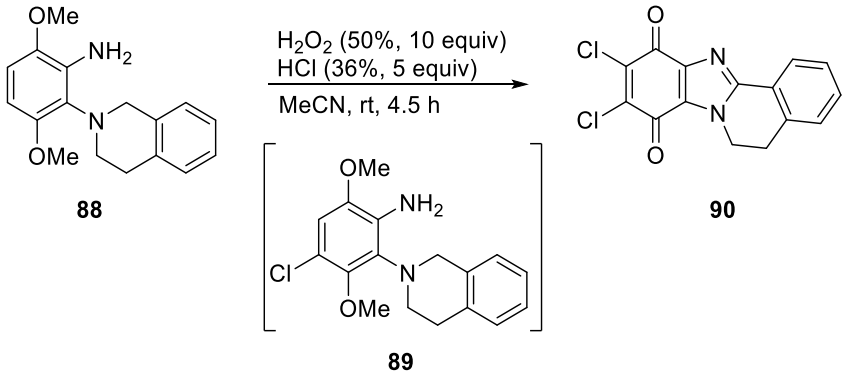

Scheme 3.27: Detection of mono-chlorinated aniline intermediate.

3.3.4 Synthesis of Azocane-Fused [1,2-*a*]Benzimidazolequinone

Based on the procedure reported by O'Shaughnessy *et al.*[198] for the conversion of a pyrrolidine-fused [1,2-*a*]benzimidazole with a fused cyclopropane ring into the corresponding benzimidazolequinone, stirring of azocino [1,2-*a*]benzimidazole **64** in HBr at reflux for 3 hours allowed demethylation of the methoxy substituents. After evaporation of the HBr, the intermediate hydroquinone was oxidized by using aqueous ferric chloride to give the desired azocino[1,2-*a*]benzimidazolequinone **65** in 52% yield after purification by flash column chromatography (Scheme 3.28).

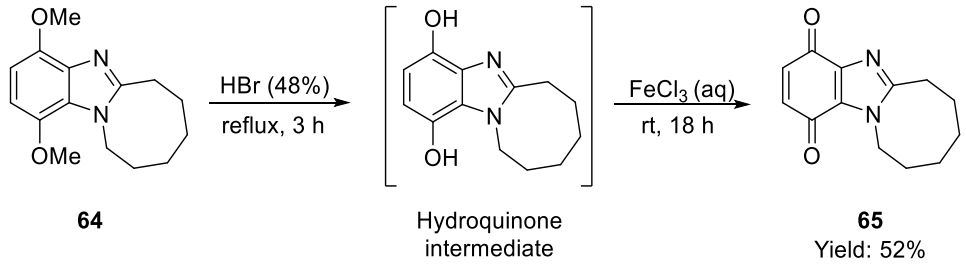

Scheme 3.28: Preparation of 6,7,8,9,10,11-hexahydroazocino[1,2-*a*]benzimidazole-1,4-dione.

3.3.5 Synthesis of Halogenated Azocino-Fused [1,2-*a*]Benzimidazolequinones

With the overall aim of carrying out a one-pot conversion of the *o*-cyclic amine-substituted aniline **63** into halogenated benzimidazolequinones, **68** and **69**, we first carried out the reaction in a stepwise manner, i.e. chlorinated azocino [1,2-*a*]benzimidazole **66** was first converted into benzimidazolequinone **68**. *In-situ* deprotection and oxidation of chlorinated azocino [1,2-*a*]benzimidazole **66** was carried out through subjection to hydrogen peroxide and hydrochloric acid in refluxing acetonitrile. This protocol gave benzimidazolequinone **68** in 40% yield after purification by flash column chromatography (Scheme 3.29). It was necessary to use high equivalents of both hydrogen peroxide and hydrochloric acid to ensure complete conversion of starting material **66**. These conditions favoured the formation of Cl_2, allowing cleavage of the methoxy ether bond.

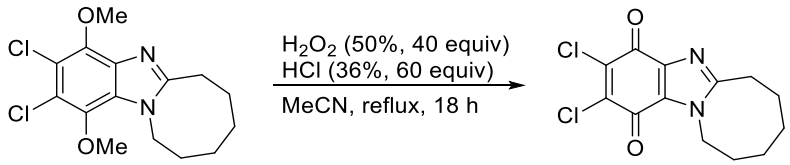

66 **68**
Yield: 40%

Scheme 3.29: Preparation of 2,3-dichloro-6,7,8,9,10,11-hexahydroazocino[1,2-*a*]benzimidazole-1,4-dione.

Similarly, benzimidazolequinone **69** was prepared from brominated azocino [1,2-*a*]benzimidazole **67** by using hydrogen peroxide and hydrobromic acid at reflux; the desired product was isolated in 55% yield (Scheme 3.30).

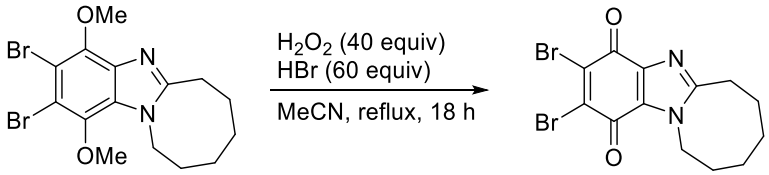

67 **69**
Yield: 55%

Scheme 3.30: Preparation of 2,3-dibromo-6,7,8,9,10,11-hexahydroazocino[1,2-*a*]benzimidazole-1,4-dione.

3.3.6 One-Pot Synthesis of Halogenated Azocane-Fused [1,2-*a*]Benzimidazole-quinones

To enable a one-pot oxidative cyclization/deprotection/oxidation of 2-(azocan-1-yl)-3,6-dimethoxyaniline (**63**) into dihalogenated quinones, **68** and **69**, conditions that favour the formation of X_2 (X = Cl or Br) were employed. When a higher molar ratio of HX is used relative to H_2O_2, the concentration of X_2 will be higher, thus allowing the 6-electron oxidation to give the benzimidazolequinone products.

2-(Azocan-1-yl)-3,6-dimethoxyaniline (**63**) was stirred in acetonitrile (MeCN) and excess HCl (180 equiv) was added. Hydrogen peroxide (50 equiv) was added over 30 mins and the reaction mixture was stirred at reflux for one hour thus giving the desired benzimidazolequinone **68** in 45% yield (Scheme 3.31).

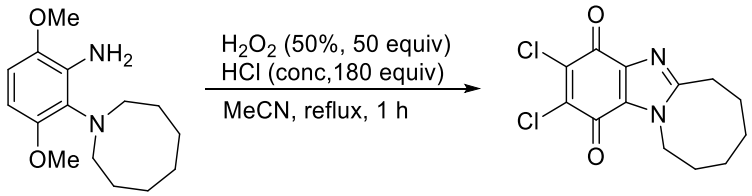

63 **68**
Yield: 54%

Scheme 3.31: One-pot synthesis of 2,3-dichloro-6,7,8,9,10,11-hexahydroazocino[1,2-*a*]benzimidazole-1,4-dione.

Performing the corresponding reaction on 2-(azocan-1-yl)-3,6-dimethoxyaniline (**63**) but using HBr instead, gave the desired benzimidazolequinone **69** in 92% yield after purification by flash column chromatography (Scheme 3.32).

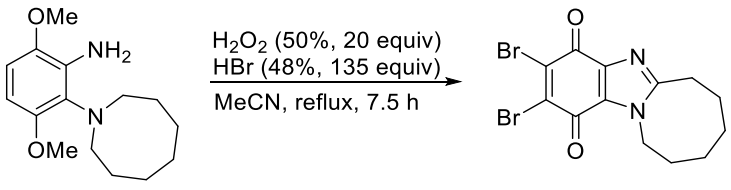

63 **69**
Yield: 92%

Scheme 3.32: One-pot synthesis of 2,3-dibromo-6,7,8,9,10,11-hexahydroazocino[1,2-*a*]benzimidazole-1,4-dione.

3.3.7 Cytotoxicity Evaluations

Cytotoxicity evaluations of a range of alicyclic ring-fused [1,2-*a*]benzimidazolequinones were carried out using the MTT assay (See Chapter 2, Section 2.3.4).

3.3.7.1 The Effect of Halogenation on the Cytotoxicity of Benzimidazolequinones

The contribution of the halogen atoms to the cytotoxicity of the piperidino[1,2-*a*]benzimidazolequinone system (Figure 3.12) was investigated (quinones **70**, **71** and **72**) on the DU-145 (prostate) and MCF-7 (breast) cancer cell lines.

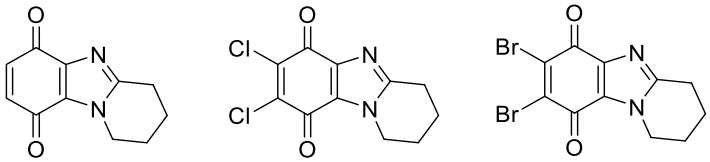

70 **71** **72**

Figure 3.12: Quinones **70**, **71** and **72** evaluated to compare the effect of halogenation of the ring-fused benzimidazolequinone moiety on cytotoxicity.

Quinones **70**, **71** and **72** showed selectivity towards the DU-145 cell line (~ 4 times more cytotoxic compared with the MCF-7 cell line). The presence of the halogen atoms had little effect on cytotoxicity against both cell lines with all quinones having similar IC_{50} values (Table 3.2). All compounds were found to be more cytotoxic than the known indolequinone anti-cancer agent, MMC (0.17 µM for DU-145[191] and 0.93 µM for MCF-7[177]).

Table 3.2: IC_{50} values[a] for quinones **70**, **71** and **72** evaluated against two human cancer cell lines, DU-145 and MCF-7.

Compound	**[a]IC_{50} DU-145 (µM)**	**[a]IC_{50}MCF-7 (µM)**
70	0.14 ± 0.01	0.44 ± 0.03
71	0.11 ± 0.01	0.52 ± 0.03
72	0.11 ± 0.01	0.89 ± 0.33

[a]IC_{50} represents the compound concentration required for the reduction of the mean cell viability to 50% of the control value after incubation for 72 h at 37 ºC, as determined using the MTT assay.

3.3.7.2 The Effect of the Size of the Fused Alicyclic Ring on the Cytotoxicity of Benzimidazolequinones

The effect of the alicyclic ring size on cytotoxicity was evaluated by comparison of five-, six-, seven- and eight-membered ring-fused benzimidazolequinones (**73**, **70**, **74** and **65**). All quinones were evaluated against the DU-145 and MCF-7 cancer cell lines (Figure 3.13).

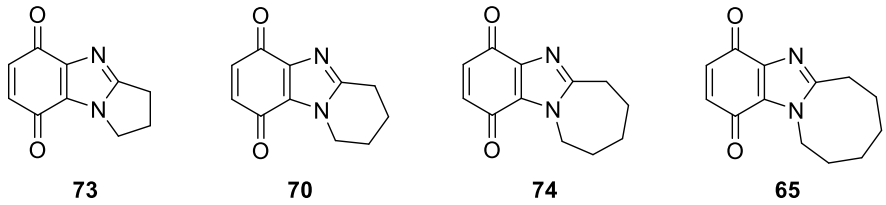

Figure 3.13: Quinones **73**, **70**, **74** and **65** evaluated against the DU-145 and MCF-7 cancer cell lines.

All quinones were found to be more cytotoxic towards the DU-145 cell line compared with the MCF-7 cell line (approximately two times more cytotoxic), except quinone **73**, which exhibited no selectivity (Table 3.3). Quinone **70** was the most cytotoxic towards both the DU-145 and the MCF-7 cell lines compared with piperidino **73**, azepino **74** and azocino **65** ring-fused analogues. The IC_{50} values of quinone **70** is comparable to MMC for the DU-145 cell line and is two times more cytotoxic towards the MCF-7 cell line compared with MMC (MMC: 0.17 µM for DU-145[191] and 0.93 µM for MCF-7[177]). Quinone **65**, containing a fused azocane ring, was the second most cytotoxic compound against both cell lines with IC_{50} values of 0.42 µM and 0.94 µM for DU-145 and MCF-7 respectively, followed by quinone **74**, contained a fused azepane ring (IC_{50} values of 0.50 µM and 0.96 µM for DU-145 and MCF-7 respectively). Quinone **73**, containing a fused pyrrolidine ring, was the least cytotoxic of all quinones towards both cell lines. Quinone **73** was seven times less cytotoxic against the DU-145 cell line and two times less cytotoxic against the MCF-7 cell line compared with the most cytotoxic quinone **70**. (Table 3.3).

Table 3.3: Comparison of the effect of alicyclic ring size on cytotoxicity towards two human cancer cell lines (DU-145 and MCF-7).

Compound	IC_{50} DU-145 (µM)	IC_{50} MCF-7 (µM)
73	1.02 ± 0.01	1.03 ± 0.01
70	0.14 ± 0.01	0.44 ± 0.03
74	0.50 ± 0.03	0.96 ± 0.04
65	0.42 ± 0.01	0.94 ± 0.03

3.3.7.3 The Effect of an Oxygen Atom Within the Fused Alicyclic Ring on the Cytotoxicity of Benzimidazolequinones

The cytotoxicity of piperidine-fused [1,2-*a*]benzimidazolequinone **70** and oxazino [1,2-*a*]benzimidazolequinone **75** against the DU-145 and MCF-7 cancer cell lines was compared to show the effect of an oxygen atom within the fused alicyclic ring of the [1,2-*a*]benzimidazolequinone moiety (Figure 3.14).

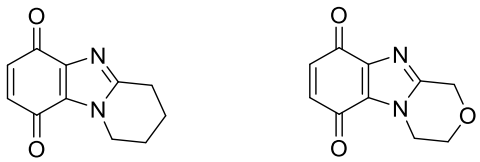

70 **75**

Figure 3.14: 1,2,3,4-tetrahydropyrido[1,2-*a*]benzimidazole-6,9-dione and 3,4-dihydro-1*H*-[1,4]oxazino[4,3-*a*]benzimidazole-6,9-dione.

Morpholine quinone **75** was five times less cytotoxic against the DU-145 cell line and three times less cytotoxic towards the MCF-7 cell line compared with piperidine quinone **70** (Table 3.4). In contrast with the other ring-fused analogues (quinones **73**, **70**, **74** and **65**, Table 3.3) morpholine quinone **75** is the least cytotoxic quinone towards both cell lines. Therefore, it is clear that inclusion of an oxygen atom within the alicyclic ring system has a significant effect on biological activity (Table 3.4).

Table 3.4: Comparison of the effect of the incorporation of an oxygen atom into the fused alicyclic ring of the piperidino[1,2-*a*]benzimidazolequinone system, evaluated against the DU-145 and MCF-7 cancer cell lines. This effect is shown by the comparison of 1,2,3,4-tetrahydropyrido[1,2-*a*]benzimidazole-6,9-dione (**70**) (with no heteroatom) and 3,4-dihydro-1*H*-[1,4]oxazino[4,3-*a*]benzimidazole-6,9-dione (**75**) (containing an oxygen atom).

Compound	IC_{50} DU-145 (μM)	IC_{50} MCF-7 (μM)
70	0.14 ± 0.01	0.44 ± 0.03
75	0.72 ± 0.06	1.14 ± 0.02

3.3.8 National Cancer Institute (NCI) – 60 Human Tumour Cell Line Screen

The NCI Developmental Therapeutics Program (DTP) facilitates the development and discovery of new anti-cancer agents (See Chapter 2, Section 2.3.3). The NCI-60 human tumour cell line screen was designed to screen small molecules against 60 different human tumour cell lines for anti-cancer activity. Cell lines from various types of cancers are used in this screen such as melanoma, leukaemia, lung, colon, central nervous system, breast, kidney, ovarian and prostate cancers. All accepted compounds are initially tested at a single high dose concentration (10^{-5} M) against the full 60 human tumour cell line range.

From the cytotoxicity evaluations carried out, the most cytotoxic of our [1,2-*a*]benzimidazolequinones towards both the MCF-7 and DU-145 cell lines was found to be piperidine fused [1,2-*a*]benzimidazolequinone **70** and halogenated analogues **71** and **72**. Therefore, these three benzimidazolequinones were submitted to the NCI and accepted for one-dose testing against the panel of 60 cancer cell lines. Quinone **70** exhibited significant cytotoxicity against the melanoma cancer cell lines, MALME-3M and MDA-MB-43 (Figure 3.15). The profiles for chlorinated quinone **71** (Figure 3.16) and brominated quinone **72** (Figure 3.17) were overall less cytotoxic compared with quinone **70**. However, both chlorinated quinone **71** and brominated quinone **72** exhibited selective cytotoxicity towards the leukaemia cell lines, CCRF-CEM and MOLT-4 (Figure 3.16 and Figure 3.17). Chlorinated quinone **71** also exhibited selectivity towards the colon cancer cell line, COLO 205 and the renal cancer cell line, ACHN (Figure 3.16). These [1,2-*a*]benzimidazolequinones (**70**, **71** and **72**) were not accepted by the NCI for further five-dose testing.

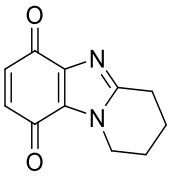

70

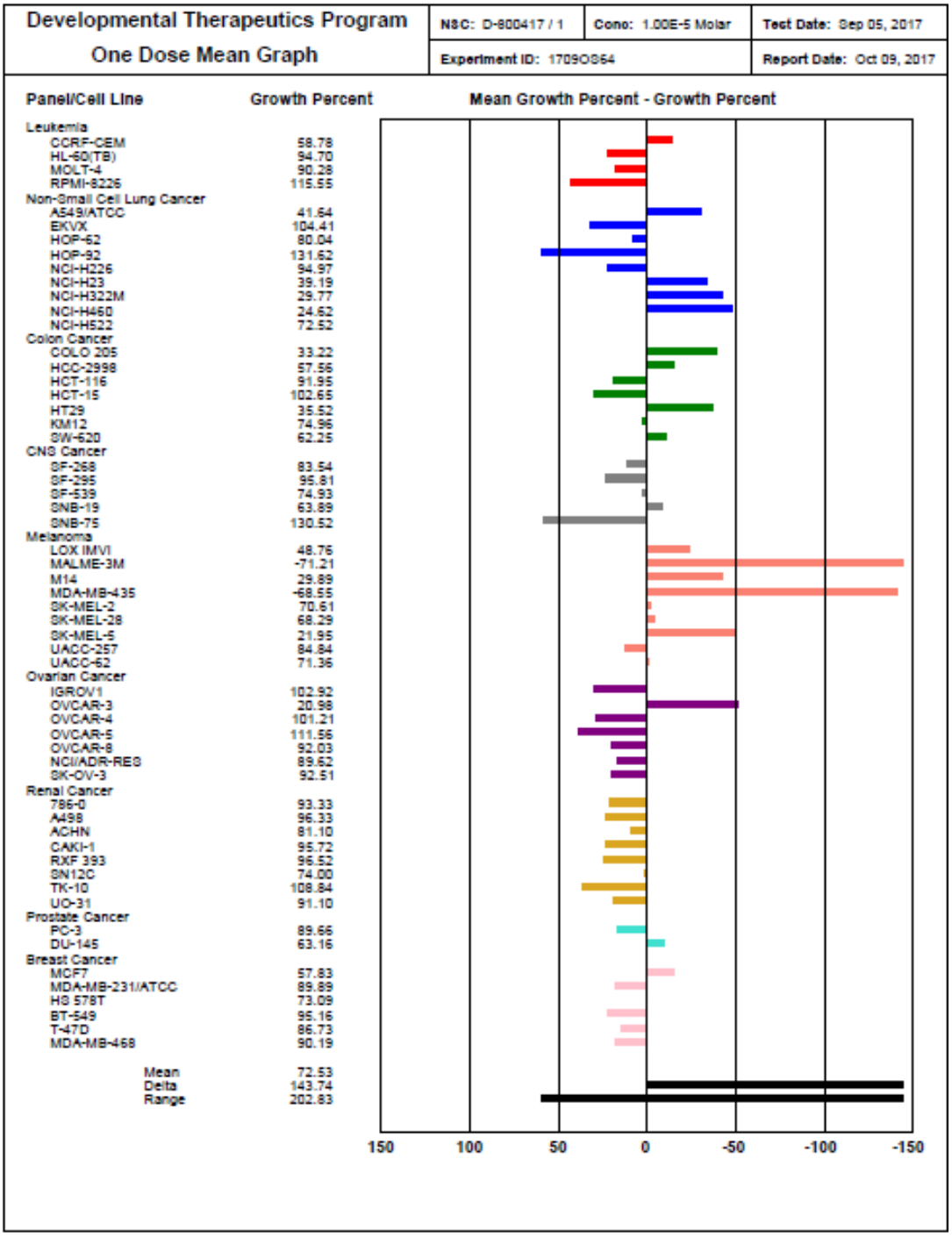

Figure 3.15: Activity of 1,2,3,4-tetrahydropyrido[1,2-*a*]benzimidazole-6,9-dione (**70**) towards the NCI-60 cell line panel.

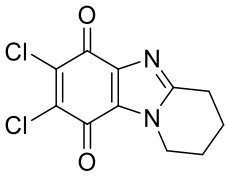

71

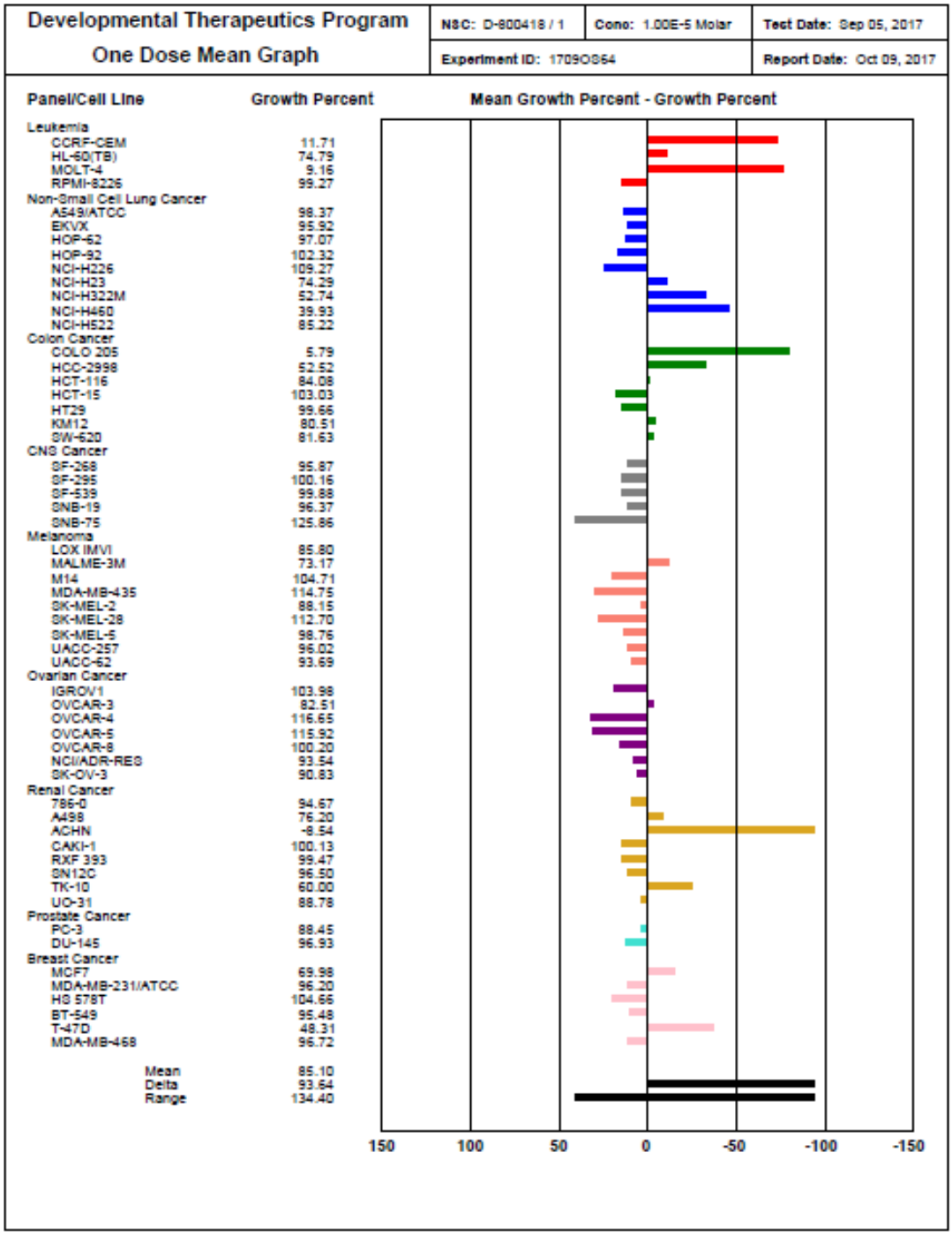

Figure 3.16: Activity of 7,8-dichloro-1,2,3,4-tetrahydropyrido[1,2-*a*]benzimidazole-6,9-dione (**71**) towards the NCI-60 cell line panel.

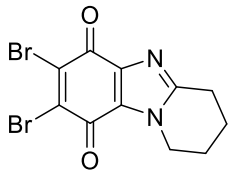

72

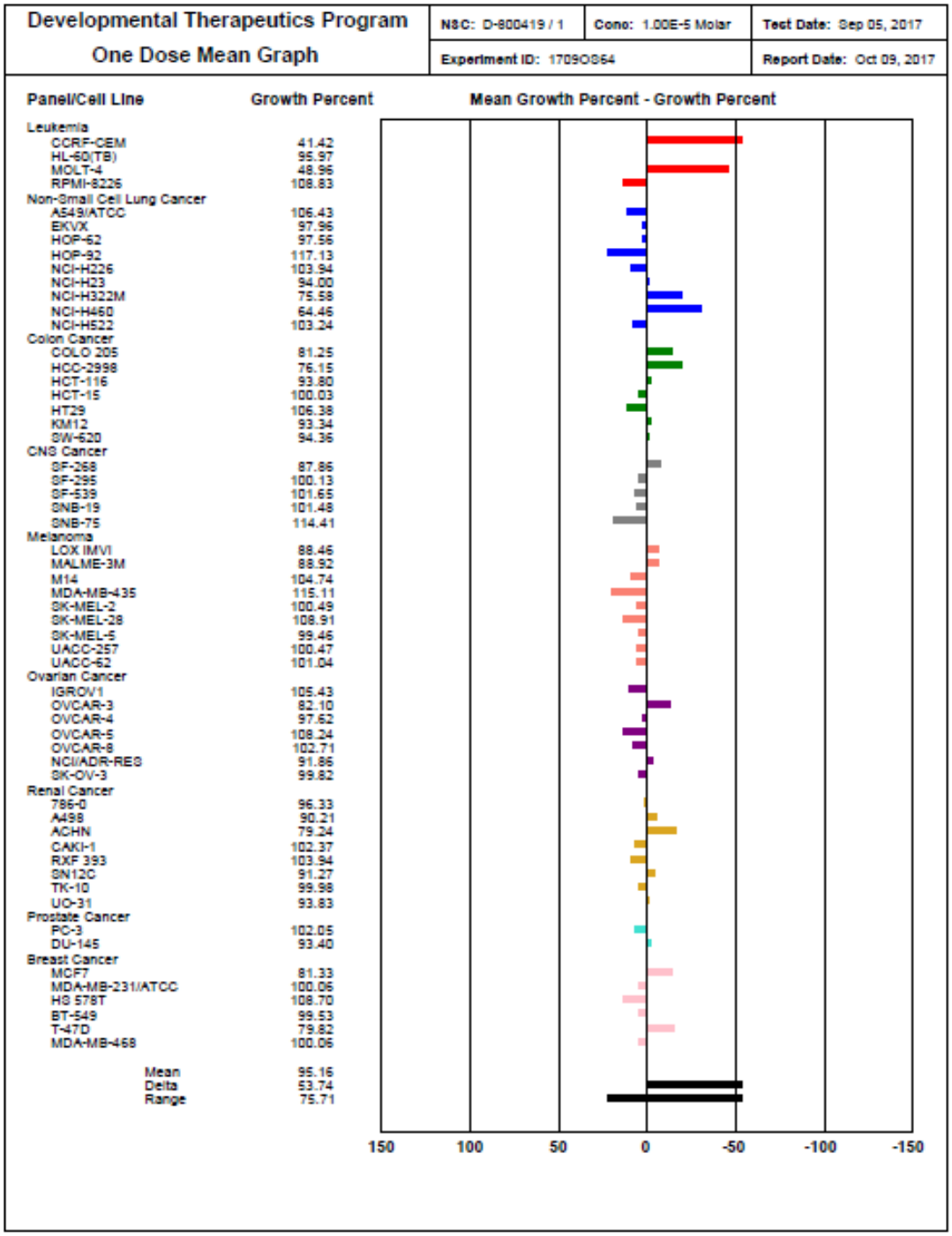

Figure 3.17: Activity of 7,8-dibromo-1,2,3,4-tetrahydropyrido[1,2-*a*]benzimidazole-6,9-dione (**72**) towards the NCI-60 cell line panel.

3.4 Summary and Conclusions

- A series of azocane-fused [1,2-*a*]benzimidazoles and benzimidazolequinones have been synthesized. The hydrogen peroxide and MSA mediated cyclization of an *o*-cyclic amine substituted aniline gave the azocane-fused [1,2-*a*]benzimidazole. Hydrobromic acid-induced demethylation followed by oxidation gave the azocino[1,2-*a*]benzimidazolequinone. Dihalogenated azocane-fused [1,2-*a*]benzimidazoles were synthesised using the H_2O_2–HX system and X-ray crystal structures of both halogenated analogues were obtained. Using the H_2O_2–HX system, a one-pot reaction involving oxidative cyclization, aromatic halogenation and demethylation of *o*-cyclic amine substituted anilines gave dihalogenated azocane-fused [1,2-*a*]benzimidazolequinones.
- A series of alicyclic ring-fused benzimidazolequinones were evaluated for anti-cancer activity against two human cancer cell lines, prostate cancer (DU-145) and breast cancer (MCF-7). All quinones were shown to be more active towards the DU-145 cell line compared with the MCF-7 cell line.
- Halogenation (chlorination and bromination) of the piperidine-fused [1,2-*a*]benzimidazolequinone has been shown to have little effect on cytotoxicity against MCF-7 and DU-145 cell lines.
- The size of the fused alicyclic ring was shown to affect cytotoxicity with the piperidine-fused [1,2-*a*]benzimidazolequinone being the most cytotoxic towards both MCF-7 and DU-145 cell lines followed by azocane, azepane and pyrrolidine rings.
- An overall decrease in cytotoxicity was observed when an oxygen atom was included in the fused alicyclic ring towards both DU-145 and MCF-7 cancer cell lines compared with the piperidine-fused [1,2-*a*]benzimidazolequinone analogue.
- In comparison with ring-fused imidazo[5,4-*f*]benzimidazolequinones, which have previously been evaluated in the Aldabbagh group, a significant increase in cytotoxicity was exhibited by alicyclic ring-fused [1,2-*a*]benzimidazolequinones towards the DU-145 cancer cell line. Piperidine-fused [1,2-*a*]benzimidazolequinone **70** was 14 times more cytotoxic compared with the corresponding dipiperidine-fused imidazo[5,4-*f*]benzimidazolequinone **29**. Azepane-fused [1,2-*a*]benzimidazolequinone **74** was 9 times more cytotoxic compared with the corresponding diazepane-fused imidazo[5,4-*f*]benzimidazolequinone **28**.

3.5 Experimental

3.5.1 General Information

Thin layer chromatography (TLC) was performed on TLC silica gel 60 F254 plates. Flash chromatography was carried out using Aldrich technical grade silica gel (particle size 40–63 microns) with the specified eluent. Melting points were measured on a Stuart Scientific melting point apparatus SMP1. Infrared spectra were recorded using a Perkin-Elmer Spec 1 with ATR attached. ^{1}H-NMR spectra were recorded using a Joel ECX 400 MHz instrument equipped with a DEC AXP 300 computer workstation. The chemical shifts were recorded in ppm relative to tetramethylsilane. ^{13}C NMR data were collected at 100 MHz with complete proton decoupling. High resolution mass spectra (HRMS) were carried out using ESI time-of-flight mass spectrometer (TOFMS). The precision of all accurate mass measurements were better than 5 ppm.

3.5.2 Materials

All chemicals were obtained from commercial sources and used without purification, except for ethyl acetate (Honeywell ACS reagent, reagent, ≥99.5% (GC)), which was purified by distillation. Methanesulfonic acid (MSA) is >99% and should be stored under an inert atmosphere. Hydrogen peroxide is 50% (w/v) in water, HBr is 48% (w/v) in water, and nitric acid is 64-66% (w/v) in water.

3.5.3 Compound Data

Preparation of 1-(3,6-dimethoxy-2-nitrophenyl)azocane (80)

1,4-Dimethoxy-2,3-dinitrobenzene (**77**) (0.800 g, 3.50 mmol), azocane (1.586 g, 14.00 mmol) and potassium carbonate (2.42 g, 17.54 mmol) were stirred in acetonitrile (10 mL) at reflux for 24 h. EtOAc (20 mL) was added and the organic layer washed with brine (40 mL). The organic extract was dried ($MgSO_4$), evaporated to dryness, and purified by column chromatography using silica as adsorbent with gradient elution of petroleum ether and Et_2O to give 1-(3,6-dimethoxy-2-nitrophenyl)azocane (**80**) in 48% yield.

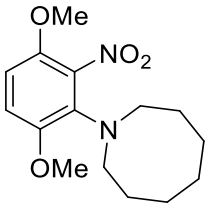

1-(3,6-Dimethoxy-2-nitrophenyl)azocane (80): (0.495 g, 48%); yellow solid; mp 99–101 ºC; R_f 0.20 (9:1 pet. ether/Et_2O); ν_{max} (neat, cm^{-1}) 2904, 2842, 1616, 1582, 1531 (NO_2), 1490, 1456, 1436, 1381 (NO_2), 1307, 1253, 1055; δ_H (400 MHz, $CDCl_3$) 1.55-1.62 (m, 10H), 2.97–3.15 (bs, 4H), 3.80 (s, 3H), 3.81 (s, 3H), 6.75 (d, J = 9.2 Hz, 1H), 6.85 (d, J = 9.2 Hz, 1H); δ_C (100 MHz, $CDCl_3$) 25.7, 26.7, 28.5, 54.7 (all CH_2), 56.0, 56.7 (both Me), 109.3, 112.8 (both CH), 137.1, 142.5, 144.1, 152.6 (all C); HRMS (ESI) *m/z* $(M+H)^+$, $C_{15}H_{23}N_2O_4$ calcd. 295.1658, observed 295.1654.

Preparation of 2-(azocan-1-yl)-3,6-dimethoxyaniline (63)

1-(3,6-Dimethoxy-2-nitrophenyl)azocane (**80**) (3.96 mmol) with iron powder (0.709 g, 12.69 mmol) and NH_4Cl (0.106 g, 1.98 mmol) were stirred at reflux in ethanol (10 mL) and water (3 mL) for 8 h. EtOAc (30 mL) was added to the cooled mixture. The organic layer was washed with brine (40 mL), dried ($MgSO_4$), evaporated to dryness and purified by column chromatography using silica as adsorbent with gradient elution of petroleum ether and EtOAc to give 2-(azocan-1-yl)-3,6-dimethoxyaniline (**63**) in 55% yield.

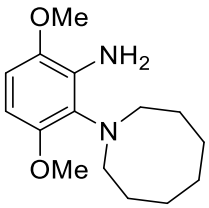

2-(Azocan-1-yl)-3,6-dimethoxyaniline (63): (0.575 g 55%); white solid; mp 74–79 ºC; R_f 0.39 (9:1 pet. ether / EtOAc); ν_{max} (neat, cm^{-1}) 3466, 3366, 2997, 2933, 2829, 1603, 1547, 1457, 1486, 1437, 1259, 1225; δ_H (400 MHz, $CDCl_3$) 1.51–1.91 (m, 10 H), 2.81–2.87 (m, 2H), 3.21–3.28 (m, 2H), 3.75 (s, 3H), 3.80, (s, 3H), 4.43–4.45 (bs, 2H, NH_2), 6.16 (d, J = 9.0 Hz, 1H), 6.54 (d, J = 9.0 Hz, 1H); δ_C (100 MHz, $CDCl_3$) 26.1, 28.2, 29.6, 54.7 (all CH_2), 55.4, 56.0 (both Me), 99.1, 107.0 (both CH), 130.3, 135.8, 142.1, 153.0 (all C); HRMS (ESI) *m/z* $(M+H)^+$, $C_{15}H_{25}N_2O_2$ calcd. 265.1916, observed 265.1901.

Preparation of 1,4-Dimethoxy-6,7,8,9,10,11-hexahydroazocino[1,2-*a*]benzimidazole (64)

2-(Azocan-1-yl)-3,6-dimethoxyaniline **63** (0.260 g, 1 mmol), H_2O_2 (1.14 mL, 20 mmol) and methanesulfonic acid (1 mmol) were stirred in EtOAc for 7 hours. EtOAc (10 mL) was added and the solution was washed with Na_2CO_3 (saturated, 2 x 10 mL) The organic extract was dried ($MgSO_4$), evaporated to dryness and purified by column chromatography using silica as adsorbent with gradient elution of EtOAc and petroleum ether (90:10) to give 1,4-Dimethoxy-6,7,8,9,10,11-hexahydroazocino[1,2-*a*]benzimidazole (**64**) in 60% yield.

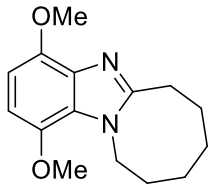

1,4-Dimethoxy-6,7,8,9,10,11-hexahydroazocino[1,2-*a*]benzimidazole (64): (0.156 g, 60%); brown oil; R_f 0.27 (9:1 EtOAc / pet. ether); ν_{max} (neat, cm^{-1}) 2929, 2857, 1615, 1520, 1466, 1443, 1403, 1253, 1223, 1159; δ_H (400 MHz, $CDCl_3$) 1.08–1.18 (m, 2H), 1.40–1.56 (m, 2H), 1.76–1.89 (m, 4H), 2.94 (t, J = 6.2 Hz, 2H), 3.83 (s, 3H), 3.90 (s, 3H), 4.39 (t, J = 6.0 Hz, 2H), 6.45 (AB_q, J 8.7 Hz, 2H); δ_C (100 MHz, $CDCl_3$) 23.6, 25.9, 27.3, 31.2 (x 2), 43.0 (all CH_2), 55.7, 55.8 (both Me), 101.0, 102.3 (both CH), 125.2, 134.8, 141.5, 145.6, 155.7 (all C); HRMS (ESI) *m/z* $(M+H)^+$, $C_{15}H_{21}N_2O_2$ calcd. 261.1603, observed 261.1600.

General Procedure for the Preparation of Ring-fused dihalogenated benzimidazoles 66 and 67

2-(Azocan-1-yl)-3,6-dimethoxyaniline **63** (0.260 g, 1 mmol), H_2O_2 (10 mmol) and HX (X = Cl, Br, 5 mmol) were stirred in MeCN (10 mL) for 20 min. At the end of the reaction, EtOAc (20 mL) was added to the cooled solution, which was washed with Na_2CO_3 (sat. soln, 2 × 10 mL). The organic extract was dried ($MgSO_4$) and evaporated to dryness to give the pure product.

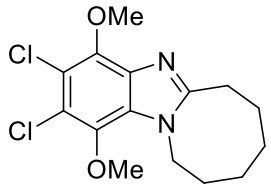

2,3-Dichloro-1,4-dimethoxy-6,7,8,9,10,11-hexahydroazocino[1,2-*a*]benimidazole (66): 0.312 g, 95%; light brown solid; mp 122-124 ºC; vmax (neat, cm^{-1}) 2934, 2851, 1512, 1481, 1467, 1427, 1389, 1236, 1059; δ_H (400 MHz, $CDCl_3$) 1.15-1.21 (m, 2H), 1.50-1.56 (m, 2H), 1.84-1.92 (m, 4H), 2.99 (t, *J* 6.1 Hz, 2H), 3.96 (s, 3H), 4.21 (s, 3H), 4.38 (t, *J* 5.9 Hz, 2H); δ_C (100 MHz, $CDCl_3$) 23.7, 25.8, 27.1, 31.0, 31.1, 42.9 (all CH_2), 61.6, 62.1 (both Me), 117.9, 120.0, 127.6, 136.3, 138.7, 144.4, 157.8 (all C); HRMS (ESI) m/z $(M+H)^+$, $C_{15}H_{19}N_2O_2{}^{35}Cl_2$ calcd. 329.0815, observed. 329.0824.

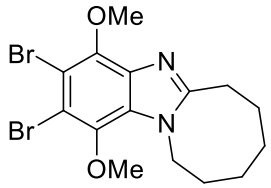

2,3-Dibromo-1,4-dimethoxy-6,7,8,9,10,11-hexahydroazocino[1,2-*a*]benzimidazole (67): 0.397 g, 95%; brown solid; mp 160-162 ºC; vmax (neat, cm^{-1}) 2927, 2857, 1672, 1594, 1507, 1440, 1468, 1409, 1390, 1252, 1056; δ_H (400 MHz, $CDCl_3$) 1.13-1.19 (m, 2H), 1.50-1.56 (m, 2H), 1.84-1.92 (m, 4H), 3.00 (t, *J* 6.2 Hz, 2H), 3.93 (s, 3H), 4.19 (s, 3H), 4.37 (t, *J* 6.0 Hz, 2H); δ_C (100 MHz, $CDCl_3$) 23.6, 25.9, 27.2, 31.0, 31.2, 42.9 (all CH_2), 61.6, 62.2 (both Me), 110.7, 112.9, 128.6, 137.2, 140.0, 145.8, 157.8 (all C); HRMS (ESI) m/z (M+H)+, $C_{15}H_{19}N_2O_2$ $^{79}Br^{81}Br$ calcd. 418.9793, observed 418.9774.

Preparation of 6,7,8,9,10,11-Hexahydroazocino[1,2-*a*]benzimidazole-1,4-dione (65)

1,4-dimethoxy-6,7,8,9,10,11-hexahydroazocino[1,2-*a*]benzimidazole (**64**) (0.260 g, 1 mmol) was stirred in HBr (10.2 mL, 90 mmol) at reflux for 5 hours. The solution was cooled and evaporated to dryness. Ferric chloride (20 mL, 0.7 M) was added and stirred at room temperature for 12 hours. The solution was extracted with CH_2Cl_2 (5 x 20 mL). The combined organic extracts were dried ($MgSO_4$), evaporated to dryness and purified by flash column

chromatography using silica as adsorbent with gradient elution of EtOAc and petroleum ether (90:10) to give the desired compound.

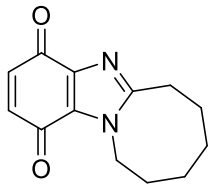

6,7,8,9,10,11-Hexahydroazocino[1,2-*a*]benzimidazole-1,4-dione (65): (0.120 g, 52%); yellow solid; mp 128–130 ºC; R_f 0.33 (9:1 EtOAc / pet. ether); ν_{max} (neat, cm^{-1}) 3062, 2925, 2853, 1674, 1755 (C=O), 1588, 1530, 1508, 1468, 1452, 1339, 1281, 1199; δ_H (500 MHz, $CDCl_3$) 1.25–1.29 (m, 2 H), 1.51–1.54 (m, 2H), 1.82–1.89 (m, 4H), 2.95 (t, J = 6.3 Hz, 2H), 4.42 (t, J = 6.1 Hz, 2H), 6.60 (ABq, J = 10.4 Hz, 2H); δ_C (100 MHz, $CDCl_3$) 23.5, 25.3, 26.4, 30.2, 30.4, 43.1 (all CH_2), 129.7 (C), 135.9, 136.1 (both CH), 141.5, 156.9 (both C), 177.9, 181.1 (both C=O); HRMS (ESI) *m/z* $(M + H)^+$, $C_{13}H_{15}N_2O_2$ calcd. 231.1134, observed 231.1130.

Preparation of 2,3-dichloro-6,7,8,9,10,11-hexahydroazocino[1,2-*a*]benzimidazole-1,4-dione (68)

H_2O_2 (2.84 mL, 50 mmol) was added over 30 mins to 2-(azocan-1-yl)-3,6-dimethoxyaniline (1 mmol) in HCl (14.8 mL, 180 mmol) at reflux. The reaction was stirred for a further 1 hour at reflux. The solution was cooled, Na_2CO_3 (sat. sol. 10 mL) added and extracted with CH_2Cl_2 (5 x 20 mL). The combined organic extracts were dried ($MgSO_4$), evaporated to dryness, and purified by column chromatography using silica as adsorbent with isocratic elution of petroleum ether and EtOAc to give 2,3-dichloro-6,7,8,9,10,11-hexahydroazocino[1,2-*a*]benzimidazole-1,4-dione (**68**) in 45% yield.

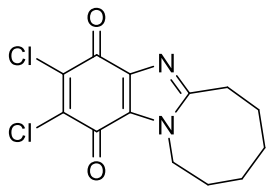

2,3-Dichloro-6,7,8,9,10,11-hexahydroazocino[1,2-*a*]benzimidazole-1,4-dione (68): 0.134 g, 45%; yellow solid; R_f 0.29 (1:1 EtOAc / pet. ether); mp 156–160 ºC ν_{max} (neat, cm^{-1}) 2920,

2851, 1693 (C=O), 1673 (C=O), 1567, 1523, 1468, 1317, 1279, 1161, 1126; δ_H (400 MHz, $CDCl_3$) 1.24–1.29 (m, 2H), 1.51–1.53 (m, 2H), 1.86-1.91 (m, 4H), 2.96 (t, *J* 6.0 Hz, 2H), 4.44 (t, *J* 6.0 Hz, 2H); δ_C (100 MHz, $CDCl_3$) 23.6, 25.5, 26.7, 30.2, 30.5, 43.8 (all CH_2), 129.3, 140.3, 140.8, 141.5, 158.7 (all C), 168.3, 171.3 (both C=O). HRMS (ESI) *m/z* $(M+H)^+$, $C_{12}H_{13}N_2O_2{}^{35}Cl_2$ calcd. 299.0354, observed 299.0340.

Preparation of 2,3-dibromo-6,7,8,9,10,11-hexahydroazocino[1,2-a]benzimidazole-1,4-dione (69)

2-(Azocan-1-yl)-3,6-dimethoxyaniline and H_2O_2 (1.14 mL, 20 mmol) were stirred at reflux in HBr (15.3 mL, 135 mmol) for 7.5 h. The solution was cooled, Na_2CO_3 (sat. sol. 10 mL) added and extracted with CH_2Cl_2 (5 x 20 mL). The combined organic extracts were dried ($MgSO_4$), evaporated to dryness and purified by column chromatography using silica as adsorbent with isocratic elution of petroleum ether and EtOAc giving 2,3-dibromo-6,7,8,9,10,11-hexahydroazocino[1,2-a]benzimidazole-1,4-dione (**69**) in 92% yield.

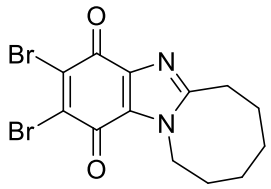

2,3-Dibromo-6,7,8,9,10,11-hexahydroazocino[1,2-*a*]benzimidazole-1,4-dione (69): 0.355 g, 92%; orange solid; R_f 0.50 (50:50 EtOAc / pet. ether); mp 172–178 ºC; ν_{max} (neat, cm^{-1}) 2930, 2862, 1687 (C=O), 1680 (C=O), 1519, 1508, 1464, 1445, 1273, 1144, 1114, 1090; δ_H (400 MHz, $CDCl_3$) 1.19–1.25 (m, 2H), 1.46–1.52 (m, 2H), 1.78–1.86 (m, 4H), 2.92 (t, *J* 6.2 Hz, 2H), 4.39 (t, *J* 6.2 Hz, 2H); δ_C (100 MHz, $CDCl_3$) 23.6, 25.5, 26.7, 30.2, 30.5, 43.7 (all CH_2), 129.0, 139.1, 139.7, 141.2, 158.5, 168.1, 171.1 (all C); HRMS (ESI) *m/z* $(M + H)^+$, $C_{13}H_{13}N_2O_2{}^{79}Br^{81}Br$ calcd. 388.9323, observed 388.9333.

3.5.4 X-Ray Crystallography Data

Table 3.5: X-ray crystallography data and structure refinement for 2,3-dichloro-1,4-dimethoxy-6,7,8,9,10,11-hexahydro[1,2-*a*]benzimidazole.

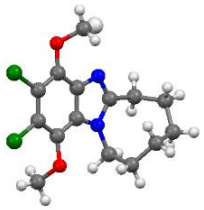

Empirical formula	$C_{15}H_{18}Cl_2N_2O_2$
Formula weight	329.21
Temperature	296.6(8) K
Wavelength	0.71073 Å
Crystal system	Orthorhombic
Space group	$Pna2_1$
Unit cell dimensions	a = 18.2099(6) Å b = 15.8757(8) Å c = 10.8517(3) Å
Volume	3137.2(2) $Å^3$
Z	8
Density (calculated)	1.394 Mg/m^3
Absorption coefficient	0.419 mm^{-1}
F(000)	1376
Crystal size	0.50 x 0.40 x 0.20 mm^3
Theta range for data collection	3.594 to 29.205°.
Index ranges	$-24 \leq h \leq 24, -20 \leq k \leq 17, -13 \leq l \leq 13$
Reflections collected	24446
Independent reflections	7285 [R(int) = 0.0398]
Completeness to theta = 25.242°	99.6 %
Absorption correction	Semi-empirical from equivalents
Max. and min. transmission	1.00000 and 0.93686
Refinement method	Full-matrix least-squares on F^2
Data / restraints / parameters	7285 / 1 / 383
Goodness-of-fit on F^2	1.118
Final R indices [I > 2sigma(I)]	R1 = 0.0678, wR2 = 0.1492
R indices (all data)	R1 = 0.0970, wR2 = 0.1746
Absolute structure parameter	−0.04(3)
Extinction coefficient	n/a
Largest diff. peak and hole	0.581 and −0.873 $e.Å^{-3}$

Table 3.6: X-ray crystallography data and structure refinement for 2,3-dibromo-1,4-dimethoxy-6,7,8,9,10,11-hexahydro[1,2-*a*]benzimidazole.

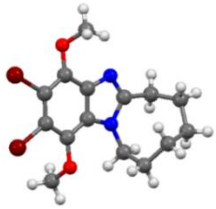

Empirical formula	$C_{15}H_{18}Br_2N_2O_2$
Formula weight	418.13
Temperature	297.3(9) K
Wavelength	0.71073 Å
Crystal system	Orthorhombic
Space group	Pna21
Unit cell dimensions	a = 18.2223(9) Å b = 16.0225(9) Å c = 11.1023(5) Å
Volume	3241.5(3) Å3
Z	8
Density (calculated)	1.714 Mg/m3
Absorption coefficient	5.007 mm^{-1}
F(000)	1664
Crystal size	0.50 x 0.40 x 0.20 mm^3
Theta range for data collection	3.587 to 29.289°.
Index ranges	$-22 \leq h \leq 23$, $-19 \leq k \leq 21$, $-14 \leq l \leq 14$
Reflections collected	24782
Independent reflections	7840 [R(int) = 0.0960]
Completeness to theta = 25.242°	99.6 %
Absorption correction	Semi-empirical from equivalents
Max. and min. transmission	1.00000 and 0.46725
Refinement method	Full-matrix least-squares on F2
Data / restraints / parameters	7840 / 13 / 384
Goodness-of-fit on F2	0.995
Final R indices [I > 2sigma(I)]	R1 = 0.0693, wR2 = 0.0890
R indices (all data)	R1 = 0.2043, wR2 = 0.1222
Absolute structure parameter	−0.014(13)
Extinction coefficient	0.00153(14)
Largest diff. peak and hole	0.826 and -0.760 e.$Å^{-3}$

3.5.5 Cell Culture and Cytotoxicity Evaluation

3.5.5.1 Cell Lines

The DU-145 (prostate cancer) and MCF-7 (breast cancer) cell lines were obtained from Dr. Stephen Rea, NUI Galway. All cell culture reagents were obtained from Sigma-Aldrich and all disposable sterile plastic ware was obtained from Sarstedt AG (Numbrecht, Germany). The MCF-7 cells were cultured in Dulbecco's modified eagle's medium (DMEM) which contained high glucose (4.5 g/mL). This media was supplemented with 10% heat-inactivated fetal bovine serum (FBS) and 1% penicillin-streptomycin. The DU-145 cells were cultured in RPMI-1640 medium. This medium was supplemented with 1% penicillin-streptomycin, 1% of 2 mM L-glutamine and 10% of non heat-inactivated fetal bovine serum (FBS). All cells grew as adherent cultures in 75 cm^3 flasks in 20 mL of medium and incubated in an autoflow CO_2 (5%) water-jacket incubator at 37 °C. All surfaces were sprayed with 70% ethanol prior to carrying out all procedures. Cells were subcultured when they were approximately 80% confluent. DU-145 cells were treated with 2X trypsin-EDTA in Hanks balance salt solution and MCF-7 cells were treated with 5X trypsin-EDTA in Hanks balance salt solution for five minutes. All cells were centrifuged at 1200 rpm in a Rotanta 300 centrifuge. The cell pellet was then re-suspended in fresh cell culture medium. When cells need to be counted (before carrying out the MTT assay) a Kova® Glasstic® slide 10 combination coverslip-microslip slide was used to determine the cell number. When cells did not need to be counted before subculturing, the MCF-7 stock suspension was seeded with 1/5 and DU-145 at 1/4 and this volume wss added to 20 mL of pre-warmed medium in a sterile 75 cm^3 flask followed by incubation at 37 °C and 5% CO_2. The cell culture medium was replaced every two–three days.

3.5.5.2 Cell Resuscitation

Both the DU-145 and MCF-7 cell lines were resuscitated though rapid thawing at 37 °C. The thawed cell suspension was added to the culture medium (1 mL) which was pre-heated to 37 °C and this mixture was added to a sterile culture flask (25 cm^3). A further 4 mL of the pre-heated culture medium was added and the cells were then incubated (37 °C and 5% CO_2). The cell culture medium was replaced after 24 h.

3.5.5.3 Cytotoxicity Measurements

Cytotoxicity evaluations were carried out on the MCF-7 breast cancer cell line and DU-145 prostate cancer cell line. The MTT (3-(4,5-dimethylthiazol-2-yl)-2,5-diphenyltetrazolium

bromide) colorimetric assay was used to determine the IC_{50} values of all compounds. Cells were added to 96-well plates at a cell density of 2000 cells per well for the DU-145 cell line (200 µL per well) and 1000 cells per well for the MCF-7 cell line (200 µL per well). The cells were allowed to adhere to the culture flask over 24 hours. Test compound solutions were added in DMSO after 24 hours (1% v/v final concentration in well). Control cells were exposed to the same concentration of DMSO without the test compound. All cells were incubated at 37 ºC and 5% CO_2 for 72 hours. After 72 h, MTT (20 µL, 5 mg/mL solution) was added. The cells were then incubated for a further 3 hours after which the supernatant was then removed from each well. The MTT formazan crystals were dissolved using DMSO (100 µL). The absorbance was determined using a plate reader at 550 nm with a reference at 690 nm. Cell viability is expressed as a percentage of the vehicle-only treated control (DMSO). Non-linear regression analysis was used to analyse the obtained dose-response curves. The IC_{50} values were determined using GraphPad Prism software, v 8.0 (GraphPad Inc., San Diego, CA, USA).

3.5.5.4 Cytotoxicity Profiles

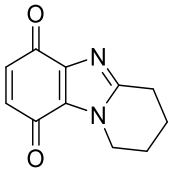

70

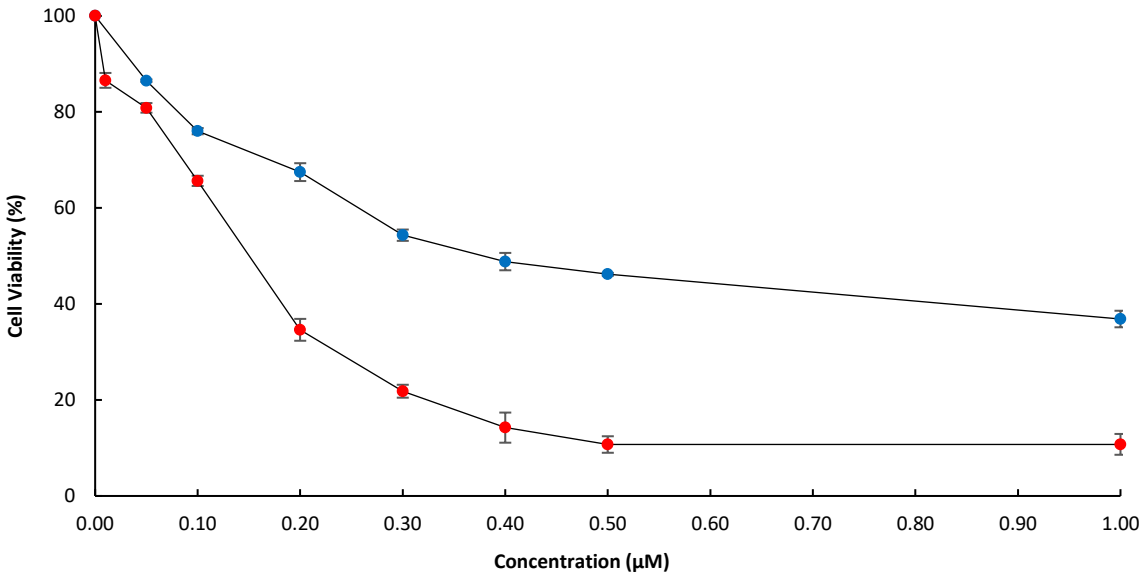

Figure 3.18: Viability of DU-145 (●) and MCF-7 (●) cell lines determined using the MTT assay following treatment with 1,2,3,4-tetrahydropyrido[1,2-*a*]benzimidazole-6,9-dione (**70**) under aerobic conditions for 72 h at 37 ºC. Each data point is the mean of at least two independent experiments. The lines shown are trend lines.

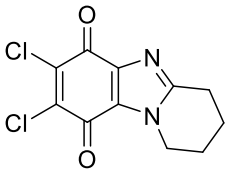

71

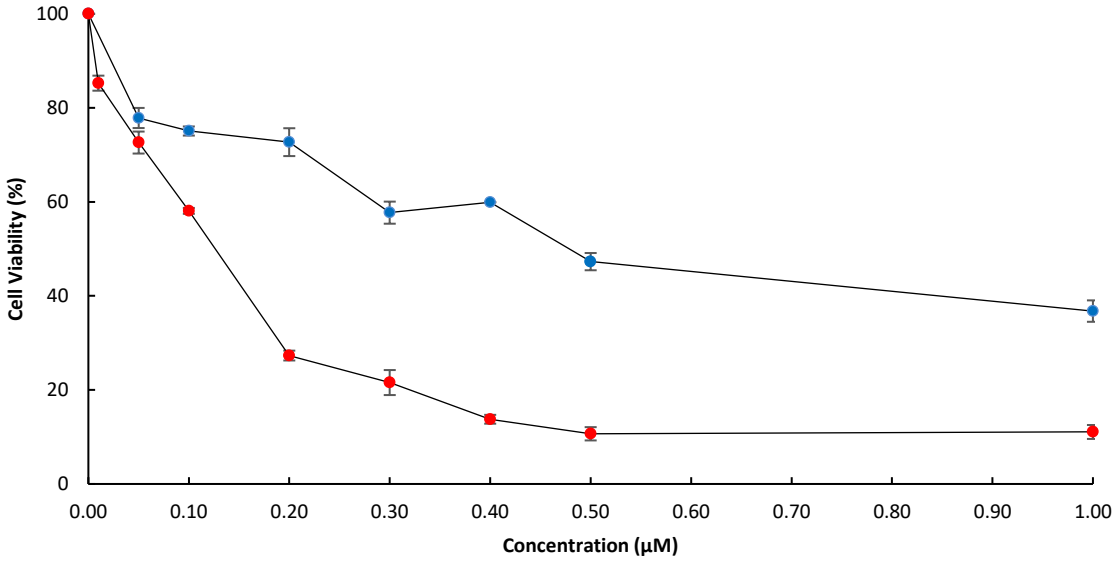

Figure 3.19: Viability of DU-145 (●) and MCF-7 (●) cell lines determined using the MTT assay following treatment with 7,8-dichloro-1,2,3,4-tetrahydropyrido[1,2-*a*]benzimidazole-6,9-dione **(71)** under aerobic conditions for 72 h at 37 ºC. Each data point is the mean of at least two independent experiments. The lines shown are trend lines.

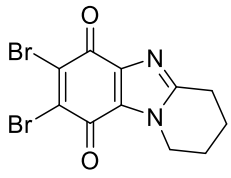

72

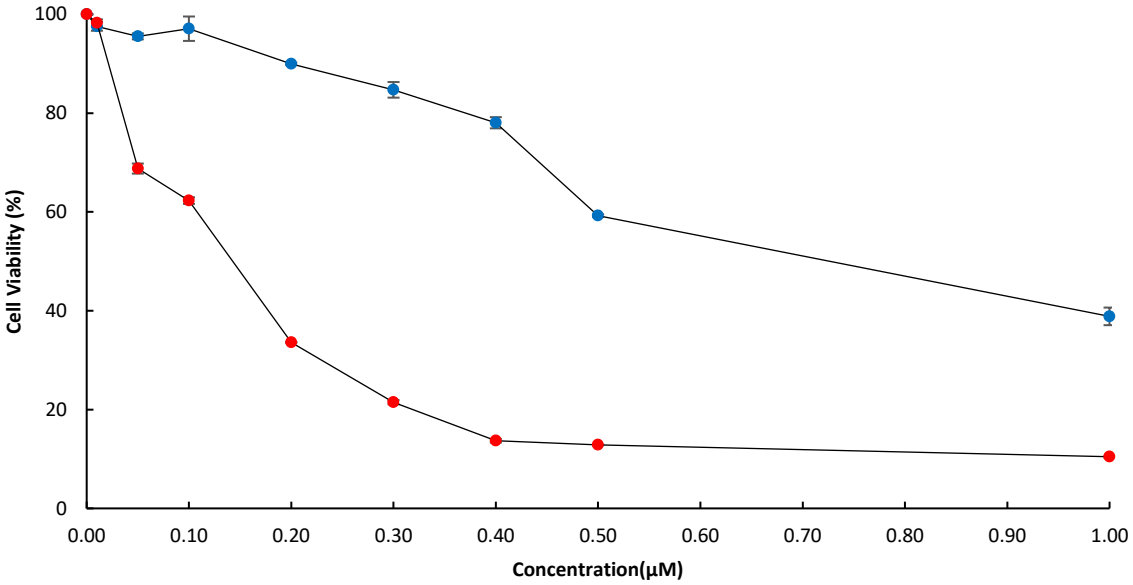

Figure 3.20: Viability of DU-145 (●) and MCF-7 (●) cell lines determined using the MTT assay following treatment with 7,8-dibromo-1,2,3,4-tetrahydropyrido[1,2-*a*]benzimidazole-6,9-dione (**72**) under aerobic conditions for 72 h at 37 ºC. Each data point is the mean of at least two independent experiments. The lines shown are trend lines.

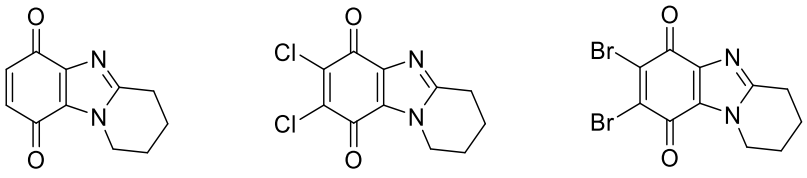

70 **71** **72**

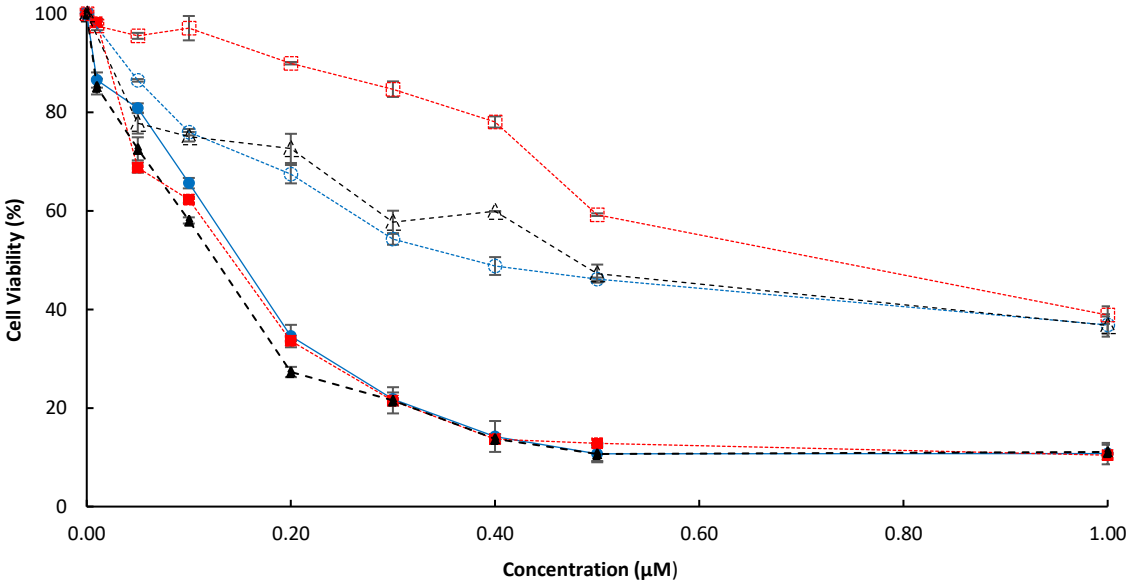

Figure 3.21: Viability of DU-145 (closed symbols) and MCF-7 (open symbols) cell lines determined using MTT assay following treatment with 1,2,3,4-tetrahydropyrido[1,2-*a*]benzimidazole-6,9-dione (**70**, ● , ○), 7,8-dichloro-1,2,3,4-tetrahydropyrido[1,2-*a*]benzimidazole-6,9-dione (**71**, ▲, Δ) and 7,8-dibromo-1,2,3,4-tetrahydropyrido[1,2-*a*]benzimidazole-6,9-dione (**72**, ■ , □) under aerobic conditions for 72 h at 37 ºC. Each data point is the mean of at least two independent experiments. The lines shown are trend lines.

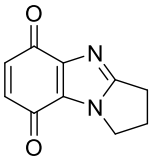

73

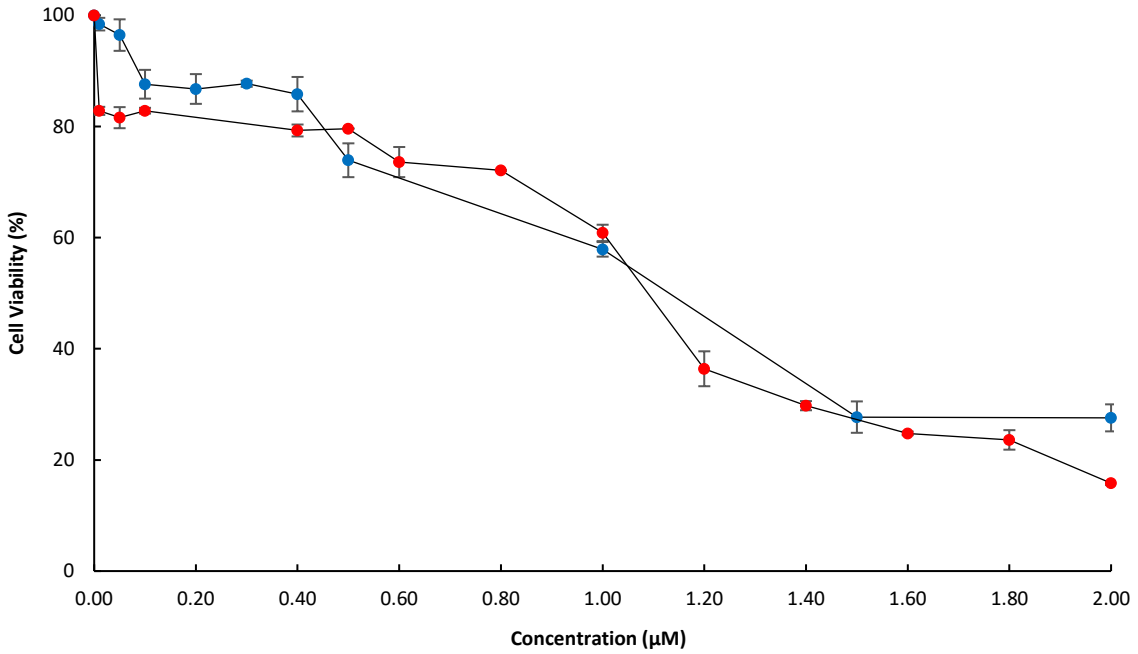

Figure 3.22: Viability of DU-145 (●) and MCF-7 (●) cell lines determined using the MTT assay following treatment with 2,3-dihydro-1*H*-pyrrolo[1,2-*a*]benzimidazole-5,8-dione (**73**) under aerobic conditions for 72 h at 37 ºC. Each data point is the mean of at least two independent experiments. The lines shown are trend lines.

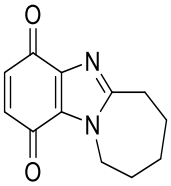

74

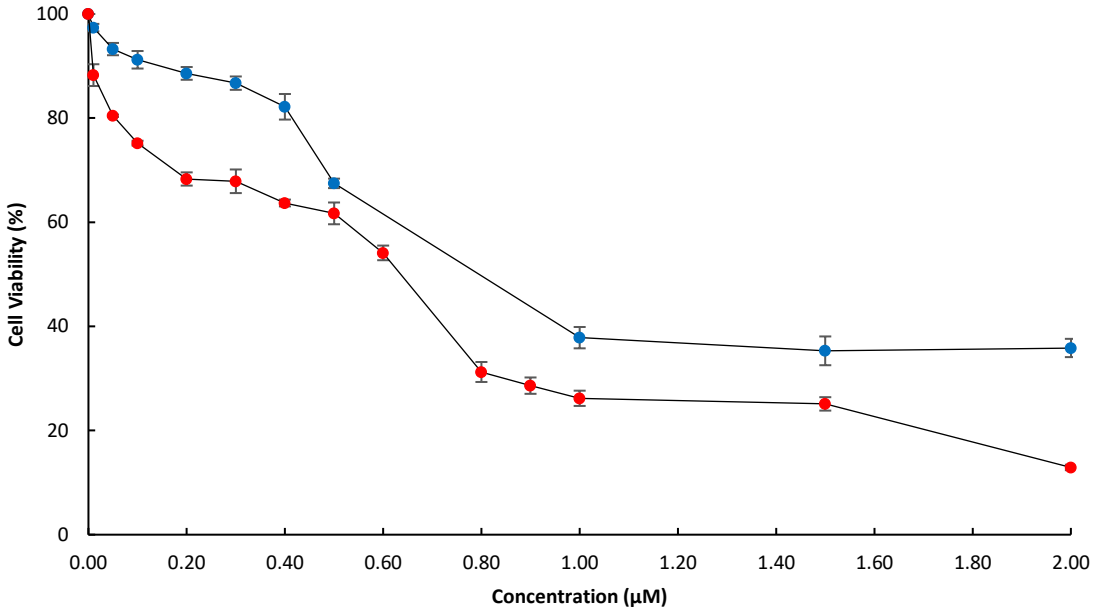

Figure 3.23: Viability of DU-145 (●) and MCF-7 (●) cell lines determined the MTT assay following treatment with 7,8,9,10-tetrahydro-4*H*-azepino[1,2-*a*]benzimidazole-1,4(6*H*)-dione (**74**) under aerobic conditions for 72 h at 37 ºC. Each data point is the mean of at least two independent experiments. The lines shown are trend lines.

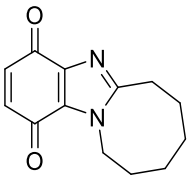

65

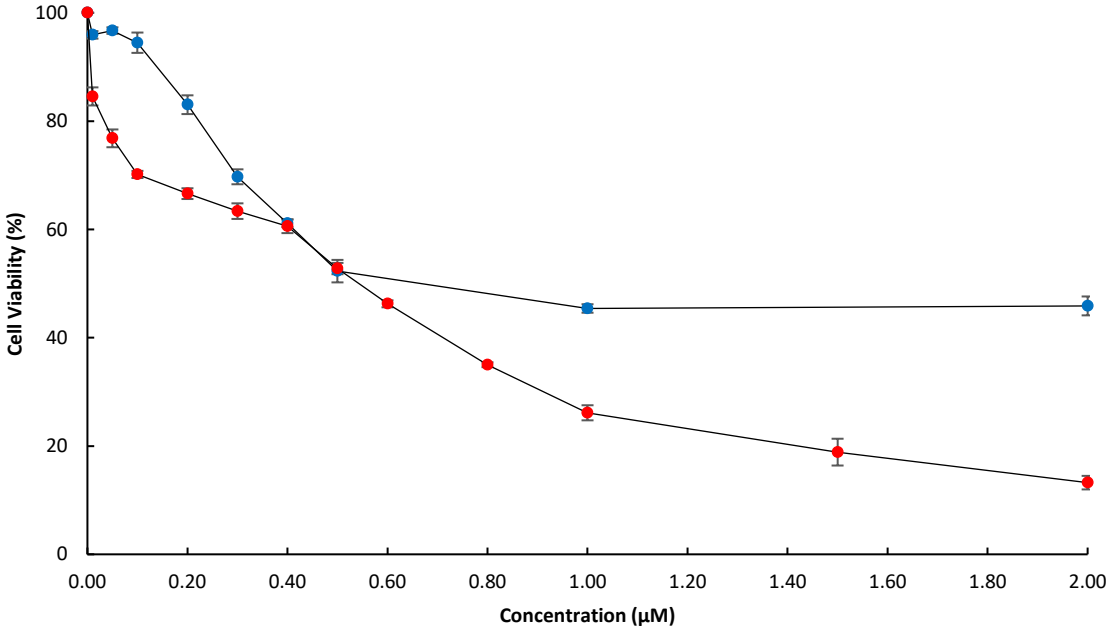

Figure 3.24: Viability of DU-145 (●) and MCF-7 (●) cell lines determined using the MTT assay following treatment with 6,7,8,9,10,11-hexahydroazocino[1,2-*a*]benzimidazole-1,4-dione (**65**) under aerobic conditions for 72 h at 37 ºC. Each data point is the mean of at least two independent experiments. The lines shown are trend lines.

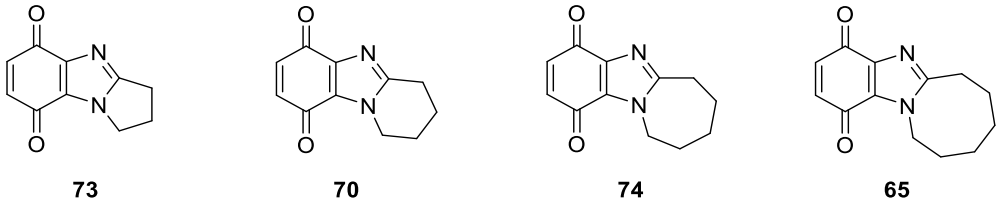

73 **70** **74** **65**

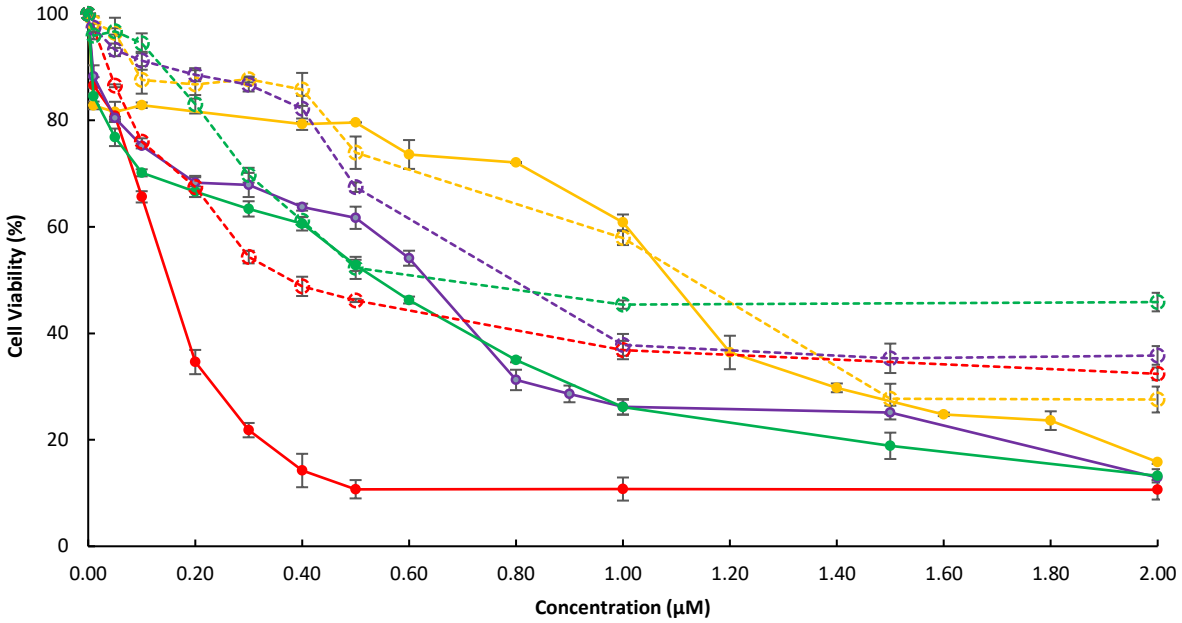

Figure 3.25: Viability of DU-145 (closed symbols) and MCF-7 (open symbols, dashed lines) cell line determined using MTT assay following treatment with 2,3-dihydro-1H-pyrrolo[1,2-a]benzimidazole-5,8-dione (**73**, ● , ○), 1,2,3,4-tetrahydropyrido[1,2-a]benzimidazole-6,9-dione (**70**, ● , ○), 7,8,9,10-tetrahydro-4H-azepino[1,2-a]benzimidazole-1,4(6H)-dione (**74**, ● , ○), 6,7,8,9,10,11-hexahydroazocino[1,2-a]benzimidazole-1,4-dione (**65**, ● , ○) under aerobic conditions for 72 h at 37 ºC. The lines shown are trend lines.

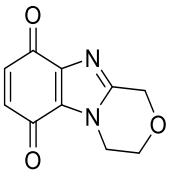

75

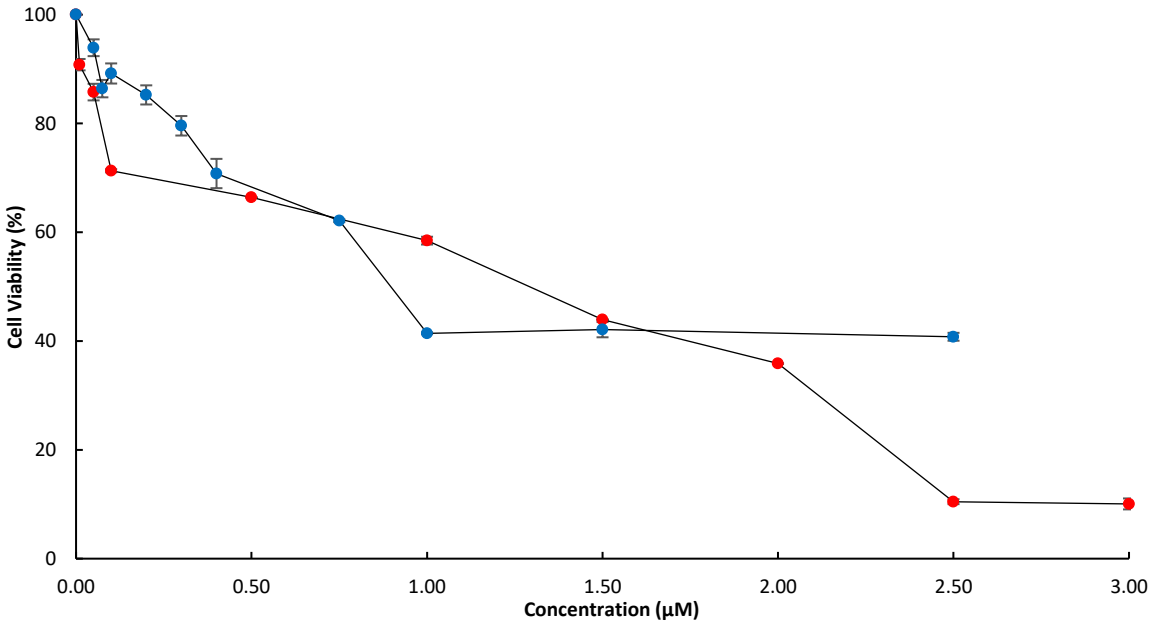

Figure 3.26: Viability of DU-145 (●) and MCF-7 (●) cell lines determined using the MTT assay following treatment with 3,4-dihydro-1*H*-[1,4]oxazino[4,3-*a*]benzimidazole-6,9-dione (**75**) under aerobic conditions for 72 h at 37 ºC. Each data point is the mean of at least three independent experiments. The lines shown are trend lines.

Chapter 4

Investigation into the Mechanism of Formation of Protein–Glucose Crosslinks

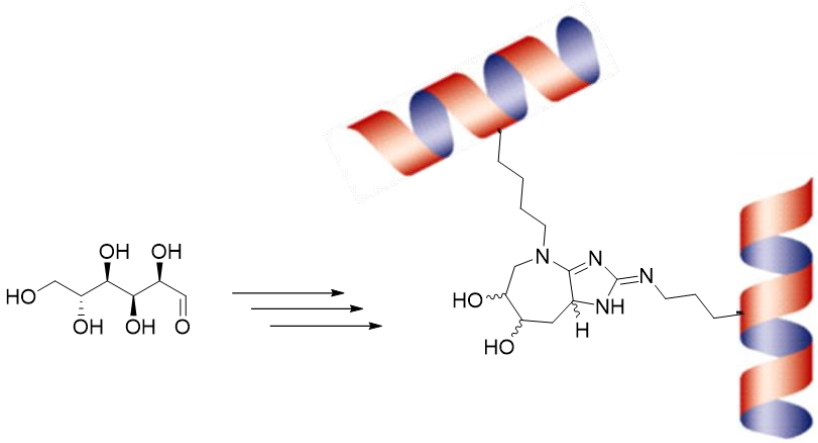

4.1 Introduction

4.1.1 Advanced Glycation End Products (AGEs)

Irreversible crosslinking can occur between proximal lysine and arginine residues through non-enzymatic reactions with glucose, thus leading to impaired protein function. Crosslinking generates several novel structures, which are part of a family of posttranslational modifications known as advanced glycation end products (AGEs). These crosslinks are found in long-lived proteins such as elastin and collagen.[199] Crosslinks naturally build up over time and are believed to be the basis for the stiffening of connective tissues and the appearance of cataractic deposits with old age. Abnormally high levels of AGEs are associated with hyperglycaemia in diabetic patients and levels of AGEs are correlated with the severity of the disease;[200,201] however, it is not known whether AGEs are the cause or a consequence of diabetes-related complications.[199] Pentosidine (Figure 4.1) is a fluorescent AGE (lysine–arginine crosslink), which is used as a biomarker for diabetes mellitus.[202] AGEs are involved in the crosslinking of collagen and this contributes to the general ageing process. Glucosepane, a lysine–arginine crosslink (Figure 4.1), is the most prevalent AGE in the extracellular matrix (ECM). This AGE is associated with many of the long-term complications of diabetes and a correlation between increased levels of glucosepane and osteoarthritis (an age-related degenerative disease) has been recently reported, although the exact mechanism for these severe types of tissue dysfunctions largely remains unknown.[203–205] Collagen is the main protein in the connective tissue of the extracellular matrix (ECM) and accounts for almost 30% of the total protein mass in humans.[206] It is a major component of bone and ligaments and is responsible for the elasticity and strength of skin.[207] More than twenty-eight different types of collagen, which are composed of different polypeptide chains, have been identified in vertebrates.[208] Type I collagen is found throughout the body except in cartilaginous tissues. Type II collagen is found in cartilage and type III is found in the walls of arteries. Collagen consists of three polypeptide chains (α-chains) that form a triple helical structure. The smallest amino acid, glycine, is present at every third residue along the chains, thus allowing three chains to form the triple helical structure.[209] Each polypeptide chain has the repeating sequence of Gly-X-Y, where X and Y can be any amino acid but are usually the amino acids proline (28%) and hydroxyproline (38%). The most common sequence is Gly-Hyp-Pro (10.5%).[208] A single triple helix is known as tropocollagen (diameter: 1.5 nm) and this is crosslinked to give fibrils, which assemble together to form fibres (diameter: 1–20 μm) that are observed in bone and tissue.[210]

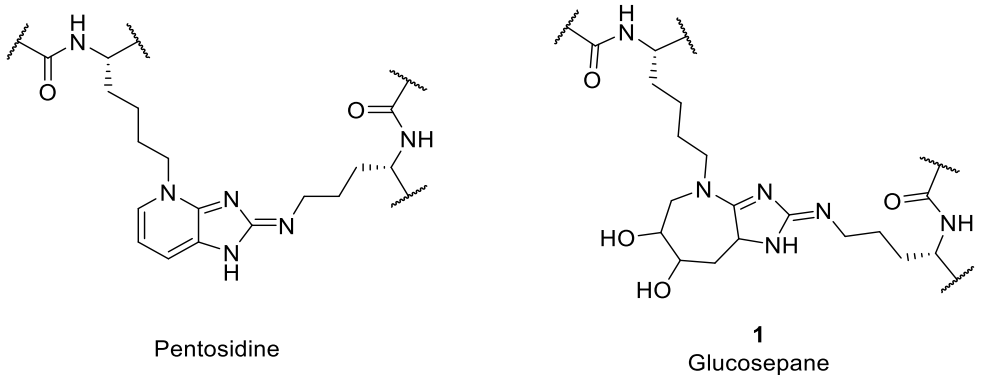

Figure 4.1: Structures of pentosidine and glucosepane.

AGEs such as glucosepane, are formed in later stages of the Maillard reaction, which is referred to as nonenzymatic glycation when it occurs *in vivo*.[211] First described by Louis Camille Maillard in 1912, the Maillard reaction is attributed to the browning and flavour in our cooked food. It involves the condensation of a carbonyl group of a reducing sugar, such as glucose, with an amino group of protein, such as the ε-amino group of a lysine residue, to form an imine (Schiff base), which isomerises to an Amadori product (aminoketose) (Scheme 4.1).

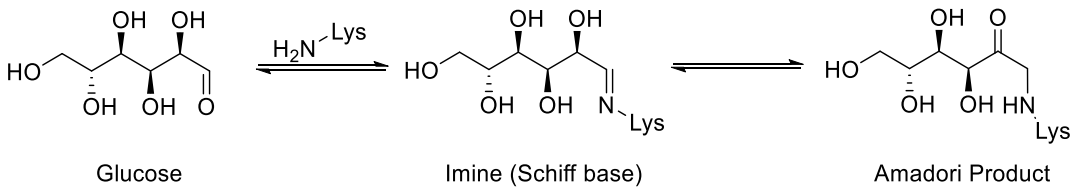

Scheme 4.1: The Maillard reaction.[211]

Later stages of this reaction involve the Amadori product undergoing a series of tautomerizations, rearrangements, condensations, and sometimes oxidation reactions, leading to the formation of AGEs, such as glucosepane and pentosidine. However, the exact details of how Amadori product is converted into these AGEs remains unclear.[212,213]

4.1.2 Glucosepane: Chemistry and Mechanism of Formation

Glucosepane is a lysine–arginine crosslink and is the most abundant protein crosslink *in vivo*.[207] It was discovered by Lederer and Bühler in 1999[214] and isolated as a mixture of two diastereoisomers from a reaction of D-glucose, α-*N*-*t*-Boc-L-lysine and α-*N*-*t*-Boc-L-arginine at 70 °C in aqueous phosphate buffer (pH 7.4) for 17 h. The seven-membered ring of glucosepane

constitutes a glucose backbone that crosslinks the two amino acid side chains of lysine and arginine. Lederer also showed that glucosepane is formed in a substantial amount when D-glucose is incubated with bovine serum albumin (BSA) (pH 7.4, 37 °C). Lederer proposed that D-glucose **2** and the ε-amino group of lysine **3** undergo a reversible condensation reaction to form unstable imine **4**. Imine/enamine tautomerization generates enaminol **5**, which can undergo further tautomerization to Amadori product **6**. Elimination of water from enaminol tautomer **5** gives ketoimine **7**. Ketoimine **7** can then condense with the guanidine side chain of arginine **8**, followed by a series of tautomerizations to imidazole **9**. Further tautomerization gives **10**, which was later named N^6-{2-{[(4*S*)-4-ammonio-5-oxido-5-oxopentyl]amino}-5-[(2*S*,3*R*)-2,3,4-trihydroxybutyl]-3,5-dihydro-4*H*-imidazol-4-ylidene}-l-lysinate, DOGDIC. A ring-closing S_N2 displacement reaction with elimination of water forms glucosepane **1**, the structure being confirmed by LC-MS and NMR analysis (Scheme 4.2).

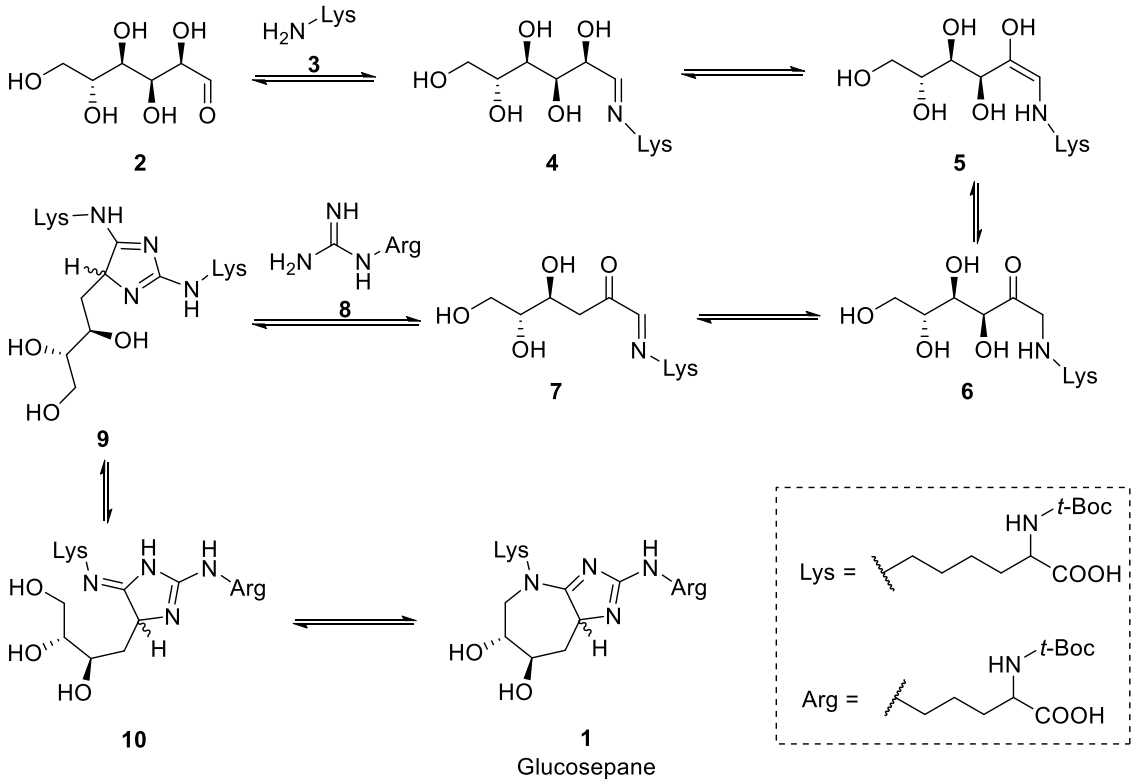

Scheme 4.2: Initially proposed mechanism for glucosepane formation.[214]

In 2001, Lederer and co-workers[215] carried out mechanistic studies into the formation of glucosepane **1**. A mixture of unlabelled D-glucose and D-glucose-$^{13}C_6$ (**2**) was reacted with α-*N*-*t*-Boc-L-lysine (**3**) and α-*N*-*t*-Boc-L-arginine (**8**) at 70 °C in aqueous phosphate buffer (pH 7.4) for 17 h. The isolation of only unlabelled and fully ^{13}C-labelled glucosepane, showed

that all six glucose carbon atoms were retained in the seven-membered ring of glucosepane **1** (Scheme 4.3) and that glucosepane **1** is not formed through the reaction of C_2, C_3 or C_4 fragments of glucose.

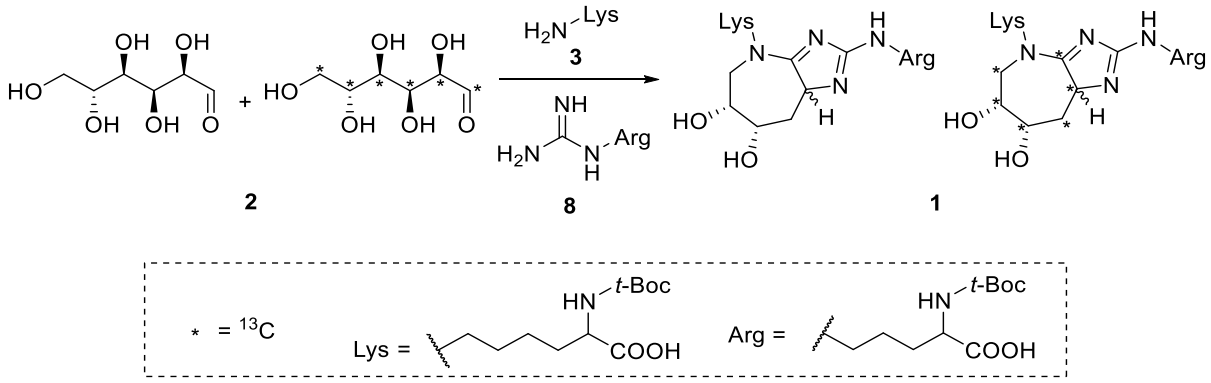

Scheme 4.3: ^{13}C labelling study showing the retention of all glucose carbons.[215]

In 2002, Lederer and co-workers[201] isolated four stereoisomers of glucosepane (rather than the single pair as previously reported)[214] after reaction of D-glucose (**2**), α-*N*-*t*-Boc-L-lysine (**3**) and α-*N*-*t*-Boc-L-arginine (**8**) at 70 °C in aqueous phosphate buffer (pH 7.4) for 17 h. Therefore, the originally proposed mechanism,[214] where the configurations at the glucosepane C6 and C7 positions, which would derive from the C4 and C5 position of glucose, are retained (glucose), thus giving only two glucosepane isomers, is incorrect. The stereochemical information in one or both of these stereocentres must be lost during the formation of glucosepane. This would allow the formation of a possible four or eight diastereoisomers, respectively.

[1-^{13}C]-D-glucose (**2**) was reacted with α-*N*-*t*-Boc-L-lysine (**3**) and α-*N*-*t*-Boc-L-arginine (**8**) to clarify whether the C3a or C5 positions of glucosepane are derived from the C1 of D-glucose. Based on the originally proposed mechanism (Scheme 4.2),[214] it was expected that C3a would be the labelled position; however, it was the C5 position of glucosepane **1** that was labelled (Scheme 4.4).[201]

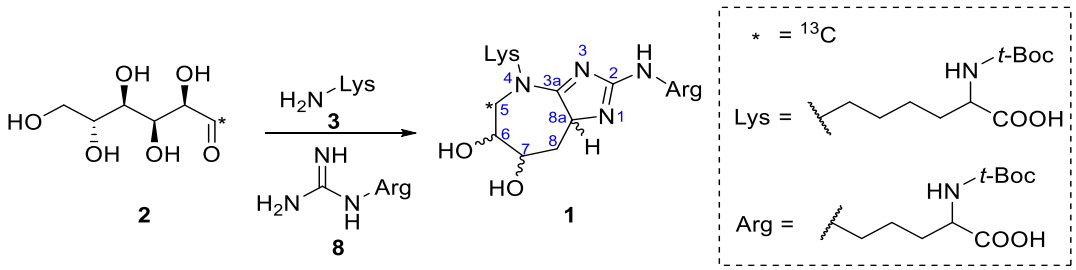

Scheme 4.4: Labelling of glucosepane's C5 position after reaction with [1-^{13}C]D-glucose.[201]

When [1-^{13}C]-D-glucose (**2**) was reacted with α-*N*-*t*-Boc-L-lysine (**3**) and aminoguanidine (**11**) in place of α-*N*-*t*-Boc-L-arginine (**8**), the expected glucosepane derivative **1** was not detected. Instead, N^6-[4-(3-amino-1,2,4-triazin-5-yl)-2,3-dihydroxybutyl]lysine (**12**) was detected with the ^{13}C label directly attached to the ε-amino group of lysine residue **3** (Scheme 4.5).[201]

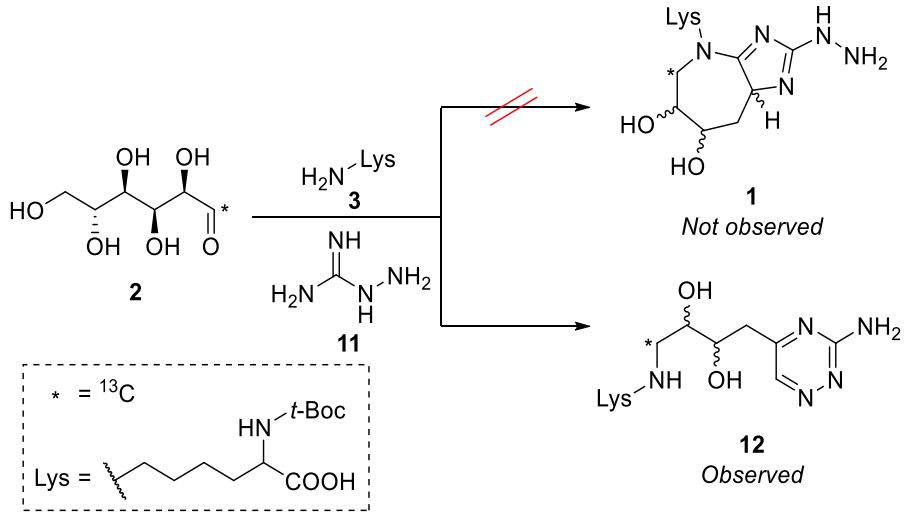

Scheme 4.5: Formation of N^6-[4-(3-amino-1,2,4-triazin-5-yl)-2,3-dihydroxybutyl]lysine rather than the expected glucosepane analogue.[201]

Because aminoguanidine (**11**) is a known trapping reagent for α-dicarbonyl compounds and N^6-[4-(3-amino-1,2,4-triazin-5-yl)-2,3-dihydroxybutyl]lysine (**12**) was detected, α-dicarbonyl, N^6-(2,3-dihydroxy-5,6-dioxohexyl)lysine (**13**) was identified as a possible intermediate for glucosepane **1** formation. The migration of the carbonyl group of Amadori product **6** through the entire carbohydrate backbone by a series of tautomerizations leads to α-dicarbonyl, **13**. Cyclization of α-dicarbonyl, **13** followed by combination with arginine **8** would generate glucosepane **1** (Scheme 4.6).[201]

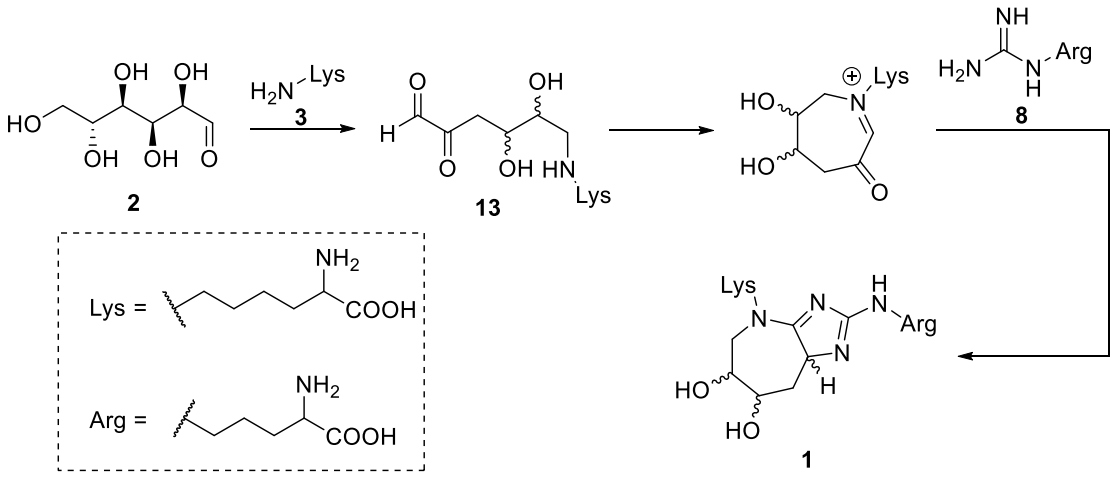

Scheme 4.6: New dideoxyosone identified as possible glucosepane intermediate.[201]

Another trapping experiment was carried out by Lederer and co-workers[201] in which [1-^{13}C]-D-glucose (**2**) was reacted with α-*N*-*t*-Boc-L-lysine (**3**) and *o*-phenylenediamine (OPD, **14**) in place of aminoguanidine (**11**) to trap α-dicarbonyl intermediate **13**. N^6-[2,3-dihydroxy-4-(2-quinoxalinyl)butyl]lysine (**15**) was obtained as a pair of stereoisomers and the ^{13}C label was directly attached to the ε-amino group of the lysine residue **3** (Scheme 4.7).

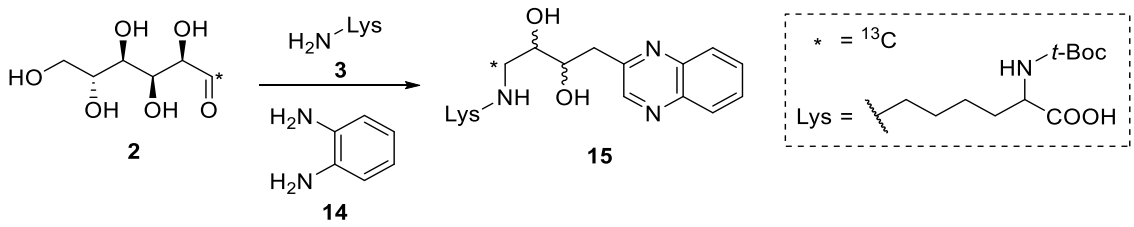

Scheme 4.7: Formation of N^6-[2,3-dihydroxy-4-(2-quinoxalinyl)butyl]lysine.[201]

Because the ^{13}C label is directly attached to the ε-amino group of the lysine residue **3** in both N^6-[4-(3-amino-1,2,4-triazin-5-yl)-2,3-dihydroxybutyl]lysine (**12**) (Scheme 4.5) and N^6-[2,3-dihydroxy-4-(2-quinoxalinyl)butyl]lysine (**15**) (Scheme 4.7), the formation of α-dicarbonyl intermediate **13** from Amadori product **6** would require the carbonyl group to shift along the carbohydrate backbone. The required series of tautomerization reactions would lead to a loss in the original stereochemical information of D-glucose (**2**) at the H–C–OH positions.[201] Cyclization of α-dicarbonyl intermediate **13** followed by dehydration would lead to seven-membered ring intermediate **16**. Intermediate **16** would then react with arginine **8** to form glucosepane **1** (Scheme 4.8).[201,216]

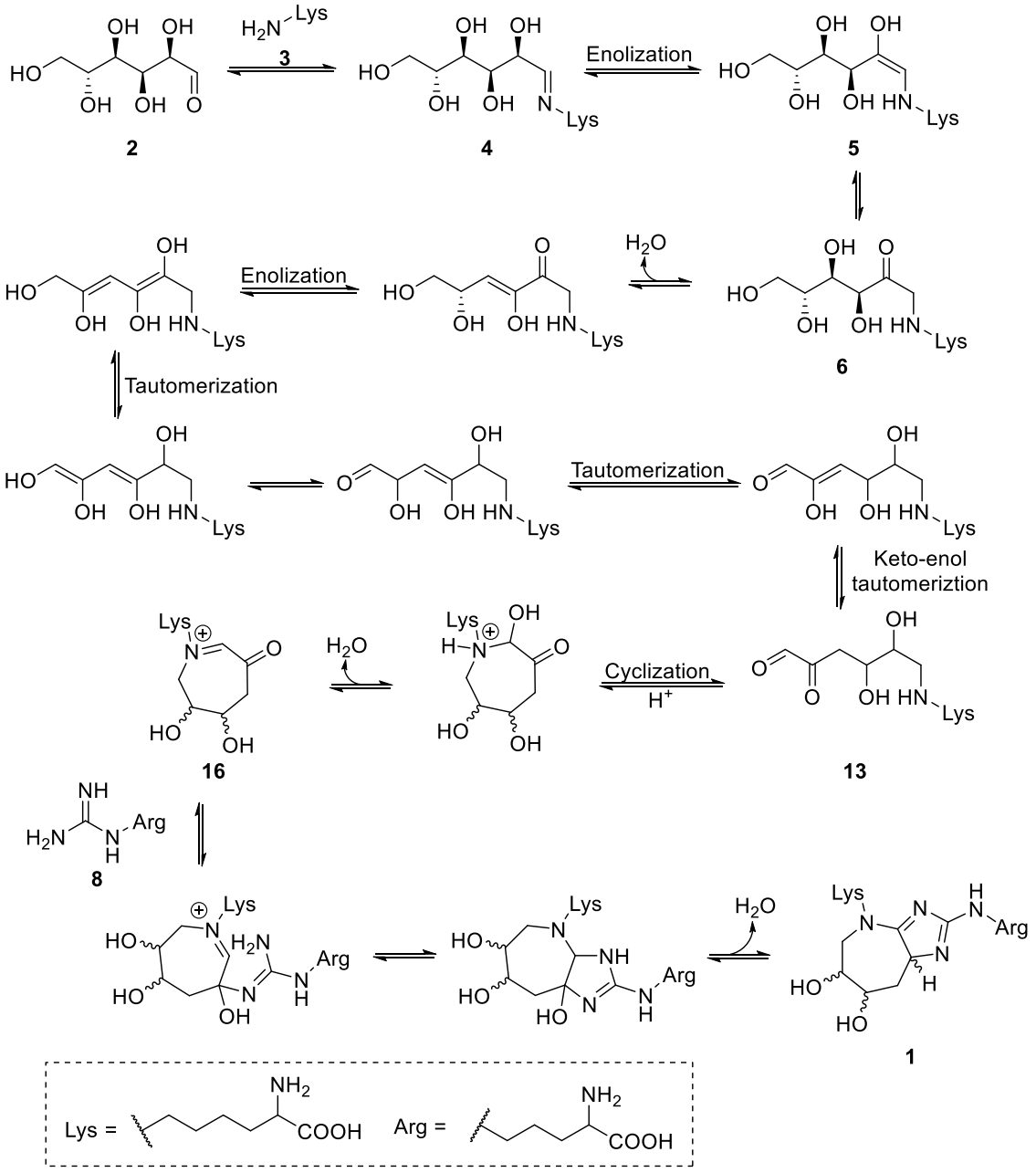

Scheme 4.8: Lederer's mechanism for glucosepane formation.[201,216]

This mechanism is supported by experiments carried out in D_2O in which N^6-[2,3-dihydroxy-4-(2-quinoxalinyl)butyl]lysine (**15**) was obtained with deuterium incorporation (D–C–OH) as proven by LC–ESI–MS and NMR analysis. Therefore, both stereogenic centres must undergo H/D exchange during keto/enol tautomerization. α-Dicarbonyl **13** is a plausible intermediate given the isolation of four diastereoisomers of glucosepane.[201]

4.2 Aims and Objectives

Previous isotopic labelling experiments have suggested that Amadori product **6** undergoes dehydration followed by migration of the carbonyl groups to the opposite end of the sugar chain, thus forming α-dicarbonyl **13**. The α-dicarbonyl moiety undergoes intramolecular condensation with the amino group followed by intermolecular condensation of the resulting seven-membered ring with the proximal arginine residue to form glucosepane **1** (Scheme 4.9).[201] Four of the possible eight diastereoisomers of glucosepane were isolated by Lederer and co-workers; however, the four diastereoisomers were not identified.[201,217]

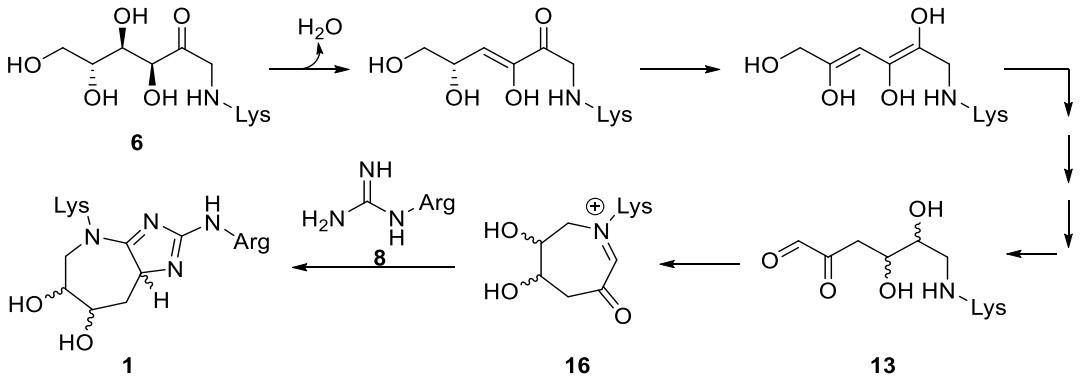

Scheme 4.9: Current understanding of the mechanism of formation of glucosepane.[201]

We will reinvestigate the mechanism of formation of glucosepane **1**, specifically the possibility that the carbonyl group of Amadori product **6** does not migrate through a series of keto–enol tautomerizations but instead through an intramolecular through-space 1,5-hydride shift. To our knowledge this possibility has not previously been considered for glucosepane formation and will be probed using isotopic labelling studies using 6-[^{2}H]$_2$-glucose (Scheme 4.10).

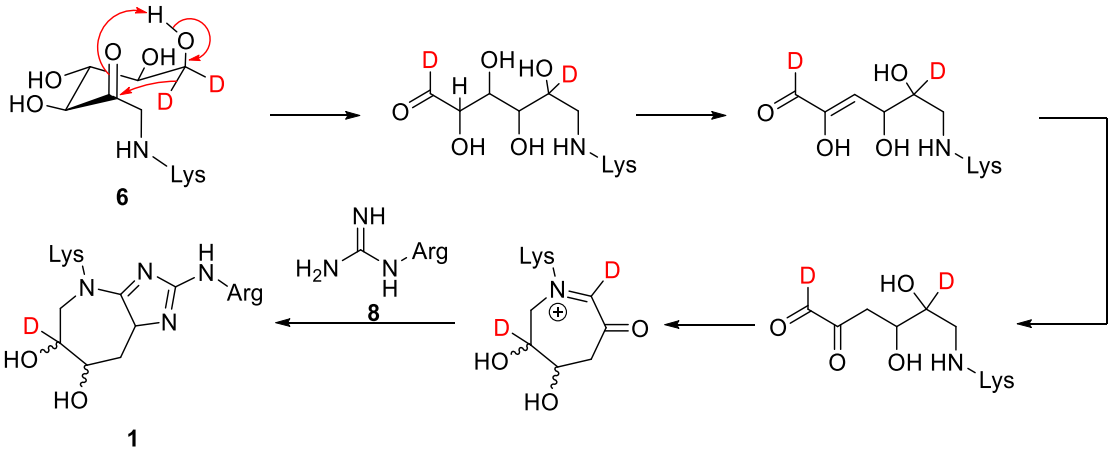

Scheme 4.10: Isotopic labelling study for investigation into glucosepane formation by 1,5-hydride shift.

1,5-Hydride shifts, which support the proposed mechanism above, have previously been reported. McQuaid *et al.*[218] reported a 1,5-hydride transfer initiated cyclization of aryl alkyl ethers **17**, which leads to dihydrobenzopyrans **18**. The hydride transfer was initiated by a Lewis acid ($Sc(OTf)_3$), which activated an electron-deficient alkene of the aryl alkyl ether (Scheme 4.11).[218]

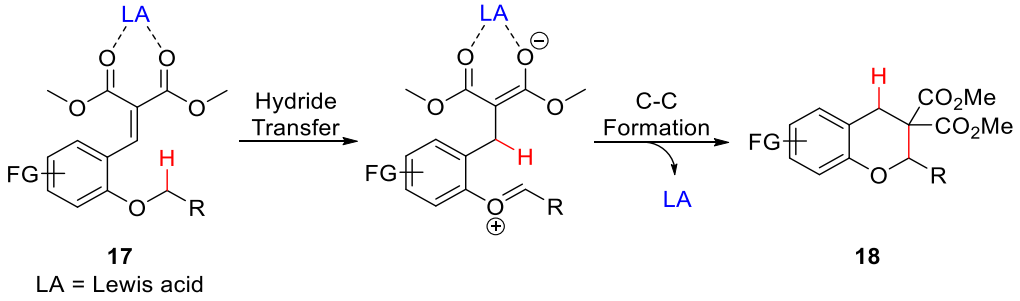

Scheme 4.11: Formation of dihydroxybenzopyran through a 1,5-hydride shift.[218]

The possibility of a 1,5-hydride shift involving protonated imine **4** will also be investigated. Protonated imine **4**, which would form directly from glucose and lysine, could undergo a 1,5-hydride shift, this time involving the hydrogen at the C5 position, thus forming ketone **19**. Tautomerization of ketone **19** to terminal aldehyde **20** followed by dehydration to α-dicarbonyl **13**, cyclization to seven-membered ring **21** and condensation with arginine **8** would lead to glucosepane **1** (Scheme 4.12). This mechanism will be probed using isotopic labelling studies with 5-[^{2}H]-glucose. Epimerization of the Amadori product could occur prior to the 1,5-hydride shift leading to a loss of stereochemistry at the C6 and C7 positions.

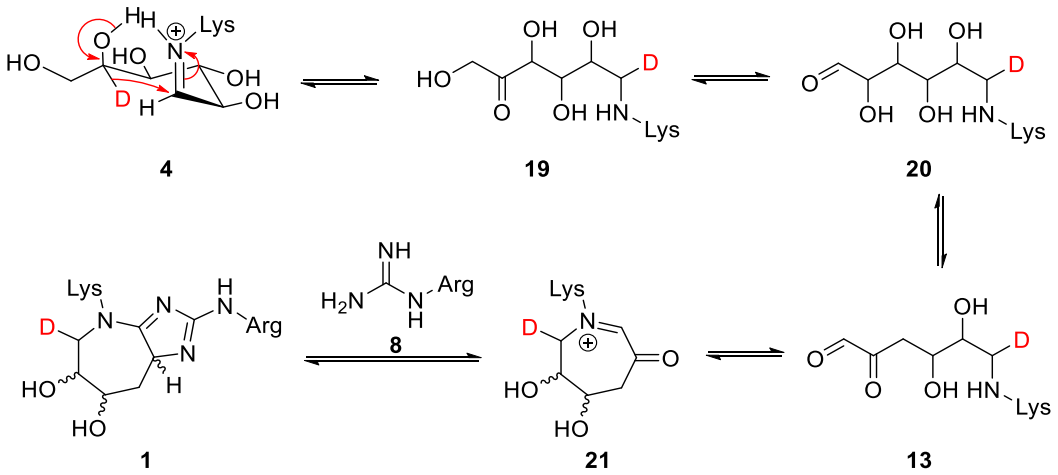

Scheme 4.12: Alternative glucosepane formation mechanism involving an intramolecular through space 1,5-hydride shift.

Interestingly, a similar 1,5-hydrogen shift involving glucose has been recently observed by Gounder and Davis[219] in which D-glucose **2** undergoes isomerization to L-sorbose **22** through an intramolecular 1,5-hydride shift in the presence of a titanium (IV) Lewis acid (Scheme 4.13). Isotopic labelling studies showed that the ^{13}C and D labels, which were placed at the C1 and C2 positions of glucose, were retained at the C6 and C5 positions of sorbose, suggesting a 1,5-hydride shift.[219] This observation would support our hypothesis of a 1,5-hydride shift involving the protonated imine **4**.

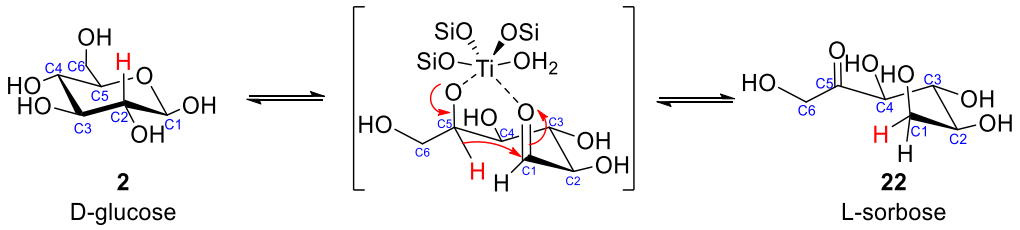

Scheme 4.13: Metal-catalysed isomerization of glucose to sorbose through a 1,5-hydride shift.[219]

4.3 Results and Discussion

4.3.1 Preparation of a Complex Mixture of AGEs Containing Glucosepane

We began our studies by preparing a protected form of glucosepane **1** in the way described by Lederer *et al.*[214] so that we could develop our analytical methods. A solution of D-glucose (**2**), α-*N*-*t*-Boc-L-lysine (**3**) and α-*N*-*t*-Boc-L-arginine (**8**) in aqueous phosphate buffer (pH 7.4) was heated at 70 °C for 17 h (Scheme 4.14). The reaction mixture changed from a colourless solution to a dark brown solution during the course of the reaction. The complex crude reaction mixture was analysed directly by LC-MS (Figure 4.2).

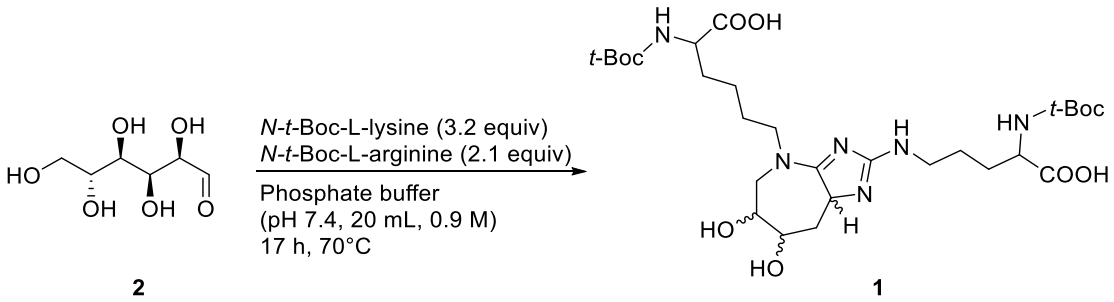

Scheme 4.14: Conversion of D-glucose into glucosepane.

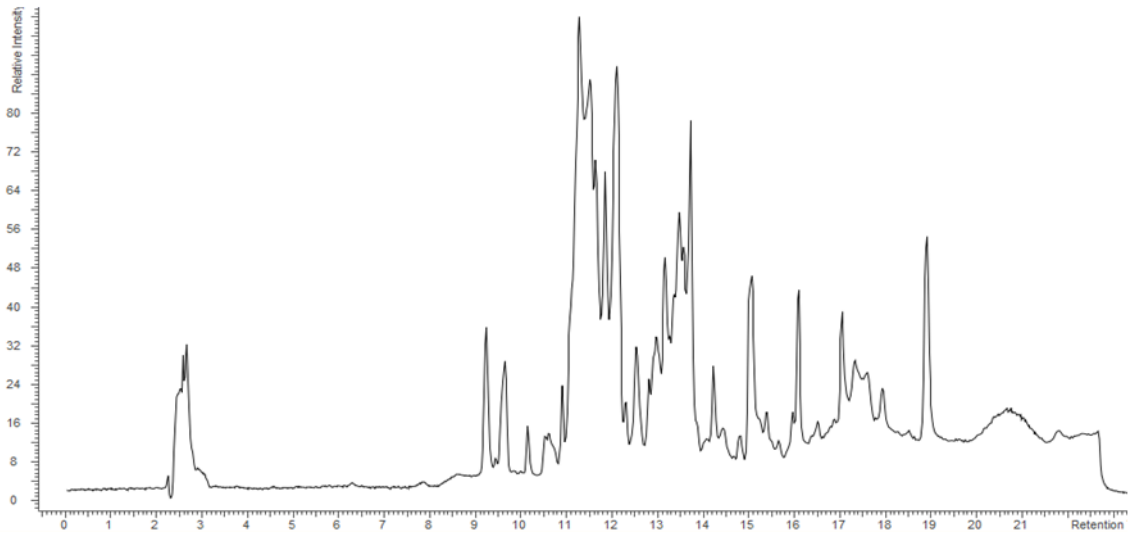

Figure 4.2: LC-ESI chromatograms for the reaction of D-glucose, α-*N*-*t*-Boc-L-lysine and α-*N*-*t*-Boc-L-arginine (see Section 4.6.2 for LC-MS parameters).

A species with a mass consistent with glucosepane **1** was observed at a retention time of 13.516 min (see Section 4.6.2 for LC-MS parameters); HRMS (ESI) *m/z* $(M+H)^+$, $C_{28}H_{49}O_6N_{10}$ calcd. 629.3505, observed 629.3487 (Figure 4.3).

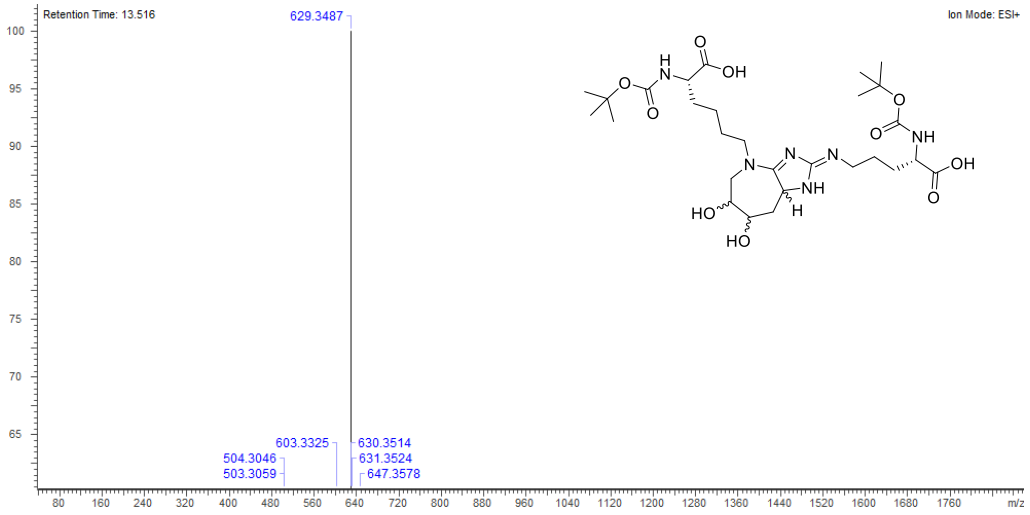

Figure 4.3: HRMS (ESI) of glucosepane at retention time 13.516 min. The single mass analysis indicates the molecular formula of the proposed structure within 5 ppm.

A species with a mass consistent with Amadori product **6** was observed at a retention time of 11.159 min (see Section 4.6.2 for LC-MS parameters); HRMS (ESI) *m/z* $(M+H)^+$, $C_{17}H_{33}O_9N_2$ calcd. 409.2176, observed 409.2176 (Figure 4.4).

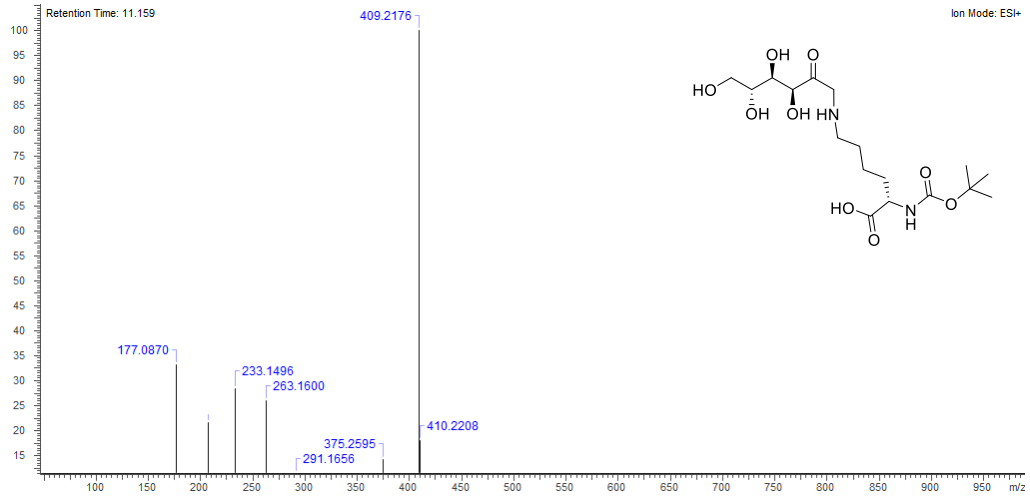

Figure 4.4: HRMS (ESI) of the Amadori product at retention time 11.159 min. The single mass analysis indicates the molecular formula of the proposed structure within 5 ppm.

A species with a mass consistent with DOGDIC **10** was observed at a retention time of 12.552 min (see Section 4.6.2 for LC-MS parameters); HRMS (ESI) *m/z* $(M+H)^+$, $C_{28}H_{51}O_{11}N_6$ calcd. 647.3610, observed 647.3591 (Figure 4.5)

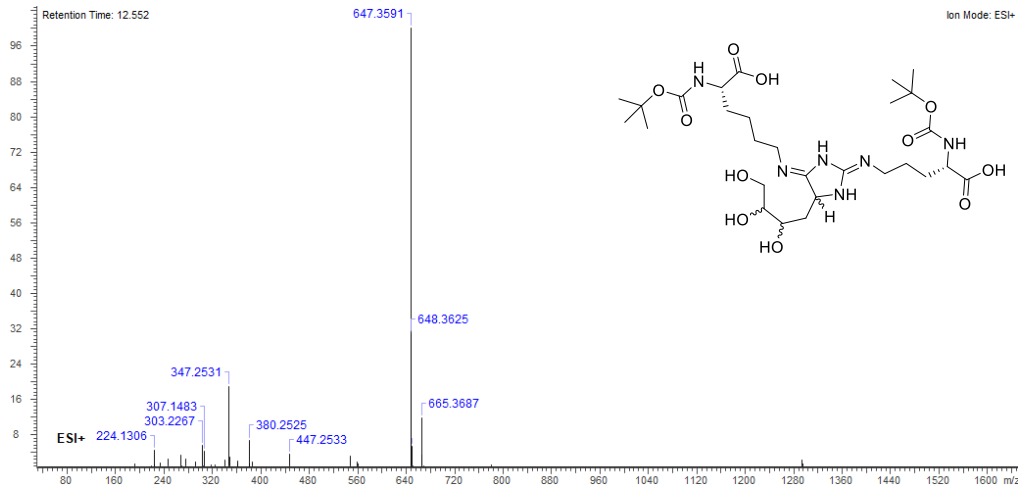

Figure 4.5: HRMS (ESI) of DOGDIC at retention time 12.552 min. The single mass analysis indicates the molecular formula of the proposed structure within 5 ppm.

Lederer and co-workers[217] have previously reported a species with a mass consistent with DOGDIC in reactions of D-glucose (**2**), α-*N*-*t*-Boc-L-lysine (**3**) and α-*N*-*t*-Boc-L-arginine (**8**) at 70 °C in aqueous phosphate buffer (pH 7.4) for 17 h. Isotopic labelling experiments, carried out by Lederer and co-workers,[217] with D-glucose-$^{13}C_6$ have shown that all of the glucose carbon atoms are retained in the DOGDIC product **10**.

4.3.2 Investigation into a 1,5-hydride Shift from the Amadori product

To investigate the possibility of a 1,5-hydride shift from the Amadori product **6**, a solution of 6-[^{2}H]$_2$-glucose (**2**), α-*N*-*t*-Boc-L-lysine (**3**) and α-*N*-*t*-Boc-L-arginine (**8**) in aqueous phosphate buffer (pH 7.4) was heated at 70 °C for 17 h (Scheme 4.15). The reaction mixture changed from a colourless solution to a dark brown solution during the course of the reaction. The complex crude reaction mixture was analysed directly by LC-MS analysis (Figure 4.6).

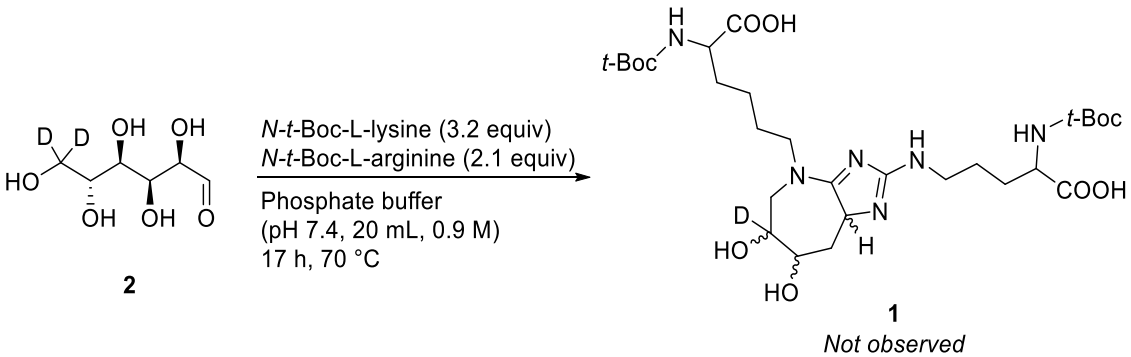

Scheme 4.15: Conversion of 6-[^{2}H]$_2$-glucose into glucosepane.

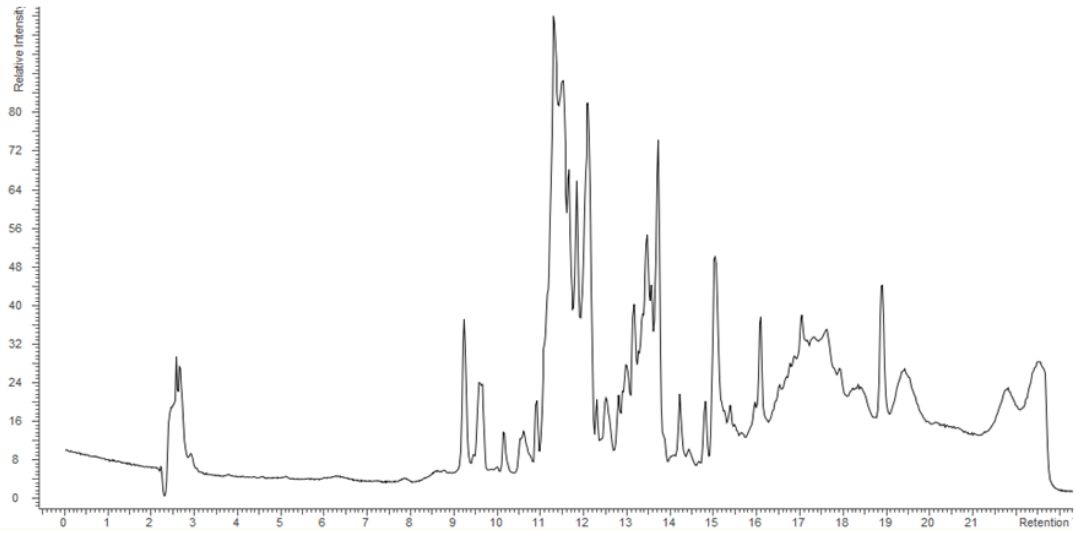

Figure 4.6: LC-ESI chromatograms for the reaction of 6-[^{2}H]$_2$-glucose, α-*N*-*t*-Boc-L-lysine and α-*N*-*t*-Boc-L-arginine (see Section 4.6.2 for LC-MS parameters).

A species with a mass consistent with glucosepane (unlabelled) **1** was observed at a retention time of 13.518 min (see Section 4.6.2 for LC-MS parameters); HRMS (ESI) *m/z* $(M+H)^+$, $C_{28}H_{49}O_6N_{10}$ calcd. 629.3505, observed 629.3479 (Figure 4.7).

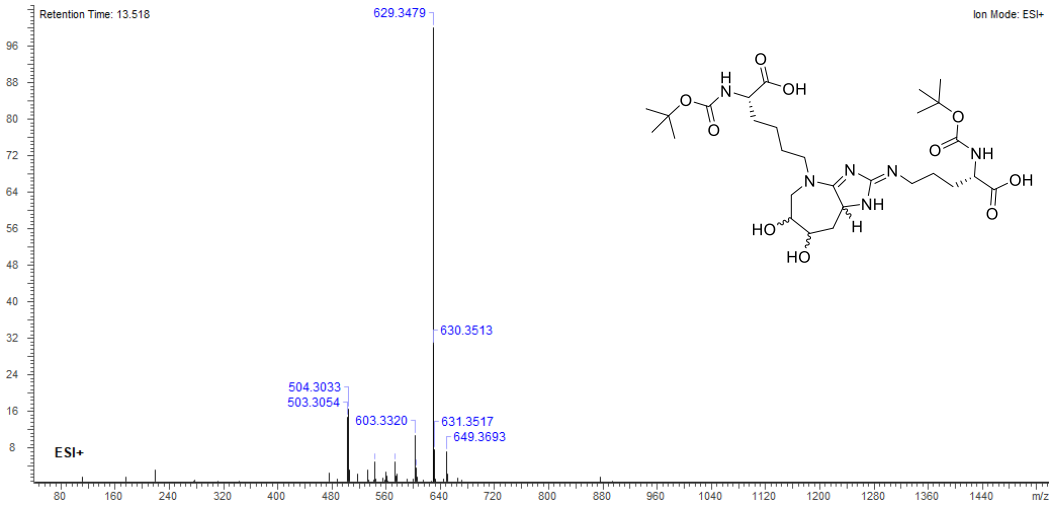

Figure 4.7: HRMS (ESI) of unlabelled glucosepane at retention time 13.518 min. The single mass analysis indicates the molecular formula of the proposed structure within 5 ppm.

The detection of a species with a mass consistent with unlabelled glucosepane **1** suggests that a 1,5-hydride shift does not occur. The result is more consistent with the original hypothesis of Lederer[201], where the isomerization occurs through a series of enol–keto tautomerizations down the carbon chain. Here the labels would wash into the solvent. The shape of HPLC profiles of the product mixtures obtained from the use of 6-[^{2}H]$_2$-glucose and unlabelled glucose **2** were similar. A species with a mass consistent with deuterium labelled Amadori

product **6** was observed at a retention time of 11.226 min (see Section 4.6.2 for LC-MS parameters); HRMS (ESI) *m/z* $(M+H)^+$, $C_{17}H_{31}D_2O_9N_2$ calcd. 411.2306, observed 411.2303 (Figure 4.8). This suggests that the deuterium label is still present after the condensation reaction with lysine, as expected.

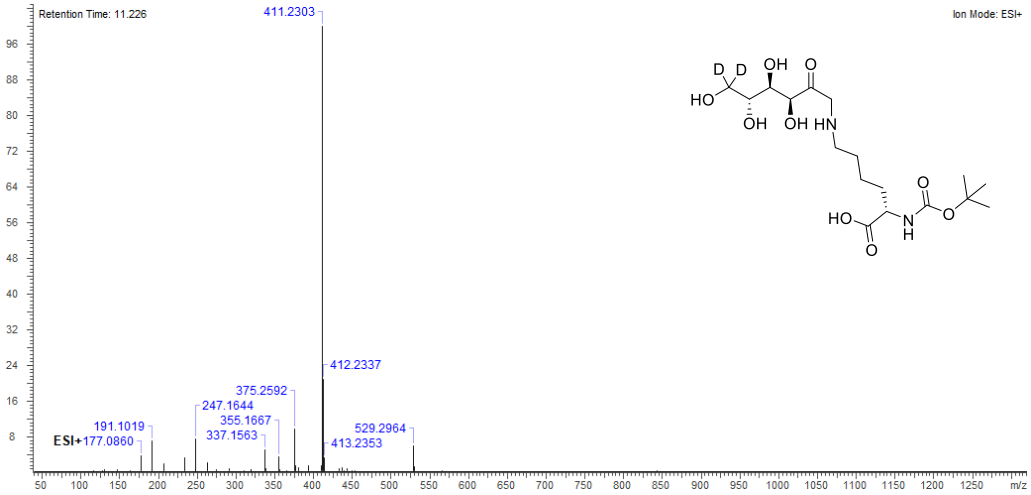

Figure 4.8: HRMS (ESI) of the deuterium labelled Amadori product at retention time 11.226 min. The single mass analysis indicates the molecular formula of the proposed structure within 5 ppm.

Surprisingly, species with masses consistent with both deuterium labelled and unlabelled DOGDIC **10** were observed at a retention time of approximately 12.569 min (see Section 4.6.2 for LC-MS parameters); Unlabelled DOGDIC: HRMS (ESI) *m/z* $(M+H)^+$, $C_{28}H_{51}O_{11}N_6$ calcd. 647.3610, observed 647.3590 (Figure 4.9).

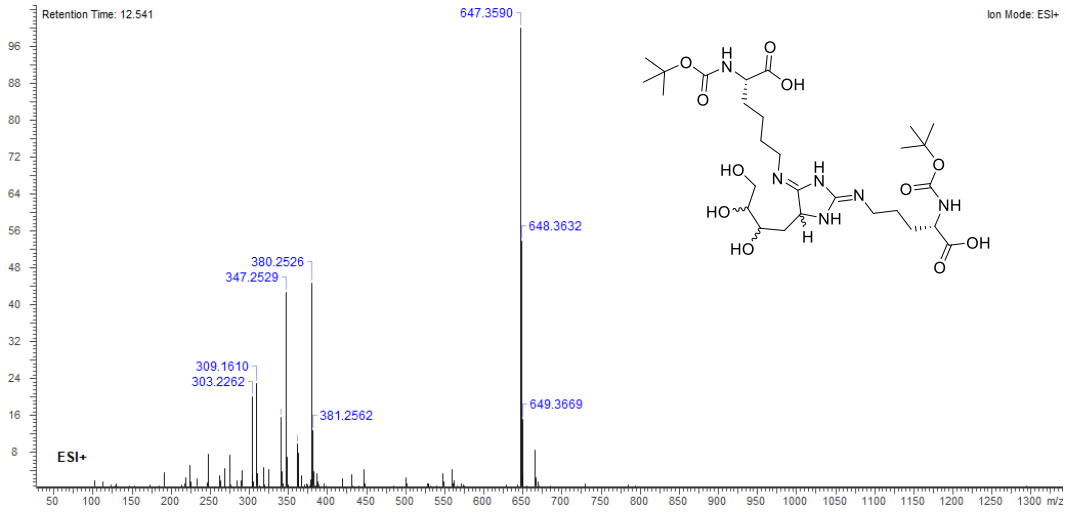

Figure 4.9: HRMS (ESI) of the unlabelled DOGDIC at retention time 12.514 min. The single mass analysis indicates the molecular formula of the proposed structure within 5 ppm.

A species with a mass consistent with DOGDIC **10** containing only one deuterium was detected; HRMS (ESI) *m/z* $(M+H)^+$, $C_{28}H_{50}DO_{11}N_6$ calcd. 648.3673, observed 648.3647 (Figure 4.10).

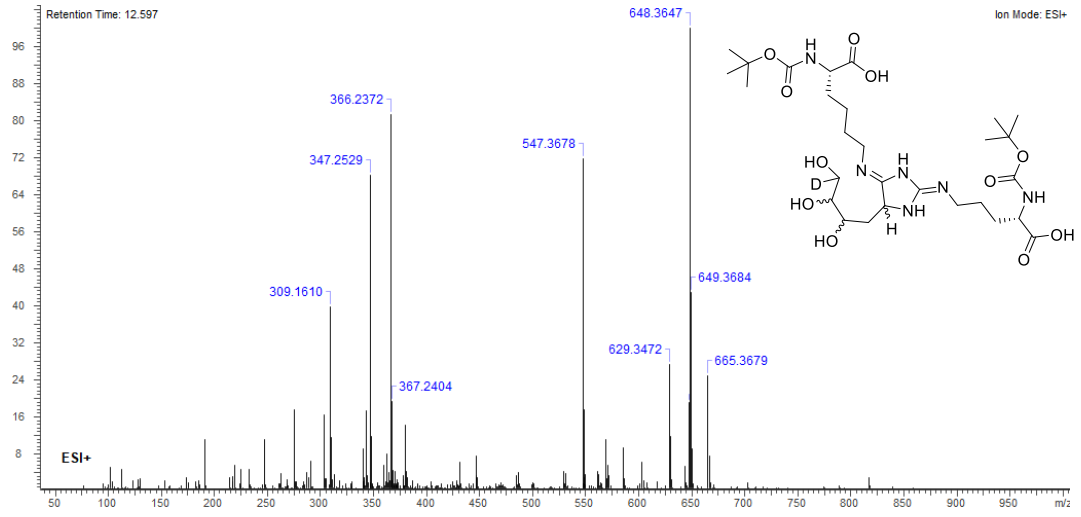

Figure 4.10: HRMS (ESI) of the deuterium-labelled DOGDIC at retention time 12.597 min. The single mass analysis indicates the molecular formula of the proposed structure within 5 ppm.

4.3.3 Investigation into a 1,5-hydride Shift from a Protonated Imine Intermediate

To investigate the possibility of a 1,5-hydride shift from protonated imine **4**, a solution of 5-[^{2}H]-glucose (**2**), α-*N*-*t*-Boc-L-lysine (**3**) and α-*N*-*t*-Boc-L-arginine (**8**) in aqueous phosphate buffer (pH 7.4) was heated at 70 °C for 17 h (Scheme 4.16). The reaction mixture changed from a colourless solution to a dark brown solution during the course of the reaction. The complex crude reaction mixture was analysed directly by LC-MS (Figure 4.11).

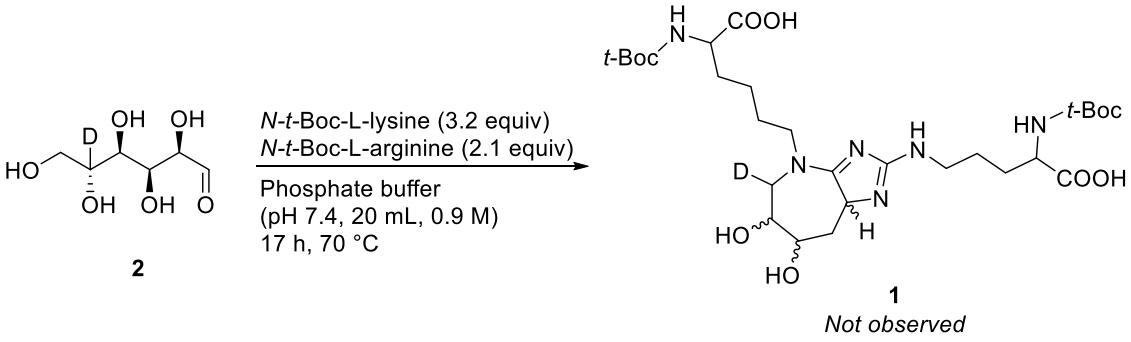

Scheme 4.16: Conversion of 5-[^{2}H]-glucose into glucosepane.

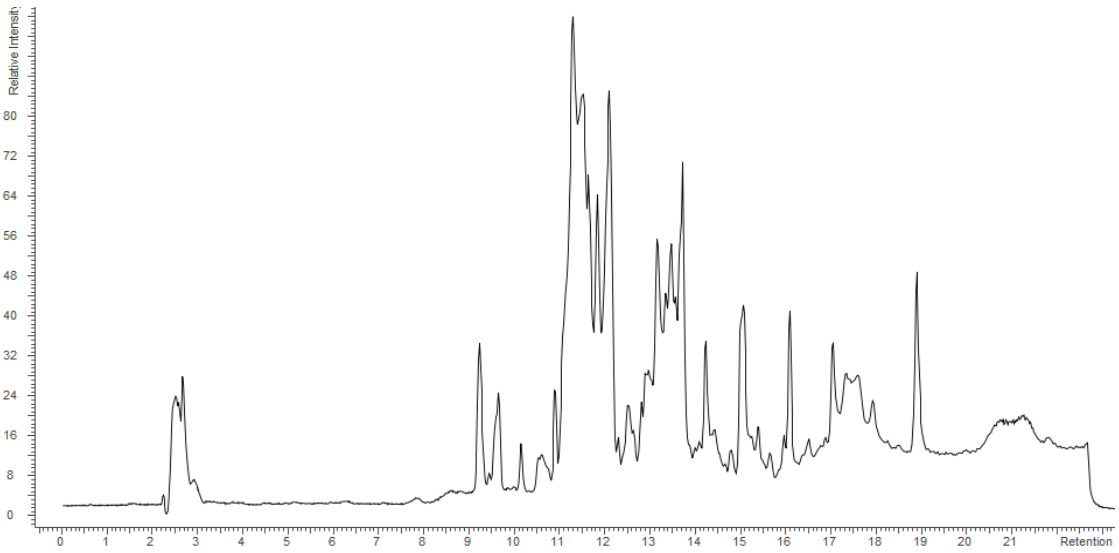

Figure 4.11: LC-ESI chromatograms for the reaction of 5-[^{2}H]-glucose, α-*N*-*t*-Boc-L-lysine and α-*N*-*t*-Boc-L-arginine.

A species with a mass consistent with glucosepane (unlabelled) **1** was observed at a retention time of 13.523 min (see Section 4.6.2 for LC-MS parameters); HRMS (ESI) *m/z* $(M+H)^+$, $C_{28}H_{49}O_6N_{10}$ calcd. 629.3505, observed 629.3489 (Figure 4.12). The detection of a species with a mass consistent with unlabelled glucosepane **1** suggests that a 1,5-hydride shift does not occur from protonated imine **4**. This result is more consistent with the original hypothesis of Lederer,[201] where the isomerization occurs through a series of enol-keto tautomerizations down the carbon chain. Here the labels would wash into the solvent. The shape of HPLC profiles of the product mixtures obtained from the use of 5-[^{2}H]-glucose were similar to the profiles obtained using unlabelled glucose and 6-[^{2}H]$_2$-glucose.

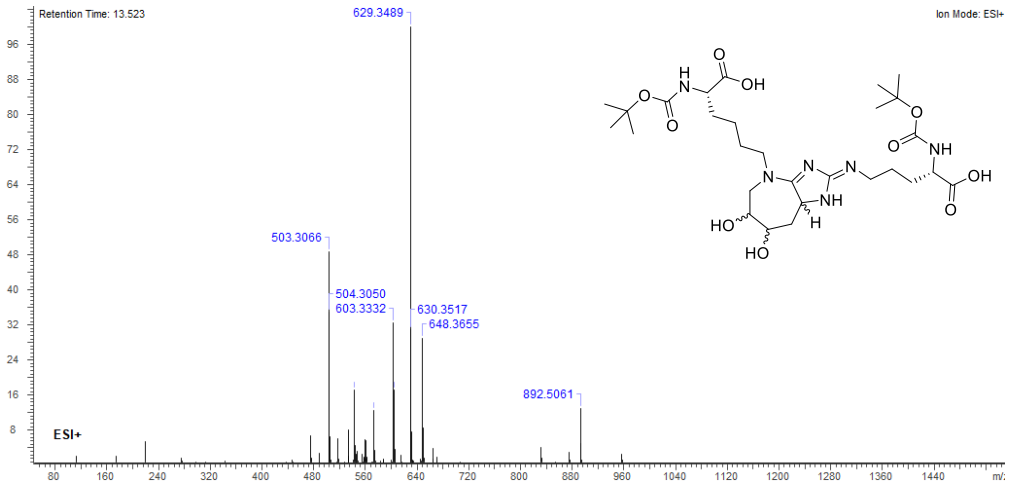

Figure 4.12: HRMS (ESI) of glucosepane at retention time 13.523 min. The single mass analysis indicates the molecular formula of the proposed structure within 5 ppm.

A species with a mass consistent with the expected deuterium-labelled Amadori product **6** was observed at a retention time of 11.196 min (see Section 4.6.2 for LC-MS parameters); HRMS (ESI) *m/z* $(M+H)^+$, $C_{17}H_{32}DO_9N_2$ calcd. 410.2243, observed 410.2245 (Figure 4.13).

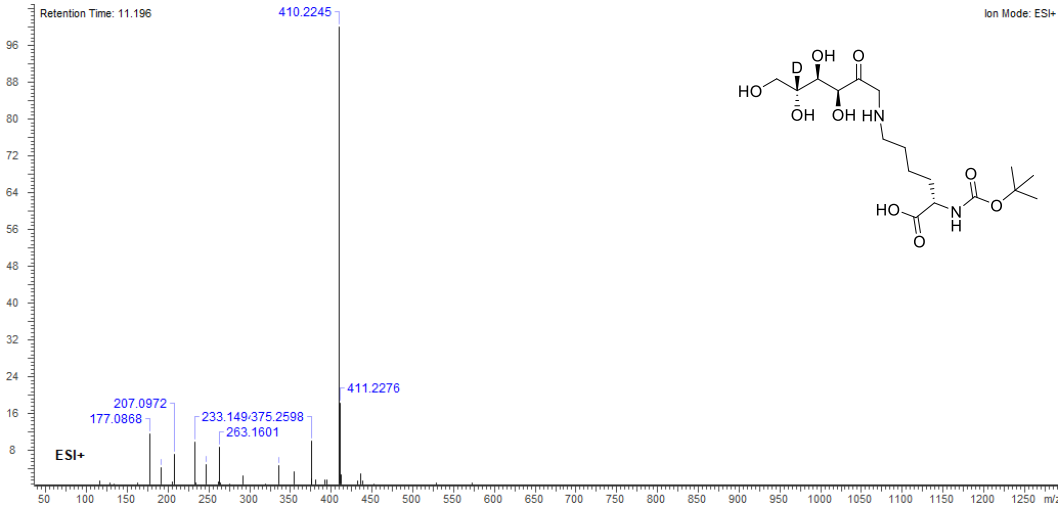

Figure 4.13: HRMS (ESI) of the deuterium-labelled Amadori product at retention time 11.196 min. The single mass analysis indicates the molecular formula of the proposed structure within 5 ppm.

A species with a mass consistent with DOGDIC (unlabelled) **10** was observed at a retention time of 12.502 min (see Section 4.6.2 for LC-MS parameters); HRMS (ESI) *m/z* $(M+H)^+$, $C_{28}H_{51}O_{11}N_6$ calcd. 647.3610, observed 647.3595 (Figure 4.14).

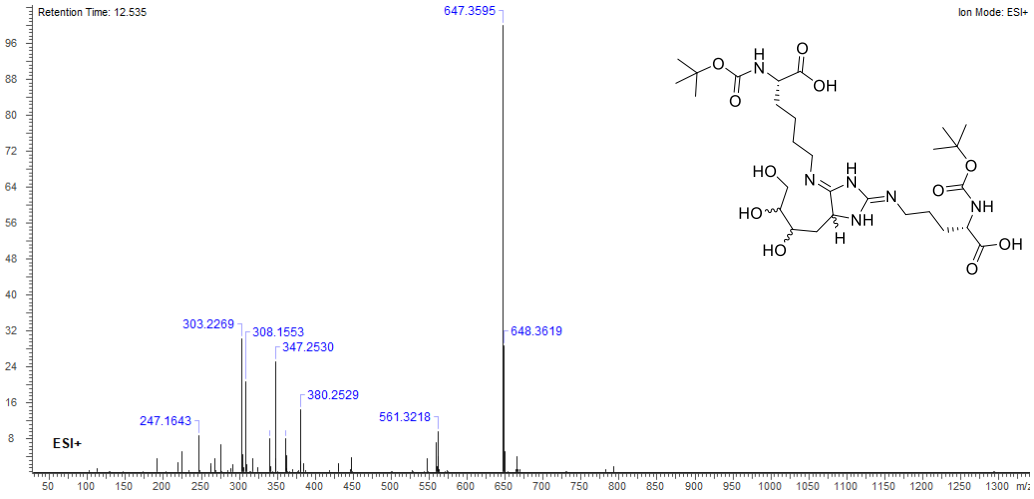

Figure 4.14: HRMS (ESI) of DOGDIC at retention time 12.502 min. The single mass analysis indicates the molecular formula of the proposed structure within 5 ppm.

4.3.4 Significance of the Observation of Deuterium-Labelled DOGDIC

The most recently accepted mechanism for DOGDIC formation (Scheme 4.17) involves D-glucose (**2**) and the ε-amino group of lysine **3** undergoing a reversible condensation reaction to form unstable imine **4**. Imine/enamine tautomerization generates enaminol **5**, which can rearrange to Amadori product **6**. Water elimination from enaminol tautomer **5**, which is in equilibrium with Amadori product **6**, gives ketoimine **7**. Nucleophilic attack of the amino group of arginine **8** onto the carbonyl group of ketoimine **7** followed by cyclization gives **23**. Dehydration followed by rearrangement gives DOGDIC **10**.[220] Two diastereoisomers of DOGDIC were isolated from a reaction of D-glucose-$^{13}C_6$ (**2**), α-*N*-*t*-Boc-L-lysine (**3**) and α-*N*-*t*-Boc-L-arginine (**8**) at 50 °C in aqueous phosphate buffer (pH 7.4) for 21 days. ^{13}C NMR and LC-MS analysis suggested the currently proposed structure of DOGDIC.[215]

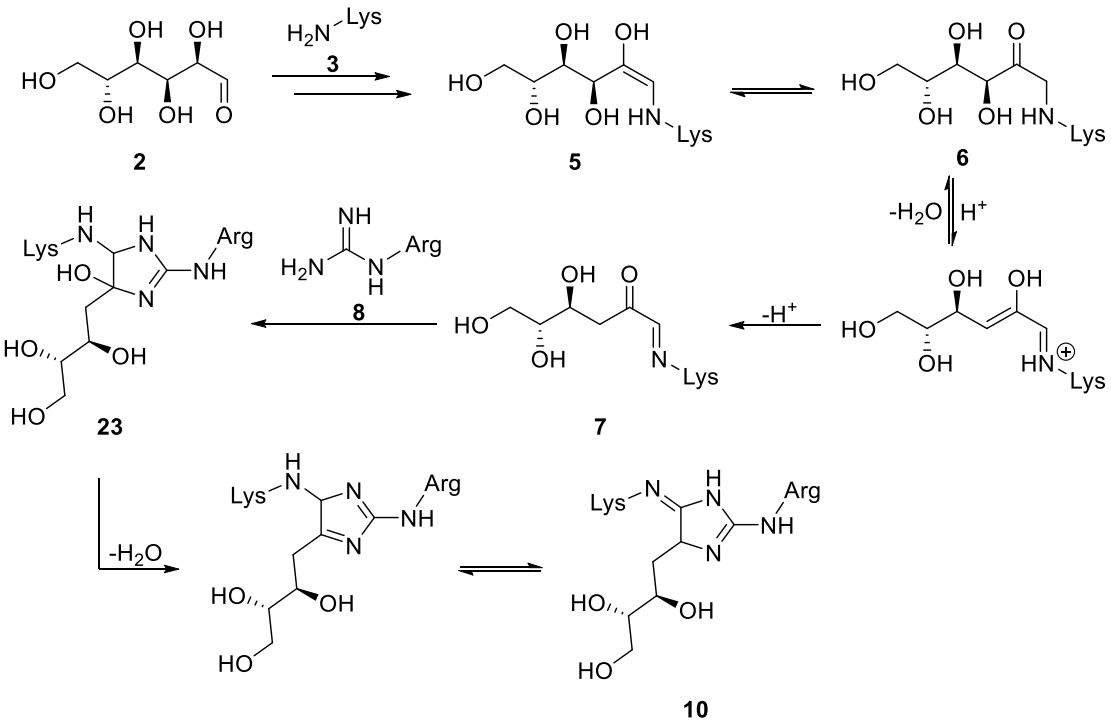

Scheme 4.17: Currently accepted mechanism for DOGDIC formation.

It was also suggested that DOGDIC is a precursor for glucosepane, i.e. upon dehydration and prototropic rearrangement glucosepane is formed (Scheme 4.2).[214] Lederer and co-workers investigated the possibility of this pathway, i.e. whether DOGDIC is a precursor to glucosepane or not. Masses consistent with both glucosepane and DOGDIC were detected from the reaction of equimolar amounts of D-glucose and D-glucose-$^{13}C_6$ (**2**) with α-*N*-*t*-Boc-L-lysine (**3**) and α-*N*-*t*-Boc-L-arginine (**8**), in which the glucose backbone was retained in both structures. Masses

consistent with both glucosepane and DOGDIC were detected from the incubation of D-glucose and bovine serum albumin (BSA); however, when 3-deoxyglucosone (3-DOG) was incubated with BSA, only a mass consistent with that of DOGDIC was detected (Scheme 4.18). The absence of glucosepane from this incubation mixture invalidated this pathway and ruled out DOGDIC as a precursor for glucosepane.[221]

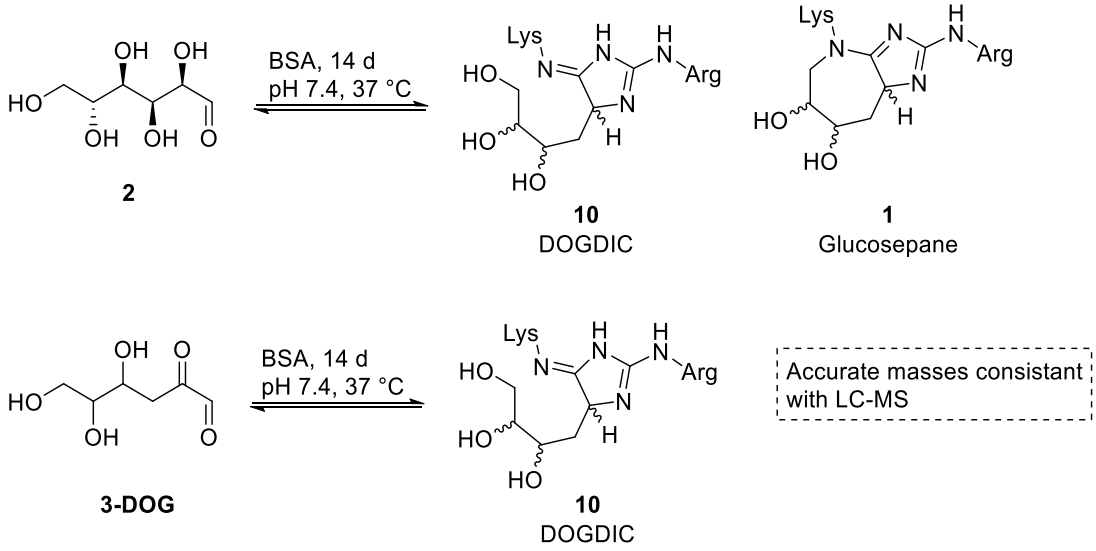

Scheme 4.18: Control experiments carried out to investigate the possibility of DOGDIC as a precursor to glucosepane.

In this work, masses consistent with that of deuterium labelled DOGDIC (containing only one deuterium) and unlabelled DOGDIC were detected after reaction of 6-[^{2}H]$_2$-glucose (**2**), α-*N*-*t*-Boc-L-lysine (**3**) and α-*N*-*t*-Boc-L-arginine (**8**). Only unlabelled DOGDIC was detected after reaction of 5-[^{2}H]-glucose (**2**), α-*N*-*t*-Boc-L-lysine (**3**) and α-*N*-*t*-Boc-L-arginine (**8**). For the currently accepted mechanism of formation of DOGDIC to be valid all deuterium labels should be present in DOGDIC after reactions using both 6-[^{2}H]$_2$-glucose and 5-[^{2}H]-glucose (Scheme 4.17). This inconsistency prompted us to suggest an alternative mechanism of formation and structure of DOGDIC in which a divergence occurs from Amadori product **6** with one pathway leading to glucosepane **1**, which is the currently accepted pathway proposed by Lederer and co-workers,[201] and another pathway leading to DOGDIC **10**, which is proposed based on this work.

This new proposed DOGDIC formation pathway (Scheme 4.19) involves the tautomerization of the carbonyl group of Amadori product **6** through the chain to give terminal aldehyde **24**. Condensation of terminal aldehyde **24** with arginine **8** gives intermediate **25**. Dehydration of

25 gives imine **26** and upon tautomerization gives enamine **27**. Keto–enol tautomerization gives ketone **28**, which can then cyclise to give imidazoline **29**. Elimination of water gives DOGDIC **10** (Scheme 4.19).

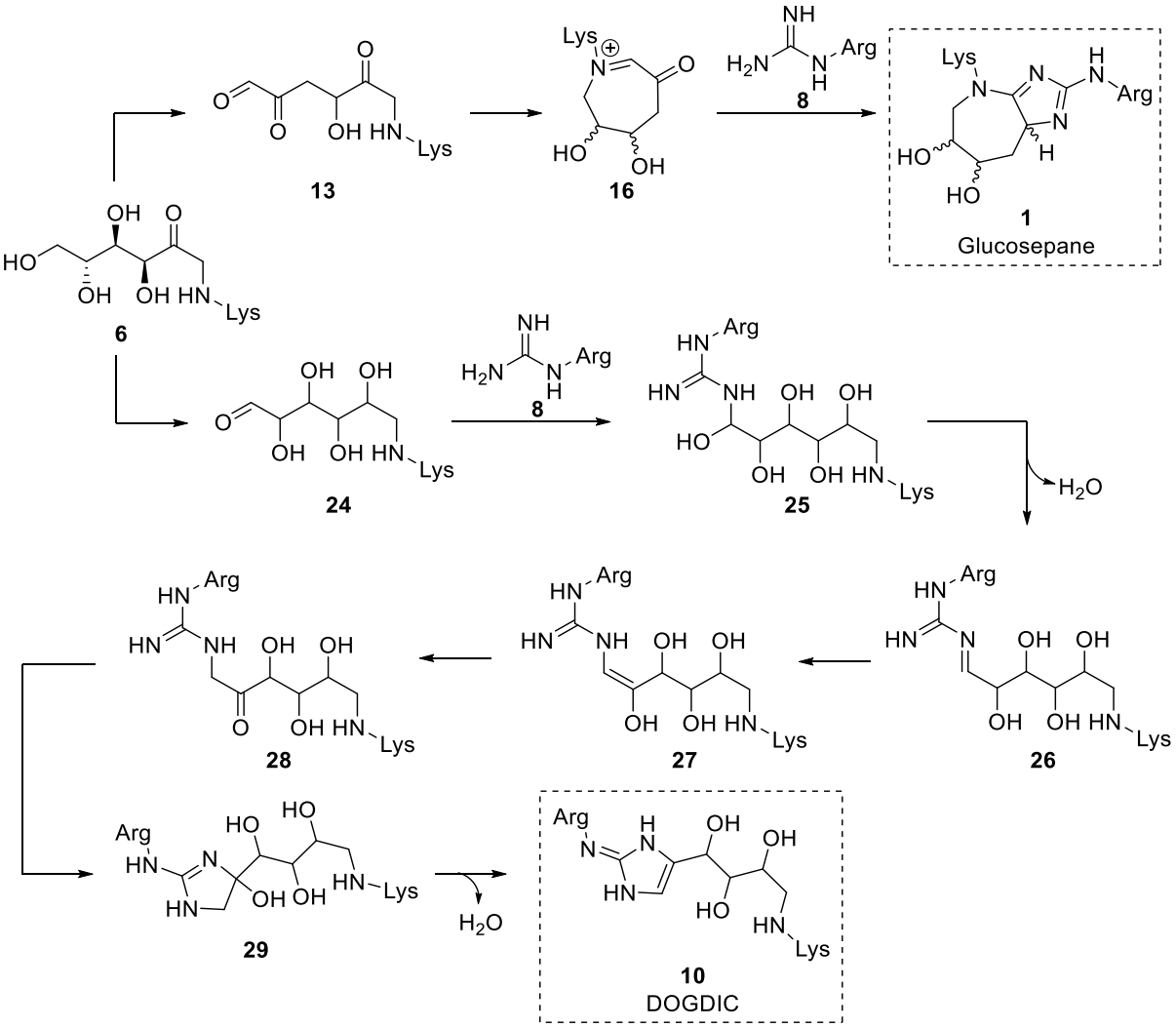

Scheme 4.19: New proposed mechanism of formation and structure of DOGDIC.

Currently, glucosepane is proposed to form by dehydration of Amadori product **6** followed by tautomerization of the carbonyl group through the chain to give α-dicarbonyl **13** (Scheme 4.8). Considering this new proposed DOGDIC formation pathway (Scheme 4.19) in which tautomerization is followed by dehydration, glucosepane could also be formed through a similar pathway in which tautomerization of the carbonyl group of Amadori product **6** through the chain is followed by dehydration to give α-dicarbonyl **13** (Scheme 4.20).

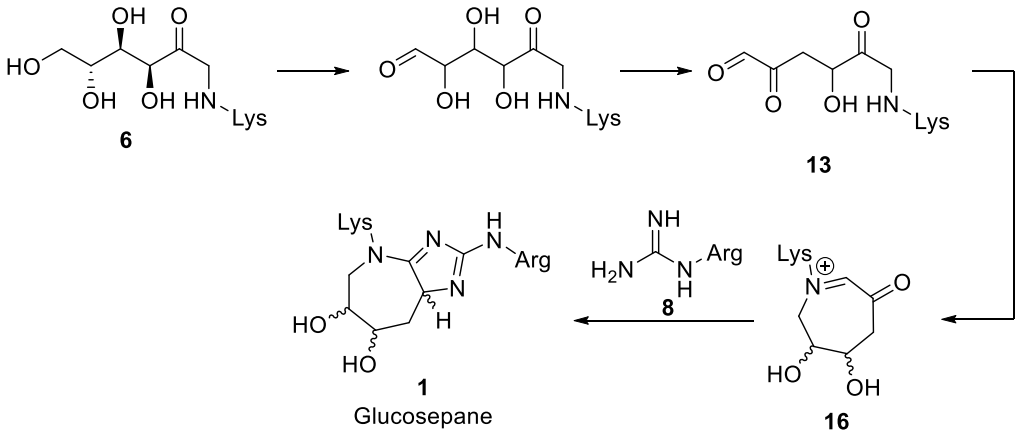

Scheme 4.20: New proposed mechanism for the formation of α-dicarbonyl **13** leading to glucosepane.

4.4 Summary and Conclusions

- Isotopic labelling studies have been used to explore the possibility of an alternative mechanism for the formation of glucosepane, involving an intramolecular 1,5-hydride shift.
- Our first hypothesis centred around a 1,5-hydride shift from the C6 position of the Amadori product to the C2 position. Isotopic labelling studies resulted in the detection of a mass consistent with that of unlabelled glucosepane, thus suggesting that a 1,5-hydride shift does not occur from this position.
- Our second hypothesis centred around a 1,5-hydride shift from the C5 position of the protonated imine to the C1 position. Isotopic labelling studies resulted in the detection of a mass consistent with that of unlabelled glucosepane, thus suggesting that a 1,5-hydride shift does not occur from this position.
- These results were more consistent with the original hypothesis of glucosepane formation with the labels likely being washed into the solvent during the keto–enol tautomerizations down the carbon chain.
- The detection of a mass consistent with that of deuterium labelled DOGDIC (containing only one deuterium) was detected when 6-$[^2H]_2$-glucose was used as starting material. The inconsistency of this observation with the currently accepted mechanism of formation of DOGDIC prompted the suggestion of an alternative mechanism of formation and structure of DOGDIC in which tautomerization of the Amadori product leads to a terminal aldehyde. Combination of the terminal aldehyde with an arginine residue could give DOGDIC rather than cyclization at the opposite end of the carbohydrate backbone, i.e. at the C2 position of the ketoimine as in the original proposed mechanism.

4.5 Future Work

To confirm the new proposed structure and formation pathway for DOGDIC it will be necessary to perform the synthesis of DOGDIC on a larger scale. This will allow a sufficient amount of material to be isolated for complete analysis by NMR.

Despite the health implications associated with AGEs, such as glucosepane, biological investigations are hampered by the lack of homogeneous material available. A total synthesis of glucosepane has been reported by Spiegel and co-workers that comprises eight steps with an overall yield of 12%.[222] A more complete understanding of how AGE crosslinks are formed would pave the way for more informed studies on their medicinal and biological implications. It is envisaged that a close analogue of glucosepane can be synthesised through a photoactivable reagent (Scheme 4.21, reagent A), i.e. a protected D-glucamine moiety, which can be substituted with a cysteine derivative and activated with UV light to generate an α-dicarbonyl moiety. Combination with an arginine residue would generate a very close analogue of glucosepane.

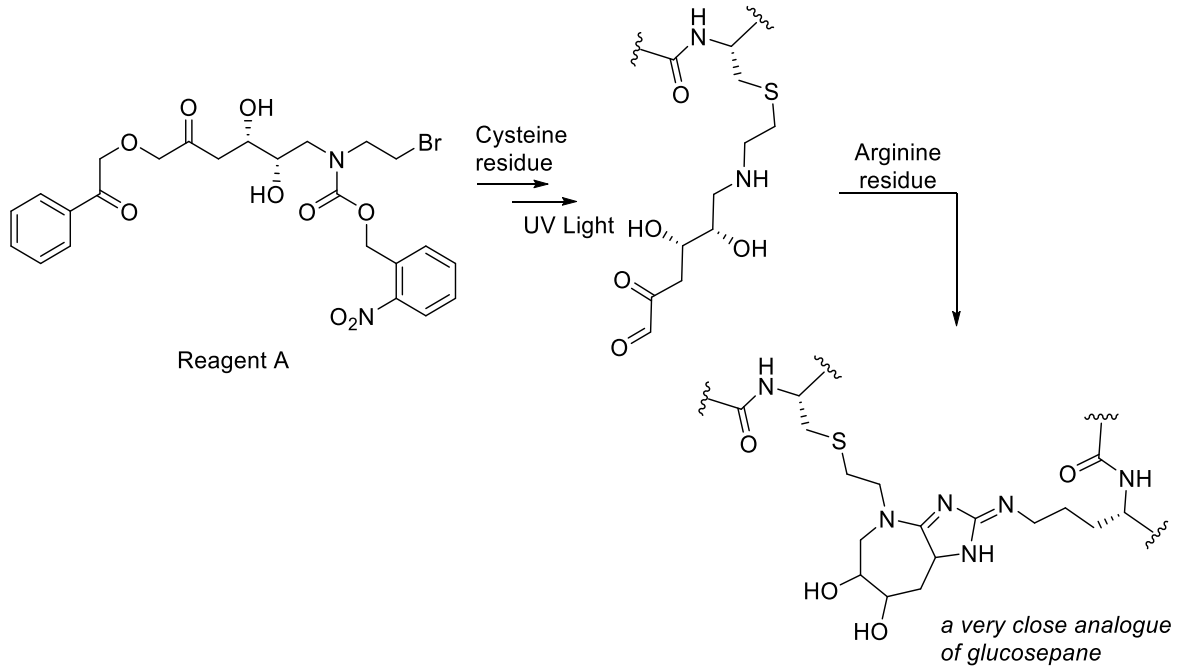

Scheme 4.21: Photoactivable reagent for the generation of a close analogue of glucosepane as well as for the study of the mechanism of formation.

Another photoactivable reagent (Scheme 4.22, reagent B) with a terminal aldehyde could also be synthesised, which upon combination with arginine followed by dehydration could produce

a close analogue of glucosepane or DOGDIC. This method of producing DOGDIC would also mimic the new mechanism for its formation as proposed from this work. These photoactivable reagents will also be used in the absence of the arginine derivative, to determine the fate of protein-bound intermediates in the absence of proximal arginine residues.

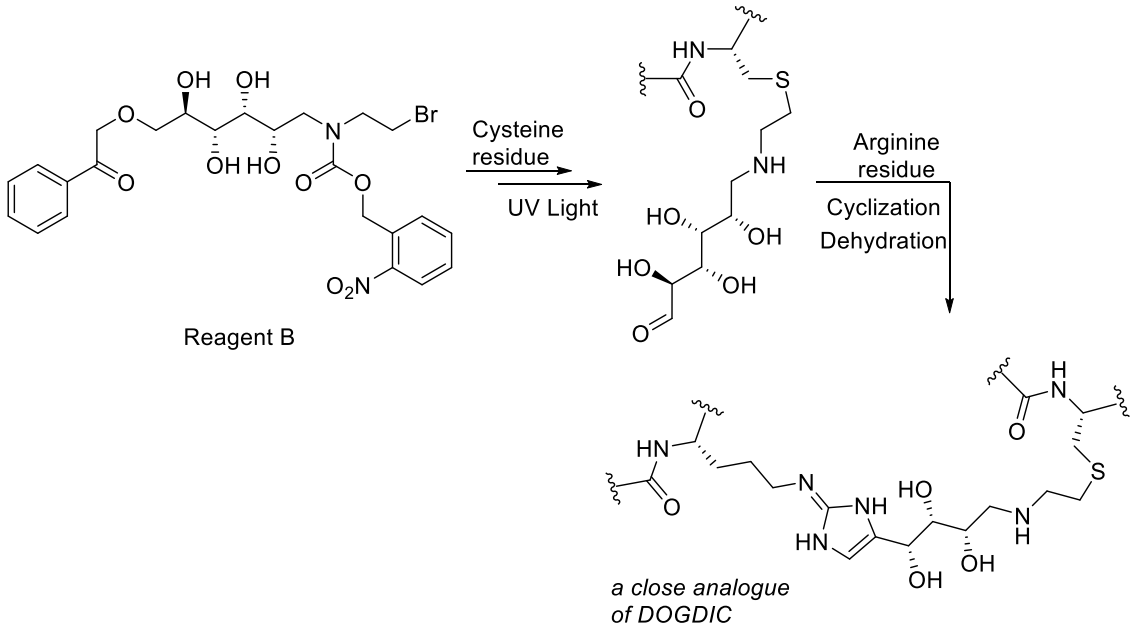

Scheme 4.22: Photoactivable reagent for the generation of a close analogue of DOGDIC.

4.6 Experimental

4.6.1 Materials

All chemicals were obtained from commercial sources and used without further purification. D-glucose and 6-[^{2}H]$_2$-glucose were obtained from Sigma Aldrich. α-*N*-*t*-Boc-L-lysine and α-*N*-*t*-Boc-L-arginine were obtained from TCI Chemicals Ltd. 5-[^{2}H]-glucose was obtained from Biosynth Carbosynth. Solvent purity is as follows: Methanol (Fisher Scientific, ≥ 99.8%), Water (Honeywell CHROMASOLV^{TM}, LC-MS grade).

4.6.2 General Experimental Procedures

LC–MS analyses were performed on a UHPLC–QTOF (Agilent 1290) coupled to high resolution mass spectrometer (quadrupole time-of-flight (QTOF), Agilent 6540) equipped with an electrospray ionization (ESI) source (quadrupole time-of-flight, QTOF, Agilent 6540). Mass spectra were acquired in positive mode with a Phenomenex® Gemini RP-C_{18}, 5 µm, 150 × 4.6 mm column. The mobile phase was prepared with: H_2O + 0.1% trifluoroacetic acid (TFA) (solvent A) and methanol (solvent B). Injection volume was set at 5 µL and flow rate at 0.7 mL/min. The elution gradient was programmed as follow: 95% A–5% B for 5 min, increasing B with a linear gradient up to 100% B from 5 to 15 min, isocratic gradient of 100% B during 15 min to 20 min, return to the initial condition from 20 to 21 min, for a total runtime of 21 min. The mass spectrometer was calibrated with a formate/acetate solution before sample analysis. This calibration solution was automatically injected before analysis for internal mass calibration. MS parameters were set as follows: nebulizer gas N_2 at 30 psig, gas temperature: 300 °C, drying gas N_2 at 7 mL/min, ion source: ESI, TOF spectra acquisition from 50 to 1600 amu, capillary voltage: 3500V.MS^2. Data was analysed using ACD/Spectrus processor 2015.

4.6.3 Preparation of a Complex Mixture of AGEs

D-glucose or D-glucose-6,6-d_2 or 5-[^{2}H]-glucose (0.01 g, 0.055 mmol), α-*N*-*t*-Boc-L-lysine (0.043 g, 0.175 mmol) and α-*N*-*t*-Boc-L-arginine (0.028 g, 0.091 mmol) were added to aqueous phosphate buffer (0.284 mL, 0.9 M, pH 7.4,) and the resulting mixture was heated to 70 °C for 17 h. The crude reaction mixture was directly analysed by UHPLC–QTOF.

References

1 J. M. Chalker, G. J. L. Bernardes, Y. A. Lin and B. G. Davis, *Chem. Asian. J.*, 2009, **4**, 630–640.

2 N. Stephanopoulos and M. B. Francis, *Nat. Chem. Biol.*, 2011, **7**, 876–884.

3 O. Boutureira and J. L. Bernardes, Goncala, *Chem. Rev.*, 2015, **115**, 2174–2195.

4 C. Zhang, E. V Vinogradova, A. M. Spokoyny, S. L. Buchwald and B. L. Pentelute, *Angew. Chemie - Int. Ed.*, 2019, **58**, 4810–4839.

5 Q. Hu, F. Berti and R. Adamo, *Chem. Soc. Rev.*, 2016, **45**, 1691–1719.

6 R. Stidl, M. Denne, J. Goldstine, B. Kadish, K. I. Korakas and P. L. Turecek, *Pharmaceuticals*, 2018, **11**, 1–16.

7 A. Papachristos, N. Pippa, C. Demetzos and G. Sivolapenko, *Drug Deliv.*, 2016, **23**, 1662–1666.

8 F. Mack, M. Ritchie and P. Sapra, *Semin. Oncol.*, 2014, **41**, 637–652.

9 J. M. Chalker, G. J. L. Bernardes and B. G. Davis, *Acc. Chem. Res.*, 2011, **44**, 730–741.

10 G. Crivat and J. W. Taraska, *Trends Biotechnol.*, 2012, **30**, 8–16.

11 O. T. Avery and W. F. Goebel, *J. Exp. Med.*, 1931, **54**, 437–447.

12 C. D. Spicer and B. G. Davis, *Nat. Commun.*, 2014, **5**, 4740–4754.

13 K. Lang and J. W. Chin, *ACS Chem. Biol.*, 2014, **9**, 16–20.

14 M. L. Blackman, R. Maksim and J. M. Fox, *J. Am. Chem. Soc.*, 2009, **130**, 13518–13519.

15 R. Bischoff and H. Schlüter, *J. Proteomics*, 2012, **75**, 2275–2296.

16 R. K. Murray, D. A. Bender, K. M. Botham, P. J. Kennelly, V. W. Rodwell and P. A. Weil, *Harper's Illustrated biochemistry*, 28th Ed., 2009, vol. 28.

17 T. E. Creighton, *Methods Enzymol.*, 1984, **107**, 305–329.

18 Z.-R. Gan, *Biochem. Biophys. Res. Commun.*, 1992, **187**, 949–955.

19 J. W. Nelson and T. E. Creighton, *Biochemistry*, 1994, **33**, 5974–5983.

20 G. B. Kallis and A. Holmgren, *J. Biol. Chem.*, 1980, **255**, 10261–10265.

21 A. R. Karala, A. K. Lappi and L. W. Ruddock, *J. Mol. Biol.*, 2010, **396**, 883–892.

22 Y.-M. Go, J. D. Chandler and D. P. Jones, *Free Radic Biol Med*, 2015, **84**, 227–245.

23 F. J. Veredas, F. R. Cantón and J. C. Aledo, *Sci. Rep.*, 2017, **7**, 1–14.

24 L. B. Poole, *Free Radic. Biol. Med. Med.*, 2015, **80**, 148–157.

25 J. Kyte, *Structure in protein chemistry*, Taylor & Francis Group, New York, Second Edi., 2007.

26 F. Brotzel and H. Mayr, *Org. Biomol. Chem.*, 2007, **5**, 3814–3820.

27 H. S. Chung, S.-B. Wang, V. Venkatramen, C. I. Murray and J. E. Van Eyk, *Circ. Res.*,

2013, **112**, 382–392.

28 O. Koniev and A. Wagner, *Chem. Soc. Rev.*, 2015, **44**, 5495–5551.

29 D. R. Goddard and L. Michaelis, *J. Biol. Chem*, 1935, **112**, 361–371.

30 F. R. N. Gurd, *Methods Enzymol.*, 1972, **25**, 424–438.

31 N. J. Davis and S. L. Flitsch, *Tetrahedron Lett.*, 1991, **32**, 6793–6796.

32 M. A. Raftery and R. D. Cole, *J. Biol. Chem.*, 1966, **241**, 3457–3461.

33 M. D. Simon, F. Chu, L. R. Racki, C. C. de la Cruz, A. L. Burlingame, B. Panning, G. J. Narlikar and K. M. Shokat, *Cell*, 2007, **128**, 1003–1012.

34 T. Climent, R. González-Luque and M. Merchán, *J. Phys. Chem. A*, 2003, **107**, 6995–7003.

35 S. G. Bodige, M. A. Me and W. H. Watson, *J. Chem. Crystallogr.*, 1999, **29**, 57–66.

36 T. Kajfe, B. Kamenar, V. Pilizota and D. Fles, *Croat. Chem. Acta*, 2003, **76**, 343–346.

37 Y. Ishii and S. S. Lehrer, *Biophys. J.*, 1986, **50**, 75–80.

38 G. Mantovani, F. Lecolley, L. Tao, D. M. Haddleton, J. Clerx, J. L. M. Cornelissen and K. Velonia, *J. Am. Chem. Soc.*, 2005, **127**, 2966–2973.

39 M. E. B. Smith, F. F. Schumacher, C. P. Ryan, L. M. Tedaldi, D. Papaioannou, G. Waksman, S. Caddick and J. R. Baker, *J. Am. Chem. Soc.*, 2010, **132**, 1960–1965.

40 M. Steiner, I. Hartmann, E. Perrino, G. Casi, S. Brighton, I. Jelesarov, G. J. L. Bernardes and D. Neri, *Chem. Sci.*, 2013, **4**, 297–302.

41 B. G. Davis, *Pure Appl. Chem*, 2009, **81**, 285–298.

42 J. M. Chalker, S. B. Gunnoo, O. Boutureira, S. C. Gerstberger, M. Fernández-González, G. J. L. Bernardes, L. Griffin, H. Hailu, C. J. Schofield and B. G. Davis, *Chem. Sci.*, 2011, **2**, 1666–1676.

43 G. J. L. Bernardes, J. M. Chalker, J. C. Errey and B. G. Davis, *J. Am. Chem. Soc.*, 2008, **130**, 5052–5053.

44 R. J. Spears and M. A. Fascione, *Org. Biomol. Chem.*, 2016, **14**, 7622–7638.

45 K. F. Geoghegan and J. G. Stroh, *Bioconjugate Chem.*, 1992, **3**, 138–146.

46 R. J. Spears and M. A. Fascione, *Org. Biomol. Chem.*, 2016, **14**, 7622–7638.

47 J. Chen, W. Zeng, R. Offord and K. Rose, *Bioconjuate Chem.*, 2003, **14**, 614–618.

48 J. M. Gilmore, R. A. Scheck, A. P. Esser-kahn, N. S. Joshi and M. B. Francis, *Angew. Chemie - Int. Ed.*, 2006, **45**, 5307–5311.

49 I. Boltes, H. Czapinska, A. Kahnert, R. Von Bu, T. Dierks, B. Schmidt, K. Von Figura, M. A. Kertesz and I. Uso, *Structure*, 2001, **9**, 483–491.

50 M. J. Appel and C. R. Bertozzi, *ACS Chem. Biol.*, 2015, **10**, 72–84.

51 M. J. Appel, K. K. Meier, J. Lafrance-vanasse, H. Lim, C. Tsai, B. Hedman, K. O. Hodgson, J. A. Tainer, E. I. Solomon and C. R. Bertozzi, *Proc. Natl. Acad. Sci. U. S.*

A., 2019, **116**, 5370–5375.

52 P. G. Holder, L. C. Jones, P. M. Drake, R. M. Barfield, S. Bañas, G. W. De Hart, J. Baker and D. Rabuka, *J. Biol. Chem.*, 2015, **290**, 15730–15745.

53 I. S. Carrico, B. L. Carlson and C. R. Bertozzi, *Nat. Chem. Biol.*, 2007, **3**, 321–322.

54 D. Rabuka, J. S. Rush, G. W. DeHart, P. Wu and C. R. Bertozzi, *Nat. Protoc.*, 2012, **7**, 1052–1067.

55 E. L. Smith, J. P. Giddens, A. T. Iavarone, K. Godula, L. Wang and C. R. Bertozzi, *Bioconjug. Chem.*, 2014, **25**, 788–795.

56 J. E. Hudak, H. H. Yu and C. R. Bertozzi, *J. Am. Chem. Soc.*, 2011, **133**, 16127–16135.

57 M. A. Gray, R. N. Tao, S. M. DePorter, D. A. Spiegel and B. R. McNaughton, *Chembiochem*, 2016, **17**, 155–158.

58 P. Thompson, B. Bezabeh, R. Fleming, M. Pruitt, S. Mao, P. Strout, C. Chen, S. Cho, H. Zhong, H. Wu, C. Gao and N. Dimasi, *Bioconjug. Chem.*, 2015, **26**, 2085–2096.

59 J. Kalia and R. T. Raines, *Angew. Chemie - Int. Ed.*, 2008, **47**, 7523–7526.

60 M. Wendeler, L. Grinberg, X. Wang, P. E. Dawson and M. Baca, *Biconjugate Chem.*, 2014, **25**, 93–101.

61 E. H. Cordes and W. P. Jencks, *J. Am. Chem. Soc.*, 1962, **84**, 826–831.

62 A. Dirksen, T. M. Hackeng and P. E. Dawson, *Angew. Chemie - Int. Ed.*, 2006, **45**, 7581–7584.

63 T. Sasaki, K. Kodama, H. Suzuki, S. Fukuzawa and K. Tachibana, *Bioorg. Med. Chem.*, 2008, **18**, 4550–4553.

64 P. I. Clark and G. Lowe, *J.C.S. Chem. Comm.*, 1977, 923–924.

65 P. I. Clark and G. Lowe, *Eur. J. Biochem.*, 1978, **84**, 293–299.

66 P. J. Wagner, *Triplet States III. Top. Curr. Chem.*, 1976, **66**, 1–52.

67 Y. Zheng, C. Duanmu and Y. Gao, *Org. Lett.*, 2006, **8**, 3215–3217.

68 C. A. G. N. Montalbetti and V. Falque, *Tetrahedron*, 2005, **61**, 10827–10852.

69 R. Subiros-Funosas, R. Prohens, R. Barbas, A. El-Faham and F. Albericio, *Chem. Eur. J.*, 2009, **15**, 9394–9403.

70 L. Fry and F. Bracher, *Encycl. Reagents Org. Synth.*, 2017, 1–3.

71 M. W. Crankshaw and G. A. Grant, *Curr. Protoc. Protein Sci.*, 1996, **3**, 15.1.1-15.1.18.

72 P. J. Wagner and E. J. Siebert, *J. Am. Chem. Soc.*, 1981, **103**, 7329–7335.

73 R. G. W. Norrish and C. H. Bamford, *Nature*, 1937, **140**, 195–196.

74 M. Oelgemoller and N. Hoffmann, *Org. Biomol. Chem.*, 2016, **14**, 7392–7442.

75 W. Horspool and F. Lenci, *CRC Handbook of Organic Photochemistry and*

Photobiology, CRC Press LLC, 2nd editio., 2004.

76 Z. Wang, *Norrish Type II Reaction (Norrish Type II Process, Norrish Type II Photoreaction, Yang Cyclization)*, John Wiley & Sons, Inc., 2010.

77 P. Klan and J. Wirz, *The Photochemistry of Organic Compounds: From Concepts to Practice*, Wiley-Blackwell, 1st ed., 2009, vol. 74.

78 G. S. Hammond and P. A. Leermakers, *J. Am. Chem. Soc.*, 1962, **84**, 207–211.

79 M. D. Schwinden, Ph.D. Thesis, Iowa State University, 1990.

80 P. J. Wagner and G. S. Hammond, *J. Am. Chem. Soc.*, 1966, **88**, 1245–1251.

81 P. J. Wagner and E. J. Siebert, *J. Am. Chem. Soc.*, 1981, **103**, 7329–7335.

82 P. J. Wagner, A. E. Kemppainen and H. N. Schott, *J. Am. Chem. Soc.*, 1973, **95**, 5604–5614.

83 A. Beckett and G. Porter, *Trans. Faraday Soc.*, 1966, **62**, 1793–1802.

84 N. C. Yang, D. S. McClure, S. L. Murov, J. J. Houser and R. Dusenbery, *J. Am. Chem. Soc.*, 1967, **89**, 5466–5468.

85 P. J. Wagner and E. J. Siebert, *J. Am. Chem. Soc.*, 1981, **103**, 7329–7335.

86 A. Nadel and J. Palinkas, *J. Heterocycl. Chem.*, 2000, **37**, 1463–1469.

87 R. B. Morin, B. G. Jackson, R. A. Mueller, E. R. Lavagnino, W. B. Scanlon and S. L. Andrews, *J. Am. Chem. Soc.*, 1969, **91**, 1401–1407.

88 P. J. Wagner and M. J. Lindstrom, *J. Am. Chem. Soc.*, 1987, **109**, 3062–3067.

89 A. Salmeen, J. N. Andersonn, M. P. Myers, T. C. Meng, J. A. Hinks, N. K. Tonks and D. Barford, *Nature*, 2003, **423**, 769–773.

90 N. Hayakawa, K. Nozawa, A. Ogawa, N. Kato, K. Yoshida, K. I. Akamatsu, M. Tsuchiya, A. Nagasaka and S. Yoshida, *Biochemistry*, 1999, **38**, 11501–11507.

91 J. R. Winther and C. Thorpe, *Biochim. Biophys. Acta*, 2014, **1840**, 838–846.

92 E. Vedejs, T. H. Eberlein and D. L. Varie, *J. Am. Chem. Soc.*, 1982, **104**, 1445–1447.

93 E. Vedejs and D. A. Perry, *J. Org. Chem.*, 1984, **49**, 573–575.

94 E. Vedejs, D. A. Perry and R. G. Wilde, *J. Am. Chem. Soc.*, 1986, **108**, 2985–2989.

95 D. Bermejo-Velasco, A. Azemar, O. P. Oommen, J. Hilborn and O. P. Varghese, *Biomacromolecules*, 2019, **20**, 1412–1420.

96 Y. Wang, Q. Chen, M. Chen, G. Guan and Y. Zhan, *Polym. Chem.*, 2019, **10**, 4844–4851.

97 G. M. Sheldrick, *Acta Crystallogr. Sect. A Found. Crystallogr.*, 2015, **71**, 3–8.

98 G. M. Sheldrick, *Acta Crystallogr. Sect. C Struct. Chem.*, 2015, **71**, 3–8.

99 P. McArdle, *J. Appl. Crystallogr.*, 2017, **50**, 320–326.

100 T. Shiraiqa, H. Tazoh, M. Sunami, Y. Sado and H. Kurokawa, *Bull. Chem. Soc. Jpn.*, 1987, **60**, 3985–3990.

101 H. J. Jin, J. Lu and X. Wu, *Bioorganic Med. Chem.*, 2012, **20**, 3465–3469.

102 V. Silvia, A. Baldisserotto, E. Scalambra, G. Malisardi, E. Durini and S. Manfredini, *Eur. J. Med. Chem.*, 2012, **50**, 383–392.

103 R. G. Hiskey and J. B. Adams, *J. Org. Chem.*, 1965, **30**, 1340.

104 K.-Y. Zee-cheng and C. C. Cheng, *J. Med. Chem.*, 1970, **13**, 414–418.

105 L. M. Tedaldi, A. E. Aliev and J. R. Baker, *Chem. Commun.*, 2012, **48**, 4725–4727.

106 M. Kirihara, Y. Asai, S. Ogawa, T. Noguchi, A. Hatano and Y. Hirai, *Synthesis (Stuttg).*, 2007, **21**, 3286–3289.

107 J. Collet and J. Messens, *Antioxidants & Redox Siganling*, 2010, **13**, 1205–1216.

108 M. Bian, R. Fan, S. Zhao and W. Liu, *J. Med. Chem.*, 2019, **62**, 7309–7321.

109 S. G. Rhee and I. S. Kil, *Annu. Rev. Biochem.*, 2017, **86**, 749–775.

110 A. Holmgren, *Ann. Rev. Biochem.*, 1985, **54**, 237–271.

111 C. H. Lillig and A. Holmgren, *Antioxidants Redox Signal.*, 2007, **9**, 26–47.

112 A. Holmgren, *Structure*, 1995, **3**, 239–243.

113 D. Mustacich and G. Powis, *Biochem. J.*, 2000, **346**, 1–8.

114 J. Folkman, *N. Engl. J. Med.*, 1971, **285**, 1182–1186.

115 D. Hedley, M. Pintilie, J. Woo, T. Nicklee, A. Morrison, D. Birle, A. Fyles, M. Milosevic and R. Hill, *Am. J. Pathol.*, 2004, **164**, 557–565.

116 T. C. Karlenius and K. F. Tonissen, *Cancers (Basel).*, 2010, **2**, 209–232.

117 M. Cha, K. Suh and I. Kim, *J. Exp. Clin. Cancer Res.*, 2009, **28**, 2085–2090.

118 A. Gallegos, J. R. Gasdaska, C. W. Taylor, G. D. Paine-murrieta, D. Goodman, P. Y. Gasdaska, M. Berggren, M. Margaret and G. Powis, *Cancer Res.*, 1996, **56**, 5765–5770.

119 J. Lu, E. Chew and A. Holmgren, *PNAS*, 2007, **104**, 12288–12293.

120 J. Ceccarelli, L. Delfino, E. Zappia, P. Castellani, M. Borghi, S. Ferrini, F. Tosetti and A. Rubartelli, *Int. J. Cancer*, 2008, **123**, 1770–1778.

121 T. Sasada, I. Satoshi, N. Sato, Y. Kltaoka, K. Hirota, K. Nakamura, A. Nishiyama, Y. Taniguchi, A. Takabayashi and J. Yodoi, *J. Clin. Invest*, 1996, **97**, 2268–2276.

122 W. J. Robbins, F. Kavanagh and A. Hervey, *Proc. Natl. Acad. Sci. U.S.A.*, 1947, **33**, 171–176.

123 I. Berdicevsky, G. Kaufman, D. J. Newman and B. A. Horwitz, *Mycoses*, 2008, **52**, 313–317.

124 S. J. Welsh, R. R. Williams, A. Birmingham, D. J. Newman, D. L. Kirkpatrick and G. Powis, *Mol. Cancer Ther.*, 2003, **2**, 235–243.

125 H. W. Moore, *Science*, 1977, **197**, 527–532.

126 P. Wipf, T. D. Hopkins, J. Jung, S. Rodriguez, A. Birmingham, E. C. Southwick, S.

Lazo and G. Powis, *Bioorg. Med. Chem. Lett.*, 2001, **11**, 2637–2641.

127 S. J. Welsh, R. R. Williams, A. Birmingham, D. J. Newman, D. L. Kirkpatrick and G. Powis, *Mol. Cancer Ther.*, 2003, **2**, 235–243.

128 D. J. Hart, H. Huang, R. Krishnamurthy and T. Schwartz, *J. Am. Chem. Soc.*, 1989, **65**, 7507–7519.

129 J. E. Biaglow and R. A. Miller, *Cancer Biol. Ther.*, 2005, **4**, 6–13.

130 D. L. Kirkpatrick, M. Kuperus, M. Dowdeswell, N. Potier, J. Donald, M. Kunkel, M. Berggren, M. Angulo and G. Powis, *Biochem. Pharmacol.*, 1998, **55**, 987–994.

131 M. Sweeney, R. Coyle, P. Kavanagh, A. A. Berezin, D. Lo Re, G. A. Zissimou, P. A. Koutentis, M. P. Carty and F. Aldabbagh, *Bioorg. Med. Chem.*, 2016, **24**, 3565–3570.

132 C. P. Constantinides, P. A. Koutentis, H. Krassos, J. M. Rawson and A. J. Tasiopoulos, *J. Org. Chem.*, 2011, **76**, 2798–2806.

133 P. A. Koutentis and D. Lo Re, *Synthesis (Stuttg).*, 2010, **12**, 2075–2079.

134 H. M. Blatter and H. Lukaszewski, *Tetrahedron Lett.*, 1968, **22**, 2701–2705.

135 A. T. Gubaidullin, B. I. Buzykin, I. A. Litvinov and N. G. Gazetdinova, *Russ. J. Gen. Chem.*, 2004, **74**, 939–943.

136 G. A. Zissimou, A. Kourtellaris, M. Manoli and P. A. Koutentis, *J. Org. Chem.*, 2018, **83**, 9391–9402.

137 J. Z. Low, G. Kladnik, L. L. Patera, S. Sokolov, G. Lovat, E. Kumarasamy, J. Repp, L. M. Campos, D. Cvetko, A. Morgante and L. Venkataraman, *Nano Lett.*, 2019, **19**, 2543–2548.

138 C. P. Constantinides and P. A. Koutentis, *Stable N- and N/S-Rich Heterocyclic Radicals: Synthesis and Applications*, Elsevier Ltd, 2016, vol. 119.

139 G. Karecla, P. Papagiorgis, N. Panagi, G. A. Zissimou, C. P. Constantinides, P. A. Koutentis, G. Itskos and S. C. Hayes, *New J. Chem.*, 2017, **41**, 8604–8613.

140 B. P. Soule, F. Hyodo, K. Matsumoto, N. L. Simone, J. A. Cook, M. C. Krishna and J. B. Mitchell, *Free Radic. Biol. Med.*, 2007, **42**, 1632–1650.

141 N. Naik and R. Braslau, *Tetrahedron*, 1998, **54**, 667–696.

142 A. Nilsen and R. Braslau, *J. Polym. Sci. Part A Polym. Chem.*, 2006, **44**, 697–717.

143 X. Guo, R. A. Mittelstaedt, L. Guo, J. G. Shaddock, R. H. Heflich, A. H. Bigger, M. M. Moore and N. Mei, *Toxicolgy Vitr.*, 2013, **27**, 1496–1502.

144 I. Novak, L. J. Harrison, B. Kovac and L. M. Pratt, *J. Org. Chem.*, 2004, **69**, 7628–7634.

145 D. Griller and K. U. Ingold, *Acc. Chem. Res.*, 1976, **9**, 13–19.

146 S. Suy, J. B. Mitchell, A. Samuni, S. Mueller and U. Kasid, *Cancer*, 2005, **103**, 1302–1313.

147 S. Suy, J. B. Mitchell, D. Ehleiter, A. Haimovitz-friedman and U. Kasid, *J. Biol. Chem.*, 1998, **273**, 17871–17878.

148 E. Moriarty, M. Carr, S. Bonham, M. P. Carty and F. Aldabbagh, *Eur. J. Med. Chem.*, 2010, **45**, 3762–3769.

149 A. A. Berezin, G. Zissimou, C. P. Constantinides, Y. Beldjoudi, J. M. Rawson and P. A. Koutentis, *J. Org. Chem.*, 2014, **79**, 314–327.

150 D. A. Close, A. X. Wang, S. J. Kochanek, T. Shun, J. L. Eiseman and P. A. Johnston, *SLAS Discov.*, 2019, **24**, 242–263.

151 M. Selby, R. Delosh, J. Laudeman, C. Ogle, R. Reinhart, T. Silvers, S. Lawrence, R. Kinders, R. Parchment, B. A. Teicher and D. M. Evans, *SLAS Discov.*, 2017, **22**, 473–483.

152 R. H. Shoemaker, *Nat. Rev. Cancer*, 2006, **6**, 813–823.

153 T. Mosmann, *J. Immunol. Methods*, 1983, **65**, 55–63.

154 P. Skehan, R. Storeng, D. Scudiero, A. Monks, D. Vistica, J. T. Warren, H. Bokesch and M. R. Boyd, *J. Natl. Cancer Inst.*, 1990, **82**, 1107–1112.

155 Y. P. Keepers, P. E. Pizao, G. J. Peters, J. Van Ark-otte, B. Winograd and H. M. Pinedo, *Eur. J. Cancer*, 1991, **27**, 897–900.

156 V. Vichai and K. Kirtikara, *Nat. Protoc.*, 2006, **1**, 1112–1116.

157 C. Asche, *Mini-Reviews Med. Chem.*, 2005, **5**, 449–467.

158 C. P. Guise, A. M. Mowday, A. Ashoorzadeh, R. Yuan, W. H. Lin, D. H. Wu, J. B. Smaill, A. V. Patterson and K. Ding, *Chin. J. Cancer*, 2014, **33**, 80–86.

159 F. J. Alcaín and J. M. Villalba, *Expert Opin. Ther. Patents*, 2007, **17**, 649–666.

160 L. Garuti, M. Roberti and D. Pizzirani, *Mini-Reviews Med. Chem.*, 2007, **7**, 481–489.

161 A. Begleiter, *Front. Biosci.*, 2000, **5**, 153–171.

162 W. T. Bradner, *Cancer Treat. Rev.*, 2001, **27**, 35–50.

163 B. M. Hoey, J. Butler and A. J. Swallow, *Biochemistry*, 1988, **27**, 2608–2614.

164 D. Jamieson, A. T. Y. Tung, R. J. Knox and A. V. Boddy, *Br. J. Cancer*, 2006, **95**, 1229–1233.

165 P. G. Penketh, W. F. Hodnick, M. F. Belcourt, K. Shyam, D. H. Sherman and A. C. Sartorelli, *J. Biol. Chem.*, 2001, **276**, 34445–34452.

166 H. A. Seow, P. G. Penketh, R. P. Baumann and A. C. Sartorelli, *Methods Enzymol.*, 2004, **382**, 221–233.

167 E. T. Oh and H. J. Park, *BMB Rep.*, 2015, **48**, 609–617.

168 V. N. Iyer and S. W, *Science*, 1964, **145**, 55–58.

169 M. Tomasz, *Chem. Biol.*, 1995, **2**, 575–579.

170 S. E. Wolkenberg and D. L. Boger, *Chem. Rev.*, 2002, **102**, 2477–2495.

171 M. A. Colucci, G. D. Couch and C. J. Moody, *Org. Biomol. Chem.*, 2008, **6**, 637–656.

172 E. B. Skibo, A. Jamil, B. Austin, D. Hansen and A. Ghodousi, *Org. Biomol. Chem.*,

2010, **8**, 1577–1587.

173 E. B. Skibo and W. G. Schulz, *J. Med. Chem.*, 1993, **36**, 3050–3055.

174 M. Lynch, S. Hehir, P. Kavanagh, D. Leech, J. O'Shaughnessy, M. P. Carty and F. Aldabbagh, *Chem. Eur. J.*, 2007, **13**, 3218–3226.

175 A. G. Siraki, T. S. Chan and P. J. O'Brien, *Toxicol. Sci.*, 2004, **81**, 148–159.

176 L. F. Scherz, E. A. Abdel-Rahman, S. S. Ali, A. D. Schlüter and M. A. Abdel-Rahman, *Med. Chem. Commun.*, 2017, **8**, 662–672.

177 S. Bonham, L. O'Donovan, M. P. Carty and F. Aldabbagh, *Org. Biomol. Chem.*, 2011, **9**, 6700–6706.

178 V. Fagan, S. Bonham, M. P. Carty, P. Saenz-Méndez, L. A. Eriksson and F. Aldabbagh, *Bioorganic Med. Chem.*, 2012, **20**, 3223–3232.

179 R. Zhou and E. B. Skibo, *J. Med. Chem.*, 1996, **39**, 4321–4331.

180 K. Fahey, L. O'Donovan, M. Carr, M. P. Carty and F. Aldabbagh, *Eur. J. Med. Chem.*, 2010, **45**, 1873–1879.

181 D. Anastasiou, E. M. Campi, H. Chaouk and W. R. Jackson, *Tetrahedron*, 1992, **48**, 7467–7478.

182 J. Huang, Y. He, Y. Wang and Q. Zhu, *Chem. Eur. J.*, 2012, **18**, 13964–13967.

183 J. M. Caroon and L. E. Fisher, *Heterocycles*, 1991, **32**, 459–467.

184 M. D. Nair and R. Adams, *J. Am. Chem. Soc.*, 1961, **83**, 3518–3521.

185 M. Gurry, M. Sweeney, P. McArdle and F. Aldabbagh, *Org. Lett.*, 2015, **17**, 2856–2859.

186 J. D. Sivey, J. S. Arey, P. R. Tentscher and A. L. Roberts, *Environ. Sci. Technol.*, 2013, **47**, 1330–1338.

187 R. Ben-Daniel, S. P. De Visser, S. Shaik and R. Neumann, *J. Am. Chem. Soc.*, 2003, **125**, 12116–12117.

188 M. Eigen and K. Kustin, *J. Am. Chem. Soc.*, 1962, **84**, 1355–1361.

189 Q. Liu and D. W. Margerum, *Environ. Sci. Technol.*, 2001, **35**, 1127–1133.

190 M. Sweeney, L.-A. J. Keane, M. Gurry, P. McArdle and F. Aldabbagh, *Org. Lett.*, 2018, **20**, 6970–6974.

191 E. Moriarty, M. Carr, S. Bonham, M. P. Carty and F. Aldabbagh, *Eur. J. Med. Chem.*, 2010, **45**, 3762–3769.

192 I. Antonini, F. Claudi, G. Cristalli, P. Franchetti, M. Grifantini and S. Martelli, *J. Med. Chem.*, 1988, **31**, 260–264.

193 P. Hammershøj, T. K. Reenberg, M. Pittelkow, C. B. Nielsen, O. Hammerich and J. B. Christensen, *European J. Org. Chem.*, 2006, 2786–2794.

194 H. Mustroph and R. Haessner, *J. F. Prakt. Chemie.*, 1989, **331**, 319–323.

195 M. R. Zhang, K. Kumata, J. Maeda, T. Haradahira, J. Noguchi, T. Suhara, C. Halldin

and K. Suzuki, *J. Med. Chem.*, 2007, **50**, 848–855.

196 V. A. Roytman and D. A. Singleton, *Science*, 2019, **363**, 1326–1329.

197 V. Fagan, S. Bonham, P. McArdle, M. P. Carty and F. Aldabbagh, *Eur. J. Org. Chem.*, 2012, 1967–1975.

198 J. O'Shaughnessy, D. Cunningham, P. Kavanagh, D. Leech, P. McArdle and F. Aldabbagh, *Synlett*, 2004, 2382–2384.

199 R. Singh, A. Barden, T. Mori and L. Beilin, *Diabetologia*, 2001, **44**, 129–146.

200 K. Nowotny, T. Jung, A. Höhn, D. Weber and T. Grune, *Biomolecules*, 2015, **5**, 194–222.

201 K. M. Biemel, J. Conrad and M. O. Lederer, *Angew. Chem. Int. Ed.*, 2002, **41**, 801–804.

202 S. K. Grandhee and V. M. Monnier, *J. Biol. Chem.*, 1991, **266**, 11649–11653.

203 V. M. Monnier, D. R. Sell, V. M. Monnier and S. Genuth, *Glycoconj. J.*, 2016, **33**, 569–579.

204 A. Nash, M. Notou, A. F. Lopez-Clavijo, L. Bozec, N. H. de Leeuw and H. L. Birch, *Matrix Biol. Plus*, 2019, 100013.

205 C. Legrand, U. Ahmed, A. Anwar, K. Rajpoot, S. Pasha, C. Lambert, R. K. Davidson, I. M. Clark, P. J. Thornalley, Y. Henrotin and N. Rabbani, *Arthritis Res. Ther.*, 2018, **20**, 131–147.

206 S. H. Kim, J. Turnbull and S. Guimond, *J. Endocrinol.*, 2011, **209**, 139–151.

207 J. S. Sjoeberg and S. Bulterijs, *Rejuvenation Res.*, 2009, **12**, 137–148.

208 M. D. Shoulders and R. T. Raines, *Annu. Rev. Biochem.*, 2009, **78**, 929–958.

209 K. E. Kadler, D. F. Holmes, J. A. Trotter and J. A. Chapman, *Biochem. J.*, 1996, **316**, 1–11.

210 S. Sasaki, T. Ikeda, S. ichiro Okihara, S. Nishimura, R. Nakadate, H. Saeki, E. Oki, M. Mori, M. Hashizume and Y. Maehara, *Sci. Rep.*, 2019, **9**, 1–10.

211 J. S. Sjöberg and S. Bulterijs, *Rejuvenation Res.*, 2009, **12**, 137–148.

212 J.-A. Lin, C.-H. Wu and G.-C. Yen, *J. Agric. Food Chem.*, 2018, **66**, 2065–2070.

213 S.-J. Cho, G. Roman, F. Yeboah and Y. Konishi, *Curr. Med. Chem.*, 2007, **14**, 1653–1671.

214 M. O. Lederer and H. P. Buhler, *Bioorg. Med. Chem.*, 1999, **7**, 1081–1088.

215 K. M. Biemel, O. Reihl and M. O. Lederer, *J. Biol. Chem.*, 2001, **276**, 23405–23412.

216 R. Nasiri, M. Zahedi, H. Jamet and A. A. Moosavi-Movahedi, *J. Mol. Model*, 2012, **18**, 1645–1659.

217 K. M. Biemel, A. D. Friedl and M. O. Lederer, *J. Biol. Chem.*, 2002, **277**, 24907–24915.

218 K. M. Mcquaid, J. Z. Long and D. Sames, *Org. Lett.*, 2009, **11**, 2972–2975.

219 R. Gounder and M. E. Davis, *ACS Catal.*, 2013, **3**, 1469–1476.

220 S.-J. Cho, G. Roman, F. Yeboah and Y. Konishi, *Curr. Med. Chem.*, 2007, **14**, 1653–1671.

221 K. M. Biemel, A. D. Friedl and M. O. Lederer, *J. Biol. Chem.*, 2002, **277**, 24907–24915.

222 C. Draghici, T. Wang and D. A. Spiegel, *Science*, 2015, **350**, 294–298.